NIPER-390
Distribution Category UC-122

# INTEGRATED RESERVOIR ASSESSMENT AND CHARACTERIZATION

Final Report for the Period
October 1, 1985-September 30, 1988

By
Matt Honarpour
Michael Szpakiewicz
Bijon Sharma
Ming-Ming Chang
Rick Schatzinger
Susan Jackson
Liviu Tomutsa
Nicida Maerefat

NIPER--390

DE89 000743

May 1989

Work Performed Under Cooperative Agreement No. FC22-83FE60149

Prepared for
U. S. Department of Energy
Assistant Secretary for Fossil Energy

Edith Allison, Project Manager
Bartlesville Project Office
P.O. Box 1398
Bartlesville, OK 74005

Prepared by
IIT Research Institute
National Institute for Petroleum and Energy Research
P. O. Box 2128
Bartlesville, OK 74005

---

TABLE OF CONTENTS

TABLE OF CONTENTS - Continued

TABLE OF CONTENTS - Continued



## TABLES

TABLES - Continued

## ILLUSTRATIONS

Figures Page

ILLUSTRATIONS - Continued

Figures | Page

Figures Page

Figures Page

## ILLUSTRATIONS - Continued

Figures | Page

# INTEGRATED RESERVOIR ASSESSMENT AND CHARACTERIZATION

By Matt Honarpour

---

## ABSTRACT

An integrated multidisciplinary evaluation of the barrier island and associated overlying valley fill deposits of the Lower Cretaceous Muddy formation at Bell Creek (MT) field was conducted for two reasons. The first objective was to improve the predictability of fluid flow and entrapment of residual oil in interwell areas through an understanding of the effects of multigeneric heterogeneities that affect each stage of production. A realistic prediction of fluid movement in clastic reservoirs subjected to enhanced oil recovery (EOR) requires the integration of depositional, diagenetic, structural, and fluid flow models that define heterogeneities encountered within barrier island hydrocarbon reservoirs. In addition, a study of analogous outcrops indicated that outcrop-derived quantitative data can supplement subsurface reservoir description. The second objective was to develop a generic methodology for characterizing barrier island reservoirs.

This report covers the development of a generic approach to reservoir characterization, the preliminary studies leading to the selection of an appropriate depositional system for detailed study, the application of outcrop studies to quantified reservoir characterization, and the construction of a quantified geological/engineering model used to screen the effects and scales of various geological heterogeneities within a reservoir. These heterogeneities result in large production/residual oil saturation contrasts over small distances.

Results of the study, based on a quantified geological/engineering model of Bell Creek field, showed that the most productive part of Unit 'A' in that field is associated with regions of well-developed, high-energy barrier island facies; low amounts of diagenetic clay cement; and the absence of structural discontinuities. The influence of the scale of heterogeneities varied at different stages of oil recovery.

Large-scale heterogeneities include fluid-related parameters, depositional features, and structural framework. Among medium- and small-scale features affecting petrophysical properties and continuity of flow units, the most influential are diagenesis and faults.

Primary production was dominantly influenced by large-scale depositional heterogeneities and moderately by medium-scale diagenetic heterogeneities. The influence of regional dip and faulting was low or negligible on primary production.

Secondary production was dominantly influenced by large-scale structural factors (structural dip but not faulting), by medium-scale diagenetic heterogeneities, and less by medium-scale depositional heterogeneities.

Tertiary production was dominantly influenced by large-, medium-, and small-scale depositional heterogeneities; locally by medium- to small-scale diagenetic heterogeneities; and to a lesser extent by faulting.

Simulations of waterflooding and micellar-polymer flooding at Unit 'A' in Bell Creek field indicated that effects of oil trapping in low-permeability layers and oil and water channeling in high-permeability layers were reflected in residual oil distribution and cumulative oil production curves.

Crossplots of density log-derived porosity versus formation resistivity and density log-derived porosity versus gamma-ray log values were effective in separating depositional facies.

Residual oil saturation distribution analysis after 10 years of linedrive waterflooding indicated that the remaining oil saturation was highest in the most geologically heterogeneous part of the reservoir. The Dykstra-Parsons coefficient was used to identify such areas. Earlier initiation of waterflooding would have provided the fastest rate of oil recovery and would not have affected cumulative production. Pattern waterflooding associated with infill drilling recovered substantial bypassed oil after linedrive waterflooding. Micellar-polymer flooding recovered a substantial amount of trapped oil from the more homogeneous part of the reservoir.

## EXECUTIVE SUMMARY

Barrier island depositional systems contain a substantial amount of the petroleum resource in the United States that can be the target of infill drilling and/or enhanced oil recovery (EOR) development. Bell Creek (MT) field was selected for this reservoir assessment and characterization research. It is a barrier island reservoir with a large remaining resource. The reservoir has been producing oil by primary and secondary methods and micellar-polymer flooding. Substantial reliable subsurface and analogous outcrop data were gathered to study various scales of heterogeneities and their influence on fluid flow and residual oil distribution.

NIPER has applied an interdisciplinary team approach to the integrated analysis of this barrier island reservoir. The reservoir characterization team consists of experienced petroleum engineers, reservoir engineers, geologists, geological engineers, geophysicists, geochemists, chemical engineers, simulation experts, core analysts, log analysts, petrographers, and geostatisticians. Through an integrated analysis, depositional, diagenetic, structural, and interstitial fluid models have been assembled and used to construct a quantitative geological model. In addition, an engineering model was constructed by integrating rock-fluid interaction data; wellbore and interwell data; and production, pressure, and drive-mechanism data. A combined quantified geological/engineering model was constructed by integrating the geological and engineering models.

This geological/engineering model was used to identify various scales of heterogeneities in a barrier island system. It also identified commonality, regional, and site-specific features of heterogeneities. The geological/engineering model also indicated trends in reservoir properties such as porosity, permeability, and mineralogy and compared data from analogous outcrops with subsurface data. Finally, the influence of various heterogeneities on fluid flow and hydrocarbon trapping was investigated. Primary recovery and waterflood simulations were performed to verify the accuracy of the geological/engineering model. Sensitivity analysis in the simulation was used to investigate the influence of various heterogeneities on fluid flow and hydrocarbon trapping. Streamline modeling and micellar-polymer simulations were performed to study fluid flow paths and residual oil saturation distributions which resulted from chemical flooding.

From the results of these 3 years of research, it was concluded that improved reservoir characterization is only possible through multidisciplinary integration and analysis of conventional data on depositional system-specific heterogeneities. Predictability on an interwell scale is enhanced through an understanding of depositional, geochemical, diagenetic, structural, fluid movement, and hydrocarbon accumulation processes.

This geological model indicates that the barrier island deposystem is commonly associated with valley cut and fill which is often of poor reservoir quality. Based on depositional characteristics of the barrier island system, superior reservoir quality is present in foreshore, upper and middle shoreface, and washover facies. These facies are distinguishable through sedimentological analyses and log and core correlations. Outcrop data were also found to be applicable to interwell-scale heterogeneity description in subsurface reservoirs.

Integration of the geological and engineering models allowed the ranking of sedimentary, tectonic, and diagenetic heterogeneities relative to different stages of the production performance. Patterned waterflooding and infill drilling after linedrive waterflooding proved to be effective in areas with permeability stratification due to depositional and diagenetic processes. Micellar-polymer flooding was responsible for much of the production after waterflood within the more homogeneous part of the reservoir.

As part of this project, a generic, comprehensive, stepwise methodology with abundant interconnection among disciplines was organized in a format that is easily adaptable to an expert system technique for effective and efficient reservoir characterization.

Projects of this type provide guidelines for effective evaluation and development of barrier island reservoirs. They also provide an interdisciplinary methodology, which is a step toward optimal and efficient exploitation of barrier island reservoirs.

This report outlines a comprehensive generic approach to integrative reservoir characterization based on a review of several DOE-sponsored EOR pilot projects (Chapter 2). This generic approach was formulated in the NIPER FY 86 Annual Research Plan for reservoir assessment and characterization research. Four criteria were considered for the selection of a deposystem for

heterogeneity research (Chapter 3). The criteria included appreciable potential reserve, presence of nearby analogous outcrops, presence of an EOR pilot, and availability of adequate specific data. Shelf ridge and barrier island deposystems were candidates for detailed heterogeneity research based on these criteria. A preliminary study of subsurface and outcrop Shannon formation (shelf ridge deposystem) sandstones was conducted (Chapter 3). A similar study of the Muddy formation sandstone at Bell creek field (Chapter 4) showed that the barrier island deposystem was better able to meet the objectives of this research as outlined in the long-term plan. Analogous outcrops were selected, sampled, and analyzed for development of a quantitative geological model to supplement subsurface data (Chapter 5). The production performance of Bell Creek field was analyzed and integrated into a geological/engineering model (Chapter 6). Sensitivity studies, waterflood simulation, and EOR simulations were performed to evaluate the effect of various heterogeneities on reservoir performance (Chapter 7). Based on experience developed during this study, a methodology for reservoir-characterization was developed (Chapter 8). Results obtained during this project are summarized in Chapter 9, and conclusions from the overall study are discussed in Chapter 10.

# CHAPTER 1. INTRODUCTION

Two broad objectives of the Department of Energy's program for petroleum production research are to develop methods for locating residual oil saturation distribution in oil reservoirs and to develop suitable methods for recovering the oil. With these broad objectives in mind, a generic approach was formulated in the NIPER FY86 Annual Research Plan for research on reservoir assessment and characterization. The specific objective was to develop a better understanding of heterogeneity factors that influence the movement and trapping of fluids in reservoirs. Accurate descriptions of the spatial distribution of critical reservoir parameters (permeability, porosity, pore geometry, mineralogy, and oil saturation) are essential for adequate mobility control, for implementation of fluid diversionary techniques, and for reliable predictions of oil recovery.

The FY86 Annual Research Plan was based on recommendations of a round-table conference convened to discuss the best generic approach to reservoir characterization. The conference was attended by representatives of NIPER/BPO and a number of eminent consultants from the petroleum industry. The research strategy adopted in the FY86 plan was to select one major depositional system based on its enhanced oil recovery (EOR) potential, and through coordinated studies of outcrops, a completed waterflood project, and a completed EOR project in a part of a field in the same reservoir, to develop and test quantitative generic methods for accurate predictions of flow patterns, recovery, and the spatial distribution of oil remaining after each process. If the methods could accurately account for the produced and remaining oil, then the applicability of the approach to other reservoirs belonging to the same deposystem could be ascertained by conducting additional reservoir studies.

The research strategy outlined in the NIPER FY86 Plan (fig. 1) was first to select a deposystem representative of several EOR target reservoirs. The barrier island system was selected. Heterogeneities that strongly influence the trapping of oil and control its movement in barrier island reservoirs were identified. This method incorporated, to the extent possible, generic factors which determine the influence of heterogeneities on reservoir performance. If the method can account for the produced oil and the remaining oil, it can be applied to other reservoirs belonging to the same deposystem.

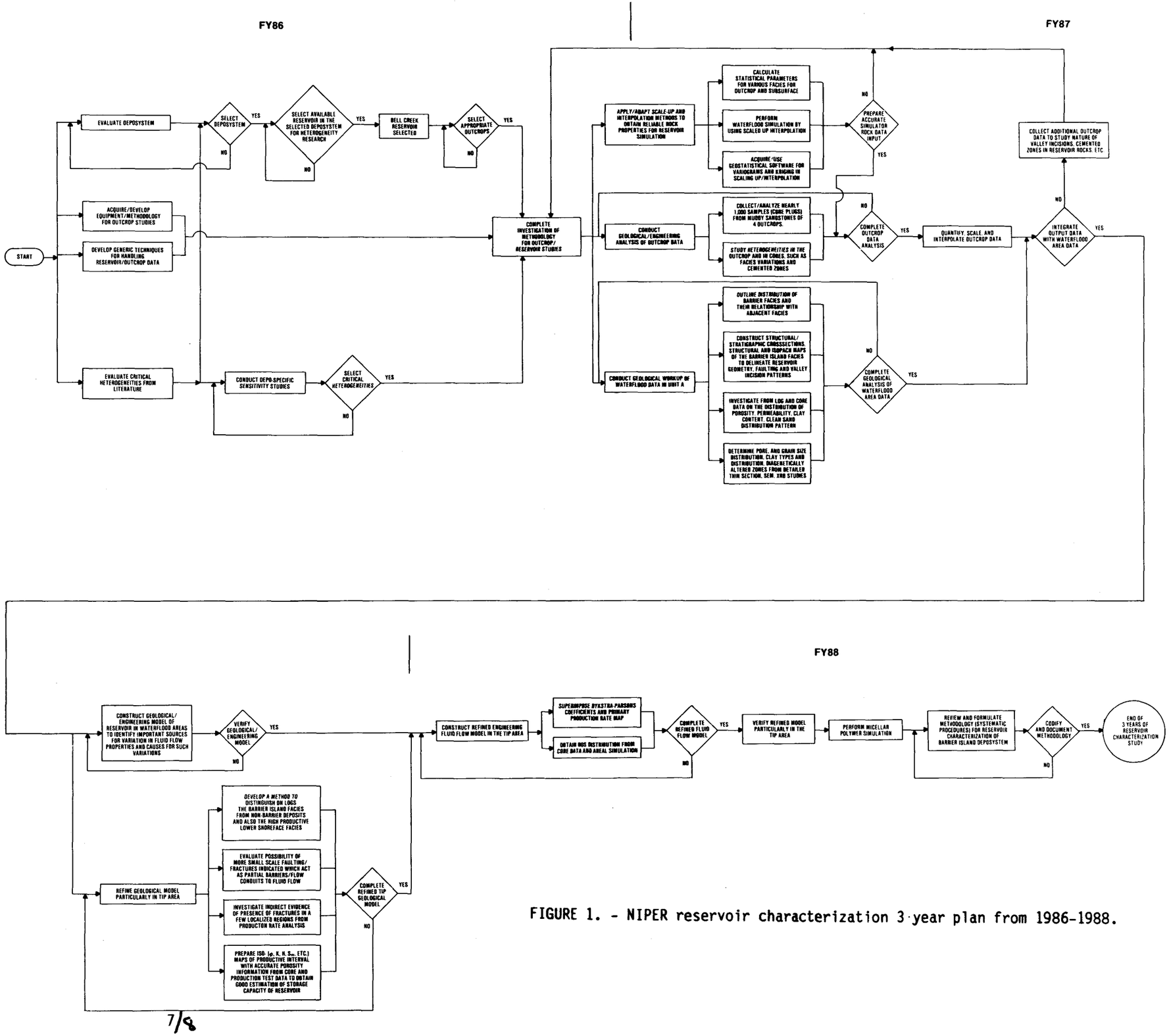


FIGURE 1. - NIPER reservoir characterization 3-year plan from 1986-1988.

Detailed analyses of heterogeneities as proposed to the FY86 Plan required the analysis of closely spaced core samples that represented locations both vertically and laterally in the pay zone. Since the only readily available source for such closely spaced data was analogous outcrops, the emphasis of the NIPER reservoir characterization program was placed on collecting ample outcrop samples and combining the resulting geological data with the reservoir data to model reservoir heterogeneities.

After a deposystem with high EOR potential was selected, the critical heterogeneities in that deposystem were selected for research. Development of equipment and methodology for outcrop studies were completed, and theoretical studies related to development of generic techniques for handling reservoir heterogeneity data were carried out. A list of selected heterogeneities was prepared, and a few critical heterogeneities from that list were selected for further research. Bell Creek field in Montana and a nearby outcrop site were selected for collecting data for studies of the fluid flow characteristics of the barrier island and genetically associated deposystem. Methods for scaling up and interpolating critical reservoir parameters were developed. Some 1,000 samples from analogous outcrops were collected from an area comparable to the tertiary incentive project (TIP) in subsurface, and reservoir data from the waterflooded part of the reservoir were gathered to construct a geological model of the reservoir in the waterflood area.

In FY87, the data collected from the outcrops and reservoir were analyzed for development of a quantitative geological model that would incorporate the effects of all the critical geological heterogeneities. Waterflood simulations were performed to investigate the influence of critical heterogeneities on waterflood performance. Reservoir data from the waterflooded portion of the reservoir were augmented with the outcrop data for further refinement of the geological model of the waterflood area. The combined quantified, calibrated, and scaled geological data were used to construct a geological/engineering model of the reservoir in a form suitable for computer simulation. The model was used to evaluate the influence of heterogeneities on reservoir performance. Additional data were collected for further improvement of the model.

In FY88, geological data from the TIP portion and surrounding area of Unit 'A' of Bell Creek field were used to refine the geological model of the

reservoir in the TIP area. Then the refined geological model of the TIP area was augmented with outcrop data to construct a refined geological/engineering model of the barrier island deposystem. This model was used to evaluate quantitatively the influence of critical heterogeneities on the reservoir performance of the TIP area. The optimized methodology was outlined and coded.

The tasks described above relate to one reservoir and several outcrops selected for study. The simplified procedure will be followed in FY89 to analyze another example of the same deposystem using the developed methodology for barrier island reservoirs and to quantify the effect of critical heterogeneities on fluid production and trapping.

This report covers the 3-year period of work, Oct. 1, 1985 - Sept. 30, 1988, performed by NIPER as Project BE1 for the U.S. Department of Energy under Cooperative Agreement DE-FC22-83FE60149.

## ACKNOWLEDGMENTS

The research team for Project BE1 gratefully acknowledges the counsel and guidance of Herbert B. Carroll, Jr of NIPER in performing this work. The team also acknowledges Min K. Tham of NIPER for his continued guidance throughout the duration of this project. The support of Aaron Cheng of NIPER and E. B. Nuckols, Project Manager, Bartlesville Project Office, U. S. Department of Energy; the encouragement and support of Bill Linville, NIPER; and the help of Edna Hatcher of NIPER who typed the manuscript for this report are acknowledged. We appreciate the support of the U. S. Department of Energy for financing this research through Cooperative Agreement DE-FC22-83FE60149. Special thanks are due to John Nikonchik of Gary-Williams Oil Producers Inc. for providing laboratory and field data and helpful comments and to R. W. Tillman for technical guidance through much of this research project. The contributions from D. H. Dailey for providing paleontological analyses, Keith Westhusing for direction in this project, 1985-87 as project manager and Mike Fowler and Ian Palmer for their efforts early in this project are greatly appreciated.

# CHAPTER 2. DEVELOPMENT OF GENERIC APPROACH TO RESERVOIR CHARACTERIZATION BASED ON THE EVALUATION OF FOUR DOE-SPONSORED EOR PILOT PROJECTS

The purpose of this continuing research is to develop a generic approach to reservoir characterization for EOR rather than to provide a technique for constructing individual reservoir models. Results of this work will bring awareness to many problems that recur in EOR projects within clastic reservoirs and that indicate the need for further refinement.

Small-scale heterogeneities, not always critical to primary and secondary recovery, may significantly affect sweep and displacement efficiencies in EOR operations. In addition to available log and core data, new methodology is needed to improve reservoir characterization in interwell areas. The importance of reconstructing the paleohistory of formations is emphasized to provide information on the variability of diagenetic, structural, and formation-fluid heterogeneities.

Improvement in reservoir characterization for EOR requires an understanding of the origin, timing, trend, and magnitude of geological events that affected the reservoir anatomy (internal structure and composition of the rock). A biased or partial approach to reservoir characterization may result in complete failure or suboptimal results. In 1979, Dickey[1] described several EOR projects that failed because the actual geology had not been considered. In 1986, Dickey[2] further stated that the most common cause of failure of EOR projects was the heterogeneity of reservoirs.

Reservoir characterization for EOR purposes should include data from all available sources (analogous reservoirs, outcrops, aquifers, etc.). The multimodel system developed from these data would include a subsequent ranking and integration of the various factors responsible for specific flow behavior.

The basic framework for a clastic reservoir description is derived from the geometry and anatomy of oil-producing formations at the time of deposition. The span of time from deposition to the present introduces a variety of changes in internal structure and composition in the formation.

Reconstruction of postdepositional conditions should include (1) interpretations of the maximum depth of burial, residence time at different depths, and tectonic history; (2) the extent of paleoexposure, erosion, weathering, and reburial conditions; and (3) knowledge of the time of

hydrocarbon entry into the reservoir. During the evolutionary history of reservoir rocks, mineral assemblages continue to equilibrate chemically with formation fluids, and intermediate byproducts are produced that contribute to the overall heterogeneity of the rocks. To determine the amount of residual oil and define the most cost-effective recovery method, reservoir parameters altered during primary, secondary, and/or tertiary recovery must be identified and quantified. In practice, however, comprehensive geological reservoir characterization is not always included in designing EOR projects.

In this research, geological data from four DOE-sponsored EOR pilot projects were analyzed to determine the effect of various geological heterogeneities on EOR performance. Results of the four case-history analyses as well as our experience with similar projects indicated that various heterogeneities assigned to four categories could best be studied through development of four static geologic models, one corresponding to each category. The requirements for optimum geological modeling of clastic reservoirs for EOR were proposed subsequent to the review of geological problems encountered in EOR pilot projects. Geological factors that affect fluid movement in reservoirs were defined, and attention was given to certain aspects of reservoir characterization--geochronology, geochemistry, and man-induced alterations. A final hydrodynamic model derived from the integration of four partial geological models provided the means for a more accurate prediction of fluid movement in a reservoir.

## Pilot Area Studies

The historical background, performance, and geological problems encountered in four EOR pilot projects (Big Muddy, WY; North Burbank, OK; Bell Creek, MT; and El Dorado, KS) reported in the literature were studied. Information from these studies contributed to the development of a generic model for improving the characterization of clastic reservoirs for EOR.

### Big Muddy Field

Production in Big Muddy field is primarily from the Second Wall Creek sandstone member of the Upper Cretaceous-Age Frontier formation.[3-4] There are three Wall Creek sandstones in the field. The upper and lower sandstones are unproductive and are separated from the middle Second Wall Creek sandstone by

20 ft and 30 ft (6.1 and 9.1 m), respectively.[3-5] Structural entrapment is within an east-plunging anticline[6] characterized by more than 300 ft (91.4 m) of closure above the oil/water contact.[5] The reservoir characteristics for the Second Wall Creek sand in Big Muddy field are summarized in table 1. Several interpretations of the depositional environment have been given (deltaic, barrier bar, and blanket sand).

Two EOR pilot projects have been implemented in Big Muddy field. Conoco began a 1-acre (0.40-ha), five-spot, low-tension surfactant-polymer flood in 1970.[3-9] In 1978, Conoco and the DOE initiated a 90-acre (36-ha) expansion pilot (nine 10-acre (4-ha), five-spots) to test surfactant flooding in a low-permeability, high-fracture-density, freshwater reservoir. The natural fracture system and geologic problems such as low-pressure parting within the reservoir were studied.[7] The daily tertiary oil-producing rates were some 220 bbl (3.5 $m^3$) lower than those predicted, possibly because of reduced injection and production rates mandated by low-pressure parting in the formation.[9]

## Big Muddy Field Geological Problems

Many geologic problems experienced during the first pilot project were circumvented before the second pilot project began. The reservoir fractured below the hydrostatic head.[9] One-half of the fluid production was from formation water influx as a result of a highly jointed system within a low-matrix-permeability reservoir. Core analyses indicated that the reservoir was of uniform thickness;[7,10-11] yet, existing interpretations of the depositional environment were contradictory. Geologic and engineering data provided evidence of an east-west fracture pattern. The general fracture orientation was determined; however, the density, distribution, and size of the fractures were not defined sufficiently to document their influence on fluid migration within the reservoir.[5,11] This definition becomes critical when fracture orientation is oblique to the natural reservoir gradient direction.[3,7] Tracer surveys and temperature logs indicated that injected fluids were migrating up-section, possibly along the annulus of old abandoned wells or within the prevailing fracture system.

Diagenesis in the form of clay alteration, patchy carbonate cements, and quartz overgrowths was observed in previously studied equivalent outcrops of

the Second Wall Creek sandstone in the Casper Arch area.[13] Diagenesis was not considered to be detrimental in the subsurface; however, little information was available to support that contention. Pressure-pulse data indicated that there were no permeability barriers across several previously defined fault traces. Further study indicated that many of the "faults" were mapped from poor-quality well logs and that what were interpreted as fault gaps were probably changes in log response resulting from changes in stratigraphy.[5] Consequently, many of the original faults were omitted from EOR structure maps. Several arguments did, however, support the concept for a highly tectonized reservoir, including the proximity to highly faulted reservoirs near the Laramie Uplift and the complexity of photo lineaments observed on Landsat imagery throughout the region.[5,14]

Knowledge of the formation anatomy, water chemistry, and effects of mineral precipitation during chemical flooding was needed to improve reservoir characterization for the prediction of EOR performance in Big Muddy. The key first required an accurate and detailed interpretation of the depositional environment because it would furnish the "map" from which diagenesis could be formulated.

## North Burbank Field

The oil reservoir at North Burbank (OK) field is a large sandstone body that was deposited in a fluvial environment on the north-central Oklahoma platform along the western shore of the Cherokee Sea during the Pennsylvanian Age. This massive sand, known as the Burbank, was created by the superimposed effect of a series of channels cut laterally into each other, which created the effect of a wide, massive body with a few internal discontinuities. The individual fluvial channels are about 1,000 ft (304.8 m) wide. Examinations of core samples have suggested that marine incursions have disrupted the continuity of the Burbank fluvial channel system periodically.[14] The Burbank structure is an undulating monocline dipping at a rate of 35 ft/mile (6.63 m/km) in a westerly direction. Several domes and synclines are present in the field.

Reservoir and fluid properties that are important in understanding the geological heterogeneities in North Burbank field are summarized in table 2. Petrographic analyses of thin-sections from well 27-W26 indicated that the

sandstone typically contained 40 to 50% quartz, with substantial amounts of cementing materials consisting of silica, dolomite, ankerite, or clays. Lesser amounts of feldspars, mica, chert, and metamorphic rock fragments were also observed. None of the clays in the North Burbank reservoir was found to be water-sensitive.

The North Burbank reservoir is an attractive target for tertiary oil recovery because more than $360 \times 10^6$ STB ($57.2 \times 10^6$ stock-tank $m^3$) of sweet 39° API (0.829 g/$cm^3$) oil will remain unrecovered when waterflooding reaches its economic limit.[15] Because of the severe vertical heterogeneities and consequent poor sweep efficiency, oil recovery by waterflooding in certain parts of North Burbank field, like the Tract 49 area, has been about half that of other parts of the unit. In Tract 97 (site of a surfactant-polymer pilot), oil recovery by waterflooding was excellent, mainly because the staggered line-drive configuration swept the reservoir fairly uniformly.

Cumulative tertiary oil production in North Burbank has been less than that predicted. In the surfactant pilot project, for example, projected ultimate oil recovery has been estimated at 300,000 bbl ($47.7 \times 10^3$ $m^3$), about half of that predicted.[16] Although oil recovery was less than that predicted, the pilot project was considered technically successful because a significant amount of tertiary oil was recovered.

## North Burbank Geological Problems

The Burbank sand is a fluvial deposit that characteristically exhibits rapid vertical and horizontal lithologic changes with corresponding changes in reservoir flow properties (see table 2). The severe permeability stratification of the reservoir rocks at North Burbank, primarily related to depositional environment, created numerous problems in the two chemical EOR pilots.

When a highly stratified reservoir like North Burbank is subjected to surfactant-polymer flooding, the high-permeability zones will be exposed to more surfactant and should have lower ultimate residual oil saturation (ROS). In a reservoir like North Burbank, however, the situation is complicated because crossflow could lead to partial resaturation of high-permeability zones by oil displaced by more slowly moving fluids in adjacent lower permeability zones. There is also the possibility of formation brine

crossflow from a low-permeability layer into a preflushed zone containing surfactant and/or polymer, causing degradation of their chemical activity. Studies of models have indicated that such crossflow could occur and may have some effect on performance of the surfactant-polymer method.[17]

Besides heterogeneities imparted to the rocks because of the fluvial nature of the deposits, a strong east-west trending, vertical jointing, or fracturing system causes preferential movement of fluid in the east-west direction. Because of this system of fractures, the effective permeability in the east-west direction is five times as great as that in the north-south direction.[17] Results of pressure falloff tests on several wells in Tract 97 and neighboring areas indicate vertical fractures in these wells ranging in length horizontally from 165 to 623 ft (50.29 to 189.9 m) and flow capacities ranging from 665 to 2,600 md-ft (203 to 792 md-m).

Pressure-interference test data from the area also suggest a roughly east/west preference in the directional permeability of the North Burbank reservoir. Radioactive tracer study performed during preflush injection showed that several wells were receiving little or no fluid from certain quadrants of their drainage areas. The flow of surfactants and polymer would also be restricted in these quadrants, and oil recovery from these areas would be low. The radioactive and subsequent chemical tracer studies also pinpointed the location of flow channels in a number of wells in the area studied. The channeling probably resulted from the directional fracture system in the pilot area.[14] This fracture system is dynamic in that the fractures open and extend to great lengths with increasing injection rates but close when fluid injection is shut off. The low formation parting pressure also prevented high injection rates.[18]

The oil-wet nature of reservoir rocks resulting from a coating of the iron-rich, clay mineral chamosite on 70% of the pore surfaces causes adsorption of sulfonate surfactant and leads to inefficient displacement of oil. The relative displacement index measured on a Burbank sandstone core from Tract 97 has an average value of -0.45,[14] indicating the highly oil-wet nature of the sand.

Formation water analysis data from two samples[19-20] indicate that the formation water from the producing sandstone at North Burbank has very high salinity and high hardness (high $Ca^{++}$ and $Mg^{++}$ content). The salinity and the

chemical composition of brine were different in the two samples. The sulfate content reported in one analysis was low (58 ppm.) The high hardness of formation water caused precipitation of calcite and sulfonate salts, thereby reducing the permeability of the medium.

The reservoir description of North Burbank was incomplete when the surfactant-polymer pilot was begun and presented a more favorable picture than was actually found.[18] Permeability stratification adversely affected the performance of the chemical flood.

Correlation and mapping of the various permeability zones from available information on depositional history and core, log, and high-resolution seismic data and integration of this information with reservoir engineering data (tracer test, pressure transient test) would be critical in assessing the magnitude of crossflow problems likely to be encountered in different parts of the reservoir.

A primary cause for the less-than-expected oil recovery at North Burbank was high consumption of injected sulfonate.[16,21] Loss of sulfonate was due to unfavorable phase behavior and mixing of micellar fluids with in-place water that has a high salinity and hardness.

In oil-wet rocks, the displacement of one non-wetting phase by a second non-wetting phase is inefficient; therefore, the preflush at North Burbank might have displaced only part of the formation water creating an unsuitable salinity and hardness environment for the micellar fluid.[16] It has been reported that compaction, authigenesis, replacement, and dissolution have altered the texture and composition of the Burbank sandstone significantly.[22]

Further research on the diagenetic effect and the wettability characteristics is needed. Careful analysis of the formation fluid would help in designing an alternate preflush to remove excess salinity and hardness from the reservoir. Further research in developing a suitable surfactant system may also prove beneficial, considering the prevailing salinity and hardness environment in the reservoir.

Natural and man-induced fractures also presented problems. Natural fractures are well developed in outcrops of Pennsylvanian limestone and sandstone and are visible on the ground and on aerial photographs.[1] The average fracture azimuth is 70° (N70°E) and is relatively constant, with only

a few less than 65° or more than 75°. Information on fracture distribution, length, and infilling (detrital or geochemical) could be obtained from correlative studies of cores, outcrops, and aerial photographs.

Another problem was the low parting pressure of the reservoir rocks, which opened the fractures whenever injection pressure exceeded the critical pressure in the reservoir. When this occurs, large volumes of fluid may circulate readily without moving much oil. Although several fracture treatments increased fluid production, it was speculated that they also induced interwell channeling. The channels were created from extension of fractures at producing wells when the micellar fluids were injected. This channeling could have prevented the polymers from following the micellar fluids at the proper sequence in all parts of the reservoir.[16]

Further research on estimating and controlling fracturing pressures and improving workover procedures is needed to improve sweep efficiency in this project area.

## Bell Creek Field

Production in Bell Creek (MT) field is from the "Zone 2" barrier bar sand of the Lower Cretaceous-Age Muddy formation. Bell Creek field is a combination of six separate waterflood units, each representing a separate barrier bar sandstone reservoir.[23-25] These stratigraphic traps are defined by updip pinchouts to the east (into lagoonal facies) and by multiple oil-water contacts along the western downdip direction.[23-24,26] Each waterflood unit has at least two sandstone intervals separated by a shale barrier.[25] The lower sand, commonly called the Zone 2 sand, is the most favorable reservoir host rock in Bell Creek field.[24,27] The flow capacity of the overlying Zone 1 sand is one-eighth that of the Zone 2 sand, and various studies have indicated very little or no communication between the two sands.[23,27] The Zone 2 reservoir is a very fine to fine-grained quartzose sandstone that is clean, moderately well sorted, and semiconsolidated. Clay and silt fractions range from 2 to 8% by weight.[27,30]

Because of the excellent reservoir qualities conducive to micellar flooding, two tertiary mode EOR pilot projects were implemented to test the Zone II reservoir, in the northernmost waterflood segment area, known as Unit 'A'.[25] Although a small gas cap was present at the time of discovery, the

Zone II reservoir in the Unit 'A' area was depleted at a faster rate than the other waterflood segment areas.[24]

Reservoir characteristics for the Zone II sand in the Unit 'A' area are summarized in table 3.

The first tertiary project in Bell Creek field was started in 1976 with the development of a 160-acre ($6.48 \times 10^5 m^2$) micellar-polymer pilot demonstration project.[26,28] Technically, the pilot was marginally successful, recovering 27,000 bbl ($4.29 \times 10^3 m^3$) of oil, or 14% of the OIP after waterflooding. Through provisions of the DOE Tertiary Oil Incentive Program, a second, 179-acre ($7.2 \times 10^5 m^2$) micellar-polymer pilot was initiated in 1981.[26] Unlike the first pilot, the second pilot was successfully located in the optimum portion of the reservoir.

The reservoir quality in the second pilot area was better than originally expected. The postwaterflood OIP was $2.773 \times 10^6$ bbl ($4.441 \times 10^5 m^2$), and the tertiary recovery was 39.6% of the OIP.[26]

## Bell Creek Geological Problems

Unexpected geological heterogeneities that adversely affected the performance of the first pilot were related primarily to the depositional environment of the Zone 2 sand.[27] Authigenic clay infilling had altered the primary porosity and permeability in the reservoir.[23] Fine-grained sands, interbedded siltstones, and shales formed a permeability barrier in the southwestern part of the pilot area that adversely affected the sweep efficiency by diverting the flow of the injected fluid out of the pilot area.[27,29] Reservoir continuity was assumed on the basis of a partial geological assessment, and drilling was continued before suspected heterogeneity problems were confirmed by a complete analysis of pressure pulse test data.[29] Brine resistivity values measured from swab-water samples and log calculations indicated two chemical types of formation water. This analysis suggested that the waterflood was not successful in displacing oil and brine in the pilot area adequately.[24]

A three-layer black oil model failed to incorporate the complex heterogeneity within the pilot area adequately. The acceptance of inadequate waterflood history-matching results and the over-optimistic determination of the ROS resulted in failure to scale up from laboratory to field application

and prediction.[28-29] Successful prediction and characterization of heterogeneity are directly correlated to the selection process of reservoir zonation. Reservoir zonation can be improved following a complete waterflood tracer study. A full understanding of the tracer survey results was not possible because of the interaction of the preflush, micellar, and polymer chemistry in the reservoir.[24] Inconsistent results were derived from the tracer survey and pressure pulse test.[29]

In a heterogeneous reservoir such as the Bell Creek barrier bar, the selection of an optimum pilot site that represents the performance behavior of the entire reservoir remains a challenge.

Reservoir heterogeneity in Bell Creek field must be sufficiently quantified before successful waterflood history-matching or EOR performance prediction can be expected. This will require not only a close cooperative effort by geologists, petrophysicists, and engineers but also a reservoir simulator designed to include the complexity of observed heterogeneities as well as the prediction of potential geochemical reactions and their products. Unfortunately, the literature does not provide comprehensive information on fracture studies, diagenesis, or phase behavior relationships--the fundamental elements for heterogeneity analysis in Bell Creek. Results of tracer surveys and pressure pulse data should be considered before new wells are drilled and expensive chemical fluids are injected.

## El Dorado Field

El Dorado (KS) field produces oil and gas from several carbonate and clastic reservoirs ranging from the Ordovician Stapleton limestone at a depth of 2,700 ft (823 m) to the Lower Permian Admire sand at a depth of 600 ft (183 m).[30-32] Structural entrapment is within an elongated asymmetrical anticline 40 miles (103.60 $km^2$) in area, directly overlying the basement granite Nemaha uplift.[31-33] Reservoir rock and shales thin radially toward the apex of the anticline.[34-35] El Dorado field was developed rapidly to furnish oil for the Allies in World War I. Oil production peaked in 1918,[31] and water injection was terminated in February 1971, when essentially all wells in the Admire sand were plugged before tertiary production was initiated.[36]

The reservoir characteristics of the Admire sand are summarized in table 4. A cost-shared, tertiary, micellar-polymer demonstration project by the DOE and Cities Service Co. was initiated in 1974.[37-43] The project included two pilot areas, and the objective was to compare two separately designed tertiary oil recovery EOR methods.[36-38] The pilot areas included 51.2 acres (20-ha) with a total of 61 wells based on 6.4-acre (2.6-ha) spacing and a five-spot pattern.[37] The project was terminated in 1982 as a marginal technical success and an economic failure.[44] The low cumulative tertiary oil recovery of only 26,734 bbl ($4.2 \times 10^3 m^3$) was a result of chemical and geological problems.[45]

The Admire sand is a sublitharenite (<75% quartz, <25% rock fragments, and <10% feldspar) deposited in a complex heterogeneous distributary channel system within a prograding delta system and proximal beach sands.[37] Nine reservoir and nonreservoir facies have been recognized within the Admire sand.[37] Distributary channel sands constitute most of the reservoir facies; however, the highest measured permeabilities are within the less extensive crevasse-splay sand facies.[37] Reservoir quality is a function of the total sand thickness and its distribution.[37] Primary porosity predominates, and secondary porosity occurs as the result of clay removal, alteration of calcite cements, leaching of plagioclase, deformation of ductile grains, and quartz overgrowths.[37]

## El Dorado Field Geological Problems

Efforts to simulate this reservoir were hampered by several factors. A primary geologic problem was the failure to spot-locate the two pilot areas within a similar facies for comparing the two EOR processes. The south pilot, the test area for Union Oil Co's. "soluble oil process," was in interdistributary bay shales, crevasse splay, and beach sands.[37] The north pilot, the test area for Shell Oil Co's. "high-water-content process," was within crevasse splay and distributary channel sand facies.[37]

Perhaps the greatest single problem resulted from a major fracture artifically induced in a south pilot area injector well which introduced complications that prevented an adequate waterflood history match, and the reservoir could not be suitably simulated.[37] A reservoir pressure gradient in a northeasterly direction in the pilot area caused fluid movement at a linear rate of 29.6 ft/d (9.0 m/d).[37,40] This prompted the invasion of the preflush

fluids by resident brine, resulting in the adsorption and neutralization of the surfactants which followed the preflush despite an initial observation of a mobilized oil bank which represented 43% of the residual OIP after waterflood.[37]

The gypsum in the reservoir was responsible for depleting the alkaline silicate preflush before it moved through the reservoir.[37] The rapid increase in produced water salinity at the onset of tertiary oil production suggests that the mobile oil moved through parts of the reservoir not swept by the preflush.[37]

The rapid changes from reservoir (distributary channel and crevasse splay) to nonreservoir (interdistributary channel) facies that occur between the 6.4-acre (2.6-ha) spacing in the pilot areas clearly indicate that the Admire sand is a very heterogeneous reservoir.[36] The 40-acre (16.2-ha) well spacing in El Dorado field does not allow the accurate reconstruction of facies and nonfacies boundaries unless improvements in reservoir characterization or additional infill drilling are made. The success of an EOR project in El Dorado field will ultimately require significant improvements in facies analysis through an understanding of depositional-environment and diagenesis models.

## Summary of Geological Problems

The geological problems encountered in the four EOR pilots may be grouped into four categories: depositional, diagenetic, structural, and interstitial fluid. Heterogeneities related to each category had a different effect on EOR performance in the four reservoirs.

The results of our studies of these EOR pilots are summarized in table 5. The data base for this report was developed from the literature; thus, all evaluations and conclusions on the case studies in table 5 are based on our evaluation. The effect of each category of reservoir heterogeneity has been evaluated and ranked (high, moderate, or low) in terms of its influence in EOR. The potential contribution from additional research in each category of reservoir heterogeneity was also evaluated and ranked (maximum, moderate, or minimum) for each reservoir studied.

This study indicates that the depositional environment defines the original framework of reservoirs and is responsible for a category of heterogeneity that has affected all four reservoirs. The potential contribution from further research is estimated to be maximum for Big Muddy, North Burbank, and El Dorado and moderate for Bell Creek. A more detailed understanding of log-to-core relationships and interpretations is needed. Combining the depositional model with engineering tests, analyses, and photogeologic interpretations from Landsat, Spot-1, SLAR, and other remote sensing data would improve EOR simulation and tertiary prediction/performance results with less risk. The postdepositional alterations (i.e. diagenesis and tectonics) are not adequately defined in all four cases. The diagenetic effect in three of the four EOR case studies was moderate except at North Burbank where it significantly affected fluid displacement in the chemical EOR pilot.

The structural component of the geological heterogeneities significantly influenced the fluid flow behavior in Big Muddy and North Burbank reservoirs and was moderately influential in Bell Creek and El Dorado reservoir pilot areas. Considering that El Dorado field directly overlies the basement Nemaha Uplift, this anticlinal structure would be expected to be fractured. No definite conclusions could be made for Big Muddy because of the paucity of data, but the effects of formation fluids on EOR performance were moderate in Bell Creek and El Dorado fields and severe in North Burbank field. These facts illustrate the need for research and development of methods to improve quantification of reservoir characteristics in the interwell region. Studies of the four categories of heterogeneity can proceed from the construction of one partial model for each category. This is discussed more fully in the next section.

## Proposed Requirements for Optimum Characterization of Clastic Reservoirs

### General Requirements for Characterization and Modeling

General requirements for characterizing clastic reservoirs for EOR are described in this section, with emphasis on certain aspects of reservoir characterization that are often neglected and underestimated. The proposed requirements address heterogeneity problems encountered not only in the four

pilot studies but also in other similar projects where EOR has been implemented.

The elements of the final fluid dynamic model constructed by integrating four static models corresponding to each category of heterogeneity are shown in figure 2.

Major reservoir heterogeneities that result from depositional patterns and postdepositional processes (tectonic and geochemical alterations) may or may not be related to the depositional environment. Reservoir paleohistory and time of major postdepositional events must be known before their diagenetic and structural influence on reservoirs can be estimated.

Postdepositional processes include products vital to EOR such as fractures or impregnation of the rock matrix by cements and authigenic clays. Fundamental processes affecting rock properties from the time of deposition until the implementation of EOR are illustrated in figure 3.

Finally, man-induced alterations from primary and secondary recovery operations can be significant in certain EOR applications and in certain types of reservoirs.

Generally, reservoir characterization for EOR should include the following steps:

1. collect reservoir information at wellbores from geologic, geophysical, and engineering sources;

2. identify the depositional environment and the implied position of the pilot area;

3. reconstruct the paleohistory of the formation;

4. integrate information from available sources and screen and rank dominant factors affecting fluid flow;

5. predict directional reservoir properties (heterogeneities and anisotropy) between injection and production wells, basis of the reservoir information, reconstruction of formation history, information from analogous reservoirs, outcrops, aquifers, and other sources such as remote sensing or mines;

6. predict current distribution of formation fluids and their composition and properties;

7. determine composition and properties;

8. predict flow paths, mobility, and sweep efficiency of injected fluids and mobilized formation fluids; and

9. predict man-induced geochemical and physical alterations that may affect reservoir performance.

A generic classification of geological factors that contribute to the final variation of effective porosity and permeability and to the fluid distribution, mobility, and pathways under imposed reservoir conditions is given in tables 6 and 7.

## Requirements Related to the Component Geological Models

### Depositional Model

In all reservoirs, the geometry and internal features were inherited from the depositional environment. Furthermore, a number of postdepositional alterations are also related to the pattern of sediment deposition (table 6). The components of a depositional model required for the comprehensive characterization of a reservoir under study are shown in table 8.

These factors may contribute directly or indirectly to variations of critical reservoir properties that influence fluid recovery in an EOR operation. Progress has been made recently in understanding the nature of sedimentological processes in a variety of depositional environments. Considerable attention is now being given to the quantification of data and to the prediction of the geometry and continuity of lithofacies.[47-53]

### Diagenetic Model

The diagenetic imprint is commonly underestimated in many EOR projects. The diagenetic effect in three of the four EOR case studies was moderate, except at North Burbank, where it was high (see table 5). Recent progress in applied geochemistry and petrology indicates that as much as 40 to 70% of the original porosity in clastic reservoirs worldwide can be destroyed by diagenetic alterations.[54-55] Cases have been reported where most pore networks are composed predominantly of secondary porosity (up to 100%).[56-57] This fact implies that any attempt to predict variations and trends in

formation matrix permeability (which is usually related to porosity) should be based on both depositional and diagenetic models.

Diagenesis has been defined as "the sum of the processes by which the original sedimentary clastic assemblages attempt to reach equilibrium with their environments."[58] In the sedimentary environment, therefore, detrital minerals are often either unstable or metastable with respect to their interstitial water.[58] Instability results in leaching or molding of original grains, mineral recrystallization or overgrowths, leaching or precipitation of cement, transformation of detrital clay minerals, and precipitation of authigenic clays and their further transformations. Changes in porosity and permeability are clearly related to diagenetic control of grains, pores, and infillings.

Diagenetic modeling incorporates both the above geochemical alterations induced into the formation during its postdepositional history and compaction resulting from physical reduction of thickness and porosity of the original sediment. The proposed elements of the diagenetic model are shown in table 8.

## Effects of Paleohistory

The time-dependent depth history of a British Carboniferous formation in two locations situated only 18.6 miles (30 km) apart reveals drastically different evolutionary stages as described by Dickson[57] (fig. 4).

An example of severe diagenetic alterations connected with paleohistoric evolution comes from the Piceance Basin in Colorado at the site of the Multi-Well Experiment (MWX) being performed by the DOE (fig. 5). There the Upper Cretaceous Mesaverde formation was buried to a depth of about 13,000 ft (4,000 m), and probably was subjected to a zone of low-grade regional thermometamorphism before being uplifted to its current depth of 7,000 ft. (2,134 m).[60]

Interpretation of diagenetic sequence in matrix and fractures for all cores in the MWX included the effects of compaction and geochemical alterations. In certain intervals, the porosity is nearly all secondary and was formed by dissolution of feldspars, lithics, and calcite cement. However, nearly all of the intergranular pore space is filled by authigenic clays. Despite the dissolution of detrital grains and cement, open space within the

matrix and fractures is rare, with permeabilities in the microdarcy range.[61-62]

Information obtained from the study of analogous deposystems, outcrops, and aquifers is useful if carefully selected. However, reservoirs of similar age and origin that were subjected to different diagenetic environments during their evolutionary history may possess quite different properties. Comparison of properties of analogous deposystems belonging to different age groups and/or different geologic settings may be even more misleading.

## Effects of Clays

The mineralogy of detrital or authigenic clays resulting in plugging of pores, pore throats, and joints is usually poorly defined in many EOR projects. The transformation of clay through geologic time is related to changes in temperature, pressure, interstitial water ionic composition, ion activity, and relations. Major rock alterations that are depth related are shown in table 9.[58]

The structural varieties (polymorphs) of final clays in shaly layers and clay/sand mixtures may react quite differently under induced conditions. For example, swelling properties are characteristic for halloysite, which is structurally the same as nonswelling kaolinite but contains a layer of water in its crystalline structure. Glauconite (a variety of nonswelling illite) may contain up to 55% of swelling layers[63] and may be quite common in certain marine clastics. Some sandstone layers may contain up to 40% of glauconite aggregates (pellets)[64] dispersed within the rock matrix and particularly concentrated in trough-bedding-laminae (fig. 6). These 0.04- to 0.08-in. (1 to 2 mm) diameter glauconitic pellets consist of myriads of tiny (2-μm) plates. If these pellets break up during EOR, pores will certainly be plugged. The behavior of glauconite under induced thermal or chemical conditions is not known.

Vermiculite, another type of clay, has a very high ion exchange capacity and when heated to about 572° F (300° C) dehydrates quickly, flakes, and expands to 18 to 25 times its original volume.[63,65] The process terminates at about 932° F (500° C). Owing to its unusual property, vermiculite may cause plugging during an in situ combustion process because the temperatures of the burning front and the combustion zone range from 600° to 1,200° F (316° to

648° C). Expansiveness resulting from dehydration is also characteristic for dickite and muscovite.[63]

Thermal effects of dehydration and pyrolysis on different clay minerals have been studied extensively by the ceramics and building industries, but little attention has been given to these alterations in reservoirs subjected to thermal EOR.

Clearly, there are many reasons to study the origin and history of clays and their proportions and structural polymorphic varieties both in clay/sand mixtures and in shale layers, drapes, or clasts. Simple identification of major groups of clay minerals may be inadequate for reservoir characterization.

## Man-Induced Geochemical Alterations

Man-induced geochemical alterations affect current and future projects in the same reservoir. The magnitude and rate of these alterations, particularly those resulting from dissolution/precipitation processes, are important because they are responsible for significant changes in reservoir properties throughout the course of field development. The prediction of these changes should be included in the diagenetic (geochemical) model and be an integral part of reservoir characterization (table 8).

Depressurizing and degassing of producing reservoirs disturb long-term established equilibrium or semiequilibrium between fluids and rocks. Reservoir porosity and permeability determined during early field development may not always be accurate for EOR planning.

Waterflooding introduces new elements to the environment, and the chemical composition of injected water may be controlled to avoid problems of precipitation and scaling. However, such controls may trigger slight changes in redox potential that may cause oxidation of formerly reduced species, such as iron or manganese, and produce particles in suspension. These suspended solids, mobile silt, and clay particles can block pore throats and prevent fluid flow.

Extensive alterations may be induced during tertiary stimulation when reservoirs are subjected to changes in the temperature and/or chemical regime. The rate of precipitation/dissolution of any substance is dependent

on concentrations of reacting ions, total salinity, temperature, partial pressure of gases, lithology, and fluid flow velocity.[66-67] The dissolution rate is fastest for strongly undersaturated solutions.[67]

The injection of $CO_2$ into such a system changes the trend and the magnitude of dissolution, particularly with respect to calcium, magnesium, and iron carbonates precipitated as cements. Excess $CO_2$ forms a highly aggressive system in reservoirs in which carbonates and significant amounts of ubiquitous iron can be mobilized. Conversely, the liberation of $CO_2$ from a calcite-saturated solution may induce carbonate precipitation.

The solubility of silica is low at 77° F (25° C) but increases rapidly at higher temperatures,[45] and siliceous minerals may corrode during steamdrive and in situ combustion. As the silica solution spreads from injection wells, decreases in temperature may cause precipitation at a certain distance and plug fluid pathways (fig. 7).

The kinetics of chemical processes under natural and induced conditions in reservoirs has recently been studied intensively.[44,66-71] One experimental study[71] revealed dramatic effects of silica dissolution/precipitation during steam injection at different flow rates, temperatures, and pH levels. Another experiment with Heart of Texas sand documented extensive dissolution of quartz grains even after 24 hours of steam treatment.[74]

Diagenetic modeling involves a variety of natural and man-made alterations that influence hydraulic properties of a reservoir under consideration for EOR. However, few of these problems were satisfactorily studied before reservoir simulation was performed.

## Structural Model

Triplex porosity (primary, secondary, and fractures) and triplex directional permeability (resulting from the combined effect of matrix, fracture, and bedding plane permeabilities) are commonly observed in reservoirs.[72] If the distribution of directional fracture permeabilities is such as that presented by Bergosh[72] (table 10) for the Monterey formation, the contribution to the overall permeability from other sources would probably be negligible. In such a situation, more attention should be given to structural modeling rather than other partial models (e.g. depositional or diagenetic models).

Although the physical and mathematical approach to modeling and simulation of naturally fractured reservoirs has been recently presented,[73-75] several geological aspects which may be important were not included. A list of geological elements required for development of a structural model is presented in table 8.

The type of fluid flow in open-fracture systems deserves special attention. For example, nonlaminar (transient or turbulent) flow was documented in heavily fractured Liassic sandstone aquifers,[76] even though reservoir simulators normally assume laminar flow. Valuable information about hydraulic behavior of the reservoir formation can be obtained from previously exploited analogous aquifers where effective permeabilities, flow units, type of flow in the combined matrix/fracture system, interference of simultaneously exploited wells, and other factors can be evaluated from results obtained during different stages of pumping tests (stepped drawdown pumping rates) in individual water wells and in interfering groups of wells.

Structural models should include the potential for cross-flow through siltstone or claystone layers (which are commonly considered to act as flow barriers) when these "barriers" are cut by fluid-conducting fractures. Previous waterflooding in the Upper Shannon formation of Naval Petroleum Reserve No. 3 (WY) probably failed because of communication between upper and lower sand benches.[77] Additional pathways for undesirable cross-formational migration of injected fluids can be created by undetected or improperly plugged/abandoned wells.

The flow pattern between matrix pores and fractures in fractured reservoirs must be determined. The matrix/fracture flow model is complex, and the process is poorly understood.[78]

Some fracture systems are sealed with detrital material, whereas others may be severely affected (infilled) by diagenetic processes. Gurzij et al.[79] show quartz, chalcedony-, calcite-, and dickite-filled joints containing bitumens in argillitic rocks at a depth of more than 23,000 ft (7,000 m). The fracture systems may diminish the fluid flow rate through the reservoir significantly or act as complete barriers to fluid flow if they are filled due to hydrodynamic or geochemical processes.[76]

Because the effect of fractures is strongly dependent upon the degree of their opening, the presence of these fractures may not be readily apparent, but subtle changes in physical and/or chemical regimes during EOR operations may easily create new barriers or high-permeability "thief" zones.

Prediction of the type and magnitude of infilling in fractures in an interwell region is as important in estimating reservoir hydraulic properties as prediction of geometry, density, and morphology of fracture systems.

## Formation Fluid Model

Before any engineering operation is implemented in the subsurface, interstitial fluid characteristics should be known (table 8). Besides residual oil, which is clearly a target of engineering operations, inadequate information on oil-associated brines may certainly cause problems.

Quantitative prediction of mass transfer between fluid and solid phases resulting in porosity and mineral alteration by a variety of driving potential (natural and forced hydrodynamic and/or convective drive) was recently proposed.[80] The pattern of alterations produced by this mechanism was described as continuous waves of field-reversible chemical reactions.

Before the startup of any EOR pilot project, formation water samples can be easily obtained either by direct sampling or by centrifugation of fresh cores. Sometimes, formation-water analyses are complete and reliable enough to permit calculations of fluid compatibility and/or chemical equilibria between rock and fluids.

## Integrated Dynamic Hydraulic Model

Screened, ranked, and integrated data obtained from depositional, diagenetic, structural, and formation fluid modeling enable final prediction of reservoir hydrodynamic response under imposed conditions. The following reservoir data required for realistic computer simulation can be obtained from such an integrated model.

1. Directional permeability distribution (matrix and fractures) between injection and production wells. (Permeability to liquids is preferred because the relationship between permeability to gases and liquids is poorly understood.)

2. Flow unit identification, direction, and rate of flow under an imposed hydraulic gradient.

Prediction of interformational crossflow.

Prediction of gravitational segregation.

Prediction of fingering within flow units.

Prediction of penetration efficiency.

Prediction of hydraulic interaction between matrix and fractures.

Prediction of rock-injected fluid interaction.

## CONCLUSIONS AND RECOMMENDATIONS

1. Many geological problems recur in clastic reservoirs.

2. Geological heterogeneities can be assigned to four categories: depositional, diagenetic, structural, and formation fluid. These heterogeneities have a different effect on the performance of projects.

3. Severe fluid flow problems in some reservoirs are the result of heterogeneities directly associated with the depositional environment. Reservoir characterization can be improved by emphasizing research on heterogeneities induced by depositional factors.

4. Data available on the effect of diagenesis on reservoir quality are limited. More emphasis on diagenetic research is essential because postdepositional geochemical alterations significantly affect reservoir quality (e.g. North Burbank).

5. The effect of structural components of heterogeneities significantly inhibited reservoir performances in Big Muddy and in North Burbank. In addition to further research to improve methodology, more emphasis is recommended for the application of existing technology (i.e. remote sensing, high resolution seismic).

6. Studies of formation fluid geochemistry should be an integral part of geological modeling because of the important role in diagenetic processes and in man-induced alterations.

7. Reservoir heterogeneities can be studied best through the development of four geological models (listed in 2 above) that consider the effects of

geochronology, geochemistry, and man-induced alterations acquired during field development.

8. Knowledge of the origin of heterogeneities, best defined by reconstruction of formation paleohistory, would improve prediction of their magnitude and distribution in interwell areas.

9. The distribution of heterogeneities, their characteristics, and interrelationships in pilot studies should be supplemented by geological data from analogous reservoirs, outcrops, and aquifers that have similar genetic and evolutionary histories.

10. The distribution, proportion, and properties of different types and polymorphs of authigenic clays need to be quantified.

11. In addition to the geometry and the morphology of fractures, structural modeling should incorporate information on the degree of their openness and the type of detrital or geochemical infilling.

12. A dynamic hydraulic model derived from the integration of four partial geological models will provide a more accurate prediction of fluid movement in a reservoir. The dynamic hydraulic model will be unique because of the triplex nature of the effective permeability distribution in each reservoir.

## REFERENCES

1. Dickey, P. A. Petroleum Development Geology, PennWell Publishing Co., Tulsa, 1979.

2. Brown, D. Geologists Eye Developing Future. In AAPG Explorer, January 1986, pp. 20-21.

3. Drilling-DCW. Big Muddy-Can a Chemical Flood Breathe New Life into a Tired Old Giant? June 1978, pp. 36-37.

4. Ogren, D. J., J. G. Davis, H. H. Ferrell, and A. A. Mostafa. Big Muddy Field Low Tension Flood Demonstration Project, Second Annual Report, April 1979 - March 1980. Dept. of Energy Report No. DOE/SF/01424-26, August 1980.

5. Troiani, L. R., J. G. Davis, H. H. Ferrel, and A. A. Mostafa. Big Muddy Field Low Tension Flood Demonstration Project, First Annual Report, April 1978 - March 1979. Dept. of Energy Report No. DOE/SF/01424-13, August 1979.

6. Haller, R. W. Big Muddy Water Flood. J. Pet. Tech., November 1955, pp. 9-12.

7. Gilliland, H. E. and F. R. Conley. Pilot Flood Mobilizes Residual Oil. Oil and Gas J. Jan. 19, 1976, pp. 43-48.

8. Davis, J. G., H. H. Ferrell, and W. C. Stewart. Big Muddy Field Low Tension Flood Demonstration Project, Third Annual Report, April 1980 - March 1981. Dept. of Energy Report No. DOE/SF/01424-39, November 1981.

9. Ferrell, H. H., M. D. Gregory, and M. T. Borah. Progress Report: Big Muddy Field Low-Tension Flood Demonstration Project with Emphasis on Injectivity and Mobility. Pres. at the 1984 SPE/DOE Enhanced Oil Recovery Symposium, Apr. 15-18. SPE/DOE paper 12682.

10. Gilliland, H. E. and F. R. Conley. A Pilot Test of Surfactant Flooding in the Big Muddy Field. SPE paper 5891, 1976.

11. Marrs, R. W. and G. R. Raines. Tectonic Framework of Powder Rive Basin, Wyoming and Montana, Interpreted from Lands at Imagery. AAPG Bull. v. 68, No. 11, 1984, pp. 1718-1731.

12. Towse, D. Frontier Formation, Southwest Powder River River Basin, Wyoming. AAPG Bull. v. 36, No. 10, 1952, pp. 1962-2010.

13. Painter, T. R., M. T. Borah, and H. H. Ferrell. Big Muddy Field Low Tension Flood Demonstration Project, Fifth Annual Report, April 1982 - March 1983. Dept. of Energy Report No. DOE/SF/01424-47, August 1983.

14. Tranthan, J. C., C. B. Threlkeld, and H. L. Patterson. Reservoir Description for a Surfactant/Polymer Pilot in a Fractured, Oil-Wet Reservoir-North Burbank Unit Tract 97. J. Pet. Tech., September 1980, pp. 1647-1655.

15. Trantham, J. C. Prospects of Commercialization, Surfactant/Polymer Flooding, North Burbank Unit, Osage County, OK. J. Pet. Tech., May 1983, pp. 872-880.

16. Keplinger and Assocs. Inc. An Evaluation of the North Burbank Unit Tertiary Recovery Pilot Test. Dept. of Energy Report No. DOE/BC/10033-2, August 1982.

17. Phillips Petroleum Co. North Burbank Unit Tertiary Recovery Pilot Test, Final Report. Dept. of Energy Report No. DOE/ET/13067-60, June 1980.

18. Trantham, J. C. and P. D. Moffitt. North Burbank Unit 1,440-acre Polymer Flood Project Design. Pres. at the 1982 SPE/DOE Enhanced Oil Recovery Symposium, Tulsa. SPE/DOE paper 10717.

19. Boneau, D. F. and R. L. Clampitt. A Surfactant System for the Oil-Wet Sandstone of the North Burbank Unit. J. Pet. Tech., May 1977, pp. 501-06.

20. Riggs, C. H. Waterflooding in the Burbank Oil Field, Osage County, Oklahoma. BuMines RI 5000, May 1954.

21. Lorenz, P. B., J. C. Trantham, and D. R. Zornes. A Postflood Evaluation of the North Burbank Surfactant/Polymer Pilot. Pres. at the 1984 SPE/DOE Enhanced Oil recovery Symposium, Tulsa, Apr. 15-18. SPE/DOE paper 12695.

22. Hufford, W. R. and T. T. Tieh. Diagenesis of Burbank Sandstone, North Burbank Field, Osage County, Oklahoma. Pres. at the 1984 AAPG Ann. Conv. San Antonio, May 20-23.

23. Burt, R. A., F. A. Haddenhorst, and J. C. Hartford. Review of Bell Creek Waterflood Performance-Powder River County, Montana. Pres. at 50th Ann. Fall Meeting of the SPE, Dallas, Sept. 28 - Oct. 1, 1975. SPE paper 5670.

24. Vargo, J. J. Site Selection, Reservoir Definition and Estimation of Tertiary Target Oil for the Bell Creek Unit 'A' Micellar-Polymer Project. Pres. at the SPE Fifth Symposium on Improved Methods for Oil Recovery, Tulsa, Apr. 16-19, 1978. SPE paper 7072.

25. Hartshorne, J. M., and J. S. Nikonchik. Micellar-Polymer Flood Success in Bell Creek Field. Pres. at the 59th Ann. SPE Tech. Conf., Houston, Sept. 16-19, 1984. SPE paper 13122.

26. Berg, R. R., and D. K. Davies. Origin of Long Cretaceous Muddy Sandstone at Bell Creek Field, Montana. AAPG Bull. v. 52, No. 10, 1968, pp. 1888-1898.

27. Gary Energy Corp. Bell Creek Field Micellar-Polymer Pilot Demonstration-Final Report--Gary Energy Corp., June 1976-Mar 1982. Dept. of Energy Report No. DOE/SF/01802-61, 1983.

28. McGregor, A. A., and C. A. Biggs. Bell Creek Field, Montana: A Rich Stratigraphic Trap. AAPG Bull. v. 52, No. 10, 1968, pp. 1869-1887.

29. Keplinger and Assocs. Inc. An Evaluation of Bell Creek Field Micellar-Polymer Pilot. Dept. of Energy Report No. DOE/BC/10033-5, December 1982.

30. Fath, A. E. Geology of the El Dorado Oil and Gas Field, Butler County, Kansas. Kansas Geol. Survey Bull. 7, 1921.

31. Reeves, J. R. El Dorado Oil Fields, Butler County, Kansas. In Structure of Typical American Oil Fields. AAPG Bull. II, 1929, pp. 160-167.

32. Uhrlaub, R. Butler County, Kansas - Geological Notes. AAPG Bull. v. 5, 1921, pp. 421-424.

33. Moore, R. C. The Relation of the Buried Granite in Kansas to Oil Production. AAPG Bull. v. 4 No. 20, 1921, pp. 255-261.

34. Bascle, B. Geological Study of the Admire 650-Foot Sandstone, Micellar-Polymer Flood Project, El Dorado Field, Butler County, Kansas. M.S. Thesis, Univ. of South Carolina, 1976.

35. Aurin, F. L., G. C. Clark, and E. A. Trager. Subsurface Pre-Pennsylvanian Stratigraphy. AAPG Bull. v. 5, 1921, pp. 141-144.

36. Van Horn, L. E. Improved Oil Recovery by Micellar-Polymer Flooding-El Dorado, Kansas, Field. Dept. of Energy Report No. DE-AC03-78ET13070, 1978.

37. Cities Service Co. El Dorado Micellar-Polymer Demonstration Project. Eighth Annual Report (Sept. 1981-Nov. 1982). Dept. of Energy Report No. DOE/ET/13070-92, 1983.

38. Cities Service Co. El Dorado Micellar-Polymer Demonstration Project. First Annual Report (January 1973-June 1975). Dept. of Energy Report No. BERC/TRP-75/1, 1975.

39. Cities Service Co. El Dorado Micellar-Polymer Demonstation Project. Third Annual Report (June 1976-Aug. 1977). Dept. of Energy Report No. BERC/TPR-77/12, 1977.

40. Cities Service Co. El Dorado Micellar-Polymer Demonstation Project. Fourth Annual Report (Sept. 1977-Aug. 1978). Dept. of Energy Report No. BETC-1800-40, 1978.

41. Cities Service Co. El Dorado Micellar-Polymer Demonstation Project. Fifth Annual Report (Sept. 1978-Aug. 1979). Dept. of Energy Report No. DOE/ET/13070-53, 1979.

42. Cities Service Co. El Dorado Micellar-Polymer Demonstration Project. Sixth Annual Report (Sept. 1979-Aug. 1980). Dept. of Energy Report No. DOE/ET/13070-63, 1980.

43. Cities Service Co. El Dorado Micellar-Polymer Demonstration Project. Seventh Annual Report (Sept. 1980-Aug. 1981). Dept. of Energy Report No. DOE/ET/13070-79, 1981.

44. Buchmann, D. and W. Dreybrodt. The Kinetics of Calcite Dissolution and Precipitation in Geologically Relevant Situations of Karst Area 2. Closed Systems. Chem. Geol., v. 50, No. 4, 1985.

45. Krauskopf, K. Introduction to Geochemistry. McGraw-Hill Book Co. Inc., New York, 1967, pp. 166-70, 208-11.

46. Tillman, R. W., and D. W. Jordan. Sedimentary Facies Analysis, El Dorado Field, Kansas, Micellar-Chemical Pilot Project. AAPG Bull. No. 5, 1981, pp. 1001-1002.

47. Sneider, R. M., C. N. Tinker, and L. D. Meckel. Deltaic Environment Reservoir Types and Their Characteristics. J. Pet. Tech., November 1978, pp. 1538-1546.

48. Haldorsen, H. H., and L. W. Lake. A New Approach to Shale Management in Field Scale Simulation. SPE paper 10976, 1982.

49. Lorenz, J. C., D. M. Meinze, J. A. Clark and C. A. Searls. Determination of Widths of Meander-Belt Sandstone Reservoirs from Vertical Downhole Data. Mesaverde Group, Piceance Creek Basin, Colorado. AAPG Bull., v. 69, No. 5, May 1985, pp. 710-721.

50. AAPG. Sandstone Depositional Environments. P. A. Shoelle and D. Spearing, eds., 1982.

51. Sneider, R. M., F. H. Richardson, D. D., Paynter, R. E., Eddy, and I. A., Wyant. Predicting Reservoir Rock Geometry and Continuity in Pennsylvanian Reservoirs, Elk City Field, Oklahoma. J. Pet. Tech., July 1977.

52. Johnson, H. D. and D. E. Krol. Geological Modeling of a Heterogeneous Sandstone Reservoir Lower Jurassic Statford Formation, Brent Field. SPE paper 13050, September 1984.

53. Geehan, G. W., T. F. Lawton, S. Sakurai, H. Klob, T. R. Clifton, K. F. Inman, and K. E. Nitzberg. Geologic Prediction of Shale Continuity Prudhoe Bay Field. Reservoir Characterization. L. W. Lake and H. B. Carroll, Jr., eds. Academic Press, Inc., New York, 1986, pp. 63-82.

54. Shanmugam, G. Secondary Porosity in Sandstones: Basic Contributions of Chepikov and Savkevich. AAPG Bull. v. 68, No. 1, January 1984, pp. 106-107.

55. Schmidt, V. and D. A. McDonald. Secondary Reservoir Porosity in the Course of Sandstone Diagenesis. Education Course Note Series No. 12, AAPG, 1979.

56. McDonald, D. A., and R. C. Surdam. Clastic Diagenesis. AAPG Memoir 37, 1984.

57. Eatough, M. O. Preliminary Results of Mineralogy and Petrology of the Fracture Zone Interval (Depth 5700-5870 ft) Drill Core MWX-1. Bendix Field Engineering Corp. Report prepared for Sandia National Laboratories Multi-Well Experiment Program, October 1982.

58. Burley, S. D., J. D. Kantorowicz and B. Waugh. Clastic Diagenesis. In: Sedimentology-Recent Developments and Applied Aspects, P. Brenchley, and B. P. Williams, eds. Blackwell Scientific Publications, 1985, pp. 189-226.

59. Dickson, A. D. Diagenesis of Shallow-Marine Carbonates, In: Sedimentology, Recent Developments and Applied Aspects, P. J. Brenchley, and B. P. Williams, eds. Blackwell Scientific Publications, 1985, pp. 183.

60. Lorenz, J. C. Tectonic and Stress Histories of the Piceance Creek Basin and the MWX Site, from 75 Million Years Ago to the Present. Preliminary Report. Dept. of Energy Report No. SAND84-2603, March 1985.

61. Eatough, M. O. Preliminary Results of Minerology and Petrology of the Fracture Zone Interval (Depth 5,700-5,870 ft) Drill Core MWX-1. Bendix Field Engineering Corp. Report prepared for Sandia National Laboratories Multi-Well Experimental Program, October 1982.

62. Stoch, L. Clay Minerals, Wydawnictwa Geologiczne, Warszawa, 1974, in Polish.

63. Tillman, R. W. and R. S. Martinsen. The Shannon Shelf-Ridge Sandstone Complex, Salt Creek Anticline Area, Powder River Basin, Wyoming. In: Siliclastic Shelf Sediments, ed. Edhington, R. L.. Society of Economic Paleontologists and Mineralogists, Special Publication No. 36, 1984.

64. Borkowska, M., and Smulikowski, K. Rock Forming Minerals, Wydawnictwa Geologiczne, Warszawa, 1973 (in Polish).

65. Haves, C. L. Simple Method Finds Barium in Oil Field Brines. Oil and Gas J., Aug. 19, 1985, pp. 130-132.

66. Herman, J. S. and White, W. B. Dissolution Kinetics of Dolomite: Effects of Lithology and Fluid Flow Velocity. Geochimica et Cosmochimica Acta, v. 49, 1985, pp. 2017-2026.

67. Baumann, J., D. Buchmann, W. Dreybrodt, and H. D. Shulz. Calcite Dissolution Kinetics in Porous Media. Chemical Geology, v. 50, No. 4, September 1985.

68. Schulman, D., and W. Chesworth. Calcium Carbonate Solubility in the C Horizon of the Southwestern Ontario, Canada, Invisol. Chemical Geology, v. 51, October 1985.

69. Southwick, J. G. Solubility of Silica in Alkaline Solutions: Implications for Alkaline Flooding. Soc. Pet. Eng. J. v. 25, No. 6, December 1985.

70. Sjoberg, E. L., and D. T. Rickard. The Effect of Added Dissolved Calcium on Calcite Dissolution Kinetics in Aqueous Solutions at 25° C. Chemical Geology, v. 49 1985, pp. 405-413.

71. Reed, M. G. Gravel Pack and Formation Sandstone Dissolution During Steam Injection. J. Pet. Tech., June 1980, pp. 941-949.

72. Bergosh, J. L., T. R. Marks, and A. F. Mitkus. New Core Analysis Techniques for Naturally Fractured Reservoirs. Pres. at the SPE Calif. Reg. Meet., Bakersfield, Mar. 27-29, 1985. SPE paper 13653.

73. Litvak, B. L. Simulation and Characterization of Naturally Fractured Reservoirs. Reservoir Characterization. L. W. Lake and H. B. Carroll, Jr., eds. Academic Press, Inc., New York, 1986, pp. 561-584.

74. International Association of Hydrogeologists Committee of USA Members. Proc. of the International Congress on Hydrogeology of Rocks of Low Permeability. Tucson, v. 1 and 2, January 1985.

75. International Association of Hydrogeologists Canadian National Chapter. Proc. of the International Groundwater Symposium on Groundwater Resources Utilization and Contaminant Hydrogeology, Montreal, Quebec, Canada, v. 1 and 2, May 1984.

76. Szpakiewicz, M. Ground-Waters in the Liassic Deposits of the Northern Margin of the Holy Cross Mountains. In: Hydrogeological Research in Poland. Geological Institute Bull. v. 3, No. 277, 1973 pp. 54-68 (in Polish with Russian and English summary and captions).

77. Doll, T. E. Polymer Mini-Injectivity Test: Shannon Reservoir, Naval Petroleum Reserve No. 3, Natrona County, WY. Pres. at the SPE Rocky Mountain Regional Meeting, Casper, May 21-23, 1984. SPE paper 12925.

78. Leung, W. F. A General Purpose Single-Phase Naturally Fractured (Carbonate) Reservoir Simulator with Regorous Treatment of Rock-Stress/Fluid-Pressure Interactions and Interporosity Flow. Pres. at the SPE Reservoir Simulation Symp., Dallas, Feb. 10-13, 1985 SPE paper 13528.

79. Gurzij, D. W., M. P. Gabinet, and A. V. Kiselev. Litologiia i Porody Kolectory na Bolshyh Glubynah v Nieftogazonosnyh Provinciah Ukrainy (Lithology and Reservoir Rock at Great Depths in Oil and Gas-Bearing Provices of Ukrainian S.S.R.), Ukrainian Academy of Sciences, published by Naukova Dumka, 1983, pp. 32-33, (in Russian).

80. Hewett, T. A. Porosity and Mineral Alternation by Fluid Flow Through a Temperature Field. Reservoir Characterization. L. W. Lake and H. B. Carroll, Jr., eds. Academic Press, Inc., New York, 1986, pp. 83-140.

TABLE 1. - Reservoir rock and fluid properties of Big Muddy field

| | |
|---|---|
| Discovery date | 1916 |
| Location | SW flank, Powder River Basin (Wyoming) |
| Formation (geologic age) | Frontier (Upper Cretaceous) |
| Reservoir of interest | Second Wall Creek Sand |
| Environment of deposition | Barrier bar, deltaic, or blanket sand |
| Entrapment | Structural (east plunging anticline) |
| Reservoir volume, acre-ft | 100,000 |
| Average depth, ft | 4,100 |
| Average thickness, ft | 68 |
| Average porosity, % | 19.4 (range: 14.7-25%) |
| Average permeability to air, md | 56 (range: 44-228) |
| Dykstra-Parsons variation | 0.61 |
| OOIP, bbl | $91.4 \times 10^6$ |
| Primary production (solution gas drive and local water drive (1917-53), bbl | $24.4 \times 10^6$, 26.7% OOIP |
| Secondary waterflood (1953-72), bbl | $6.9 \times 10^6$, 7.5% OOIP |
| ROIP after waterflood for EOR, bbl | $60.1 \times 10^6$, 65.7% OOIP |

All data obtained from the literature.

TABLE 2. - Reservoir rock and fluid properties of North Burbank field

| | Track 97 | Track 49 | North Burbank |
|---|---|---|---|
| Discovery date | | 1920 | |
| Area, acres | 90 | 160 | 18.312 |
| Reservoir depth, ft | 3,000 | 3,000 | 3,000 |
| Pay thickness, ft | 43 | 37 | 47 |
| Porosity, % | 16.5 | 10-32 | 16.8 |
| Permeability range, md | 1-450 | 1-2,000 | 1-2,000 |
| Average permeability, md: | | | |
| Entire sand | 50 | | |
| Upper high permeability zone | 389 | | >500 |
| Lower tighter zone | | <100 | |
| Average D-P permeability variation | 0.40-0.65 | 0.87 | |
| Wettability characteristics (average relative displacement index) | -0.45 | | |
| Viscosity at res. temp, cP | | | |
| Oil | 3.0 | 3.0 | 3.0 |
| Water | 0.65 | 0.6 | |
| Water-oil mobility ratio | 2.5 | | |
| Oil gravity, °API | 39 | 38 | 38-40 |

All data obtained from the literature.

TABLE 3. - Reservoir rock and fluid properties of Bell Creek field

| | |
|---|---|
| Discovery date | 1967 |
| Location | NW flank, Powder River Basin (Montana) |
| Formation (geologic age) | Muddy (Lower Cretaceous) |
| Reservoir of interest | Zone II sand, waterflood Unit 'A' |
| Environment of deposition | Barrier bar sand |
| Entrapment | Stratigraphic (OWC w/updip pinchout) |
| Size, acres | 7,219 |
| Average depth, ft | 4,500 |
| Average thickness, ft | 11.5 |
| Average porosity, % | 25.5 |
| Average permeability to air, md | 1,175 (range: 130-6,573) |
| Dykstra-Parsons variation | 0.34-0.7 (fieldwide) |
| OOIP, bbl | $122 \times 10^6$ |
| Primary production solution gas drive: 1967-70, bbl | $2.19 \times 10^6$, 17.9% OOIP |
| Secondary waterflood (1970-76), bbl | $25.7 \times 10^6$, 21.1% OOIP |
| ROIP after waterflood for EOR | $74.4 \times 10^6$, 61% OOIP |

All data obtained from the literature.

TABLE 4. - Reservoir rock and fluid properties of El Dorado field

| | |
|---|---|
| Discovery date | 1915 |
| Location | Nemaha Uplift (Butler County, Kansas) |
| Formation (geologic age) | Wabaunsee (Lower Permian) |
| Reservoir of interest | 65-ft Admire Sand |
| Environment of deposition | Distributary channel, crevasse splay |
| Entrapment | Structural (anticline over basement high) |
| Size, acres | 6,200 |
| Average depth, ft | 650 |
| Average thickness, ft | 18 |
| Average porosity, % | 24 (range: 18-29%) |
| Average permeability to air, md | 240 (range: to 1500) |
| Dykstra-Parsons variation | 0.463 |
| OOIP, bbl | $108.10^6$ |
| Primary production (solution gas drive) and secondary waterflood (1915-1971), bbl | $36.6 \times 10^6$, 33.8% OOIP |
| ROIP after waterflood for EOR, bbl | $71.5 \times 10^6$ |

All data obtained from the literature.

**TABLE 5 - Review and ranking of geological problems of EOR pilots and assessment of contribution from further research**

| | FOUR-COMPONENT GENERIC MODEL FOR CLASTIC RESERVOIR CHARACTERIZATION | | | | | | | |
|---|---|---|---|---|---|---|---|---|
| | ENVIRONMENT OF DEPOSITION | | DIAGENESIS | | STRUCTURE | | FORMATION FLUID | |
| | INFLUENCE ON PILOT | ADDITIONAL RESEARCH POTENTIAL | INFLUENCE ON PILOT | ADDITIONAL RESEARCH POTENTIAL | INFLUENCE ON PILOT | ADDITIONAL RESEARCH POTENTIAL | INFLUENCE ON PILOT | ADDITIONAL RESEARCH POTENTIAL |
| BIG MUDDY | HIGH | MAXIMUM | MODERATE | MODERATE | HIGH | MAXIMUM | [1] | [1] |
| BELL CREEK | HIGH | MODERATE | MODERATE | MODERATE | LOW | MINIMUM | MODERATE | MODERATE |
| EL DORADO | HIGH | MAXIMUM | MODERATE | MODERATE | MODERATE | MAXIMUM | MODERATE | MODERATE |
| NORTH BURBANK | HIGH | MAXIMUM | HIGH | MAXIMUM | HIGH | MAXIMUM | HIGH | MODERATE |

[1] Insufficient information for conclusion.

TABLE 6. - Factors related to depositional environment

| Sedimentary | Postsedimentary |
|---|---|
| Lithostratification | Compaction pattern resulting from burial and pressure regime[1] |
| Geometry, continuity of strata, and boundaries | Deformation of layers resulting from dewatering and clay collapsing |
| Bedding and internal sedimentary structures | Distortion of continuity and geometry of shale drapes |
| Texture and related original porosity | Geochemical alteration of original detrital grains |
| Detrital mineralogy | Fracture pattern related to the thickness of rock layers layers |
| Chemistry of synsedimentary fluids | Fracture pattern related to the type of lithologies |
| Redox potential of depositional environment | Detrital filling of fractures related to alternating lithologies |
| Early biogenic and geochemical processes and products | |
| Contemporaneous tectonics | |

[1] Hydrostatic and under- or overpressured regimes in open or closed systems.

TABLE 7. - Postsedimentary factors not related to depositional environment

| Geochemical | Tectonic |
|---|---|
| Lithification and resulting brittleness | Subsidence, uplifting |
| Dissolution/precipitation/mineral transformation | Folding, faulting, overthrusting, tilting, flexuring |
| Eogenetic stage | Fracture generations resulting from the history of shear stresses |
| Mesogenetic stage | Fracture pattern related to the position on folds |
| Telogenetic stage, resulting from chemical | Fracture pattern related to the brittleness of layers |
| Late biogenic alterations and products | Man-induced reopening of natural joints |
| Man-induced geochemical alterations since primary production | |
| Final properties and distribution of formation fluids | |

## TABLE 8. - The elements of geological models for reservoir characterization for EOR

DEPOSITIONAL MODEL

- depositional geometry and boundaries
- environment of deposition
- inferred position within deposystem
- type of stacking of depositional units
- stratigraphy
- lithology
- lithologic barriers and their continuity
- bedding and internal sedimentary structures
- original detrital mineralogy
- trends in mineralogic composition
- trends in grain size
- sorting and packing
- original porosity distribution
- rate of deposition
- rate of subsidence
- synsedimentary pore fluids
- synsedimentary temperature, pH, Eh
- synsedimentary bioactivity and products
- synsedimentary deformations

DIAGENETIC MODEL

- overall paleohistory: burial, uplift, paleoerosion paleoweathering, reburial; residence time at all stages
- diagenetic facies: eogenic, mesogenic, telogenic and related processes
- maximum depth of burial
- paleoheat-flow
- paleohydrodynamics and hydrogeochemistry
- compaction in open and closed systems
- lithification (type and degree)
- alteration and transformation of minerals framework
- generation, alteration and transformation of authigenic minerals
- time of oil arrival and rock-fluid-organics interaction products
- secondary porosity (matrix and joints)
- final fluid characteristics and state of equilibrium with rock minerals
- final properties of clay mineral (detrital and authigenic)
- man-induced diagenetic alterations since primary production
- predicted induced alterations during EOR

STRUCTURAL MODEL

- present reservoir geometry
- folds, overthrusts, flaxures, faults, dipping
- unconformities
- in situ stress
- joint system (3D)
  - origin and generations
  - zonation
  - scale
  - orientation
  - density
  - apertures
  - morphology
  - connectivity
  - termination
  - filling
    - detrital
    - chemical
    - reopenings
- joint's ability to transmit fluids (fracture permeability)
- reservoir susceptibility to hydraulic fracturing

FORMATION FLUID MODEL

- fluid content (Sw, So, Sg)
- fluid distribution
- fluid composition
- fluid properties
- fluid rock state of thermodynamic equilibrium
- condition of fluid mobilization

INTEGRATED DYNAMIC HYDRUALIC MODEL

based on screened and ranked data from static models

**TABLE 9. - Summary of depth-related diagenetic stages and important reactions in mudrocks which may contribute solutes to sandstones via the associated trends in pore water evolution and expulsion. After Burley, et al., 1985.**

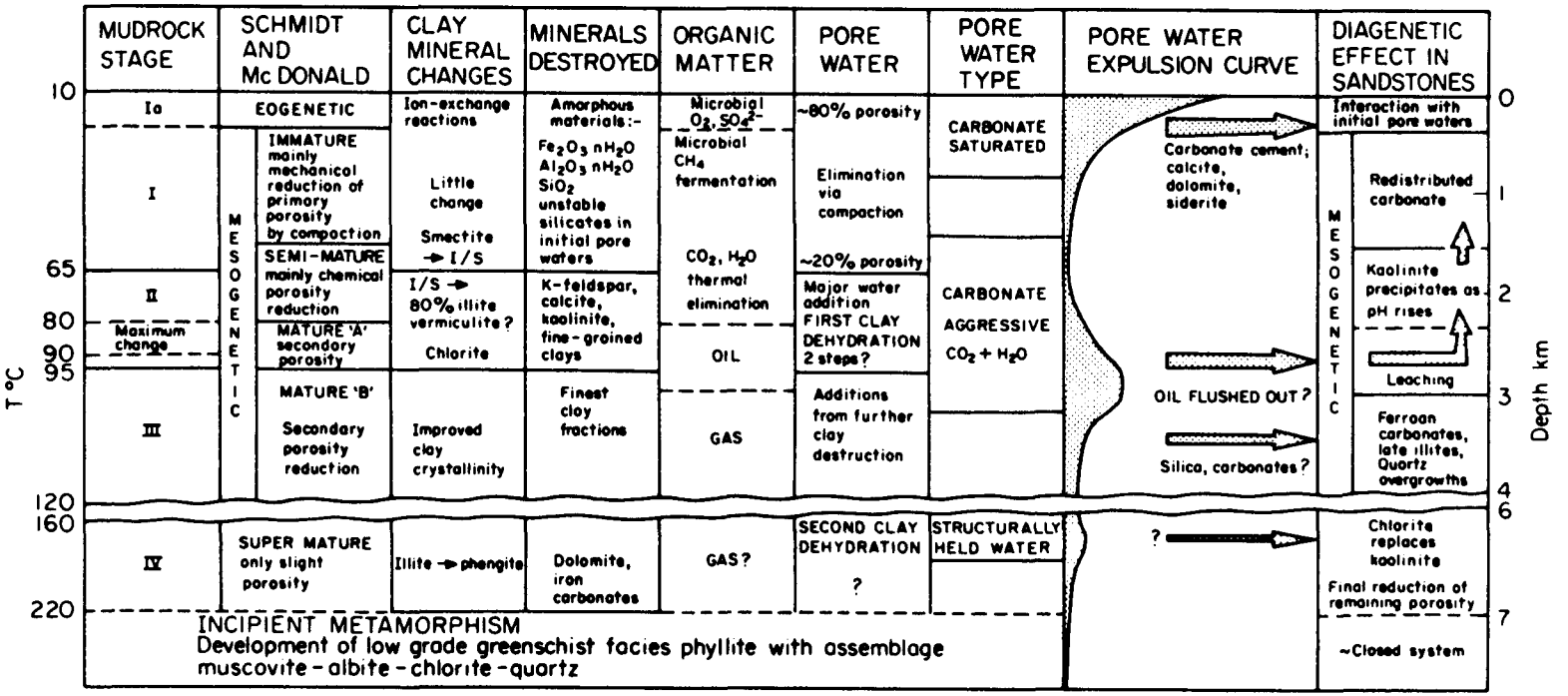

TABLE 10 - Full-diameter whole-core directional permeability and plug data versus orientation. After J. Bergosh et al., 1985

| Sample number | Azimuth location | | | | | | |
|---|---|---|---|---|---|---|---|
| | 255°-285° | 285°-315° | 315°-345° | 345°-15° | 15°-45° | 45°-60° | Plug |
| | Permeability, millidarcies | | | | | | |
| 1 | 39.0 | 45.0 | 44.3 | 45.0 | 44.3 | 39.0 | 48.00 |
| 2 | 13.5 | 12.0 | 20.3 | 28.5 | 45.0 | 8.3 | 13.30 |
| 3 | 5.9 | 4.2 | 4.1 | 3.8 | 4.7 | 7.5 | 0.13 |
| 4 | 426.0 | 1,145.0 | 12.0 | 18.0 | 4.65 | 1,052.0 | 0.06 |
| 5 | 1,293.0 | 1,323.0 | 1,132.0 | 1,192.0 | 1,190.0 | 1,350.0 | 0.10 |
| 6 | 488.0 | 587.0 | 1,262.0 | 1,709.0 | 948.0 | 435.0 | 0.17 |
| 7 | 2.93 | 3.9 | 5.78 | 18.0 | 24.8 | 3.15 | 0.90 |
| 8 | 23.3 | 12.1 | 7.8 | 5.3 | 6.6 | 10.0 | -- |
| 9 | 48.1 | 55.2 | 27.2 | 21.4 | 15.3 | 28.7 | -- |
| 10 | 2.8 | 3.5 | 1.5 | 0.4 | 0.6 | 0.8 | -- |
| 11 | 24.9 | 23.6 | 8.8 | 6.6 | 9.4 | 21.6 | -- |
| 12 | 139.0 | 96.4 | 56.4 | 24.4 | 85.1 | 51.6 | -- |

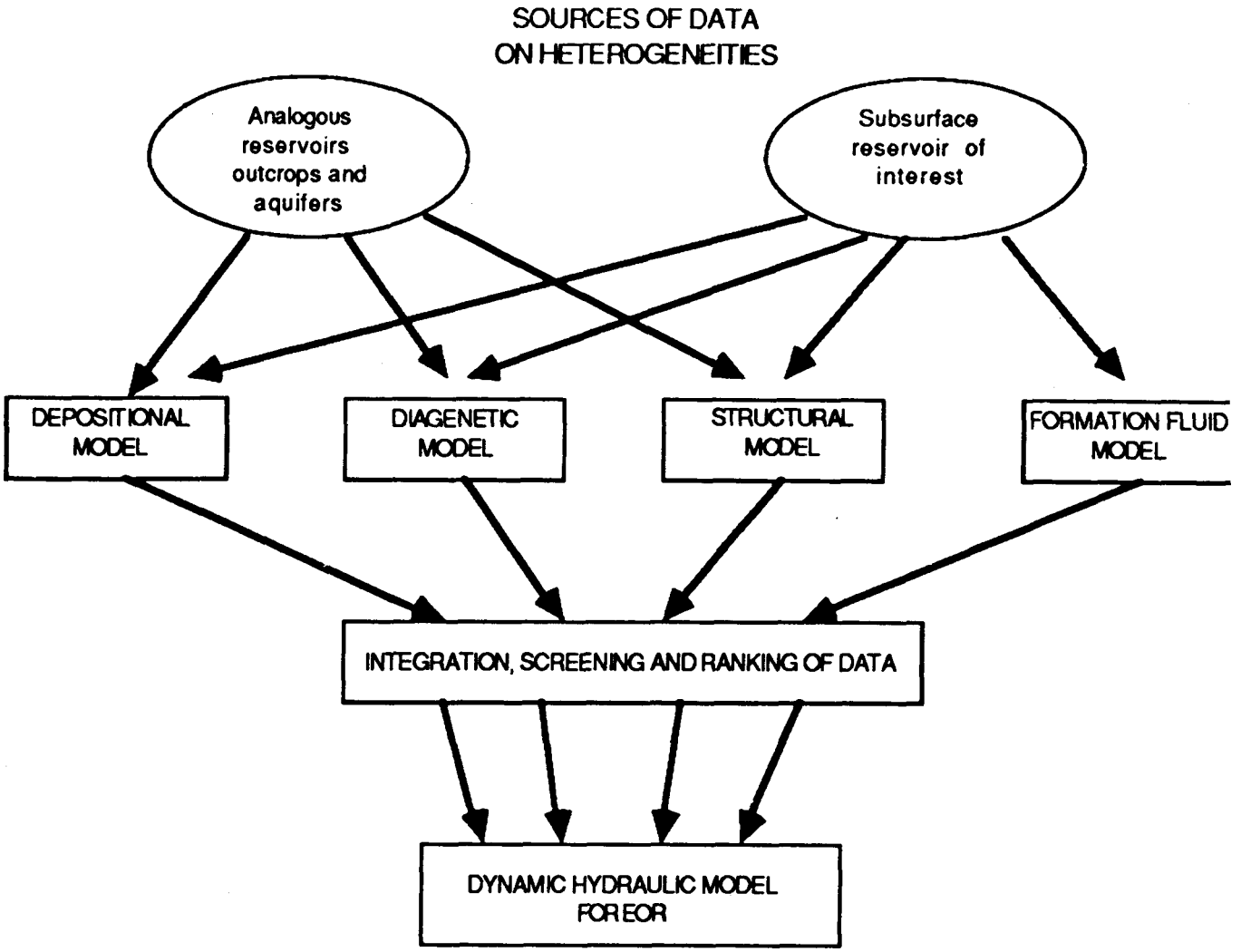


FIGURE 2. - Reservoir modeling for EOR.

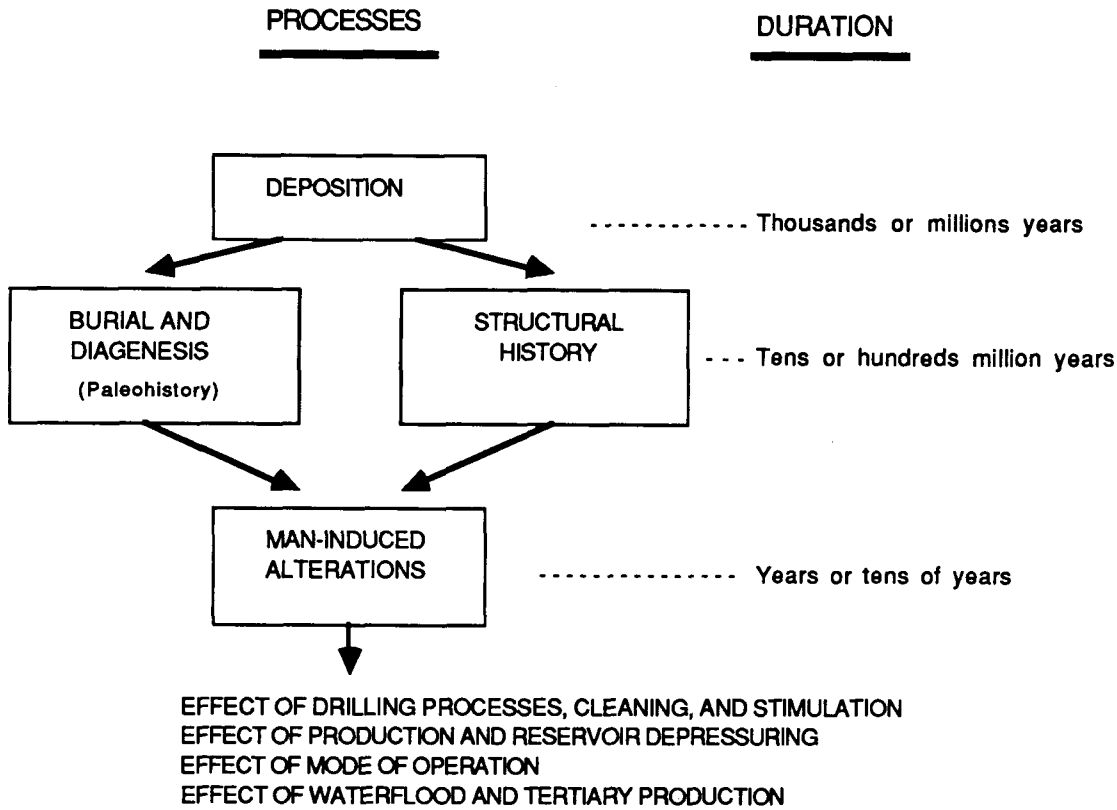


FIGURE 3. - Processes affecting reservoir properties and their duration.

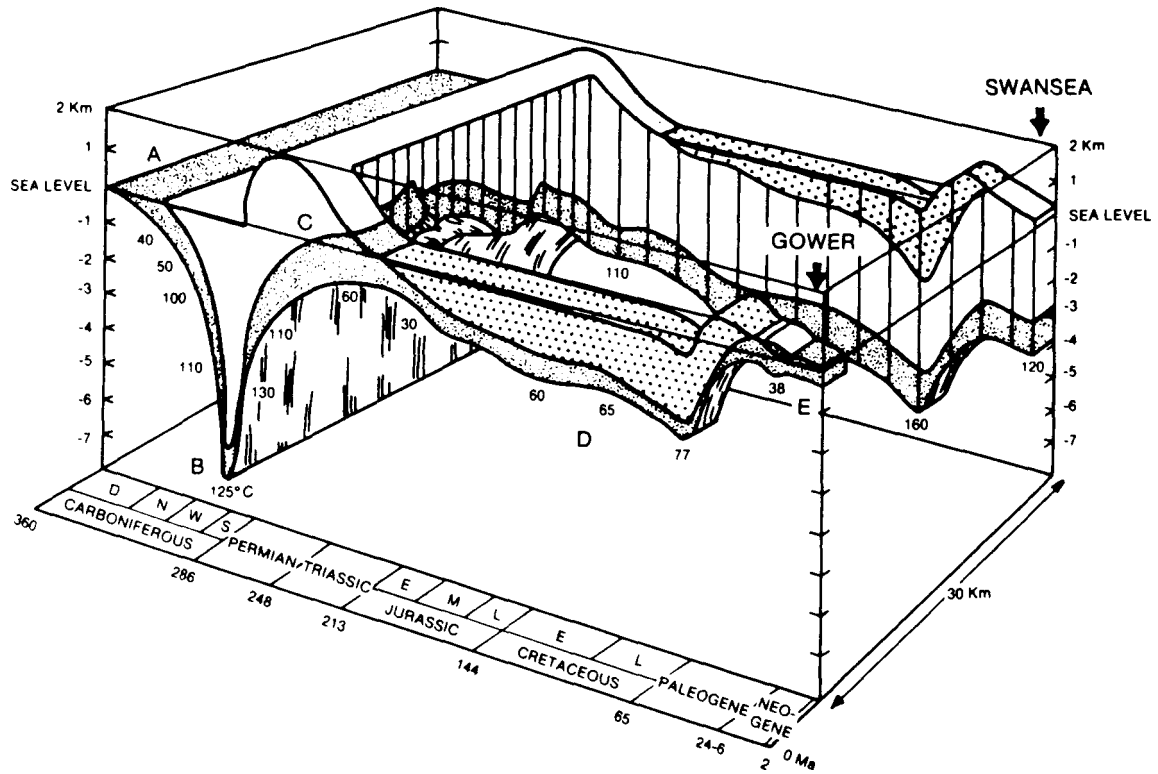


FIGURE 4. - Perspective time-depth reconstruction to show history of South Wales Dinantian sediments from their deposition through burial to their present position. Dinantian sediments shown in fine stipple; Mesozoic sediments in coarse stipple. Temperatures shown at base of Dinantian in degrees Celsius. After J. Dickson, 1985.

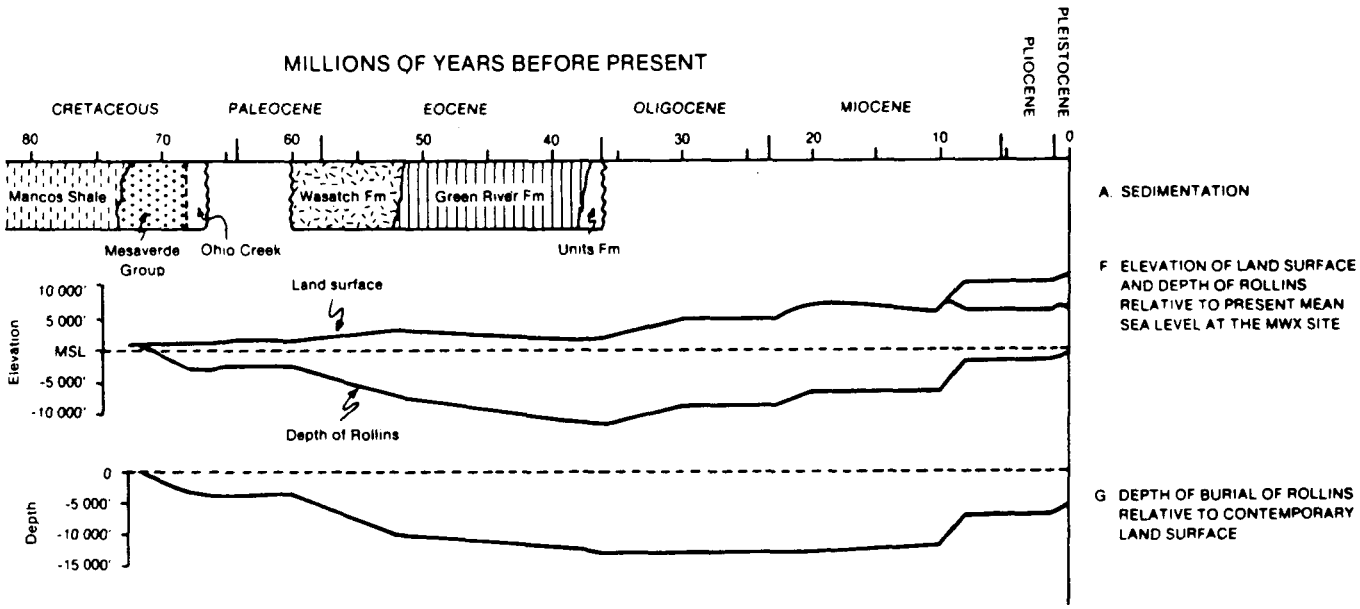


FIGURE 5. - Geological History of the Piceance Creek Basin at the MWX site. Simplified after J. Lorenz, 1985.

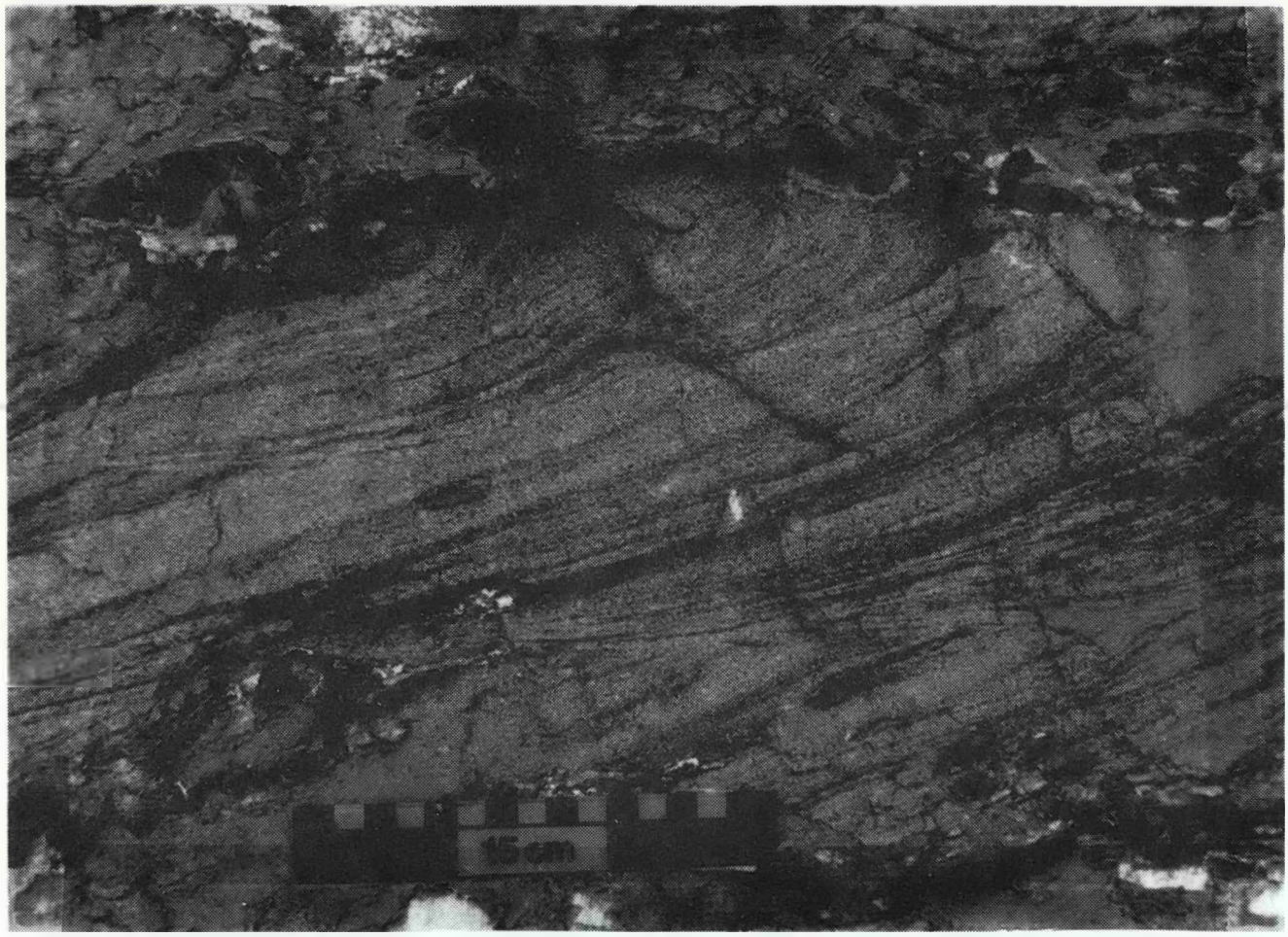


FIGURE 6. - Glauconite concentrations emphasizing trough-bedding laminae in the high energy shelf ridge margin lithofacies of the Shannon formation in the Powder River Basin. Note the glauconite concentrations (black) in the cross-bedded layer above the scale. Outcrop W1B, zone 2.

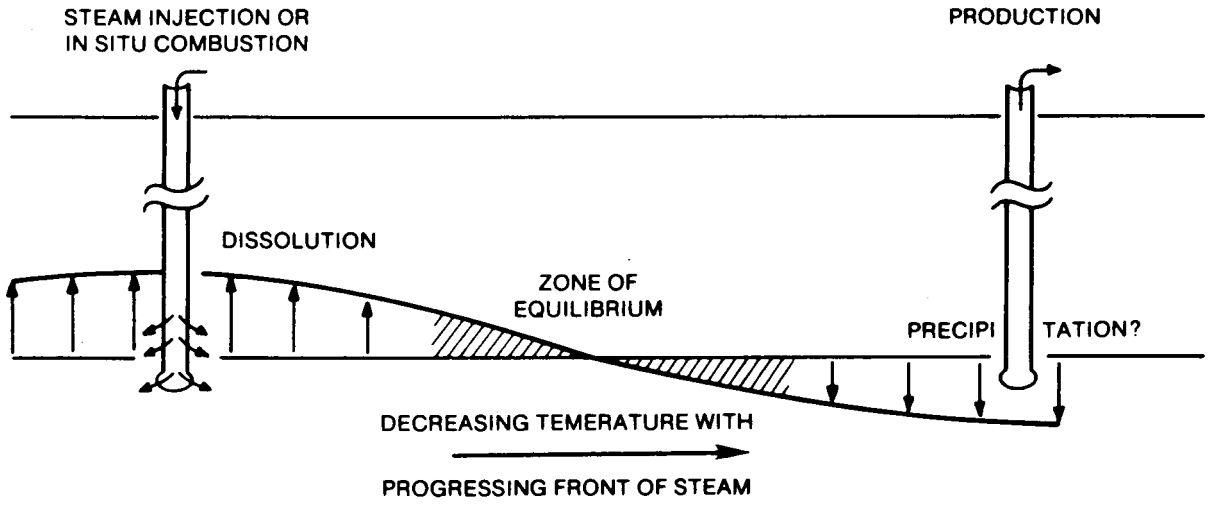


FIGURE 7. - Predicted trend in dissolution/precipitation of silica during thermal EOR processes.

# CHAPTER 3. SELECTION OF DEPOSYSTEM FOR HETEROGENEITY RESEARCH

## A. Selection of Deposystem Based on Pseudo-Dykstra-Parsons Coefficient

NIPER reservoir characterization research was initiated by selection of a suitable deposystem for conducting reservoir heterogeneity research. It was decided that the ideal deposystem for such research should be a major habitat of oil and gas and should have potential for enhanced oil recovery.

One approach to the selection was based on the analysis of pseudo-Dykstra-Parsons coefficients ($V_{PDP}$) calculated in the 1984 National Petroleum Council (NPC) study for a large number of reservoirs. Obtained from theoretical investigations with the Higgins-Leighton streamline model,[1] $V_{PDP}$ coefficients are expected to give not only a measure of aggregate reservoir heterogeneities (usually obtained from Dykstra-Parsons coefficients, $V_{DP}$, for a stratified reservoir) but also volumetric sweep efficiency and the mobility ratio of a reservoir. It was postulated that if reservoirs from various deposystems could be grouped in terms of calculated $V_{PDP}$ values, information would be provided not only about aggregate heterogeneities in reservoirs from various deposystems but also about volumetric sweep efficiencies and mobility ratios in the reservoirs. It was concluded that the ideal candidate deposystem for heterogeneity research should have relatively poor sweep and displacement efficiencies so that there would be good potential for significant oil recovery through improved reservoir characterization and heterogeneity research.

### Collection of Data

Relevant geological data from 26 Department of Energy (DOE) cost-shared EOR projects were first extracted from the DOE Reservoir Data Base. That data consisted of field and reservoir names, lithology, average reservoir porosity and permeability values, and calculated pseudo-Dykstra-Parsons coefficients ($V_{PDP}$) for those reservoirs. Information on the environment of deposition was gathered through a computer search of geological information for each reservoir studied. The search required a review of available information for most reservoirs since information on depositional environment was not readily available. Besides the environment of deposition, the literature review also included any information available on permeability variation in the reservoir,

such as Dykstra-Parsons coefficients calculated from individual well permeability data.

## Interpretation of Data

Results of the analysis of the $V_{PDP}$ data and environment of deposition for 16 of the DOE cost-shared EOR projects are shown in table 11. The reservoirs belonged to four main environments (fluvial, deltaic, barrier, and offshore bars and turbidites) with some of them in a transition zone between two environments. As shown in table 11, $V_{PDP}$ values were not diagnostic of any particular environment of deposition. For example, $V_{PDP}$ values ranged between 0.5 (or less) and 0.90996 in fluvial and fluvial-deltaic environments. The fluctuation of $V_{PDP}$ values in turbidites was from 0.92 to 0.60.

Even within a single field, sometimes there were large variations in reservoir heterogeneities ($V_{DP}$ values), depending upon the location of the reservoir in the deposystem from where the permeability information was obtained. As an example, in North Burbank field (fluvial environment), the coefficients varied from 0.40 to 0.87 within a distance of 4 to 5 miles. The variation in $V_{DP}$ could be even larger in other areas in the same environment. A second example is Bell Creek (MT) field which has been classified as a barrier island reservoir. In Bell Creek field, the calculated $V_{PDP}$ value is 0.50 although the Dykstra-Parsons permeability variations range from 0.34 in the more homogeneous central part to 0.70 or higher in the lagoonal side or the more diagenetically altered parts. Again, the variation could be even larger in other areas of the bar.

## Results of Study and Conclusion

Results of this limited study indicate that calculated $V_{PDP}$ values in various deposystems are not confined within narrow limits. Even in a single field within a particular deposystem, $V_{DP}$ coefficients sometimes show wide variations due to appreciable lateral geological heterogeneities. It may be concluded that calculated $V_{PDP}$ coefficients are not diagnostic of aggregate heterogeneities within a given deposystem. Owing to their large variations, $V_{PDP}$ coefficients cannot be construed to give a reliable measure of the sweep efficiency or the aggregate reservoir heterogeneity within a deposystem. It would seem that any conclusion as to geological heterogeneity or sweep

efficiency in reservoirs in a given deposystem based on the $V_{PDP}$ coefficient could be erroneous.

An alternative method for selecting a suitable deposystem was proposed in the FY86 Research Plan plan which was based upon a literature search for deposystems with most significant oil accumulations and good EOR potential.

## B. Selection of Deposystem Based on Production Potential and Availability of Data

The initial approach was to use the pseudo-Dykstra-Parsons ($V_{PDP}$) coefficient recorded in the NPC study as a method to assess aggregate heterogeneities of various deposystems. However, results of a previous NIPER study[2] indicated that because of large variations, no correlation could be made between $V_{PDP}$ and depositional environment. Therefore, aggregate heterogeneities of depositional environments could not be classified according to $V_{PDP}$ coefficient values listed in the 1984 NPC report on enhanced oil recover.[4]

An alternative procedure was based on the selection of a depositional environment that had high original-oil-in-place (OOIP) and high residual oil saturation (ROS) after waterflooding. Because poor recovery performance during primary and secondary recovery operations is usually due to geological heterogeneities, it is in studies of reservoirs such as these that heterogeneity research has the potential for significant contributions. This criterion was therefore the primary criterion upon which the selection of a deposystem was based.

Three other criteria not specifically associated with the depositional environment but essential for the execution of the project were as follows:

1. The productive formation is exposed near a producing field. This is important because the research strategy involves using outcrop data to supplement subsurface data.

2. Subsurface data from the producing field are available to the public. This limits the choices to fields having data in the public domain.

3. The producing field has an EOR project. This is necessary for testing the model, once developed, with actual field data.

These factors were weighed along with the EOR potential of the depositional environment in the final selection.

It should be emphasized, however, that since the overall objective was to develop and test a methodology applicable to many reservoirs of diverse origins, it was not necessary to choose a depositional environment with the highest OOIP and the highest ROS after waterflooding. Rather, an environment that was relatively important as a reservoir and EOR target and that reasonably met the other criteria was required. It should also exhibit a degree of complexity appropriate for the initial development of a methodology.

Deltaic and turbidite environments, although prolific producers, were not considered for heterogeneity research because (1) they form extremely complex reservoirs, which is undesirable for the initial development of a methodology, and (2) no field was known that satisfied the three criteria: (a) the productive formation is exposed nearby, (b) subsurface data are available to NIPER, and (c) the field has an EOR project.

## Reserves

Two depositional environments satisfied the above requirements: barrier island/strandplain deposits and shelf sand ridge deposits. More than one-half (51%) of North America's giant oilfields produce from clastic reservoirs interpreted by Moody et al[3]. to be shallow marine and near-shore (littoral) deposits (fig. 8). Results of a survey of 77 fields producing from barrier/strandplain deposits and 22 from shelf deposits indicated that both environments were economically important on this continent. (See appendix A.) Of these, six barrier fields and two shelf fields were found to be U.S. giant oilfields (ultimate recovery > 100 million bbl). Thirteen fields producing from barrier deposits and three fields producing from shelf deposits were found to have ultimate recoveries estimated at more than 50 million bbl (tables 12 and 13).

Names of fields producing from a combination of barrier/strandplain and shelf sands are presented in table 14. Two of these fields have ultimate recoveries of >500 million bbl.

This survey of fields provided a partial list (tables A-1 and A-2) and was intended only to illustrate examples of economically important fields producing from the depositional environments of interest. A complete list,

useful for statistical comparisons, would be difficult and extremely time-consuming to compile for the following reasons:

1. Depositional environments are often not well understood, have conflicting interpretations, or are not reported in the literature.

2. Many fields produce from multiple zones representing diverse depositional environments; production and reserve figures are not calculated for individual zones.

3. Reservoirs producing from shelf sand ridge deposits probably are not well represented in the literature because only recently have shelf ridge sand deposits been described and recognized as discrete deposystem types.

4. Areas where large amounts of data are available (e.g., Texas) tend to bias the data set.

## EOR Potential (ROS After Waterflood)

Information and data resulting from 22 EOR projects conducted in barrier/strandplain deposits and four projects conducted in shelf deposits are presented in tables 15 and 16, respectively. The data illustrate that both types of deposits are EOR targets. Residual oil saturation (ROS) after primary and secondary recovery in the 15 barrier fields sampled ranges from 31.5 to 55% and averages 38.7%. The difference between ROS after primary and secondary recovery and ROS after tertiary recovery ranges from 24 to 1% and averages 7.6%. This comparison suggests that barrier/strandplain reservoirs are good candidates for EOR and that improvements could be made in recovery efficiency. Insufficient data exist for shelf sand ridge fields to make comparisons.

## Other Criteria

Reservoirs in both barrier/strandplain and shelf sand ridge deposystems satisfy the other criteria of (1) an existing outcrop-reservoir pair, (2) available subsurface data, and (3) existing reservoir with an EOR project. Bell Creek field produces from a barrier/strandplain deposit, the Muddy sandstone, which crops out nearby. Much of the published subsurface data are available in DOE reports. Two micellar-polymer EOR projects have been implemented in Bell Creek field.

Teapot Dome field in Naval Petroleum Reserve No. 3 (NPR-3) produces from the Shannon sandstone which is extensively exposed within 5 miles of the reservoir. Most of the well logs and core analyses from the field are available at NIPER; additional data are available from the NPR office in Casper. Three pilot EOR projects (polymer, in situ combustion, and steam), have been implemented in the Shannon in the Teapot Dome reservoir.

## PRELIMINARY EVALUATION OF SHANNON FORMATION, A SHELF RIDGE DEPOSIT

Teapot Dome field, a shelf sand ridge deposit, and Bell Creek field, a barrier island deposit, both in the Powder River Basin, were selected as candidates for heterogeneity research.

The Shannon sandstone (which produces in Teapot Dome field) met all four criteria for selection of a deposystem. Therefore, preliminary studies were conducted to determine the degree to which Shannon outcrop data could supplement the reservoir data from Teapot Dome field.

The Shannon sandstone, a shelf sand ridge deposit in the Powder River Basin, Wyoming, was studied. Sedimentologic and petrophysical features of an outcrop exposure of the high-energy ridge-margin (HERM) facies within the Shannon were compared with those from a Shannon sandstone reservoir in Teapot Dome field.

Comparisons of outcrop and subsurface permeability and porosity histograms, cumulative distribution functions, correlation lengths, and natural logarithms of permeability versus porosity plots indicated a strong similarity between Shannon outcrop and Teapot Dome HERM facies petrophysical properties.

Permeability classes found in outcrop samples could be related to crossbedded zones and shaley, rippled, and bioturbated zones. Similar permeability classes related to similar sedimentologic features were found in Teapot Dome field.

The similarities of outcrop and Teapot Dome petrophysical properties, which are from the same geologic facies but from different depositional episodes, suggested that rocks deposited under similar depositional processes within a given deposystem have similar reservoir properties. The results of

the study indicated that the use of quantitative outcrop information in characterizing reservoirs might provide a significant improvement in reservoir characterization.

The results of the study of the shelf ridge example were published.[4]

Although the Shannon sandstone outcrops and Teapot Dome field provided an excellent situation for this preliminary pilot study, further investigation of candidate outcrop/reservoir pairs indicated that the Muddy formation and Bell Creek field were better suited for obtaining the goals of the research project, which are described in the next chapter.

## Results of Study

1. Criteria for the selection of a depositional environment for study were as follows: (a) it must be of relatively important economic value, (b) it must be a good EOR candidate, (c) the productive formation must be exposed near a producing field, (d) subsurface data for the producing field must be available to NIPER, and (e) the producing field must have an EOR project.

2. Barrier/strandplain deposits and shelf sand ridge deposits meet criteria a, b, c, and e. Criterion d was also investigated for both candidate deposystems for final selection of a specific reservoir within these deposystems for further study.

## REFERENCES

1. Craig, F. F., Jr. The Reservoir Engineering Aspects of Waterflooding; SPE-AIME Monograph, v. 3, 1971, p. 82.

2. Sharma, B. Determining Possible Correlations Between Pseudo Dykstra-Parsons Coefficient and Deposystem Types. Dept. of Energy Report No. NIPER-145, March 1986, p. 6.

3. Moody, J. A., J. W. Mooney, and J. Spivak. 1968 Giant Oil Fields of North America. In Geology of Giant Petroleum Fields, M. T. Halbouty, ed., AAPG Memoir 14, 1970.

4. Jackson, S., M. Szpakiewicz, and L. Tomutsa. Geological Characterization and Statistical Comparison of Outcrop and Subsurface Facies: Shannon Shelf Sand Ridges. Dept. of Energy Report No. NIPER-214, 1986, p. 60.

TABLE 11. -- Pseudo Dykstra-Parsons coefficients and depositional environments for DOE cost-shared EOR projects

| Field name | Reservoir name | $V_{PDP}$ | Environment of deposition | Comments |
|---|---|---|---|---|
| North Burbank | Burbank/Burbank Sand | 0.6821 | Fluvial | Dykstra-Parson coefficients indicate large variations in the field. For example in Tract 97 it ranges from 0.40 to 0.65. In Tract 49, it has a value of 0.87. |
| Weeks Island | "S" Sand Reservoir | 0.50 | Fluvial | A $V_{PDP}$ value of 0.50 indicates that the calculated permeability variation was less than 0.50. |
| Kern Front | Main/Chanac | 0.73168 | Fluvial | |
| El Dorado | All/Admire | 0.90996 | Fluvial-Deltaic | |
| Bradford | Bradford/Third Sand | 0.65792 | Deltaic | |
| Big Muddy | Frontier/Frontier | 0.70215 | Barrier Island | A complete interpretation of the environment of deposition has not yet been made. Some claim that sands in the reservoir were deposited under deltaic environment. |
| Bell Creek | Muddy/Muddy | 0.50 | Barrier Bar | The calculated Dykstra-Parsons coefficient in the 160 acre pilot ranged from 0.34-0.70. |
| Stanley Stringer | Burbank/Burbank | 0.72 | Offshore bar | The average value of 0.72 was assigned to reservoirs for which insufficient data was available to calculate the permeability variation. |
| Huntington Beach | Hunt Ave Area/Puente | 0.92388 | Turbidites | |
| Coalinga | Temblor/Temblor Zone | 0.67822 | Turbidites | |
| Midway Sunset | Republic/Spellacy | 0.78505 | Turbidites | |
| Wilmington | East Area Block VI/Puente | 0.76639 | Turbidites | |
| Wilmington | Harbor Area Fault/Puente | 0.6175 | Turbidites | |
| Wilmington | Terminal Area Fault/Puente | 0.65343 | Turbidites | |
| Wilmington | Terminal Area Fault/Puente | 0.60857 | Turbidites | |
| Wilmington | Terminal Area Fault/Puente | 0.6778 | Turbidites | |

TABLE 12. - Reservoirs producing oil from barrier/strandplain deposits (Ultimate recovery >50 million bbl)

| Field | State | Payzone | OOIP | Cumulative production | Ultimate recovery |
|---|---|---|---|---|---|
| | | | | millions of barrels | |
| Tom O'Connor 5900 | TX | Frio | 549 | 246.3 | 337.0 |
| Tom O'Connor 5800 | TX | Frio | 422 | 244.0 | 252.0 |
| Greta 4400 | TX | Frio | 313 | 124.7 | 147.0 |
| Tom O'Connor 5500 | TX | Frio | 261 | 77.7 | 140.0 |
| West Ranch Greta | TX | Frio | 223 | 73.9 | 111.0 |
| West Ranch 41-A | TX | Frio | 203 | 84.6 | 94.0 |
| Magnet-Whithers | TX | Frio | 163 | 78.6 | 91.3 |
| Big Piney/ LaBarge | WY | Almy | -- | 65 | 91 |
| Govt Wells, North G W | TX | Jackson-Yegua | 50 | 77.3 | 78.0 |
| Lake Pasture H-440S | TX | Frio | 132 | 37.7 | 74.0 |
| Old Ocean Armstrong | TX | Frio | 136 | 67.3 | 69.0 |
| White Point E Brighton | TX | Frio | 119 | 64.5 | 66.0 |
| Seven Sisters | TX | Jackson-Yegua | 142 | 35.0 | 56.0 |
| Plymouth Heep Greta | TX | Frio | 113 | 53.4 | 55.4 |
| Withers North | TX | Frio | 100 | 49.0 | 50.0 |

TABLE 13. - Reservoirs producing oil from shelf sand ridge deposits (Ultimate recovery >50 million bbl)

| Field | State | Payzone | OOIP | Cumulative production | Ultimate recovery |
|---|---|---|---|---|---|
| | | | | millions of barrels | |
| Sussex | WY | Shannon/Sussex | -- | 59 | 66.3 |
| Hartzog Draw | WY | Shannon | 350 | 32 | 100 |
| Meadow Creek | WY | Shannon/Sussex | -- | 92 | 108 |
| Teapot East | WY | Shannon/Frontier Muddy | -- | 10.7 | 54 |

TABLE 14. - Reservoirs producing oil from combined barrier/strandplain and shelf sand ridge deposits

| Field | State | Payzone | OOIP | Cumulative production | Ultimate recovery |
|---|---|---|---|---|---|
| | | | | millions of barrels | |
| Pembina | Canada | Cardium | -- | 436 | 1,773 |
| Salt Creek | WY | Frontier FM (Second Wall Creek) | 1518 | 576 | 789 |
| Viking | Canada | Viking | 320 | -- | 110 |
| Big Muddy | WY | Frontier | 91.4 | 52 | 53 |
| Garrington | Canada | Cardium | 190 | -- | 40 |
| Bisti | NM | Gallup | 200 | 33.4 | 34.6 |
| Elk Basin | WY/MT | Frontier FM (Second Wall Creek) | 998 | 467 | -- |
| Teapot Dome | WY | Muddy/Frontier/ Shannon | 275 | 13.7 | -- |
| Crossfield | Canada | Cardium | 160 | -- | 16 |

## TABLE 15. - EOR projects in barrier island/strandplain reservoirs

| Field | State/County | Payzone | EOR process | k, md | Ø, % | Depth, ft | Previous production | ROS, % Start | ROS, % End | Project evaluation | Profit |
|---|---|---|---|---|---|---|---|---|---|---|---|
| La Barge | WY/Sublette | Almy | Steam | 100 | 25 | 850 | WF | 55 | 55 | Disc(4/83) | No |
| Ruben | WY/Sublette | Almy | Polymer | 1-56 | 14 | 330.0 | Prim | 45.4 | 42 | Succ | Yes |
| McDonald Draw | WY/Sublette | Almy | Polymer | 1-200 | 18 | 320.0 | WF | 43.8 | 29.1 | Succ | Yes |
| McDonald Draw | WY/Sublette | Almy | Polymer | 2-59 | 16.7 | 305.0 | WF | 40.3 | 36.7 | Succ | Yes |
| Isenhour | WY/Sublette | Almy | Polymer | 1-25 | 15-20 | 360.0 | Prim | 38.1 | 27.0 | Succ | Yes |
| Long Island/ Star Corral | WY/Sublette | Almy | Polymer | 1-50 | 15.5 | 355.0 | Prim | 43.6 | 23.9 | Succ | Yes |
| Tip-Top Shallow Unit | WY/Sublette | Almy Mesaverde | Polymer | 1-200 | 12-20 | 1150 | Prim | 41.3 | 36.9 | Disc (1983) | No |
| Sage Spring Creek-Unit 'A' | WY/Natrona | Dakota | Polymer | 50 | 13 | 7400 | WF | 45 | 21 | Succ | Yes |
| Big Muddy | WY/Converse | Wall Creek | Polymer | 52 | 19.5 | 3180 | Prim/WF | -- | -- | Disc (10/85) | No |
| Clareton | WY/Weston | New Castle | Polymer | 1-15 | 15-18 | 6000 | Prim | -- | -- | Term | |
| Mush Creek | WY/Weston | New Castle | Polymer | 1-15 | 15-18 | 4400 | Prim | -- | -- | Succ | Yes |
| Bison Basin | WY/Fremont | Frontier | Alkaline | 144 | 22 | 1300 | Prim | -- | -- | Prom | -- |
| Horseshoe Gallup | NM/San Juan | Gallup | Polymer | 14 | 15 | 1200 | WF | -- | -- | Disc | No |
| Bell Creek | MT/Powder | Muddy | Micellar Polymer | 1218 | 24.9 | 4500 | WF | 33 | 21.5 | Succ | Yes |
| Bell Creek | MT/Powder | Muddy | Micellar Polymer | 1050 | 27.0 | 4650 | WF | 35 | 25 | Disc | No |
| Bridger Lake | UT/Summit | Dakota | Hydrocarbon Miscible | 70 | 12.8 | 15,600 | WF | 37 | 32 | Disc | No |
| Withers, North | TX/Wharton | Frio (Withers N) | $CO_2$ Immiscible | 1050 | 25 | 5,250 | Prim | 35 | 32 | Prom | Yes |
| Withers, North | TX/Wharton | Frio (C-Sand) | $CO_2$ Immiscible | 400 | 25 | 5,320 | WF | 32 | 30 | Disc (Term. 1/85) | No |
| Plymouth | TX/San | Frio Patricro | $CO_2$ Immiscible | 350 | 31 | 4,650 | Prim | 31.5 | 20 | Disc (Term. 1/85) | No |

## TABLE 15. - EOR projects in barrier island/strandplain reservoirs - Continued

| Field | State/County | Payzone | EOR process | k, md | Ø, % | Depth, ft | Previous production | ROS % Start | ROS % End | Project evaluation | Profit |
|---|---|---|---|---|---|---|---|---|---|---|---|
| Pickett Ridge | TX/Wharton | Frio | $CO_2$ Immiscible | 1,200 | 30 | 4,600 | Prim | 29 | 28 | -- | No |
| Magnet Whithers | TX/Wharton | Frio | $CO_2$ Immiscible | 1,700 | 23 | 5,500 | Gas injection | 35 | 31 | Succ | Yes |
| Magnet Whithers Pierce Estates B&C | TX/Wharton | Frio | $CO_2$ Immiscible | 1,700 | 23 | 550 | Gas injection | 35 | 34 | Succ | Yes |

Prom = Promising
Succ = Successful
Disc = Discontinued
Term = Terminated

## TABLE 16. - EOR projects in shelf sand ridge deposits

| Field | State/County | Payzone | EOR Process | k, md | Ø, % | Depth, ft | Previous production | ROS, % Start | ROS, % End | Project evaluation[1] | Profit |
|---|---|---|---|---|---|---|---|---|---|---|---|
| NPR-3 Teapot Dome | WY/Natrona | Shannon | Polymer | 63 | 18 | 550 | Prim | 40 | 29 | Disc | No |
| NPR-3 Teapot Dome | WY/Natrona | Shannon | Combustion | 135 | 18 | 270-425 | Prim | 40 | 12-15 | -- | -- |
| West Sussex Unit | WY/Johnson | Shannon | $CO_2$ Miscible | 121 | 19.5 | 3040 | -- | -- | -- | Term | -- |
| Dugot Creek | WY/Johnson | Shannon | $CO_2$ Miscible | 120 | 22 | 2000 | WF | -- | -- | Prom | -- |

[1]Project evaluation:
Prom. = Promising
Succ. = Successful
Disc. = Discouraging
Term. - Terminated

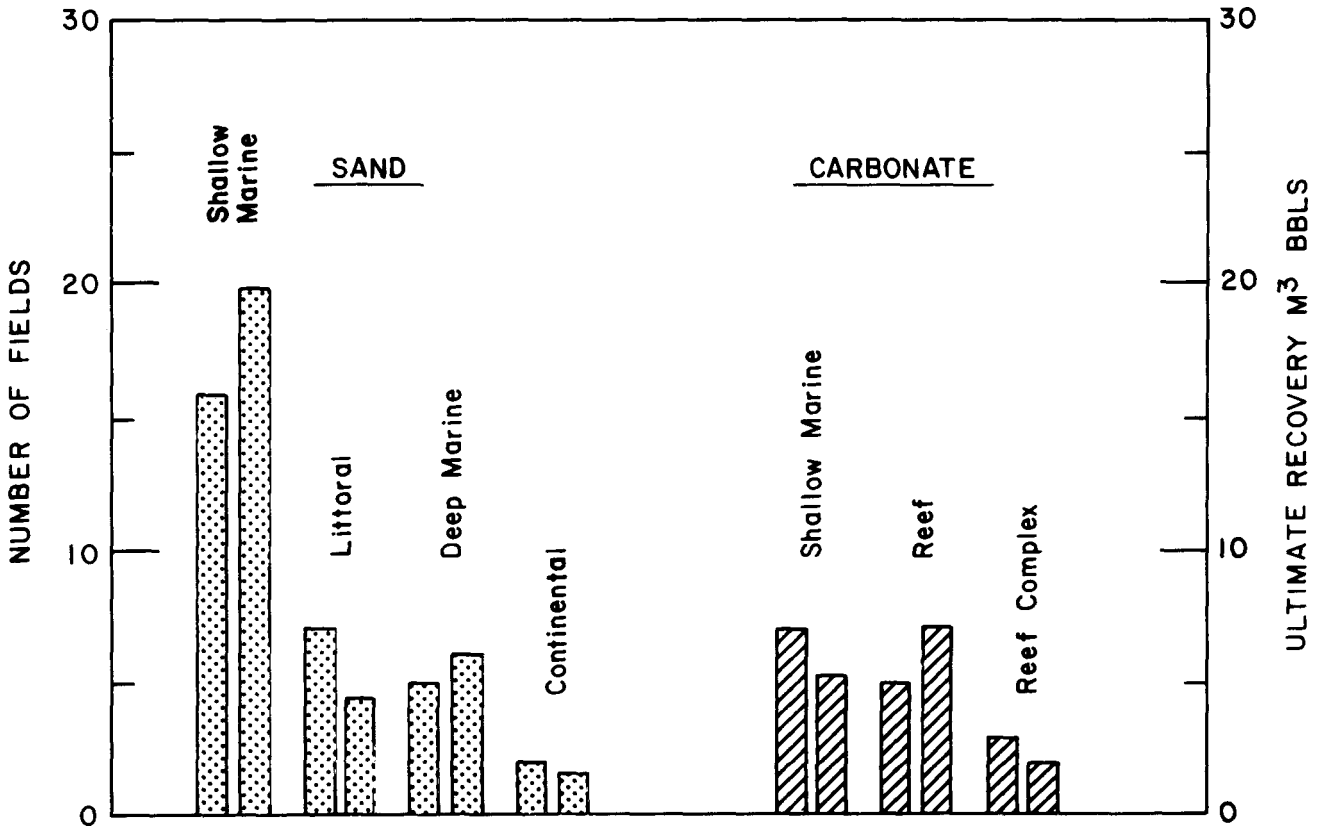


FIGURE 8. - Reservoir lithology by depositional environment of 45 North American giant oilfields. Note: Bars are paired: left-hand bar of each pair gives number of fields, right-hand bar gives ultimate recovery. After Moody et al., 1968.

# CHAPTER 4. RESERVOIR CHARACTERIZATION OF BELL CREEK FIELD

Barrier island reservoirs are prolific hydrocarbon producers in the United States, and they are more abundant than shelf ridge reservoirs. The shelf ridge candidate reservoir, Teapot Dome, is highly tectonized and unrepresentatively shallow; therefore, the Muddy formation in Bell Creek, (MT) field was selected for reservoir characterization research.

An integrated geological and engineering evaluation was conducted for the Upper Cretaceous Muddy formation barrier island sedimentary complex which is unconformably overlaid by valley fill deposits at Unit 'A' of Bell Creek field. Emphasis was on a 4-square mile area in the center of production Unit 'A' surrounding an enhanced oil recovery project from which 18 cores were sedimentologically interpreted. Extensive study of geologically analogous outcrops in north-east Wyoming provided valuable information for an improved characterization of the subsurface barrier island and genetically associated environments of deposition.

Few published geological models of ancient barriers contain sufficient detail to predict reservoir heterogeneities and explain variations of reservoir properties occurring at different scales. This study was made to provide such a model. The productive interval in Unit 'A' comprises several stacked upward-shallowing barrier island sandstones which are laterally confined by nonproductive valley infills on the basinward side and paralic facies on the landward side. Postbarrier erosion removed the top part of the barrier island sequence and significantly reduced the thickness of the best productive reservoir sandstones. Nonbarrier sediments generally have low permeability and contribute little to overall oil production.

Depositional, diagenetic, and structural heterogeneities of a variety of scales define the geometry, continuity, and petrophysical properties of flow units. Distribution of effective porosity, dominant grain size, sorting, horizontal permeability, anisotropy, and dominant clay type and content characterize the productive barrier island depositional facies. Changes of lateral continuity and thickness of flow units related to faults and erosional cuts were evaluated, and the influence of geological heterogeneities on fluid flow and production was studied. This chapter identifies the common geological properties of barrier island deposits which may be encountered in other reservoirs of this type; the unique geological properties which

differentiate barrier island systems from other environments; and the site-specific reservoir features.

The major features common to barrier island systems comprise stratigraphy of facies within individual sedimentary cycles, stacking of several sedimentary cycles, and postbarrier erosional valleys filled with continental and/or paralic facies. A unique feature of this system is the separation of reservoirs by shale-filled as well as productive channel cuts and genetic association with productive ebb and flood tidal deltas. The entire system is subjected to the unique early diagenesis resulting from exposure to the open marine, atmospheric, and brackish or hypersaline solutions. Among site-specific features affecting petrophysical properties and continuity of flow units, the most influential are diagenesis and tectonics.

In this research, the predictability of heterogeneities was evaluated, and the most predictable heterogeneities in the barrier island deposystem were identified.

The Muddy formation and the Bell Creek reservoir have been a target of extensive geological studies during the past two decades.[1-7] Major geological problems encountered in the Muddy formation of Bell Creek field and their influence on tertiary oil production have been compared with problems encountered in other formations and deposystems.[8]

The barrier island reservoir selected for detailed analysis in this study is located in Unit 'A' of Bell Creek field in Carter and Powder River counties, Montana, on the northeastern flank of the Powder River Basin (figs. 9 and 10). Bell Creek field consists of six hydraulically independent producing units 'A', 'B', 'C', 'D', 'E' and Ranch Creek. The largest and the most productive is Unit 'A'. Since 1976, two tertiary oil recovery pilot projects have been completed within the confines of Unit 'A'. The northernmost pilot (fig. 10) was less successful because of unanticipated geological complexity, whereas the southern pilot implemented through the DOE tertiary oil incentive program (TIP) was more successful because it was in a more homogeneous part of the field.[9-11]

This geologic and engineering study on the productivity of the Muddy formation was concentrated in the 4-square mile (10.4 square km) area (sections 22, 23, 26 and 27) of Unit 'A' located in T8S, R54E where the

tertiary incentive project (TIP) was implemented. However, core and log data were also used from adjacent areas in order to construct a broader geologic context. The data presented in this report are mostly from the tertiary incentive project (TIP) and surrounding area located in the south-central part of Unit 'A'.

This integrated geological/engineering study (fig. 11) is expected to improve predictions of flow patterns, distribution of residual oil saturation, and performance of various EOR operations. The study of this barrier island deposystem will not end with an analysis of Bell Creek field, rather the methodology used to improve an understanding of geologic limitations on production in this field will be incorporated as a "base line study" with which to compare and ultimately to improve predictive capabilities in other barrier island reservoirs.

The succession of lithology, sedimentary structures, and textures in the Muddy formation barrier island sandstones at Bell Creek field is similar to the succession observed in Holocene barrier island deposits near Galveston, Texas, and in other barrier island reservoirs.[12] The Muddy formation barrier differs from many described barriers in that it is at least in part a transgressive barrier. The characterization of Bell Creek field using abundant log, well test, production, and core data may shed light on heterogeneities encountered in similar barrier bar deposits. Emphasis in this report is on the synthesis of the reservoir core and outcrop geological and production information.

## Reservoir Case History

Bell Creek field is the northernmost major oil field in the Powder River Basin and has produced 125 million bbl of oil through 1987.[12] This field was discovered in June 1967. The field was developed rapidly on 40-acre spacing, and the primary production was primarily by the solution gas drive mechanism. The downdip sandstone developments indicated the presence of several aquifers; however, their effectiveness was limited. There were several gas wells in the field initially, but the gas accumulation was local, and primary performance indicated no significant gas-cap drive. The original oil-in-place (OOIP) for the field was calculated to be 242.9 MMSTB with an ultimate primary recovery of 48.4 MMSTB or 19.9% of the OOIP. Unit 'A'

accounts for approximately one-half of the oil-in-place at Bell Creek field. The rock and fluid properties and production data from Unit 'A' are summarized in table 17. The primary production from Unit 'A' was 22 MMSTB.[13]

Waterflooding of Unit 'A' was begun in August 1970. Linedrive waterflooding was initiated at the northwestern (downdip) edge of the unit. In 1978, an additional line of injectors was located in eastern sections of Unit 'A'. The injected water generally pushed the oil into the updip part of the barrier which interfingers with backbarrier and lagoonal facies. Waterflooding of Unit 'A' succeeded in recovering more than 35% of the OOIP. The total primary (20%) and secondary (35%) production exceeded 55% of the OOIP.[13]

In June 1976, a 160-acre, DOE cost-shared micellar-polymer pilot project was implemented in the watered-out, northern portion of the Unit 'A' reservoir. This project recovered 28% of the remaining 40 to 45% of the OOIP at the beginning of the tertiary preflush.[10]

In 1980, a second tertiary project was undertaken in Unit 'A'. This 179-acre micellar-polymer DOE tertiary incentive project (TIP) was initiated near the center of the Unit 'A' reservoir, in the watered-out portion of the linedrive waterflood about 3.6 miles (5.8 km) south of the first tertiary pilot. It consisted of 12 injector-centered, 20-acre, five-spot patterns, nine of which were chemical injectors. The other wells were designed for patterned waterflooding. The entire project was also surrounded by 18 water injection wells. It is estimated that the micellar-polymer TIP project recovered 39% of the remaining oil in place at the start of the preflush.

## Geological Setting

The Bell Creek oil reservoir produces from the Lower Cretaceous Muddy formation at an average depth of 4,500 ft (1,373 m). The Muddy formation dips westward toward the center of the Powder River Basin. The stratigraphic position of the Muddy (Newcastle) sandstones within the Lower Cretaceous suite of sediments in the region is presented in figure 12. The productive and non-productive sandstones of the Muddy formation are underlain by a thick series of marine shelf Skull Creek shale and are overlain by Shell Creek and Mowry shales. Outcrops analogous to the reservoir rocks are exposed in northeastern Wyoming on the flank of the Black Hills Uplift approximately 30 miles southeast of Bell Creek field (fig. 13).

A regional isopach map reveals a variation of the total thickness of the Muddy formation near Bell Creek field from less than 60 ft (18.3 m) to almost 100 ft (30.5 m).[3] However, the maximum documented thickness of stacked barrier island sandstones in Unit 'A' of Bell Creek field does not exceed 30 ft (9.2 m). The thickest preserved sequence of stacked barrier island sandstones which occur in outcrops (New Haven type of Newcastle-Muddy sandstone) was 28.4 ft (8.6 m).

According to the original engineering interpretation,[14] the production in Bell Creek field is from the "Zone 2" barrier bar sand of the Lower Cretaceous Muddy formation structurally interpreted as a gently dipping monocline. Faults were not reported in early studies. Bell Creek field consists of six separate units, each representing a distinct, stratigraphically trapped barrier bar sandstone reservoir. The original position of formation fluids (oil, gas, and brine) in the hydraulically isolated production units of Bell Creek field is diagramatically illustrated in figure 14.

Stratigraphic traps in production Unit 'A' are defined by updip pinchouts to the east (into lagoonal facies) and by multiple oil-water contacts along the western downdip direction.[1,15-16] Each waterflood unit has at least two sandstone intervals separated by a shale barrier.[10] The lower sand, designated in early reports as the Zone 2 sand, is the most favorable reservoir in Bell Creek field.[16-17] The flow capacity of the overlying Zone 1 sand is one-eighth that of the Zone 2 sand, and various studies have indicated that these zones have significantly different production characteristics.[15,17] The Zone 2 reservoir is a very fine- to fine-grained quartzose sandstone that is clean, moderately well sorted, and semiconsolidated. Clay and silt fractions range from 2 to 8 wt %.[1,17]

Detailed sedimentological analysis of existing cores (this study) showed that the Lower Cretaceous Muddy formation, which produces oil from Unit 'A' in Bell Creek field, is composed of two genetically different major sandstone reservoir units interpreted as (1) barrier islands (littoral marine bars) and (2) valley fills.

The Muddy formation barrier island and related environments of deposition (lagoon, estuary, tidal flat, tidal channel, valley fill, etc.) are underlain and overlain by marine shales: Skull Creek shale and Shell Creek/Mowry shale, respectively.

Hydrocarbon production in Unit 'A' of Bell Creek field is controlled by at least five geological factors:[1,18-19]

(1) stratigraphic relation of the barrier sandstones to the valley fill deposits;

(2) development and architecture of the barrier island facies
- internal distribution of facies within the dominant sedimentary cycle of the barrier island deposit, and
- stacking or overlap of subsequent fragmental cycles of barrier deposition;

(3) depth and width of erosional cuts into the top of barrier island and type of their infilling;

(4) distribution, type, and degree of importance of diagenesis (clay filling, compaction); and

(5) local faulting which appears to modify fluid flow patterns between individual wells and groups of wells.

## Depositional History of Muddy Formation in the Bell Creek Area

Paleogeographic and paleotectonic reconstructions of the Muddy formation[1-3,6,20-21] show the interrelationship between continental (delta channels and deltaic plain); brackish marine (lagoon, estuary, and tidal flat); and coastal marine (barrier islands) sedimentation in the northeastern Powder River Basin where Bell Creek field is located.

Characteristics common to Bell Creek and supportive of a barrier island interpretation are: (1) washover facies predominate in cores on the landward side of Bell Creek; (2) washover sandstones are interbedded with lagoonal mudstones, indicating contemporaneity of these facies; (3) foraminiferal species indicate less than normal marine salinities in lagoonal facies; underlying Skull Creek shales are normal marine; (4) shoreface sandstones are thin or absent in wells on the landward side of the field; (5) in analogous outcrops and cores in the field, foreshore and upper shoreface deposits locally are present above middle shoreface deposits; and (6) backshore deposits with landward (SE) flow directions occur above washover deposits in analogous outcrops. The barrier island model presented herein also requires that the barrier be, in part, transgressive over lagoonal deposits.

At least four different concepts regarding relationships between barrier-bar sandstones and valley fill deposits in the northeastern part of the Powder River Basin have been presented:

1. The barrier deposits lie stratigraphically above an unconformity which separates them from the underlying Skull Creek shale.[3-4]
2. The barrier islands and valley fills are in part synchronous.[2]
3. Valleys (and their subsequent fills) are incised into barrier island deposits and are stratigraphically younger. The barrier island deposits are generally related to the Skull Creek shale.[5]
4. Two periods of valley cut and fill have incised the barrier. The earlier valleys are distributed over a large portion of the barrier. The later channels were narrow and were filled primarily with marine shale.

In some cores from Unit 'A', the lower shoreface barrier island facies conformably overlie the marine Skull Creek shales. There are indications, however, that lagoonal deposits also underlie part of the barrier sandstones in the Bell Creek Unit 'A' area. Lagoonal deposits also occur below analogous barrier island sandstone outcrops exposed near New Haven, Wyoming, about 30 miles (48 km) southeast of Bell Creek field. Foraminiferal analysis indicates that the suite of foraminifers in samples interpreted sedimentologically as lagoonal deposits are distinct from those in the underlying Skull Creek marine shale. Incision of valley fills into the top of barrier deposits is, however, commonly observed in Bell Creek cores,[19] and strongly supports Weimer's concept (see number 3 above).

If the Bell Creek barriers were deposited on a tectonically uplifted high as suggested by Forgotson and Stark (1981),[20] and Weimer and Davies (1988),[7] it would be possible to accept at least two independent periods of valley erosion and fill during and after deposition of the barrier and associated deposits. In the Bell Creek area, therefore, the Muddy formation is a complicated system of barrier sandstones with channel cuts and subsequent valley fills unconformably superimposed. This model finds numerous recent analogues along the Texas Gulf Coast and elsewhere. Holocene patterns of barrier island sedimentation in the United States indicate that valley fill sediments, either underlying or incised into the tops of barrier islands (as is the case in Bell Creek), occur commonly together and should be considered a typical association of this type of near-shore sandstone deposits.

A question concerns the influence of eustacy on sandstone occurrence, erosional cuts, and infilling of valley incisions with non-marine sediments in the Bell Creek area. Figure 15 shows the correlation and the stratigraphic sequence of the Lower Cretaceous (Albian) periods of deposition and erosion with sea level high and low stands. Skull Creek shales and barrier island sandstones were deposited during $T_4$ and $T_5$ time intervals, respectively. When sea level dropped during $T_6$, the valleys incised into the barrier tops. The accumulation of valley fills took place during a subsequent sea level rise, marked $T_7$ on the diagram. Deposition of the Muddy formation, with an average total thickness in the study area of about 40 ft (12 m) as interpreted from logs, was completed during $T_7$. Further continuous deepening of the sea (transgression period) in the Bell Creek area resulted in enveloping the Muddy formation in Albian Shell Creek/Mowry shale and Cenomanian (Upper Cretaceous) Belle Fourche shale. The stacking of barrier island facies resulting from minor fluctuations of sea level during the $T_5$ period is discussed further in this report.

## Architecture and Depositional Characteristics of Barrier Island and Valley Fill Deposits -- Muddy Formation, Bell Creek Field

Depositional features commonly provide the predominant control of reservoir performance in EOR projects, including the Bell Creek.[8] Thus, construction of the geological model of the barrier island deposit at Bell Creek was initiated by interpreting the depositional framework. More detailed investigation of the stratigraphy, lithology, sedimentary and biogenic structure, grain size distribution, and cementation distribution of the different facies was based on examination of 26 completely or partially preserved cores from the northern part of Bell Creek field. Locations of cores used in this study are presented in figure 16. Eighteen of the cored wells were within the TIP area or in its immediate vicinity. Representative examples of verified core descriptions are presented in appendix B. Other verified core descriptions are available from NIPER's Open File[19] and are accessible at NIPER during office hours.

In addition to the subsurface cores, 21 outcrops representing a variety of analogous barrier island and valley fill facies were described and interpreted in the New Haven area, Wyoming (fig. 17). Some of the outcrops; e.g., no. 22

and 1/86, offered almost continuous lateral exposure for distances of thousands of feet -- distances that are comparable to interwell distances in Bell Creek field (600-1,320 ft). Representative outcrop profiles are included in appendix C. Other outcrop profiles used in this report are available on Open File,[19] accessible at NIPER during office hours. Four of the outcrops (nos. 22a, 22, 23, and 3/86) were extensively cored in order to characterize the petrophysical properties of barrier island facies (fig. 17). Photographs of selected outcrops illustrate general stratigraphy, characteristics of facies, and type of contacts (fig. 18).

The position of the four thoroughly studied reservoir sections in Unit 'A' of Bell Creek field have been related to adjacent environs of the subsurface barrier island depositional system. A resulting sketch map (fig. 19) of the inferred depositional setting in the 16-square mile area (40 $km^2$) was based on geological interpretation of available cores and logs from wells located at the edges of production Unit 'A', within production Units B, C, and D, and eastward and westward of them in nonproductive areas. Similar interpretations based on 21 documented outcrop profiles (fig. 20) have been made.

The purpose of this preliminary, broader scale interpretation was to allow comparison of the position of individual outcrops within the deposystem with the position of a similar, studied area in the subsurface. Both sketch maps (figs. 19 and 20) suggest general similarity in the distribution of barrier island and genetically associated facies within the subsurface and outcrop depositional systems. It was concluded that framework information regarding facies distribution, stacking pattern, and continuity of sandstone units could be applied from outcrops to the subsurface in Unit 'A'.

A typical stratigraphic cycle of major barrier island facies exhibited predictable characteristics (fig. 21). Dominant sedimentologic features of genetically related barrier island sandstone units are summarized in table 18. The reservoir quality and productivity potential of barrier-island sediments coincided with (1) patterns of vertical stacking of facies, (2) changes in thickness of barrier island deposits due to erosion, and (3) the range of permeability values in the productive facies (table 19). Stacking of several barrier cycles was recognized in Bell Creek cores; for example, in well W-16 where 21 ft (6.4 m) of shoreface and foreshore facies is underlain by 2.8 ft of (1.0 m) barrier-washover facies and overlain by another 2.4 ft

(0.8 m) of possible barrier-washover facies. For locations of production (P) wells, chemical injection (C) wells, and water injection (W) wells within the TIP area, see figure 22. The thickness of barrier island sandstones representing one or more overlapping sedimentary cycles is 32 ft (9.8 m).

In addition to local thickening resulting from the deposition of more than one barrier cycle, total barrier thickness is seldom preserved because of erosional processes during and after deposition of individual barrier island genetic packages. Aeolian deposits which commonly occur at the top of barrier island sequences (figs. 21 and 23) are most susceptible to erosion and are rarely preserved in ancient shoreline deposits. However, thin layers of dune deposits overlying foreshore facies were observed in some Bell Creek cores; for example, in well C-8 (fig. 10). Foreshore and shoreface (supratidal, intertidal, and subtidal) facies have a better preservation potential, and they comprise most of the producing barrier island sandstone interval. Stacking of foreshore and shoreface sequences results from relative sea level drop (regression) and sea level rise (transgression). During periods of regression, the older barrier island sequences were partially eroded, and during subsequent transgressions, additional barrier island sequences were deposited above remnants of the previous one. In a series of events subsequent to and independent of barrier building, valley cuts locally removed significant portions of the upper part of the barrier complex. Locally, only remnants of the original barriers were preserved, and in extreme cases the entire barrier was removed by erosional processes which cut near or below the base of the barrier (figs. 23 through 27). Significant erosional reduction of thickness of barrier island sediments (including local complete removal) strongly affects their storage capacity and transmissivity to fluids. Complete hydraulic disconnection of the reservoir may occur, as is the case between production Units 'A' and 'B' (figs. 24 and 26).

There are indications of two stages of valley incision during late Muddy deposition: an earlier stage affecting, in most cases, only barrier island deposits, and a later stage, affecting barrier island and valley fill deposits of the first stage.

A ribbon-like incision filled with very low-energy shaley/silty sediments of the second stage of erosion cuts down about 35 ft (10.7 m) into the Muddy deposits (almost to or below the base) and creates a steep and narrow (about

500 ft/153 m wide) barrier to hydraulic conductivity between Bell Creek production Units 'A' and 'B'. This barrier has been documented in several logs from dry holes within the barrier (fig. 24). Different pressure regimes and different positions of water-oil contacts on both sides of the barrier reflect effective isolation of the two production units (fig. 25). Thickness of sandstone units is similar on both sides of the deep incision suggesting that the position of the barrier-front is west of Unit 'A'. No significant faulting between production Units 'A' and 'B' is indicated. The gamma ray log signature above 4-ft-thick (1.2 m) remnants of eroded barrier island or inlet fill (fig. 26) suggests probable marine, shaley fill acting as a hydraulic barrier. The argillaceous material was deposited in a deep cut probably eroded by strong subsea currents. Superposition of the deep bifurcating cuts illustrated in figure 27 provides an analogy to the position of Unit 'A' in the Bell Creek system. The cut on the left-hand side corresponds to the western limit of production Unit 'A'. The cut on the right-hand side may belong to the valley system documented east of Unit 'A' in dry hole Superior Lornegan No. 1. (Core description is available on Open File at NIPER.)[19]

Valley cuts into the barrier island and into synsedimentary lagoonal deposits within production Unit 'A', east of the major hydraulic barrier, were filled with argillaceous fluvial (continental) and marine deposits of much lower reservoir quality before and during the transgressive stage. Several types of valley fills are shown in figure 23 and table 20.

Most of the valley fills depicted in Bell Creek cores from Unit 'A' are of non-marine origin, have very fine mean grain size (75 to 125 microns), and contain abundant clay matrix. X-ray diffraction analyses of barrier island and valley fill sandstone samples from the subsurface and from analogous outcrops reveal significantly different clay assemblages (table 21). In barrier island sandstones, kaolinite and illite predominate, and only traces of smectite are present, whereas smectite as well as kaolinite occur commonly in valley fill sandstones and siltstones. Clay types and percentages related to core-derived geologic profile and log responses of barrier island and valley fill facies identified in well W-7 are shown in figure 28.

Valley fill sandstone in Unit 'A' of Bell Creek field may immediately overlay the barrier island sandstone as in well W-7 (less common case) or may be separated by shaley or silty lagoonal, estuarine, or low-energy, inactive

alluvial silty channel deposits. (See figure 29 for photos of slabbed core.) The vertical sequence of valley fill sandstone on barrier sandstone suggests possible local hydraulic communication between the two most distinctive productive and potentially productive types of Muddy sandstones. Such a juxtaposition of facies differs from earlier models that present them as parts of the reservoir continuously separated by impermeable (lagoonal) facies without hydraulic communication. Predominant sedimentologic features of typical valley fill sandstones overlying the barrier island complex in Bell Creek are summarized in table 22.

Lithogenetic cross section A-A' (fig. 30), is parallel to the structural strike of the Muddy formation in a SW-NE direction. It was constructed to document the interrelationship between barrier island and valley fill deposits along the northwest side of the TIP area in sections 27, 22, and 23. Gamma ray, SP, and resistivity wireline log signatures from 16 wells and sedimentologic core descriptions from six wells were used for geological correlation of the major lithogenetic units. (The log responses were geologically calibrated in several cored wells in which genetic units had been identified with a possible error of ±0.5 ft/0.2 m). The calibration included major facies changes, observed unconformities, and comparison of subsurface gamma ray log response to core gamma ray log responses (where available).

The base of the barrier island sandstone facies conformably or unconformably overlies the Skull Creek marine shale and is associated with the characteristic change of log signature that defines the base of the Muddy formation. Both the top and the base of the Muddy formation can be identified on logs within 2 ft (0.6 m) without core control.

The top of barrier island sandstones in cores consists of a disconformity between barrier sandstones and overlying valley fill deposits. This contact is not always readily identifiable on logs although the resistivity log commonly shows an increase in conductivity upward within the valley fill deposits in contrast to the usually low-conductive (oil-rich) barrier island complex. Separation of these two genetic units is almost impossible on the basis of a SP log alone. A gamma ray log shows more detailed lithologic variations, and sonic logs help to locate the contact based on porosity changes.

Resistivity log profiles in well W-10 (fig. 30) show similar responses in barrier island and overlying sandstones, indicating the productivity potential of the "Zone 1" sandstone. The porosity log, however, indicates a significant decrease of average porosity in the valley fill section. In this well, the change in porosity allows separation of the two lithogenetic units.

Cross-section A-A' runs parallel to the general elongation of the barrier and shows only a 20% variation of barrier island thickness (table 23).

Total thickness of the Muddy formation varies from 42.5 to 49.0 ft (12.9 to 14.9 m). The slight increases in barrier thicknesses are locally compensated by decreases in total valley fill thickness. The average thickness of valley fill sandstones overlying the barrier sandstones is 8 ft (2.4 m), but variations in thickness may reach 65% with significantly lower values toward the northeast. The top part of the Muddy formation along the trend of the cross section consists primarily of silty and clayey valley fill facies. Identification and distribution of productive facies within the Muddy infill can be determined only in wells with core control. Inference of lateral continuity and vertical distribution of individual facies in non-cored wells requires further work and a more comprehensive method of log analysis.

Relief on the disconformity at the top of the barrier is minimal in cross-section A-A' (fig. 30). However, small-scale, deeper incisions that locally remove more of the barrier island sequence cannot be entirely ruled out between interpreted wells. In Unit 'A', at least two scales and geometries of valley incisions into the productive barrier island sandstones have been documented: a narrow, steep, and deep type (figs. 23 and 24) and a broad type with only moderate relief (fig. 30).

Barrier island and related nonbarrier facies documented in Bell Creek cores can be grouped, from an engineering point of view, into three classes according to the decreasing turbulence of the environment of deposition (table 20).

Class 'A' sediments, when not severely affected by diagenesis, have the best reservoir properties and have permeabilities in the range of hundreds and thousands of millidarcies, whereas in class 'B' deposits, permeabilities rarely exceed hundreds of millidarcies. Nonproductive sediments of class 'C' usually have low permeabilities ranging from near zero to tens of millidarcies. The lateral extent and continuity of facies of the three

classes can be predicted from the depositional models. In the central part (TIP pilot area) of Unit 'A' in Bell Creek field, a fair quality class 'B' and mostly nonproductive facies class 'C' are significantly thinner than the high-quality upper shoreface and foreshore facies (class 'A'). The barrier core (central portion of the barrier) has better reservoir quality potential than the distal part of the barrier (back-barrier) where thinner and lower energy facies intercolate with nonproductive members of adjacent depositional environments. Thus, oil productivity in the "barrier core" should be directly proportional to the total thickness of barrier deposits because class 'A' and higher energy class 'B' sediments predominate in the geological sequence. Barrier deposits may be conformably underlain by marine class 'C' Skull Creek shale or be disconformably underlain by lagoonal siltstones. The barrier facies are locally unconformably overlain by continental brackish and shallow marine valley fills (class 'B' and 'C') and/or marine deposits (class 'C'), as shown in figure 23 and table 24.

The productivity of individual wells and the water and chemical injectivities within the barrier core will also depend on spatial variation in site-specific transmissivity and hydraulic connectivity between groups of wells resulting from diagenetic alterations (addressed further in this report) and on local faulting. Engineering and production data as well as core, log, and outcrop interpretations indicate significant geological complexities in the study area of Bell Creek field.

## Structural Characteristics

The Muddy formation in Unit 'A' of Bell Creek field generally strikes in a NE-SW direction and dips northwest at an average 100 ft/mile (19 m/km). Structural analyses reveal several previously unrecognized faults in the TIP and adjacent areas. The faults commonly strike 50° (N50E) and 140° (N40W) (fig. 31).

The faults are discontinuous and are generally parallel to the NW and NE trending lineaments recognized throughout the Powder River Basin.[6,21] The direction of principal stress in the area near the Wyoming, Montana, and South Dakota border is 50° (NE-SW), according to the regional stresses mapped in the United States[22] (fig. 32). Major linear features (fig. 33) mapped from Lansat imagery in Highlight field, located south of Bell Creek field, reveal azimuths

of 50°-55° and 145°-150°.[23] The similarity of directions obtained from a variety of sources and from different locations in the northeastern part of the Powder River Basin is striking and strongly suggests that the structural framework is common for the entire area.

The most common vertical displacements of the postdepositional faults (which cut both the base and the top of the Muddy formation) in Bell Creek field are from 10 to 20 ft (3 to 6 m), although displacements greater than 40 ft were also identified in Sec. 27 (fig. 34). Separation of the barrier island reservoir into small tectonic blocks has highly influenced the continuity of sedimentary and diagenetically controlled flow units and has resulted in locally anomalous sweep efficiencies in numerous five-spot EOR patterns. The ratio of vertical displacement to the net pay varies from 0.5 to 1.5, indicating the possibility of local restriction or disconnection of fluid flow. Within the TIP area, 0.5- to 1.0-square mile (0.6 to 2.6 $km^2$) gently tilted blocks include several wells in which the hydraulic communication of flow units has not been complicated by additional faulting (fig. 31).

Natural fractures were not obvious in the 16 examined cores from the TIP area, but their presence cannot be entirely excluded because many of the cores were incomplete.

Field observations in New Haven outcrops[19] and elsewhere in analogous sediments indicate that the density of natural fractures decreases rapidly outside the fault plane in "soft," less-well-cemented sediments. The width of heavily fractured zones in "soft sediments" should not exceed 100 to 200 ft (30 to 60 m) in this case. In brittle, more cemented layers, however, the density of tectonic fractures increases, and the fractured zone associated with faulting may be much wider.

The average distance between wells in the TIP area is about 600 ft (183 m), and fractures related to faulting may not be detected in wells drilled a distance greater than 200 to 300 ft (60 to 90 m) from a fault zone.

Downthrown tectonic blocks would be expected to produce less oil but high total fluids because of the natural tendency of oil to concentrate in structurally high wells. Well P-14 (fig. 31), which is structurally low due to faulting, produced 76,000 bbl of oil and more than 2.5 million bbl of total

fluids during the 1980-87 period. Adjacent well P-11, located in an uplifted tectonic block, produced 40% more oil and 35% less total fluids during the same period.

The overall influence of structural features on primary, secondary, and tertiary production in the TIP area of Bell Creek field are summarized in table 25. The documented faulting affected very little the primary and secondary production in the study area but had moderate to high effect on tertiary production.[13]

## Diagenesis of Barrier Island Facies

Thin section analysis was based on samples from cored wells containing barrier island facies, most of which were from the TIP area of Bell Creek field, Unit 'A'. The major diagenetic phases within barrier island sandstones have been identified primarily from core samples in the TIP area, and their relative timing has been established (table 26). The following discussion is based on samples from the productive portions of the barrier bar system which include shoreface, foreshore, and washover facies. The microscopic aspects of these facies are illustrated in figures 36 through 41. The effects of early diagenesis, particularly leaching, are of significant importance with respect to modification of the pore space in the Bell Creek reservoir. Virtually all subsequent diagenetic phases affected the evolution of the reservoir rocks in a potentially negative sense.

## Mineralogy of Barrier Island Sandstones

Foreshore, shoreface, and washover facies have similar petrographic characteristics, but lower shoreface and some washover samples tend to contain more clay cement and matrix. These sandstones comprise moderately to well sorted, very-fine to fine-grained quartzarenite and subarkose. When the skeletal component is recalculated to 100% and plotted on a quartz-feldspar-rock fragment diagram (fig. 42), the quartz-rich nature of these producing sandstones becomes evident. Individual barrier facies cannot be distinguished by either skeletal framework mineralogy or clay content alone.

X-ray diffraction analysis of barrier island and valley fill sandstone samples from the subsurface and analogous outcrops confirmed the high quartz content and revealed significant differentiation of clay assemblages (table

21). Within the barrier island sandstones the clays exhibit a 2:1 ratio between kaolinite and illite and comprise less than 15% by weight. In valley fill sandstones and mudstones, smectite and kaolinite dominate the clay assemblage.

In a regional study, Stone (1972)[3] concluded that the clays in shales are dominantly illite and montmorillonite (smectite group), whereas clays in sandstones are almost exclusively kaolinite.

Most of the clay in the Bell Creek barrier island reservoir facies is diagenetic kaolinite which was derived from the decomposition of feldspars and other less-stable grains such as rock fragments. Chert is the most common surviving lithic fragment, and K-feldspars are virtually the only type of feldspar represented. Based on thin section studies, feldspars generally account for no more than 2 to 3% of total rock volume.

The diagenetic phases and comments about their relative timing (paragenesis) are as follows:

### Early Leaching

Leaching occurred very early in the paragenetic sequence. Feldspars (fig. 43) and chert show the most obvious effects of leaching. All degrees of feldspar corrosion and polycrystalline quartz disassociation are associated with the collapse of surviving silt-size remnants; for example, well W-10 (fig. 43 C). Leached chert (fig. 43 D) and polycrystalline quartz are microporous. Sedimentary rock fragments were leached from most samples throughout the field. The leaching of unstable grains, particularly sedimentary rock fragments, is believed to be responsible for the creation of numerous oversized pores (fig. 45). Oversized pores are diagnostic of widespread leaching throughout the barrier island sandstones. Sandstones that might not otherwise be highly porous contain scattered oversized pores, some of which are partitioned by clay bridges (fig. 44) or contain grain remnants. In such samples, the feldspars are generally corroded, and remnants are not abundant. Clean, relatively uncompacted, poorly cemented sandstone which contains oversize pores or other evidence of secondary porosity may locally have a permeability greater than 5 darcies (fig. 46).

Substantial early leaching of the barrier island facies was controlled by infiltrating fresh water and the establishment of one or more meteoric lenses. Because the barrier island is surrounded by marine or marine-to-brackish waters, the dominant source of meteoric waters must have been atmospheric. In addition to the leaching of unstable terrigenous grains, these oxygenated, slightly acidic atmospheric waters would have been undersaturated with respect to calcite and aragonite. Therefore, any marine molluscan fauna in the barrier island facies would have been leached. Additional meteoric phreatic or brackish waters could have entered the barrier island system during subsequent valley cut-and-fill episodes.

The meteoric lens migrated along with the barrier island system through progradational and transgression cycles. The meteoric lens and associated mixing zone created a very dynamic diagenetic system. The diagenetically active upper part of the meteoric lens may have migrated through the same sediments more than once very early in their history because of the fluctuations of sea level required to form stacked barriers. Repeated exposure to meteoric waters may, in part, explain the high porosity and anomalously high permeability within the reservoir facies throughout much of the field.

The net result of early leaching was twofold: first, abundant secondary (interparticle and intraparticle) porosity was created, enhancing the fluid storage capacity of the reservoir facies; secondly, leaching resulted in kaolinization of some feldspars. When the kaolinized skeletal grains were compacted, some clays collapsed into pore throat regions (fig. 44) and thereby slightly reduced permeability. Kaolinized feldspars also explain the small amount of diagenetically early (precompaction and pre-quartz overgrowth) clay cement.

Existing porosity within the better portions of reservoir facies is commonly about 30%; associated permeability generally ranges from 1 to 3 darcies or greater. These permeability values are greater than those expected from reservoir sandstones of this age at this depth. Early leaching must, therefore, have been severe, and its effects have been well preserved and have greatly influenced the porosity and permeability of this reservoir.

## Siderite

Siderite ($FeCO_3$) occurs early in the paragenetic sequence. Interpenetrating grain margins were found to be present in a few thin sections (figs. 45 and 47 A); therefore, siderite precipitated prior to compaction. Siderite is not abundant in cores from the barrier island facies and generally does not occur where mineralogical cross-cutting relationships could establish its exact timing. Siderite locally replaced matrix and rock fragments or precipitated as a void-filling cement shortly after the first (significant) stage of leaching.

As slightly acidic meteoric water migrated through the barrier sandstones leaching unstable grains, its pH would have increased, and it may have locally become stagnant (negative Eh). Moderately low Eh ($\simeq$0.1) meteoric waters carrying $Fe^{+2}$ then contacted marine or brackish pore waters from adjacent facies which were of equal or lower Eh and questionably higher pH. Abundant organic matter within marine or lagoonal sandstones would have ensured that a reducing environment was maintained within these sediments. If sufficient $Fe^{+2}$ and $HCO_3^-$ or $CO_3^{-2}$ were available, the mixing with waters of equal or lower Eh and higher pH (>7) would have caused local siderite precipitation. Krauskopf (1967)[24] also noted that siderite forms within partly consolidated sediments from groundwater solutions whose dissolved oxygen content has been depleted. A terrestrial-fluvial source of ferrous iron is not required because of the small amount of siderite precipitated within the barrier sandstone facies. Percolating meteoric waters that leached unstable grains within the barrier sandstones may have provided the small amounts of ferrous iron.

## Compaction

As the barrier island sandstones were buried by thick shales, overburden pressures caused physical compaction. The major results of early compaction included grain reorientation and collapse of surviving remnants from previously leached unstable grains. As subsidence continued, overburden pressure increased, and a chemical compaction phase occurred. The net result of chemical compaction by a solution-reprecipitation process was to increase the breadth of grain contacts and the interpenetration of grains to a moderate extent (fig. 47 B). Grain shape eccentricity was enhanced by compaction, and

grain sphericity decreased. Compaction and quartz, calcite, and clay cements produced a rock capable of withstanding greater overburden pressures, and further compaction was stopped or was severely retarded.

In well W-16 (fig. 48), the increase in clay content of the foreshore facies from less than 1 to 4% over an interval of 1 ft (0.3 m) at depths of 4,312 and 4,311 ft (1,315.2 and 1,314.9 m) is accompanied by an unexpected significant increase in permeability from 269 to 1,935 md. Greater permeability at 4,311 ft (1,314.9 m) is due to relative changes in compaction. Increased compaction was observed in thin sections to result in increased packing and smaller pores. Samples at 4,308 (1,313.9 m) and 4,312 ft (1,315.2 m) are highly compacted resulting in lower permeability (197, 269 md) and porosity (19.7, 20.2%) values, whereas the sample at 4,311 ft (1,314.9 m) is undercompacted and has higher permeability (1,935 md) and porosity (26.7%) relative to the samples above (4,308 ft/1,313.9 m) and below (4,312 ft/1,315.2 m). These observations indicate that although changes in percentage of total clay generally reflect permeability trends and indicate changes in depositional facies (low "k" values in lagoonal and lower shoreface facies, higher "k" values in upper shoreface and foreshore facies), compaction may be locally the most important diagenetic heterogeneity affecting permeability. It follows that in portions of the reservoir affected by diagenesis, permeability may not necessarily reflect depositional facies because the diagenetic overprint (authigenic clay content and compaction) may be dominant.

### Silica Overgrowths

Diagenetic silica occurs as syntaxial overgrowths on relatively few detrital grains. Fine "dust rims" of clay (fig. 47B) rarely separate the host grains from authigenic cements. Overgrowths almost never form on all sides of detrital grains and are rarely euhedral (fig. 49). Because of this, it is frequently difficult to identify the overgrowths in thin sections. Nevertheless, silica cement, comprising no more than 2% of the rock, provided sufficient reinforcement to halt compaction of the sandstone. The presence of sutured grain boundaries and the anhedral to subhedral nature of most overgrowths suggest that silica was derived by local solution reprecipitation

rather than migrating diagenetic solutions. In addition, the transformation of feldspars to kaolinite during the previous leaching phase liberated excess silica which may also have been used to form secondary quartz overgrowths.

Almon and Davies (1979)[4] state that some kaolinite booklets in Bell Creek sandstones are partly enclosed by quartz overgrowths implying that formation of authigenic kaolinite preceeded silica cementation. Unfortunately, Almon and Davies did not provide well or depth information, and their example may be from valley filling sediments rather than the barrier sandstones. Only rarely were small amounts of kaolinite that were enveloped within quartz cement observed. The onset of quartz overgrowth cementation preceeded clay precipitation, but because clays are trapped within younger portions of some quartz overgrowths, some clay precipitation occurred concurrent with later stages of overgrowth formation.

In well C-8 (4,372.6 ft/1,333.6 m - upper or middle shoreface) an anhedral, 30-micron-thick quartz overgrowth partly encircled a detrital quartz grain. A faint submicron-size "dust trail" delimits the contact between host and overgrowth. Approximately half of the overgrowth adjacent to the detrital quartz grain is inclusion-free; however, the outer portion of the overgrowth contains numerous inclusions, some of which are clay inclusions. In most cases, however, quartz overgrowths clearly formed before clay precipitated (figs. 45 and 50). Two major stages of clay formation were indicated: first, a very early one associated with leaching of unstable grains, particularly feldspars; secondly, a more important later stage that generally postdated compaction and silica cementation. Late-stage clays will be discussed in a following section.

### Calcite Cementation

Calcite comprises medium-to-coarse crystalline, subhedral to euhedral poikilotopic pore-filling cement (fig. 51A). It also replaces a small amount of the margins of detrital grains. Compaction can be shown to predate calcite (well C-6, 4,423.5 ft/1,349.2 m) based on the packing of the detrital grains adjacent to the calcite and by the presence of calcite between the bent, splayed-open books of compacted micas. Because clay is generally not present within calcite-cemented pores, it is thought that calcite probably preceded the second and most important stage of clay precipitation.

Although calcite cement is only sporadically present in cores from the reservoir, where it does occur it has a strong negative effect on porosity and permeability. Calcite does not exceed 20% in any thin sections, but when more than 2 to 5% calcite is present, permeability is generally less than a few 10's of millidarcies.

Calcite in nodules and calcite-cemented beds could have been derived from the dissolution of a marine molluscan fauna included in Muddy sediments. No traces of shells are preserved in the cores, nor are broken or abraided fragments preserved in thin sections. Given the marginal marine setting at the time of deposition, it seems likely that such a fauna must have existed. Percolating meteoric waters could have easily dissolved the aragonitic shells and later reprecipitated the $CaCO_3$ as calcite cement. The trigger for calcite cementation must be conjectural on the basis of the evidence but could have included deoxygenation, a shift toward more alkaline pH conditions, fluid temperature changes, or other factors which cause supersaturation with respect to calcite.

### Late-Stage Leaching

A diagenetic late-stage leaching event is indicated by at least three lines of evidence: first, the outer margins of calcite cement are locally corroded; secondly, poikilotopic calcite cement-filled primary pore spaces surround secondary pores that contain remnants of feldspar. Such a physical configuration indicates that calcite was present before corrosion of the detrital grain. The third line of evidence includes the presence of a compacted siliceous framework of grains around oversize pores; for example, well C-8, 4,370.5 ft (1,319.9 m). In thin sections with a compacted framework, compacted sedimentary rock fragments (pseudomatrix) and oversize pores are the same size (fig. 45), and both are significantly larger than the other detrital components of the sandstone. Undoubtedly, portions of the pseudomatrix that survived compaction were subsequently leached to create the oversize pores. The unstable fabric that exists today (oversize pores in a compacted rock) could not exist unless some leaching postdated compaction.

In addition, thick quartz overgrowths with wavy or irregular margins suggest (but do not prove) that postcompaction leaching removed neighboring grains from a well-fitted fabric.

Late-stage leaching can have two possible sources: first, decarboxylation of organic matter and migration of organic acids before hydrocarbon entrapment; or secondly, re-establishment of a fresh-water (meteoric) lens. The volume of secondary porosity created by the decarboxylation-organic acid process is generally considered small.[25] We infer that the Bell Creek reservoir has a significant amount of late-stage leaching. In this example, the late-stage leaching documented here may reflect the effect of two (or more) meteoric leaching phases within the same rocks.

## Clay Cement

Clay cement found within the barrier island sandstones is dominantly kaolinite with minor amounts of illite (table 21 and fig. 28). These observations are in agreement with those of Almon and Davies (1979)[4] who classified Muddy formation sandstones from Bell Creek reservoir as belonging to a diagenetic zone characterized by authigenic kaolinite and quartz overgrowths. The secondary, authigenic nature of kaolinite cement was established by textural indicators[26] observed both through petrographic examination (concentric color zonation; monomineralic nature; radial crystal arrangement) and with scanning electron microscopy (coarse, well crystalline morphology, see fig. 40B).

Based on petrographic evidence, clay cement in Unit 'A' of Bell Creek field precipitated from diagenetic fluids primarily after compaction and precipitation of siliceous overgrowths. Based on analysis completed at this time, we infer that calcite cementation and late-stage leaching predate the dominant phase of clay cement precipitation.

Kaolinite cement commonly forms 5- to 30-micron-thick coatings on detrital grains (figure 51B). Individual crystals are often oriented perpendicular to the surface of the substrate and thereby produce a radial texture. Less commonly pore-filling by clay cement is microporous and monomineralic and consists of coarsely crystalline masses. Clay cements vary in abundance throughout the TIP area from 0 to more than 15%. Middle to upper shoreface and foreshore facies commonly contain only traces of clay cement; however, areal and vertical heterogeneity of clay content is great. Although the amount of clay in these facies is generally low and corresponding permeabilities may be high (several darcies), the presence of only 1 to 2%

clay cement concentrated in pore throat regions can be shown to drastically reduce permeability. For example, in well C-6 the foreshore sample at 4,411.7 ft (1,345 m) has 1% clay cement and 1,799 md permeability. In contrast, the foreshore sample at 4,414.5 ft (1,346 m) contains 3% clay cement, and permeability has been reduced to 1,113 md. Other than for the small increase in clay cement, the petrographic characteristics of these two samples are very similiar. The decrease in permeability caused by a small increase in clay cement is further accentuated by even slight changes in compaction. In well C-8, for example, an increase of 2% clay cement in samples from 4,370.5 ft (1,333 m), which is uncompacted, and 4372.6 ft (1,333.6 m), which is slightly compacted, is associated with a decrease in permeability from 5,498 to 919 md. Because of the ability for such a small amount of diagenetic clay to readily alter permeability, authigenic clay (cement) is considered the most crucial limiting diagenetic factor with regard to well performance.

## Oil Migration and Entrapment

Oil staining in thin sections is not common, possibly because of the method used for thin section preparation. In the few samples with entrapped oil droplets, the oil appears to stain clay within primary and secondary pores. We have not yet determined whether oil droplets are present as fluid inclusions in various early cements; however, because much of the microporosity between diagenetic clay particles contains oil, we know that the oil was the last phase to enter the reservoir rocks. This relationship agrees with the relative timing of oil migration and entrapment in other reservoirs where it has been shown that at the time of oil entrapment diagenesis virtually ceases.[27]

## Distribution of Clays

As indicated by Almon & Davies (1979),[4] diagenesis in an open system may produce multiple diagenetic zones that cut across stratigraphic boundaries. Because the direction of fluid movement (the geohydrology) is a critical factor in such a system, permeability at the time of diagenetic alteration should be a major control of diagenetic mineral occurrence. It follows that the distribution of particular diagenetic phases may approximate the distribution of permeability within a sandstone body. Maps of clay

distribution in the TIP area were constructed to determine whether a relationship exists between diagenesis and petrophysical parameters or production performance.

The distribution of diagenetic clay within middle and upper shoreface and foreshore facies of the barrier island section (fig. 52) is, in part, controlled by the pattern of faults. Partial fault control of diagenetic clay is significant because faulting may have provided pathways for diagenetic fluids. Secondly, within the unfaulted eastern portion of the TIP area, diagenetic clay is least abundant.

The amount of matrix (interstitial fines deposited at the time of deposition -- dominantly clays in Bell Creek field) within the middle and upper shoreface and foreshore facies is generally very low except in the area around well W-11 (fig. 53). An increase of matrix in this area reflects increased heterogeneity in the lithology of the reservoir sandstone.

The distribution of total clay (fig. 54) in middle and upper shoreface and foreshore facies is similar to the distribution of diagenetic clay (fig. 52) and indicates the dominant influence of cement, rather than matrix over most of the TIP area. By comparing the maps for diagenetic clay (fig. 52) and for matrix clay (fig. 53) one can determine that the high total clay content near well W-11 is due to increased matrix. In addition, the total clay map is quite similar to the distribution of average horizontal air permeability for the study area. It is similar to the residual oil saturation distribution obtained from routine core analysis, and it is somewhat similar to the tertiary cumulative production distribution. Based on these similarities, it is evident that clay distribution has had a significant influence on primary, secondary, and tertiary production patterns.

The distribution of the maximum amount of matrix within any stratigraphic level of the barrier island facies is shown in figure 55. The general northeast-southwest orientation of the "cleanest" (best) part of the TIP area sandstones is evident. The increasing matrix toward the southeast and toward the northwest shows the greater influence of nonbarrier interbeds along the margins of barrier facies in those directions. The maximum matrix in the barrier facies distribution (fig. 55) is similar to that of diagenetic and total clay maps; however, the area of "best sands" is shifted slightly westward in the maximum matrix in barrier map. The map of maximum matrix in

barrier island facies distribution (fig. 55) is comparable with the tertiary cumulative production map (fig. 97) and again emphasizes the significant effect that clays had on the micellar-polymer pilot project.

## Petrophysical Properties

### Distribution of Average Porosity, Average Permeability, and Net Pay

The net pay of Unit 'A' of Bell Creek field was determined from detailed core descriptions, porosities, permeabilities, and wireline logs. Values of 50 md permeability and 5% oil saturation cutoff in conjunction with information from lithologic and diagenetic core descriptions and conventional logs such as gamma, spontaneous potential, electrical resistivity, and core gamma logs were used for determination of net pay. Zones with permeability lower than 50 md did not contribute to overall transmissivity. Net pay greater than 20 ft (6.1 m) occurred mainly in Sec. 22 and the northern and western portion of Sec. 27 as well as the northwestern corners of sections 23 and 26 (fig. 56). The highest net pay values (26 ft/7.9 m +) were determined for the area where the barrier island is thickest; net pay and barrier sandstones thin toward the east on the lagoonal side of the barrier.

Average core porosities, and average horizontal air permeability data from zones I and II were mapped and are shown in figures 57 and 58. Core plug porosities and horizontal air permeabilities have the highest values in a north-south direction in the western portion of Sec. 23 and the northeastern quarter of Sec. 26. Higher porosities and air permeabilities were also found in the western portion of sections 22 and 27 extending westward into the adjacent sections. Higher average porosities and permeabilities result from the presence of thicker and less-clay-cemented foreshore and upper shoreface facies that have superior reservoir properties.

An obvious trend exists between the natural log of air permeability and porosity data (fig. 59). A comparison of reservoir and outcrop $k/\phi$ scatter plots indicates parallel but offset trends for data from the same facies (fig. 60) because subsurface samples have slightly lower porosities. The similarity of $k/\phi$ scatter-plot trends suggests that subareal exposure of outcrop rocks did not significantly alter petrophysical properties from those rocks in the subsurface. This finding offers further possibility to applying laterally continuous outcrop data to interwell areas in the Bell Creek reservoir.

Porosity and permeability related to modal grain size and sorting for individual facies and environments of deposition are exemplified for wells W-16 (table 27) and 26-3 (C-1) (table 28).

Relatively low-permeability sediments prevail in most valley infillings at Bell Creek. An example is found in well 26-7, 4,547 ft (1,386 m) (fig. 61) where brackish marine to continental facies overlie a major unconformity. The low ratio of vertical to horizontal permeability (kv/kh = 0.3 to 0.6) is characteristic for valley fills overlying the most productive barrier island facies that have a kv/kh ratio of about 0.7 for the upper and middle shoreface and about 1.0 for foreshore facies (fig. 61). These numbers indicate a tendency for retardation of vertical fluid displacement within the valley fill deposits. Also, because of similar log characteristics and comparable horizontal permeability values, the upper shoreface and foreshore barrier island facies have been characterized, to date, as one flow unit. The kv/kh ratio in well 26-7 (fig. 61) indicates, however, significant differences in the flow potential of these two facies. Portions of the barrier immediately underlying the unconformity at the base of the valley fills are at least locally strongly affected by diagenetic processes.

Limited data from permeability measurements conducted using air, brine, and distilled water on samples covering a large permeability range (20 to 4,500 md) show that absolute air permeabilities of the rocks examined do not differ significantly from brine or distilled water permeabilities.[13] X-ray diffraction analysis of rock samples showed that expandable clay is generally absent from barrier island sandstones in the area surrounding Unit 'A'. A similar conclusion was indicated by normal and reverse flow tests conducted on a few core samples; therefore, air permeability data provided good estimates of absolute brine permeabilities.

Maps of reservoir storage capacity and fluids transmissivities were constructed from data on core porosities, air permeabilities, and net pay (figs. 62 and 63). The areal distribution of average porosities was also calculated based on density logs. Density-log-derived porosities were higher than core porosity values in the western and southeastern portions of Unit 'A'. Porosity derived from density logs was generally 4% lower than the porosity determined from core measurements. This cannot be explained by the possible occurrence of damage to dispersed illite clay in the cores during the

cleaning process or difficulties in measuring porosities of friable rocks such as those found in Unit 'A'. Similar contrasts in porosity values have been identified in cores relatively free from clay as well as in well-cemented cores; therefore, handling was not critically responsible for differences between log-derived and core-derived porosity values. Removal of the net confining stress of more than 3,000 psi may account for such a large contrast because a pore volume compressibility close to $40 \times 10^{-6}$ vol/vol/psi was found in pressure-transient analysis between wells C-4 and P-11, and C-4 and P-12.

## Vertical Distribution of Permeability

Available core air permeability data were used to construct a map (fig. 64) showing the distribution of Dykstra-Parsons coefficients (D-P) of vertical permeability variations of the barrier sandstone in the study area. The Dykstra-Parsons plots for a few wells (mainly in the periphery of the study area) were rejected because permeability distributions are obviously not log normal, and in a few others some discretion was necessary in drawing the best straight-line fit. The map, nevertheless, reflects the general trend in the vertical distribution of permeability of the barrier island deposit.

Figure 64 shows that the central part of the bar deposit and the area slightly east of it are the most homogeneous (low Dykstra-Parsons values), and the area immediately southwest of the bar axis is the most heterogeneous because of large-scale permeability stratification. The area northwest of section 22 is again relatively more homogeneous.

## Distribution of Geometric Means of Permeability

Another way to obtain an overall idea about the general permeability distribution in the sandstone deposit is to plot the geometric means of air permeabilities from core measurements (fig. 65).

This map indicates that the highest geometric mean permeabilities also trend in a northeasterly direction in the central part of the study area, in the direction of the depositional strike. The area of highest mean permeabilities also coincides with areas where the sands are the cleanest (fig. 66).

Although no reliable method to obtain permeability information from log data is yet available, the crossplots of core air permeability and porosity data from the study area gave a strong correlation except in heavily cemented areas where the relationship becomes less clear. This suggests that a good estimate of permeabilities in most parts of the study area may be obtained from correlation with porosity data, an accurate estimation of which is available from interpretations of density logs.

## Wireline Log Analysis for Formation Evaluation

### Facies Analysis

The producing Muddy formation in Bell Creek field is composed of two genetically different systems: barrier island and nonbarrier sediments (marine or nonmarine valley fill sediments). Usually, the petrophysical properties of each system are different (fig. 67), and a method to distinguish the two sandstones on logs is needed for analysis of fluid production characteristics of the Muddy sandstone. A method is also needed to distinguish, as far as practicable, the highly productive and the less productive barrier island facies so that their reservoir characteristics and distribution can be studied individually. The nonbarrier and barrier facies and the different facies of the barrier island sandstone have been distinguished and lithologically described using cores obtained from several wells. Although subtle at times, differences have been noted from detailed core examinations and petrographic studies between the barrier island and nonbarrier facies and also within the different barrier island facies in lithology, mineralogy, clay content, grain size distribution and sorting, sedimentary structures, etc. All of these different reservoir properties will affect petrophysical properties (porosity, permeability, and water saturation) of the different facies to varying degrees, as illustrated by the plots in figure 67.

The sedimentary facies identified in cores were correlated laterally, as far as practicable, using typical responses of gamma ray, spontaneous potential, resistivity, sonic, and density logs. If log responses of the various facies were sufficiently unique, then visual inspection alone would be adequate to distinguish different sandstone facies. There is, however, not always an appreciable difference in petrophysical properties between different

facies so that for reliable facies mapping some other technique is required to distinguish important sandstone facies on logs.

Figure 67 clearly illustrates good petrophysical properties of high productive facies (mainly foreshore and shoreface facies) and the comparatively poorer quality of the nonbarrier sandstone as well as the clay-rich lower shoreface barrier island facies. Clay-rich sandstones (from both valley fill and lower shoreface facies) normally tend to have higher water saturations than highly productive barrier island facies. Also, mainly because of clay content, these sandstones tend to have lower porosities. These two reservoir properties, porosity and water saturation, have been exploited in distinguishing highly productive barrier facies from lower shoreface and nonbarrier valley fill sediments in the proposed method. The methodology developed is based on the application of Pickett's crossplot of formation resistivity, $R_t$, obtained by plotting induction log against the log-derived porosity, $\phi$, obtained from the density log. Formation resistivity values have been plotted against corresponding porosity values for each depth interval. Figure 68 shows that for well P-2 such a crossplot clearly separates highly productive barrier island facies from nonbarrier and lower shoreface facies. Facies boundaries indicated in this plot, however, were obtained from previously completed core descriptions. A similar plot for well C-6 (fig. 69) also separates highly productive barrier facies from less productive barrier and nonbarrier facies. Facies boundaries in this plot were obtained not from core descriptions (the top part of the core from well C-6 was missing) but from pattern recognition after studying typical patterns in distributions of points in crossplots for a number of wells for which facies descriptions were available (such as in well P-2). Further subdivision of highly productive facies into foreshore and shoreface facies was not always possible in the crossplot because of their similar petrophysical properties.

### Distribution of Highly Productive Barrier Island Facies

The technique discussed above was used to map highly productive barrier island facies (mainly foreshore and shoreface facies) at Bell Creek. An isopach contour map was constructed of the highly-productive facies from analyses of crossplots from wells for which density and induction logs were available (fig. 70). In a few critical areas where density logs were not

available, porosity information was supplemented by sonic logs after taking adequate precautions for the clay-filled nature of the reservoir sandstones. For delineation of the thickness trend of barrier island sandstones, ideally, the study should have been extended over a wider area, but the method of interpretation discussed is based upon combined interpretation of reliable porosity and resistivity logs. Unfortunately, density logs (for porosity estimation) were not available to extend this investigation to other areas.

The highly productive barrier island facies assumes a maximum thickness of about 32 ft in the central part of the study area in Unit 'A', and the thickness decreases in the lagoonal as well as in open sea directions. The maximum sand development is in the NE-SW direction, along the depositional strike. This trend in thick sand development is broken at places where the sandstones are much thinner.

The sharp reduction in barrier island thickness along a linear zone could be due to valley incisions. The sharp swings in the isopachs could also be reflective of structural discontinuities like faults. These structural heterogeneities may have significant effect on barrier thickness development and consequently on fluid movement in the reservoir. Some of these features are marked in figure 70.

### Structural Contours on Top of the Barrier Island

The technique discussed previously for distinguishing barrier from nonbarrier sandstones was used to construct an accurate structural contour map at the top of the barrier island sandstones (fig. 71). The surface, of the top of the barrier island deposit has a general northwesterly dip of about 90 to 100 ft/mile. The sharp swings in structural contours are again suggestive of sharp discontinuities like faults or valley incisions.

The general information obtained from the structural contour map is that the top of the barrier island deposit is not always a smooth surface, and different types of structural features may considerably affect the topography of the sandstone deposit. Fluid flow patterns in such a reservoir will also be affected by various structural heterogeneities.

## Variations in Internal Architecture and Reservoir Quality

Variations in thicknesses of facies, stratigraphy, and sedimentary structures in the barrier island deposit have been studied from two stratigraphic crosssections: one parallel (section AA') and the other perpendicular (section BB') to the strike direction (fig. 72). Gamma ray logs with superimposed porosity and permeability profiles (obtained from core data) were used in constructing the cross sections. In these cross sections, the thickness variations of the highly productive unit "BS" (consisting predominantly of foreshore and shoreface facies) and the lower shoreface facies are indicated.

Cross section AA' indicates that the thickness and reservoir quality of the barrier island sandstone improve from southwest to northeast near the central part of the barrier deposit. Good reservoir quality and high rates of oil production from well P-2 (fig. 72) are due to crossbedded-to-massive appearing sandstones in the upper shoreface and the foreshore facies of the bar. These crossbedded intervals contain subhorizontal to low-angle, plane parallel laminae. In well C-8, facies development and related sedimentary structures within the barrier are similar to those encountered in well P-2, but the top of the sandstone is more silty and clayey, and the reservoir quality in the barrier sandstone is reduced in this portion of the well. Further southwest, in well 27-14, the reservoir quality in the barrier is diminished mainly because of a still higher percentage of clay cementation through much of the productive interval.

Along section BB', the reservoir quality is strongly influenced by cementation by different types of clays and by compaction.

## Log Interpretation of Petrophysical and Petrographic Properties

The distribution of porosity, permeability, and oil saturation in certain parts of the barrier island deposit at Bell Creek was investigated from integrated studies of log, core, and petrographic data. Vertical distributions of total clay content and porosity at 1-ft intervals determined from log interpretations were correlated with facies descriptions obtained from cores and permeability, porosity, and oil saturation measurements obtained from core plugs.

## Porosity Distributions

Porosity is one of the most important reservoir parameters for calculations of reserves and fluid production, and information on the distribution of porosity in a barrier island deposit and the factors controlling it are vitally important.

Sonic, density, and neutron logs were available for determining porosities of reservoir rocks at Bell Creek. The logs run at Bell Creek have all been affected to various degrees by dispersed clays filling the pores.[14] Of all the logs, the density logs seem to be least affected by clay infilling, and they give a good measure of the effective porosity because tests run in the laboratory found that the clay density was between 2.60 and 2.63 g/cm$^3$, which is near the matrix density of quartz (2.65 g/cm$^3$). The effect of dispersed clays on density logs should, therefore, be small, and porosities derived from density logs should be a good representation of the true or effective reservoir porosity of the barrier sandstone. Moreover, in relatively clean formations (such as in well P-2, fig. 67) the agreement between core porosity and density log porosity is excellent. This is because slight enhancement (around 2 porosity units in well P-2) of core porosity had to be considered due to the release of overburden pressure. The observed reduction in porosity due to the net overburden pressure agrees very well with published curves[27] of porosity response with net overburden pressure. This is also an indirect confirmation that the matrix density of 2.65 g/cm$^3$ assumed for porosity calculations was very nearly the correct value. Any other value would make porosity values incompatible with core measurements. The grain density measured in laboratories was slightly lower, around 2.625 g/cm$^3$. The slightly low grain density values obtained from core measurements could also be a measurement error because all evidence (such as petrographic) points to the fact that the average grain density should be closer to 2.65 g/cm$^3$. Other workers[28] also used a grain density of 2.65 g/cm$^3$ even though the measured grain density was lower (around 2.61 g/cm$^3$).

Average porosities of the total barrier sandstone unit obtained from foot-by-foot analyses of 51 density logs from the study area have been contoured in figure 73. Zones with the highest porosity values are near the axis of the bar and slightly to the east. There are intervening zones with low porosity values in between the highly porous zones. Immediately to the west of the

axial position are elongated zones (in sections 22 and 27) with distinctly lower porosities. The porosity distribution in these areas seems to have been affected by structural or diagenetic features previously discussed under reservoir framework and petrographic studies. The porosity distribution in the extreme northern parts of sections 26 and 27 seems to have been affected by a possible northwest, southeast trending fault as interpreted from sharp changes in the porosity contour pattern in this area (fig. 73).

Proper caution is necessary in interpreting the reserves potential of an area based on the average porosity map of a stratified reservoir such as Bell Creek. This is because the real potential of a thin highly porous zone may be masked if the other parts of the sandbody are very tight due either to diagenetic alterations or some other reasons.

## Distribution of Clay Content

We mentioned previously that the distribution of total clay content in reservoir sandstones has a dominant effect on the distribution of petrophysical properties. A reliable estimate of the distribution of clay content in a barrier island deposit may be obtained from an interpretation of sonic and density log data.

In a friable sandstone, such as the barrier island sandstone at Bell Creek, a sonic log measures the total porosity of the rock matrix because dispersed clays respond like slurries to the sonic tool, and there is a dampening of transit times in the clay-filled zones.

In a sandstone having dispersed clays, the sonic porosity, $\phi_s$, is given by

$$\phi_s = C_p\ (\phi + V_{dis}) \qquad (1)$$

where $C_p$ is a compaction factor which is greater than 1, $\phi$ is the effective porosity, and $V_{dis}$ is the volume of dispersed clay.

In uncompacted formations, a value for $C_p$ may be obtained by comparing $\phi_s$ and $\phi_d$ (porosity from density logs) in clean, liquid-filled sands. A few clean sandstones from the study area were identified by crossplotting the density and sonic transit time values for a large number of sandstone samples. Having identified the clean sandstones, the compaction factor, $C_p$,

is obtained as follows:

$$C_p = \frac{d_s}{d_d} \qquad (2)$$

The average value for $C_p$ obtained for the study area is 1.17.

In equation 1, the density logs provide good estimates of d in filtrate invaded and in water sands because the density of dispersed clays (about 2.60 to 2.63 g/cm$^3$) is near the matrix density of the sand which is 2.65 g/cm$^3$. Therefore, in clean water sands we can assume that $d = d_d$.

The clay volume indicator, q is defined as $V_{dis}/d_{im}$ where $d_{im}$ is the intermatrix porosity which includes all of the space occupied by fluids and dispersed clays. For Bell Creek field, a reliable estimate of $d_{im}$ may be obtained from sonic log data from the relationship $d_{im} = \frac{d_s}{C_p}$ .

From equation 1,

$$\frac{d_s}{C_p} = d + V_{dis} = d_d + V_{dis} \qquad (3)$$

$$\text{and } \frac{\frac{d_s}{C_p} - d_d}{\frac{d_s}{C_p}} = \frac{\frac{d_s}{C_p} - d_d}{d_{im}} = q \qquad (4)$$

Because permeability in the study area has been strongly influenced by clay content and compaction (see the discussion on Petrography, Porosity, and Permeability), the distribution of "q" values is expected to correlate with fluid recovery trends in the study area. The distribution of "q" values, plotted as a percentage of intermatrix porosity, is shown in figure 74. The map indicates elongated, relatively clay-free zones in the central and eastern part of the mapped area, with intervening zones of high clay content. The clay content increases to the west and southwest of the central part of section 27 and directly north of it. The distribution of clay content has strongly influenced permeability and porosity distributions and hence fluid production.

## Determination of 'Cleanness' of Sands - Heterogeneity Index

A method for quick determination of the 'cleanness' of reservoir sandstones was developed based solely on interpretations of sonic log data. Analysis of sonic log data from Bell Creek field indicates that sonic deflections from the baseline are strongly influenced by inhomogeneities in the sandstones. In a purely homogeneous sandstone, deflections are nearly uniform through most of the reservoir interval; however, as more and more heterogeneities are introduced, sonic deflections become nonuniform. The amount of deviation of sonic deflections from the perfectly homogeneous case is an indication of the type and degree of heterogeneity in the sandstone "framework."

The sonic response, $T_C$, across a perfectly homogeneous, clean sandstone zone is dependent upon the matrix velocity of the sandstone, the sonic velocity of the pore fluid, porosity, rock compaction, etc. In the more heterogeneous sandstone, the average deflection, $T_{AV}$, is closely related to factors influencing the homogeneous sandstone, but fluctuations in deflections will be largely determined by inhomogeneities in the sandstone matrix. An estimate of the amount of fluctuation (which is a function of the degree of heterogeneity) can be obtained by taking the standard deviation of the sonic deflections. The standard deviation (hereafter called the log-derived heterogeneity index, LHI) can be estimated as follows:

$$LHI = \sqrt{\frac{\sum_{i=1}^{N} (T_i - T_{AV})^2}{N}} \qquad (5)$$

where $T_i$ is the sonic deflection in the ith interval and N is the total number of deflections in the heterogeneous sandstone.

The LHI is a general heterogeneity index that will respond to all types of inhomogeneities in the sandstone. The magnitude of LHI values is dependent upon sonic velocities of inhomogeneities in the sandstones.

In the study area, 48 sonic logs were analyzed to provide average LHI values of the main barrier island sandstone at well locations. The distribution of LHI values shown in figure 66 indicates that low LHI values are clustered in the center of the mapped area near the axis of the bar (areas with high permeability and porosity) and slightly to the east. Sandstones in

this area are relatively "cleaner" and contain comparatively little clay or other cements, or their pores are relatively free from compaction. The high LHI values extending north-south through sections 22 and 27 indicate a higher degree of cementation and clay filling. In the extreme northwestern corner of section 22 and the extreme southwestern corner of section 27, LHI values are small, indicating good, clean reservoir rocks.

There is good correspondence of the LHI map with permeability maps derived from core data and also with the porosity map obtained from density logs.

The main observations and conclusions drawn from these investigations and statistical analysis performed for a number of wells are as follows:

1. The clay content has a strong inverse relationship with porosity in all wells studied.

2. For low to moderate clay content, the clay quantity only has moderate inverse correlation with log of permeability, but as the clay content increases there is sharp reduction in permeability due to widespread clogging of pore throats.

3. The grain size distribution in well P-2 determined from measurements of the mean quartz grain size indicates that this parameter has a strong direct relationship with permeability. Therefore, permeability distribution in certain parts of the barrier island deposit depends on more than one variable.

4. The sedimentary structures have considerably affected permeability distributions. For example, the massive crossbedded parts of the sandstones seem to have the best permeabilities.

5. In well W-7, the gamma ray count in the backshore facies of the barrier island deposit was at least 10 API units higher than that for the middle shoreface facies. Petrographic studies indicate that this higher count could be due to a higher total percentage of mica, organic material, and/or feldspar in the backshore facies. This points to the possible application of modern gamma ray logs for detailed studies of certain barrier island facies.

6. Besides potassium feldspar, mica, etc., gamma ray logs respond to clays like illite and montmorrillonite but will not respond to potassium-free kaolinite which is the main clay type in wells where petrographic studies have so far been completed.

All of these observations and conclusions are illustrated by plots of core and log-derived petrophysical properties and clay content in wells P-2 and W-7 (figs. 67 and 75). The clay content in well P-2 is uniformly low, and the minor variations in k and $\phi$ in this well are believed to be primarily due to the distribution of grain size and sorting and sedimentary structures. On the other hand, porosity and permeability curves show much wider fluctuations in well W-7 (fig. 75), and this is primarily due to variable clay content in the reservoir sandstones.

## Determination of Oil and Water Saturations

To determine how different heterogeneities have affected oil entrapment in a barrier island type of depositional environment, information on vertical and lateral distribution of oil saturation is vitally important. Ideally, for a rigorous investigation of the role of different heterogeneities during each recovery phase (primary, secondary, and tertiary), information on oil saturation is needed after each stage of production. Such a detailed investigation will permit location of pockets of by-passed oil that could be targets of enhanced oil recovery.

Difficulties of obtaining accurate water saturation information from core plugs are well recognized mainly because of flushing of cores by mud filtrate and difficulties of preserving original fluid saturations in core samples. Therefore, log data will have to be used to obtain more reliable and detailed information on saturation distribution for heterogeneity research.

Because of the high clay content in certain parts of Bell Creek field coupled with relatively fresh formation water (from 6,400 to 7,400 ppm of total dissolved solids) the conventional use of Archie's equation[29] for water saturation calculations may lead to serious errors. It was demonstrated by Waxman and Smits[30] that the plot of laboratory-derived $R_0$ (resistivity of formation 100% water saturated) versus $R_w$ (formation water resistivity) did not always equal a constant as predicted by Archie.[29] This divergence was particularly prominent in clayey formations where the saturating fluid had a high resistivity (such as at Bell Creek). In these low-salinity, highly-resistive formations, the values of $R_0$ are much lower than those anticipated from Archie's formula. This apparent decrease in $R_0$ is attributed to the fact

that clays in the pore space and the saturating fluid both contribute ions which together define the total conductivity of the rock.

For reliable estimation of water saturation in such clayey and low-salinity formations, Waxman and Smits[30] have proposed an equation which requires calculation of a value for the cation exchange capacity (CEC) of the pay interval. The cation exchange capacity is a property of the shales or clays in an interval affecting the resistivities of that interval. A quantitative measure of the effective clays (clays that have significant electrical effect) is available with modern spectral gamma ray logs. Since such logs and laboratory measurements of CEC from Bell Creek are not available, an indirect method is needed to obtain information on the effective clays and the cation exchange capacity of the pay zone.

### Determination of 'Effective Clay' and Cation Exchange Capacity`

We attempted to estimate the CEC from a combined interpretation of the available gamma ray log and the previously calculated total shale volume indicator calculated from sonic and density logs. From petrographic studies (thin section and XRD), the clays in the study area are known to be predominantly kaolinite (which are electrically nearly inert). Minor amounts of other clays like illite and montmorillonite with significant electrical effects have also been reported. Since gamma ray logs are practically unresponsive to potassium-deficient clays like kaolinite and chlorite, the gamma ray response could be attributed to either effective clays (like illite or montmorillonite) or to certain non-clayey minerals like k-feldspar, mica, or uranium etc. which have been reported from petrographic studies. A good estimate of the total clay volume in the reservoir was previously obtained from interpretation of sonic and density logs. A comparison of the distribution of total clay volume with the effective clay volume can fairly accurately isolate high gamma ray readings due to non-clayey radioactive minerals.

Effective clay values obtained at every foot of vertical depth were next converted into effective CEC values using a formula which has been shown to be valid in two different basins: MacKenzie Delta and Gulf Coast.[31] The relationship can be expressed as

$$V_{CL} = CEC\ (1.661\ R_{Sh} - 0.567) - 0.001\ R_{Sh} - 0.0072 \qquad (6)$$

where $R_{Sh}$ is the resistivity of shales adjacent to the pay zone. The cation exchange capacity along with other reservoir parameters is then added to the Waxman and Smits equation for calculating $S_{Wt}$, the total water saturation as a fraction of total pore volume. This equation is

$$S_{Wt}^{n} = \frac{R_t\ (1 + R_W B Q_V / SW_t)}{a\phi_t^{-m^*} \cdot R_W} \qquad (7)$$

where

$R_t$ = Formation resistivity, Ω-m

$R_W$ = Formation water resistivity, Ω-m

$Q_V$ = CEC $(1-\phi)\beta/\phi$

B = Specific counterion inductance which is expressed as

$$B = 4.6\ (1 - 0.6 - \exp\ (-.77/R_{W2})$$

where

$$R_{W2} = R_W \text{ at } 77^\circ \text{ F}$$

m = Cementation exponent

n = Saturation exponent

a = Tortuosity factor

The technique for obtaining vertical distribution of water saturation values will be illustrated from an example in well W-7. Log and core-derived petrophysical properties along with the distribution of total clay content indices (q) for the well are shown in figure 75. Well W-7 can be considered as moderately clay-filled, and from petrographic and XRD studies, the clays are known to be mostly kaolinite which do not have an appreciable electrical effect. There are minor amounts of non-clay radioactive materials, but the total percentage of these is very small.

After the calibration was checked, the gamma ray curve was normalized. For each foot of depth interval, gamma ray indices were calculated by use of the following equation.

$$I_{GR} = \frac{GR_{log} - GR_{min}}{GR_{max} - GR_{min}} \qquad (8)$$

From this index, $V_{CL}$ (effective clay) was calculated either from a published chart or from the following formula given by Clavier.[32]

$$V_{CL} = 1.7 - (3.38 - (I_{GR} + .7)^2)^{\frac{1}{2}} \qquad (9)$$

These values of $V_{CL}$ were plotted for each depth (fig. 76). Total clay values ($V_{CLT}$) obtained from an interpretation of sonic and density logs are also indicated alongside effective clay values.

Note that although the total clay content in this well is fairly significant, the effective clays are almost entirely distributed in the lower shoreface and in parts of backshore and middle shoreface facies.

The $S_W$ values obtained from application of Waxman and Smits formula are plotted along with values obtained from $S_W$ measurements on core plugs. The agreement between the two sets of $S_W$ values is good in areas of clean sand development, but it deteriorates in the clayey and shaly parts of the pay zone.

## Fluids and Rock-Fluid Interaction

The components of an engineering model required for a comprehensive characterization of a reservoir are shown in table 29. The chronology of data gathering for each stage of field development is illustrated in figure 77. The reliability of data sources for reservoir characterization is summarized in table 30.

### Formation Fluid Characteristics

Muddy formation water in Unit 'A' of Bell Creek field is of the general chloride-bicarbonate-sodium ($Cl-HCO_3-Na$) chemical type. Total dissolved solids in the formation water average 7,000 mg/L and have low divalent cation (calcium and magnesium) and sulfate content.[33] The origin and spatial

variation in chemical characteristics of the oil-associated formation water are not known.

Madison formation water was used during waterflooding and chemical injection into the Muddy formation. Madison formation water was of the chloride-sulfate-bicarbonate-calcium ($Cl$-$SO_4$-$HCO_3$-$Ca$) chemical type with total dissolved solids of 1,200 mg/L.[33] Madison water was treated by ion exchange to replace calcium and magnesium ions with sodium ions to prevent precipitation of calcite in the presence of bicarbonate in the Muddy formation water. Madison formation water temperature was thermally compatible with the Muddy formation temperature. Activities of abundant sulfur-reducing bacteria in the presence of sulfates and iron in the injected water were responsible for hydrogen sulfide production and potential problems resulting from possible iron sulfide precipitation.

The barrier island sandstone in Bell Creek field contains negligible amounts of water-sensitive clays;[11] however, other clays are locally abundant. Therefore, the formation was not susceptible to permeability reduction when Madison formation water was injected into the reservoir. Preflush injection before micellar-polymer injection was intended to reduce the adsorption of the sulfonate onto clay particles. Analysis of produced water during the tertiary recovery project revealed a large $SiO_2$ content (from the sodium silicate preflush) in the producing wells located in high-permeability, low-clay-content areas. It may be concluded that the injected preflush was diverted toward high-permeability regions and did not appear in appreciable amounts in regions with high clay content and low permeability.

The API gravity of the paraffinic crude oil in the Muddy formation varies from 31.5° to 40°. The increase in API gravity occurred within a distance of 8 miles from the northern tip of Unit 'A' because of the increase in $C_5$ to $C_{10}$ hydrocarbon components. Hydrocarbon gases in Unit 'A' consist mainly of methane (92.94%) and nonhydrocarbon gases such as carbon dioxide (0.42%) and nitrogen (0.63%).[33] The PVT and compositional properties of the crude oil and gas have been measured, reported,[14,33] and used in simulation studies.

### Relative Permeability and Wettability

Several water-oil, steady-state, and unsteady-state relative permeability tests were performed on core samples from sections 1, 6, 7, 12, 22, and 27 in

Unit 'A'.[14,34] Measurements were conducted on cores having a range of permeabilities from 299 to 2,450 md. Cores were solvent extracted, and flow experiments were performed with nonreservoir fluids. A set of oil-water imbibition-drainage relative permeability curves indicating the water-wet behavior of the samples is shown in figure 78. Irreducible oil saturation obtained from laboratory flow tests ranged from 27 to 40%, with an average of 33.3%. Results of imbibition tests performed on two fresh samples showed that at least as much oil was imbibed as water. Oil saturation values obtained from cores recovered from the TIP area in 1980 following waterflooding indicated oil saturations in the range of 14 to 20% which is substantially lower than irreducible oil saturations exhibited by laboratory flow tests and areal simulations. Water relative permeabilities calculated from pulse tests and falloff tests conducted in 1980 were as high as 27%. A history match of the field data by areal simulation showed lower oil relative permeability values at high oil saturations and higher values of oil relative permeabilities at lower oil saturations compared to laboratory tests. The relative permeability to water obtained from history matching was higher than the results obtained from laboratory flow tests. These results combined with imbibition tests and constant waterflood production rate decline characteristics implied that high waterflood recovery efficiency may be indicative of mixed wettability behavior.

Several laboratory gas-oil drainage relative permeability measurements were conducted.[14,33-34] Results were highly scattered, partly because of the experimental difficulties associated with obtaining reliable data in high-permeability cores. Laboratory gas relative permeability values were higher than those obtained from history matching.

## Initial Electrical Resistivity Distribution and Its Change After 10 Years of Waterflooding

Thickness-weighted, average induction log values of the productive interval for each well drilled in 1967-68 in the 4-section area enclosing the TIP were mapped (fig. 79). The average value varied from 30 to 175 Ω-m, and the distribution resembled the average permeability distribution, as shown in figure 59. The 1967-68 resistivity map shows that the resistivity in high-permeability regions is higher than 50 Ω-m coresponding to lower water

saturation. Air-brine drainage capillary pressure tests were conducted by the conventional porous plate method on six samples ranging in permeability from 29 to 4,320 md (fig. 80). A centrifuge speed equivalent to a capillary pressure of 100 psi was used to extend the pressure range of porous plate capability beyond the 35 psi level. A good correlation was found between air permeability and irreducible water saturation from capillary pressure curves at 100 psi displacement pressure (fig. 81).

Electrical resistivity logs were obtained in 1980 from newly drilled wells in the TIP area after 10 years of waterflooding the unit with water from the Madison formation.[14] Madison formation water has one-sixth the salinity (TDS) of Muddy formation water.[14] As a result, the salinity of the produced water gradually decreased during waterflooding to that of the injected water. Changes in electrical resistivity were, therefore, due to both increases in water saturation (with associated decreases in oil saturation) and the reduction in salinity.

The ratio of 1980 to 1967 electrical resistivity was mapped in the TIP area (fig. 82) and ranged from 20 to 130%. The ratio was from 10 to 40% in the region with better reservoir quality, and the resistivity ratios ranged to 130% in the most heterogeneous part of the reservoir. Effects of oil depletion and water-saturation increases (higher oil sweep efficiencies) were more dominant than the effect of water-salinity reduction in the regions with good reservoir properties. The increase in water saturation in the heterogeneous part of the reservoir was not high enough to offset the effect of the reduction of salinity on electrical resistivity.

Regions with a lower electrical resistivity ratio had better sweep efficiencies, and these same regions are those having superior reservoir quality and low Dysktra-Parsons coefficients. In contrast, regions with relatively inferior reservoir quality and higher Dykstra-Parsons coefficients did not have good sweep efficiencies.

### Residual Oil Saturation (ROS) Distribution

Samples from cores recovered during 1980 were used to determine the distribution of residual oil saturation (ROS) in the Tertiary Incentive Project (TIP) area of Unit 'A', Bell Creek field following waterflooding and before the initiation of chemical flooding EOR operations. Oil saturation

measurements were determined from cores from 19 wells after 10 years of waterflooding. Oil-saturation data were obtained by solvent extraction during conventional core analysis. Oil saturations were measured for each foot of the productive zone, and a weighted average was used (fig. 83).

The average waterflood residual oil saturation measured from cores within the TIP area (fig. 83) was low, in the range of 12 to 22.4%. The residual oil saturation was lowest in regions where the permeability was high and the Dykstra-Parsons coefficient was low, and where the formation consisted mainly of foreshore and middle and upper shoreface facies. The residual oil saturation in the TIP area was relatively high around well C-10 where considerable faulting had occurred. The average residual oil saturation values in the TIP area were at least 5% lower than results from any of the water-oil relative permeability and laboratory waterflood tests. Dynamic flushing by drilling fluids and decompression from formation to atmospheric pressure may have reduced oil saturations below the residual oil remaining after waterflooding.

Higher residual oil saturations from cores as of 1980 (fig. 83) were evident in the northern and the southern parts of the TIP area. These regions of high average oil saturation correspond to areas with strong sedimentary or diagenetic layering. In these areas, vertical variations in residual oil saturations often ranged from 10 to 30% in each well. When corrected for mobility ratio, Dykstra-Parsons coefficient, oil formation volume factor, and sweep efficiencies,[35] 26% ROS was obtained after 10 years of waterflooding in areas with a low Dykstra-Parsons coefficient. Close to 60% ROS was obtained in regions having a high Dykstra-Parsons coefficient.

The 1980 residual oil saturation for the TIP area was also obtained from areal field simulations of Unit 'A'. Primary and secondary production were history matched, and residual oil saturation distribution was mapped (fig. 84). The spatial distribution of residual oil saturation obtained from simulation showed a good agreement with corrected core measurements at 1980 in the TIP area. The ROS values ranged from 25 to 55%. The combined effect of transmissivities and the location of the injectors were responsible for this variation. The highest average residual oil saturation occurred in the southern tip of the TIP area.

The 1980 residual oil saturation map prepared from conventional core analysis (fig. 84); the map generated by areal simulation (fig. 84); and the 1980/1967 resistivity ratio map (fig. 82) have many similarities. A comparison of these maps indicates that the resistivity ratio map is a very good indicator of ROS distribution and sweep efficiency, while simulation provides the magnitude and the distribution of ROS.

## SUMMARY AND CONCLUSIONS

Integration of sedimentologic, diagenetic, structural, and petrophysical data from outcrops and subsurface with wireline logs, well test results, and production/injection performance has provided a more predictive geological/engineering model for the barrier island/valley fill reservoir at Unit 'A', Bell Creek (MT) field. In addition to a genetic classification of heterogeneities, the predictibility of common, unique, and site-specific heterogeneities has been evaluated for barrier island reservoirs based on their occurrence in the Muddy formation.[36]

Common features which can be ascribed with a good deal of confidence to all barrier island systems include the sequence of facies and original properties inherited from depositional processes, geometry and continuity of major flow units, and stacking pattern in progradational or regressive cycles. Features unique to the barrier island depositional system include significant early diagenesis caused by the interaction of marine, meteoric, and continental-derived waters with unconsolidated sediment and the lateral association of paralic lagoonal or estuarine facies with marine-transitional facies including ebb and tidal deltas. Diagenesis and faulting are the most important site-specific heterogeneities.

Fluctuations of relative sea level ensure that barrier island facies are inherently associated with valley filling sediments. Tops of barrier cycles were eroded over most of Unit 'A', but deeper erosional cuts removed almost the entire barrier on the west side of production Unit 'A'. Nonbarrier infillings within erosional cuts by continental or marginal-marine facies may either be productive; for example, in nearby Recluse field, or dominantly nonproductive, as in Bell Creek field. However, it needs to be clearly stated that stratigraphic position and type of infilling differ in both fields.[7] The intimate association of valley fill and barrier island facies may be the most

characteristic stratigraphic features of barrier island depositional systems; however, the actual pattern of erosive cuts is site-specific.

Integration of the core- and outcrop-derived geological model with production/injection data allowed the ranking of the importance of sedimentary, tectonic, and diagenetic heterogeneities relative to overall production performance. Based on data from Unit 'A', Bell Creek field, primary production was most strongly influenced by depositinal heterogeneities and less so by diagenetic heterogeneities. Secondary production was mostly affected by structural dip and distribution of diagenetic heterogeneities. Tertiary production, in contrast, was influenced by depositional and diagenetic heterogeneities as well as by faulting.

Lateral changes of facies within the barrier core define continuity of flow units unless disruptions result from faults or diagenetic facies.

On the barrier periphery, a subdivision of flow units results primarily from stacking of two or more sedimentary cycles where less permeable facies intercolate or interfinger with productive sandstones; for example, washovers divided by a lagoonal sequence, as in well 13-11 or 35-13.

The barrier island flow units are confined on top by low- and high-relief valley incisions filled with predominantly low quality or nonreservoir sediments. Internal vertical subdivision of flow units is predominantly related to faults and diagenetic layering.

There are two dominant effects of diagenesis on the distribution of reservoir quality sandstones in Bell Creek field:

1. Strong leaching occurred very early in the paragenetic sequence and was shown to significantly increase porosity. The leaching process specifically created intraparticle secondary porosity, created oversize pores, (late-stage leaching), and removed less stable components, such as feldspars and sedimentary rock fragments, locally including chert. The effect of all subsequent phases recognized in the paragenetic sequence (siderite, silica, calcite, and clay cementation and compaction) was to reduce porosity and permeability. Therefore, the importance of leaching, particularly leaching that occurred early in the paragenetic sequence, cannot be overemphasized relative to reservoir development.

2. The distribution and magnitude of late-stage clay cementation within the barrier island sandstone is the most crucial limiting diagenetic factor relative to fluid flow paths and ultimately well performance.

Better petrophysical properties and reservoir quality potential have been found in the barrier core, rather than in distal parts of the barrier where thinner and lower energy facies intercolate with nonproductive members of adjacent depositional environment.

Superior reservoir properties were documented for foreshore, shoreface, washover, tidal channel, and delta splay facies. Low-permeability sediments prevail in most alluvial valley fills. Storage capacity and flow capacity tend to decrease toward the backbarrier side of the buildup but are highly variable within the barrier.

The highest net pay (20 to 26 ft/6.1 to 7.9 m) is present in the central part of Unit 'A', where the barrier island deposits are thickest. Net pay sharply decreases toward the lagoonal side of the barrier.

There is an obvious trend between natural logarithm of air permeability and porosity within Muddy barrier island and valley fill sediments. Variation in distribution of core-derived average porosities and permeabilities depends primarily on clay distribution in the TIP and surrounding areas. Average porosity and permeability distribution is not obviously dependent on position within the barrier, but tends to parallel the general strike of the barrier in the study area.

Barrier island and valley fill sandstones contain different assemblages of clays both in outcrops and in subsurface. In barrier island sandstones, kaolinite and illite predominant, whereas smectite and kaolinite occur commonly in valley fill sediments.

A parallel trend of permeabilities exists for the same facies between outcrops and reservoir, but porosity is characteristically 5 to 10 % greater for outcrop facies.

The vertical and horizontal permeability ratio ($k_v/k_h$) varies from about 1.0 for foreshore facies to 0.7 for upper and middle shoreface. A low ratio of vertical-to-horizontal permeability ($k_v/k_h$ - 0.3 to 0.6) is characteristic for lower shoreface and for valley fill deposits.

The overall influence of geological heterogeneities depends on production strategy and stage of production. The role of depositional heterogeneities is very important at all stages of production, although diagenetic effects may moderately to severely deteriorate reservoir quality. Structural features play a different role, depending on the stage of production, well spacing, and injection-production pattern.

The best tertiary recovery occurred in areas of (1) favorable development of barrier island sandstone, (2) negligible diagenetic effects, (3) good sedimentary and structural continuity, and (4) proper well pattern which allowed sweep by four chemical injectors surrounding a producing well. Only one well in the TIP area fulfilled all of those requirements, well P-6. The well had an exceptionally good tertiary oil recovery (1.8 million bbl).

Monitoring of changes in electrical resistivity provides a good indication of volumetric sweep and displacement efficiencies during the depletion of reservoirs.

Separation of highly productive barrier island facies from nonbarrier and lower shoreface facies, based on application of Pickett's crossplot of formation resistivity obtained by plotting induction log values against density log derived porosity proved successful.

Indices for clay content and log-derived heterogeneity index were successfully used for determining relative inhomogeneity in the reservoir sandstone.

## REFERENCES

1. Berg, R. R. and D. K. Davies. Origin of Lower Cretaceous Muddy Sandstone at Bell Creek Field, Montana. AAPG Bull., v. 52, 1968, pp. 1888-1889.

2. McGregor, A. A. and C. A. Biggs. Bell Creek Field, Montana. A Rich Stratigraphic Trap. AAPG Bull., v. 52, 1968, pp. 1869-1887.

3. Stone, W. D. Stratigraphy and Exploration of the Lower Cretaceous Muddy Formation, Northern Powder River Basin, Wyoming and Montana. The Mountain Geologist, v. 9, 1972, pp. 355-378.

4. Almon, W. R. and D. K. Davies. Regional Diagenetic Trends in the Lower Cretaceous Muddy Sandstone, Powder River Basin, in P. A. Scholle, and P. R. Schluger, eds., Aspects of Diagenesis. Soc. Econ. Paleontologists and Mineralogists Special Publication 26, 1979, pp. 379-400.

5. Weimer, R. J. New Age Interpretation of Bell Creek Sandstone, Powder River Basin, Montana and Wyoming. AAPG Bull., v. 69, 1981, p. 870.

6. Weimer, R. J., J. J. Emme, C. L. Farmer, L. O. Anna, T. L. Davis, and R. L. Kidney. Tectonic Influence on Sedimentation, Early Cretaceous, East Flank Powder River Basin, Wyoming and South Dakota. Colorado School of Mines Quarterly, v. 77, 1988, p. 61.

7. Weimer, R. J., C. A. Rebne, and T. L. Davies. Geologic and Seismic Models, Muddy Sandstone, Lower Cretaceous, Bell Creek - Rocky Point Area, Powder River Basin, Montana and Wyoming (abs.). AAPG Bull., v. 72, 1988, pp. 883-884.

8. Szpakiewicz, M., K. McGee, and B. Sharma. Geologic Problems Related to Characterization of Clastic Reservoirs for Enhanced Oil Recovery: Pres. at Fifth SPE/DOE Symposium on Enhanced Oil Recovery, Tulsa, 1986. SPE/DOE paper 14888; SPE Formation Evaluation, December 1987, pp. 449-460.

9. Holm, L. W. Correlation of Oleic and Aqueous Micellar Processes for Tertiary Oil Recovery. Pres. at Fifth SPE Symposium on Improved Methods for Oil Recovery, Tulsa, Apr. 16-19, 1978. SPE paper 7066.

10. Hartshorne, J. M. and S. J. Nikonchik. Micellar-Polymer Flood Success in Bell Creek Field. Pres. at the SPE Ann. Tech. Conf. and Exhib., Houston, 1984. SPE paper 13122.

11. Sharma, B., M. Honarpour, M. Szpakiewicz, and R. A. Schatzinger. Critical Heterogeneities in a Barrier Island Deposit and Their Influence on Primary Waterflood and Chemical EOR Operations. Pres. at the SPE Ann. Tech. Conf. and Exhib., Dallas, Sept. 27-30, 1987. SPE paper 16749.

12. Reinson, G. E. Barrier Island and Associated Strand Plain System, in R. G. Walker, ed., Facies Models. Geoscience Canada, Reprints Series, No. 1., 1984, pp. 119-140.

13. Honarpour, M., M. J. Szpakiewicz, R. A. Schatzinger, L. Tomutsa, H. B. Carroll, Jr., and R. W. Tillman. Integrated Geological/Engineering Model for Barrier Island Deposits in Bell Creek Field, Montana. Pres. at the Sixth SPE/DOE Symposium on Enhanced Oil Recovery, Tulsa, Apr. 14-20, 1988. SPE/DOE paper 17366.

14. Gary-Williams Oil Producers Inc. 1969 Engineering and Geological Report, Bell Creek Field, Unit 'A'. Prepared by Frank E. Farnham, Gary-Williams Oil Producers, Inc., Denver, 1969.

15. Burt, R. A., F. A. Haddenhorst, and J. C. Hartford. Review of Bell Creek Waterflood Performance--Powder River County, Montana. Pres. at the SPE Ann. Tech. Conf. and Exhib., Dallas, Sept. 28-Oct. 1, 1975. SPE paper 5670.

16. Vargo, J. J. Site Selection, Reservoir Definition and Estimation of Tertiary Target Oil for the Bell Creek Unit, a Micellar-Polymer Project. Pres. at the Fifth SPE Symposium on Improved Methods for Oil Recovery, Tulsa, Apr. 16-19, 1978. SPE paper 7071.

17. Gary Energy Corp. Bell Creek Field Micellar-Polymer Pilot Demonstration. 1982 Final Report. June 1976-March 1982. Dept. of Energy Contract No. DOE/SF/0180261.

18. Tillman, R., M. Szpakiewicz, M. M. Honarpour, and S. Jackson. Reservoir Description and Production History; Bell Creek Field, Muddy Stone, Barrier Island and Valley Fill Deposits. AAPG Bull., v. 72, 1988, p. 254.

19. Szpakiewicz, M., R. Tillman, S. Jackson, and G. deVerges. Sedimentologic Description of Barrier Island and Related Deposits in the Bell Creek Cores, Montana and Analogous Outcrops Near New Haven, Wyoming. NIPER Open File. Available for review at NIPER.

20. Forgotson, J. M. Jr. and P. H. Stark. Well Data Files and the Computer: A Case History from Northern Rocky Mountains. AAPG Bull., v. 56, 1981, pp. 1114-1217.

21. Slack, P. B. Paleotectonics and Hydrocarbon Accumulation, Powder River Basin, Wyoming. AAPG Bull., v. 65, 1981, pp. 730-743.

22. Zorback, M. L. and M. Zorback. State of Stress in the Conterminous United States. Geophy. Res., v. 85, 1980, pp. 6113-6156.

23. Michael, C. R. and E. S. Merin. Tectonic Framework of Powder River Basin, Wyoming and Montana From Lansat Imagery. Discussion in AAPG Bull., v. 70, 1986, pp. 453-455.

24. Kaauskopf, K. B. Introduction to Geochemistry. McGraw Hill International Series in the Earth and Planetary Sciences, McGraw Hill Book Company, New York, 1967, p. 721.

25. Lundegard, D. D., L. S. Land, and W. E. Galloway. Problems of Secondary Porosity: Frio Formation (Oligocene), Texas Gulf Coast. Geology, v. 12, 1984, pp. 399-402.

26. Dickinson, W. R. Interpreting Detrital Modes of Graywacke and Arkose. Sed. Petrology, v. 40, 1970, pp. 695-707.

27. Feazel, C. T. and R. A. Schatzinger. Prevention of Carbonate Cementation in Petroleum Reservoirs, in Schneiderman, N. and P. M. Harris, eds., Carbonate Cements. Soc. Econ. Paleontologists and Mineralogists, Special Pub. No. 36, 1985, pp. 97-106.

28. Collins, H. N. An Intergrated Approach to Unconsolidated Sand Evaluation. Pres. at the Sixth Formation Evaluation Symposium of the Canadian Well Logging Society, in Calgary, Oct. 24-26, 1977.

29. Archie, G. C. The Electrical Resistivity Log as an Aid in Determining Some Reservoir Characteristics. Trans., AIME, v. 146, 1941, pp. 54-67.

30. Waxman, M. H. and L. J. M. Smits. Electrical Conductivities in Oil-Bearing Shaley Sands. Trans., Soc. Pet. Eng. J., v. 243, 1968.

31. Johnson, W. L. and W. A. Linke. Some Practical Applications to Improve Formation Evaluation of Sandstones in the MacKenzie Delta. Pres. at the SPWLA 19th Annual Logging Symposium, June 13-16, 1978.

32. Clavier, C. Quantitative Interpretation of Thermal Neutron Decay Lime Logs. J. Pet. Tech., v. 23, 1971, p. 751.

33. Gary-Williams Oil Producers Inc. A Reservoir Engineering Study to Determine Feasibility of Tertiary Recovery Operations, Bell Creek Field. Prepared by Charles R. Smith and Associates, Denver, 1974.

34. Core Laboratories, Inc. Special Core Analysis Study, Warford No. 22-3 Well, Bell Creek Field, Powder River County, Montana. Available from Gary-Williams Oil Producers Inc., Denver, 1968.

35. Kazemi, H. Determination of Waterflood Residual Oil Saturation From Laboratory Tests. J. Pet. Tech., February 1973, pp. 175-185.

36. Szpakiewicz, M., R. Schatzinger, M. Honarpour, M. Tham and R. Tillman. Geological/Engineering Evaluation of Heterogeneity, Petrophysical Properties and Productivity of Barrier Island/Valley Fill Lithotypes in the Bell Creek Field; Muddy Sandstone, Powder River Basin, Montana. Submitted to the RMAG's 1989 Guidebook. Sandstone Reservoirs of the Rocky Mountains, 1988.

TABLE 17. - Rock, fluid properties and production data from Unit 'A', Bell Creek Field, Muddy formation

| | |
|---|---|
| **GENERAL INFORMATION** | |
| Location | NE Flank, Power River Basin, Montana |
| Date discovered | June 29, 1967 |
| Formation | Muddy Sandstone (Lower Cretaceous) |
| Depositional environments | Barrier island/valley fill sandstones |
| Average depth, ft. (m) | 4500 (range 4300-4700) |
| Type of trap | Stratigraphic (OWC w/updip pinch out) |
| Regional dip | WNW 100 ft/mile |
| Average gross pay, ft (m) | 25.7 |
| Average net pay, ft (m) | 22.9 |
| Productive area, acres | 7,219 |
| Bulk volume, acre-ft | 86,189 |
| Primary producing mechanism | solution gas drive |
| Gas cap size/oil zone size, % | 3.9 |
| Initial GOC, ft, subsea (total of 3) | 550 (sec 25 & 26), 650 (sec 6), 671 (sec 7) |
| Initial WOC, ft, subsea (total of 3) | 797 (sec 11) 784 (sec 21 & 22), 714 (sec 28 & 29) |
| Reservoir temperature, °F (°C) | 110 |
| Initial reservoir pressure, psia, at 800 ft. subsea | 1,204 |
| Bubblepoint pressure, psia, at 800 ft. subsea | 1,204 |
| Original oil in place, MMSTB | 127.0 |
| **FLUID PROPERTIES** | |
| Oil Gravity, ° API | 32.5 (range 31.5-40) |
| Solution GOR, scf/bbl (std $m^3/m^3$) | 200 |
| Original FVF, vol/vol | 1.112 |
| FVF at start of waterflood | 1.05 |
| Viscosity at initial reservoir P&T of live crude, cP | 2.76 |
| Viscosity at 300 psia, cP | 4.4 |
| Oil type | paraffinic |
| Formation water TDS, ppm | 6,400-7,400 |
| Formation water resistivity at 68° F, Ω-m | 1.08 |
| Injected water TDS, ppm | 1,070-1,200 |

TABLE 17. - Rock, fluid properties and production data from Unit 'A', Bell Creek Field, Muddy formation -- Continued

| | |
|---|---|
| **ROCK AND ROCK-FLUID PROPERTIES** | |
| Dominant clay type | Illite/kaolonite |
| Clay/silt content, percent | 5-17 |
| Average sandstone porosity from cores, % | 28.5 (range 6-36) |
| Permeability, geometric mean, md | 915 (range 0.1-13,000) |
| Arithmetic mean, md, | 2250 (range 0.1-13,000) |
| Harmonic mean, md | 370 (range 0.1-13,000) |
| Dykstra Parsons coefficient | 0.5 (ranges 0.3-0.8) |
| Critical gas saturation, % | 2.5 (range 1.5-5) |
| Waterflood residual oil saturation, % (Aug. 1980) | 35 (25-65) |
| Wettability | water-wet (possibly mixed or intermediate) |
| **PRODUCTION DATA** | |
| Type of secondary recovery method | waterflood |
| Date secondary recovery installed, Unit 'A' | July 1970 |
| Flooding pattern | Linedrive |
| Primary & secondary production well spacing, acres | 40 |
| Ultimate primary oil recovery, MMSTB | 21.96 |
| Water production during primary production | Negligible |
| Cumulative secondary oil recovery, (Aug. 1987), MMSTB | 46.6 |
| Cumulative water production (Aug. 1987), MMSTB | 162.8 |
| Water injection wellhead pressure, psia | 50-1,750 |
| Type of tertiary recovery method | micellar-polymer flood |
| Date first tertiary recovery pilot installed | 1975 |
| Size of first tertiary recovery pilot, acres | 160 |
| Date second tertiary recovery pilot (TIP) installed | 1981 |
| Size second tertiary recovery pilot (TIP), acres | 179 |
| Cumulative tertiary oil production (TIP) (Aug. 1987), MMSTB | 1.37 |
| Cumulative water production (TIP) (Aug. 1987), MMSTB | 31.4 |

TABLE 18. - Dominant features identified in Barrier Island Sandstones, Muddy formation (Bell Creek cores and New Haven outcrops)

| | |
|---|---|
| **UPPER FORESHORE** | Sandstone 150-200 μ, swash deposit.<br>Moderately to well-sorted,<br>low-angle to subhorizontal stratification.<br>Trace to 5% burrowed (Skolithos, Corophioides Diplocraterion).<br>Trace of shale (rip-up clasts) and siltstone.<br>Interruptions in sedimentation (subunits), poorer sorting, more burrowing and local bioturbation may indicate backshore deposit. |
| **LOWER FORESHORE** | Sandstone 125-150 μ, intertidal deposit.<br>Moderately to well sorted.<br>Subhorizontally laminated to low-angle troughs, wavy-bedded, not swash-laminated.<br>Less than 10% burrowed.<br>Trace of shale laminae. |
| **WASHOVER** | Sandstone 100 - 175 μ, storm overwash deposit.<br>Poor to fair sorting.<br>Massive appearing or subhorizontally to horizontally laminated planar beds. Possible ripple-form bedding.<br>Typically nonburrowed and clean. |
| **UPPER SHOREFACE** | Sandstone 125 - 175 μ, fairweather current and/or wave deposit (subtidal). Occurs only rarely. Fair sorting. Cross-bedded or massive appearing, swaly cross-stratification (SCS), wave and current ripples. Hummocky cross stratification (HCS) absent. Few burrows (Diplocraterion, Rosellia, Ophiomorpha)<br>Shaley siltstone up to 25%. |
| **MIDDLE SHOREFACE** | Sandstone 100 - 175 μ, wave dominated deposits at depth into which long shore bars and trough ridges have migrated.<br>Poor, or moderate to good sorting.<br>Mostly massive due to burrowing (up to 60%) or bioturbation (>75%).<br>Very low relief troughs to subhorizontal lamination.<br>Shale drapes common but discontinuous |
| **LOWER SHOREFACE** | Sandstone 100 - 150 μ.<br>Poor sorting. Shale and siltstone 25-60% increasing downward.<br>Low angle to subhorizontal stratification, Hummocky cross-stratification (HCS), rippled.<br>Commonly bioturbated, burrowed 10-90% (Thallasinoides, Asterosoma, Rosellia, Corophioides). |

TABLE 19. - Essential elements of the depositional model and their effects on production related problems in barrier island deposystem.

| Element | Effect |
|---|---|
| Environment of deposition | Field-wide geometry, general rock properties, reservoir boundaries. |
| Facies | Drainage volume, interwell continuity, fluid storage capacity and conductivity. |
| Stacking of facies | 3-D shape of sandstone bodies, increase in net-pay, layering of rock types, and flow units. |
| Unconformities, contacts | Boundaries and 3-D shape of flow units. |
| Erosional cuts and infill | Reduction of net-pay, modification of flow units, barriers to flow. |
| Geochemical environment | Early cement, decrease of porosity and permeability, interfacies layering of properties. |

TABLE 20. - Classification of productive and nonproductive facies of Muddy formation sediments in Bell Creek reservoir

| CLASS | | FACIES | | B - BARRIER NB - NON-BARRIER |
|---|---|---|---|---|
| A | PRODUCTIVE | FORESHORE[1] (UPPER/LOWER) | - B | |
| | | AEOLIAN | - B | |
| | | AEOLIAN FLAT | - B | |
| | | UPPER SHOREFACE | - B | |
| | | MIDDLE SHOREFACE | - B | |
| | | WASHOVER (TAIL & CORE) | - B | |
| | | CHANNEL CUT FILL (HIGH ENERGY) | | - NB |
| | | MARINE VALLEY FILL (HIGH ENERGY) | | - NB |
| B | PRODUCTIVE | LOWER SHOREFACE | - B | |
| | | WASHOVER (INTO LAGOON) | - B | |
| | | MARINE VALLEY FILL (LOW ENERGY) | - NB | |
| | | CHANNEL CUT FILL (LOW ENERGY) | - NB | |
| | | ALLUVIAL VALLEY FILL (HIGH ENERGY) | | - NB |
| | | ESTUARY FILL | - NB | |
| | | WINDBLOWN SAND IN LAGOON | - NB | |
| C | NON-PRODUCTIVE | LAGOON FILL | - NB | |
| | | ALLUVIAL VALLEY FILL (LOW ENERGY) | - NB | |
| | | SWAMP & MARSH | - NB | |
| | | MARINE TRANSITION TO THE BARRIER | - NB | |

[1]Dominant facies are underlined.

TABLE 21. - Quantitative XRD determination of mineralogy for subsurface samples from Bell Creek field and a nearby outcrop (GM = Green Mountain outcrop)

| Well | Depth, ft | Depositional setting | Mineralogy in percent | | | | | | | | | | | |
|---|---|---|---|---|---|---|---|---|---|---|---|---|---|---|
| | | | Quartz | Feldspar | Calcite | Dolomite | Anhydrite | Barite | Pyrite | Kaolinite | Illite | Smectite | Ill./Smectite | Siderite |
| Subsurface) | | | | | | | | | | | | | | |
| C-8 | 4351 | Lagoon | 76 | 3 | - | 4 | - | - | - | 7 | 8 | tr | - | 2 |
| 27-16 | 4303-3 | Washover | 88 | 2 | tr | tr | - | - | - | 6 | 4 | - | tr | tr |
| W-14 | 4309.3 | U./L/Shoreface | 89 | 3 | tr | tr | - | - | tr | 5 | 3 | tr | - | - |
| 27-14 | 4309.5 | U. Shoreface/foreshore | 94 | tr | tr | tr | - | - | - | 4 | 2 | tr | - | - |
| 27-14 | 4331.5 | U. Shoreface/foreshore | 90 | 2 | - | 2 | - | - | tr | 4 | 2 | tr | 1 | - |
| W-16 | 4308.6 | Foreshore | 91 | 2 | 1 | 1 | - | tr | - | 3 | 2 | 1 | - | - |
| W-16 | 4318 | U. Shoreface | 88 | 2 | 1 | 1 | - | tr | - | 5 | 3 | tr | - | - |
| W-7 | 4405.5 | Estuarine | 88 | 4 | - | tr | - | - | - | 2 | tr | 6 | - | - |
| W-7 | 4410.0 | Estuarine | 79 | 4 | - | - | - | - | - | 2 | tr | 15 | - | - |
| W-7 | 4417.5 | Swamp | 92 | 3 | - | - | - | - | - | 3 | tr | 2 | - | - |
| W-7 | 4418.9 | Alluvial Channel | 96 | 1 | - | - | - | - | - | 3 | tr | tr | - | - |
| W-7 | 4419.5 | U. Shoreface | 94 | 2 | - | - | - | - | - | 2 | 2 | tr | - | - |
| W-7 | 4431.3 | U. Shoreface | 91 | 3 | - | - | - | 2 | - | 2 | 2 | tr | - | - |
| Outcrop | | | | | | | | | | | | | | |
| GM | 0 | Fluvial channel ss | 93 | 2 | - | tr | 1 | - | - | 3 | 1 | tr | | |
| GM | 10 | Fluvial channel ss | 97 | tr | - | - | - | - | - | 2 | tr | 1 | | |
| GM | 52 | Continental sits. | 96 | tr | - | tr | tr | - | - | 2 | tr | 2 | | |
| GM | 65 | Fluvial ss | 97 | tr | - | tr | tr | - | - | 1 | tr | 22 | | |

TABLE 22. - Sedimentologic division of typical valley fill sandstones associated with barrier island deposits, Muddy formation

(Dominant features identified in Bell Creek cores and New Haven outcrops)

| | |
|---|---|
| | **Continental** |
| **FLUVIAL CHANNEL FILL** (High Energy) | Sandstone 100-200 ), alluvial deposit. Fair to moderately well sorted. Abundant troughs, horizontally or subhorizontally laminated in thin sets; massive appearing where thoroughly rooted, sometimes recognizably rooted or burrowed; 5-10% current ripples associated with shale. Carbonaceous (5%) Trace of shale as rip-up clasts or drapes on ripples. Lower boundaries erosional and abrupt. |
| | **Brackish Marine** |
| **SANDY ESTUARY OPEN LAGOON** | **Sandstone 75-125 ) interlaminated with silt** (30%) and shale (30%). Carbonaceous (15%) Very poorly sorted. Massive appearing or horizontally to subhorizontally very finely laminated; subordinate wavey bedding; low amplitude current ripples; common soft sediment deformation. Burrowed (5-50%); locally thoroughly bioturbated or rooted. |
| **TIDAL CHANNEL AND DELTA** | **Sandstone 150-175 ), current deposit.** Poorly sorted Cross-bedded or low-relief planar tabular laminations. Poorly burrowed (Skolithos). |

TABLE 23. - Comparison of formation thickness along cross section A-A' based on interpretation of gamma ray, SP, and resistivity logs and available cores (in feet)

| | Well No. | Barrier island sandstone | Valley fill sandstone | Total valley fill | Total Muddy formation |
|---|---|---|---|---|---|
| SW | 27.5 | 17.5 | 9.0 | 25.0 | 42.5 |
| | W-14[1] | 18.0 | 10.0 | 25.5 | 43.5 |
| | P-20 | 20.0 | 8.0 | 25.5 | 45.5 |
| | W-13 | 18.0 | 10.0 | 28.0 | 46.0 |
| | C-10[1] | 20.0 | 11.0 | 29.0 | 49.0 |
| | P-13 | 20.5 | 7.0 | 25.0 | 45.5 |
| | W-10[1] | 21.0 | 10.0 | 24.0 | 45.0 |
| | C-9 | 20.0 | 7.0 | 24.0 | 44.0 |
| | P-12 | 19.5 | 6.0 | 25.0 | 44.5 |
| | C-4[1] | 21.0 | 5.5 | 26.0 | 47.0 |
| | W-9 | 20.5 | 7.5 | 24.0 | 44.5 |
| | P-5 | 21.0 | 7.5 | 21.5 | 43.5 |
| | W-6[1] | 20.0 | 9.5 | 23.0 | 43.0 |
| | C-3 | 22.0 | 5.0 | 20.0 | 44.0 |
| | P-4 | 21.5 | 5.5 | 22.0 | 43.5 |
| NE | W-4[1] | 21.0 | 4.0 | 21.5 | 42.5 |

[1]Core control on these wells.

TABLE 24. - Prevailing stacking patterns documented in Muddy formation sediments in the central part of Unit 'A', Bell Creek field

| COMMON | | LESS COMMON | |
|---|---|---|---|
| C<br>A<br>B<br>C | C<br>B<br>A<br>B<br>C | C<br>A<br>C | C<br>B<br>C |

A = Best reservoir-quality sandstone facies.
B = Poor reservoir-quality sandstone facies.
C = Nonreservoir quality facies.

TABLE 25. - Overall influence of geological heterogeneities on production performance in TIP area, Bell Creek field

| Production | Depositional facies (Stacking and continuity) | Diagenetic (Clay cement) | Structural | |
|---|---|---|---|---|
| | | | Faulting | Structural dip |
| Primary | Very High | Moderate | Low | Negligible |
| Secondary | Moderate | Moderate to Very High | Negligible | Very High |
| Tertiary | Very High | High to Very High | Moderate to High | Negligible |

TABLE 26. - Major diagenetic phases identified within the barried sandstone facies and their potential effect on porosity and permeability Muddy formation, Bell Creek field, Unit 'A'

| Diagenetic phase | Suggested cause | Potential effect |
|---|---|---|
| Dominant leaching<br>creates secondary porosity<br>creates oversize pores<br>effects chert, feldspars, sed. rock fragments<br>early kaolinization | Meteoric water lens | Major $\phi$ increase |
| Siderite cement | Mixing of waters at low Eh | Insignificant $\phi$ decrease |
| Compaction<br>increases rock heterogeneity<br>disjoints pore system<br>creates silt size detritus<br>creates pseudomatrix | Overburden pressure | Major k decrease |
| Silica overgrowths<br>increase grain eccentricity<br>reduce pore throats<br>increased grain contact | Solution-reprecipitation | Minor $\phi$ decrease<br>Minor k decrease |
| Calcite cement<br>usually fills all porosity<br>beds subdivide facies<br>stops compaction | Deoxygenation, pH and/or temperature changes causing oversaturation | Major $\phi$ decrease<br>Major k decrease |
| Later leaching<br>corrodes grains and prior cements | Reestablished meteoric water lens | Major or Minor $\phi$ increase<br>Major k increase |
| Clay cement<br>fills or lines pores<br>blocks throats<br>creates microporosity | changing subsurface water chemistry; new diagenetic fluids along faults | Minor $\phi$ decrease<br>Major k decrease |
| Hydrocarbon migration | Hydrodynamic forces | Retards or stops diagenesis<br>Oil trapped |

TABLE 27. - Relation of porosity and permeability to modal grain size and sorting for individual facies in well W-16. Muddy Formation, Bell Creek field, Unit 'A', TIP area

| UNIT NUMBER | ENVIRONMENT OF DEPOSITION | $\bar{K}$(md) | $\bar{K}$(md) "NON-CEMENTED" ONLY | $\bar{\phi}$(%) | MODAL GRAIN SIZE (μ) | SORTING |
|---|---|---|---|---|---|---|
| 6 | "LAGOON" | 247 | — | 18 | 60 | POOR |
| 5 | SUBTIDAL SANDSTONE | 507 | — | 26 | 150 | FAIR |
| 4 | BACKBARRIER WASHOVER | 1189 | — | 27 | 150 | POOR |
| 3 | FORESHORE (BEACH) | 746 | 823 | 24 | 175 | FAIR TO MODERATE |
| 2 | MIDDLE SHOREFACE | 182 | 494 | 20 | 100 | POOR |
| 1 | BACKBARRIER WASHOVER | 1070 | — | 28 | 125 | FAIR |

TABLE 28. - Relation of porosity and permeability to modal grain size and sorting for individual facies in Well C-1. Muddy Formation, Bell Creek field, Unit 'A', TIP area

| ENVIRONMENT | $\overline{Kv/Kh}$ | $\bar{\phi}$ | $\overline{Kv}$(md) | $\overline{Kh}$(md) | GRAIN SIZE |
|---|---|---|---|---|---|
| CONTINENTAL | 0.79 | 26 | 288 | 366 | 100 |
| BRACKISH MARINE | 0.37 | 24 | 51 | 168 | 110 |
| ? | 0.75 | 28 | 2508 | 3382 | 115 |
| FORESHORE (U) (BEACH) | 0.85 | 29 | 4001 | 4757 | 150 |
| UPPER SHOREFACE | 1.00 | 29 | 5561 | 5127 | 165 |
| WASHOVER | 0.76 | 31 | 4613 | 6085 | 150 |
| LAGOON OR LOWER SHOREFACE | 0.03 | 18 | 0.1 | 3.3 | — |

TABLE 29. - Engineering components required for reservoir characterization models

Rock Characteristics

Petrophysical properties
Lithology/mineralogy
Mechanical properties
Pore volume compressibility
Sonic properties
Thermal properties
Core gamma spectroscopy

Fluid Characteristics

Crude oil/gas/injected composition
P.V.T. properties
- Saturation pressure
- Thermal expansion
- Liquid compressibilities
- Density, gravity
- Viscosity/compositional phase viscosity
- Formation volume factor vs pressure
- Solution gas vs pressure

BS & W
Brine-oil-micellar phase behavior
Acid number
Interfacial tension
Emulsion formation
Low temperature oxidation of fuel deposit
Minimum miscibility pressure
Watson characterization
Precipitation of asphaltenes
Density & compressibility of $CO_2$ saturated oil
Metals in oil
Water analysis
Total dissolved solids/total suspended solids
Presence of multivalentions in injection water and reservoir water
Turbidity
Redox potential, Eh
Biological analysis
Water-softening tests
Properties of carbonated water
Molecular weight

TABLE 29. - Engineering components required for reservoir characterization models - Continued

Rock-Fluid Interaction Characteristics

Saturations
Chemical reactions
Formation damage susceptibility
Critical velocity, water sensitivity tests
Cation exchange capacity (CEC)
Chemical absorption and desorption
Chemical precipitation
Wettability
Capillary pressure/capillary number
Relative permeability
Electrical resistivity properties
Dispersivity/molecular diffusivity
Mobility of stabilized oil bank
Polymer resistance factor
Polymer residual resistance factor in accessible pore volume

Well Drainage Area/Model

Saturations/ROS
Porosity
Mineralogy
Fractures/faults/pinchout/contacts
Layerings
Formation damage
Average permeability
Flowing pressure/static pressure
Interwell flow continuity
Thickness
Drainage area/volume
Well data/completion data

Production/Injection Rates Pressure, Drive Mechanism

Water, oil, gas production rates
Water, gas injection rates
Pressure history
Variation in drive indices
Gas cap size/aquifer size

TABLE 30. - Sources of data and their relative merits (After Timmerman, 1980).

| Time | Predrilling | | | | | | | During drilling | | | | | | | | | | | Post development | | | | | | |
|---|---|---|---|---|---|---|---|---|---|---|---|---|---|---|---|---|---|---|---|---|---|---|---|---|---|
| Operation | Gravity | Seismic | | | | Geology-Eng study | | Well bore operations | | | | | | | | | | | Production | | | | | Special studies | |
| | | | | | | | | | | | | | Logs | | | | | Wire line | | | | | | | |
| | Gravity | Time | Velocity | Amplitude | Character | Analogy Regional knowledge and maps | Depositional environment | Drill rate | Mud log | Cuttings | Cores | Drillstem | Electric | SP | Acoustic | Density | Gamma ray | Neutron | Test | Cores | Flow test | Pressure | Water cut GOR | History | Analogy | Engineering and geology |
| Depth markers | | 2 | 2 | | | 2 | 2 | 3 | 3 | 2 | 1 | 1 | 1 | 1 | 1 | 1 | 1 | 1 | 2 | 1 | 2 | | | | | 1 |
| Structure and area | 2 | 2 | 1 | 3 | 3 | 2 | | | | | | 4 | | | | | | | | | 2 | 2 | 3 | 3 | 1 | | 1 |
| Hydrodynamics | | | | | | 1 | | | | | | | | | | | | | | | 2 | | | | 3 | 1 | 1 |
| Gross thickness | | | 2 | | 3 | 2 | 2 | 2 | 2 | 3 | 2 | 4 | 1 | 1 | 1 | 1 | 1 | 1 | | | 2 | | | | | | 1 |
| Net Thickness | | | | 2 | 2 | 2 | 2 | 3 | 3 | 4 | 1 | 4 | 1 | 1 | 1 | 1 | 1 | | | | 2 | | | | | | 1 |
| Lithology | | | 2 | 2 | 3 | 2 | 2 | 3 | | 2 | 1 | | 3 | 3 | 2 | 2 | 2 | 3 | | 3 | | | | | 2 | | 1 |
| Mechanical properties | | | 2 | 2 | 3 | 2 | 2 | 3 | | 2 | 1 | | | | 2 | 2 | 2 | 3 | | 2 | | | | | 2 | | 1 |
| Contacts | | | 2 | 2 | 2 | 4 | | | 3 | 2 | 2 | 2 | 1 | 2 | 1 | 1 | | 1 | 1 | 2 | 1 | | 2 | 2 | 2 | | 1 |
| Pressure | | | 2 | 3 | | 1 | | | 3 | | | 1 | | | | | | | 2 | | 1 | 1 | | | | 1 | 1 |
| Porosity | | | 2 | 2 | 3 | 2 | 2 | 4 | | 3 | 1 | | 3 | | 1 | 1 | | 1 | | 2 | 4 | | | | | 2 | 1 |
| Permeability | | | | | 4 | 2 | 2 | | | 4 | 1 | 1 | 4 | | 3 | 3 | | 3 | 2 | 3 | 2 | 1 | | | | 2 | 1 |
| Relative permeability | | | | | | | | | | | 1 | | | | | | | | | | 1 | 2 | 2 | 2 | 2 | 2 | 1 |
| Fluid saturation | | | 3 | 3 | 3 | 4 | | | 3 | 3 | 2 | 1 | 1 | 3 | 2 | 2 | | 2 | 2 | 3 | 1 | | 1 | 1 | 2 | | 1 |
| Pore Sizes | | | | | | 2 | | | | 2 | 1 | 4 | 4 | 4 | 4 | 4 | 4 | 4 | | 3 | | | | | 2 | | |
| Producing mechanism | | 4 | 3 | 3 | 3 | 2 | 3 | | | | | | | | | | | | | | | | 1 | 1 | 1 | 1 | 1 |
| Hydrocarbon properties | | | 4 | 4 | | 2 | | | 3 | 4 | 3 | 1 | | | 4 | 4 | | 4 | 2 | 4 | 1 | 2 | | 1 | | 2 | 1 |
| Water properties | | | | | | 1 | | | | | 4 | 1 | | | | | | | 2 | | 1 | | 1 | | 2 | | 1 |
| Production rate | | | | | | 2 | 2 | | | | 2 | 2 | | | 4 | 4 | | 4 | 2 | 3 | 1 | 1 | | 1 | 2 | | 1 |
| Fluids produced | | | | | | | | | | | | 1 | | | | | | | | | 1 | | 1 | 1 | 1 | 2 | 1 |
| Well damage | | | | | | | | | | | | | | | | | | | | | 1 | 1 | | 1 | | | 1 |
| Recovery efficiency | | | | | | | | | | | | | | | | | | | | | | | 2 | 2 | 1 | 2 | 1 |

Code: 1. Best source 2. Good data source 3. Average data source 4. Poor data source

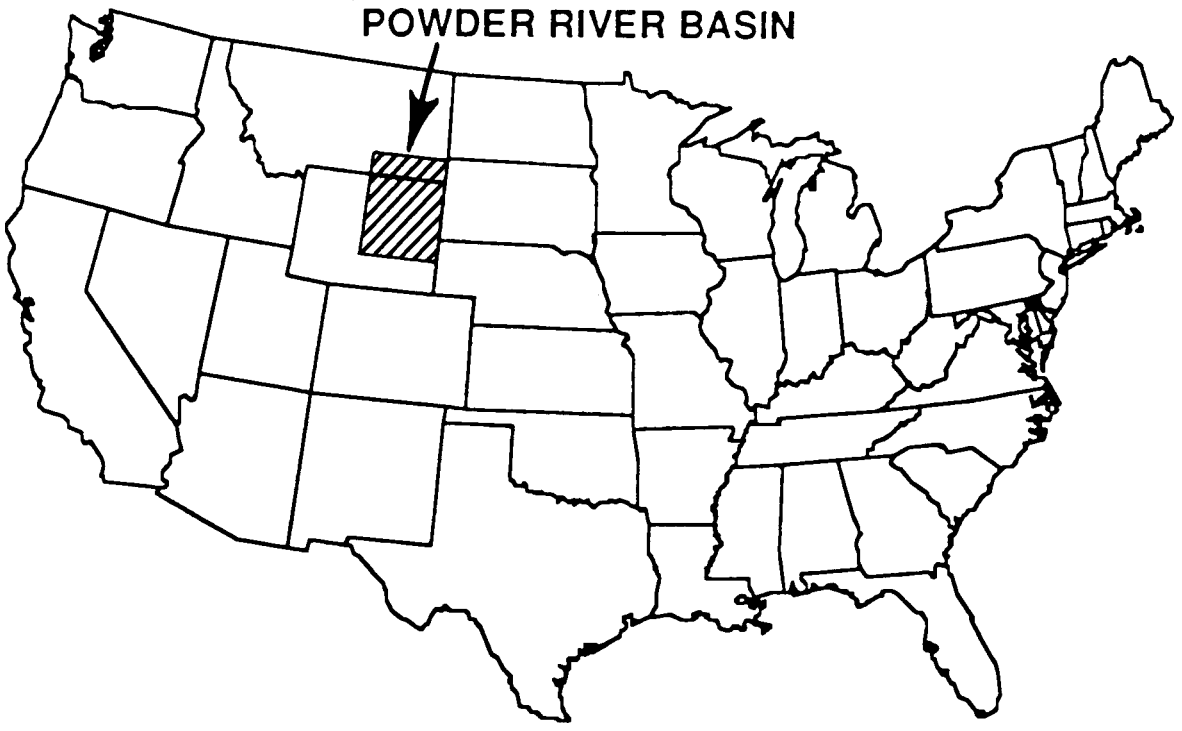


FIGURE 9. - Location of the Powder River Basin within the Continental United States.

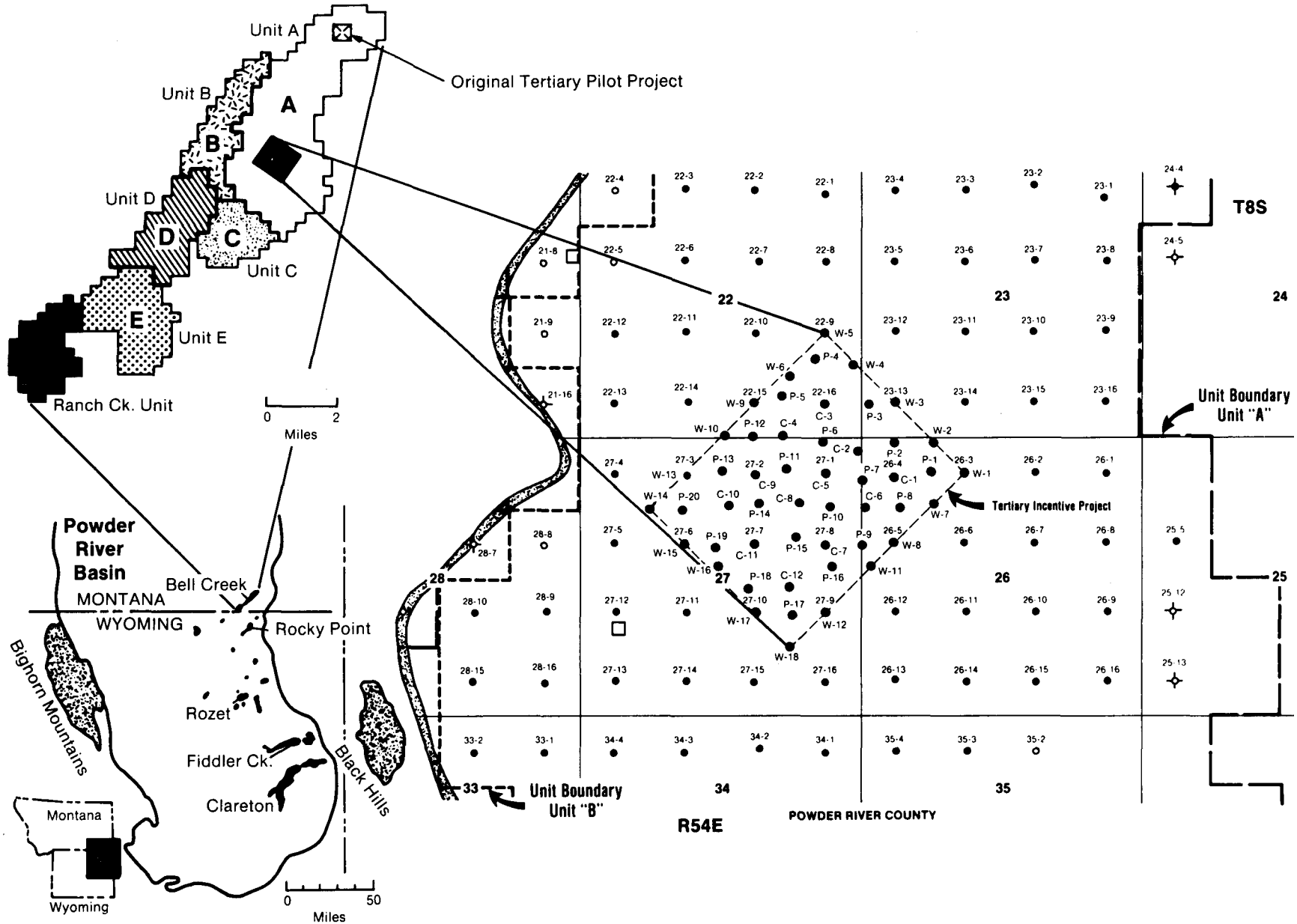


FIGURE 10. - Location map of the Bell Creek field and study area (Secs. 22

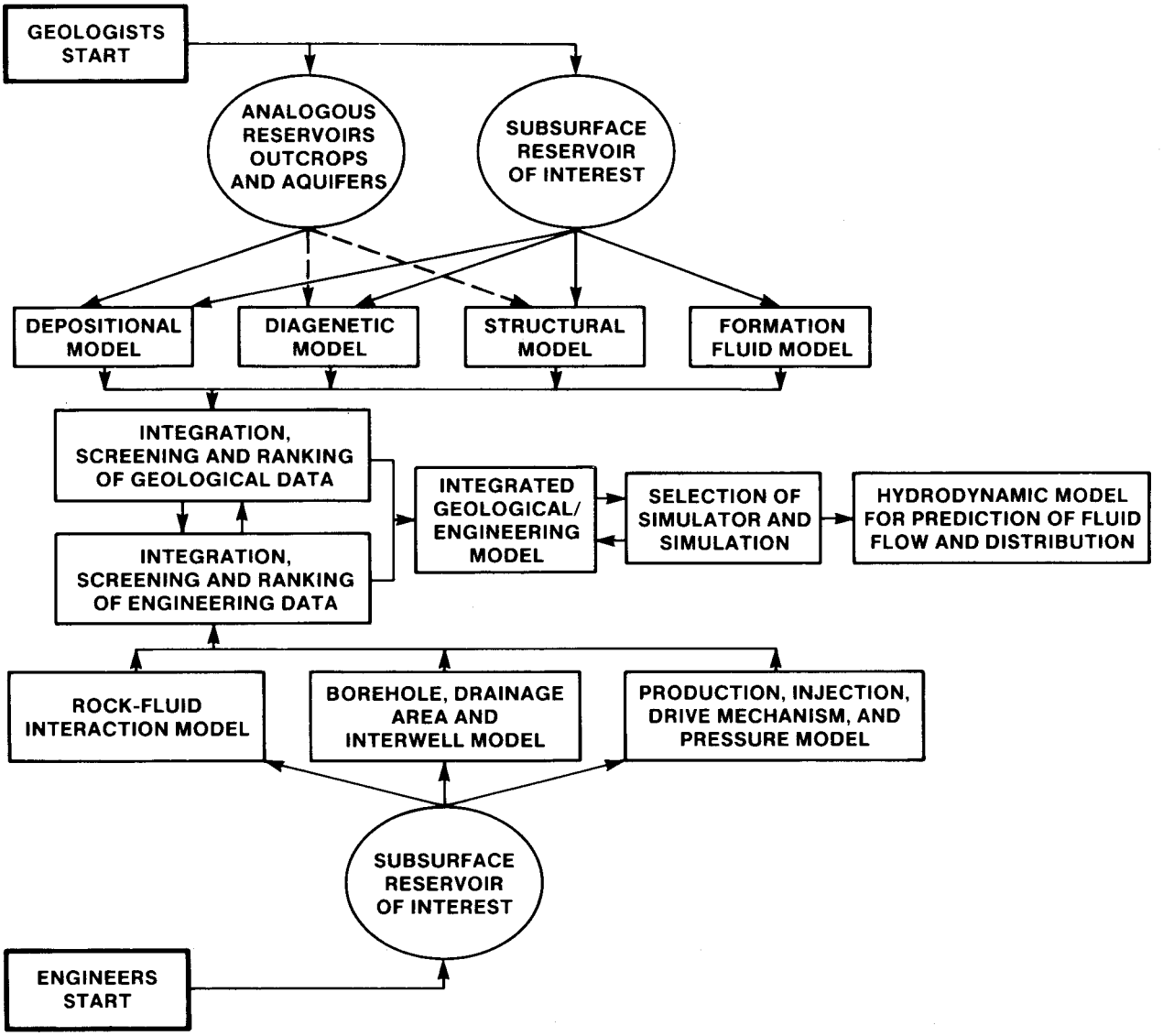


FIGURE 11. - Procedure chart used by authors for integrating geological and engineering study for advanced reservoir characterization.

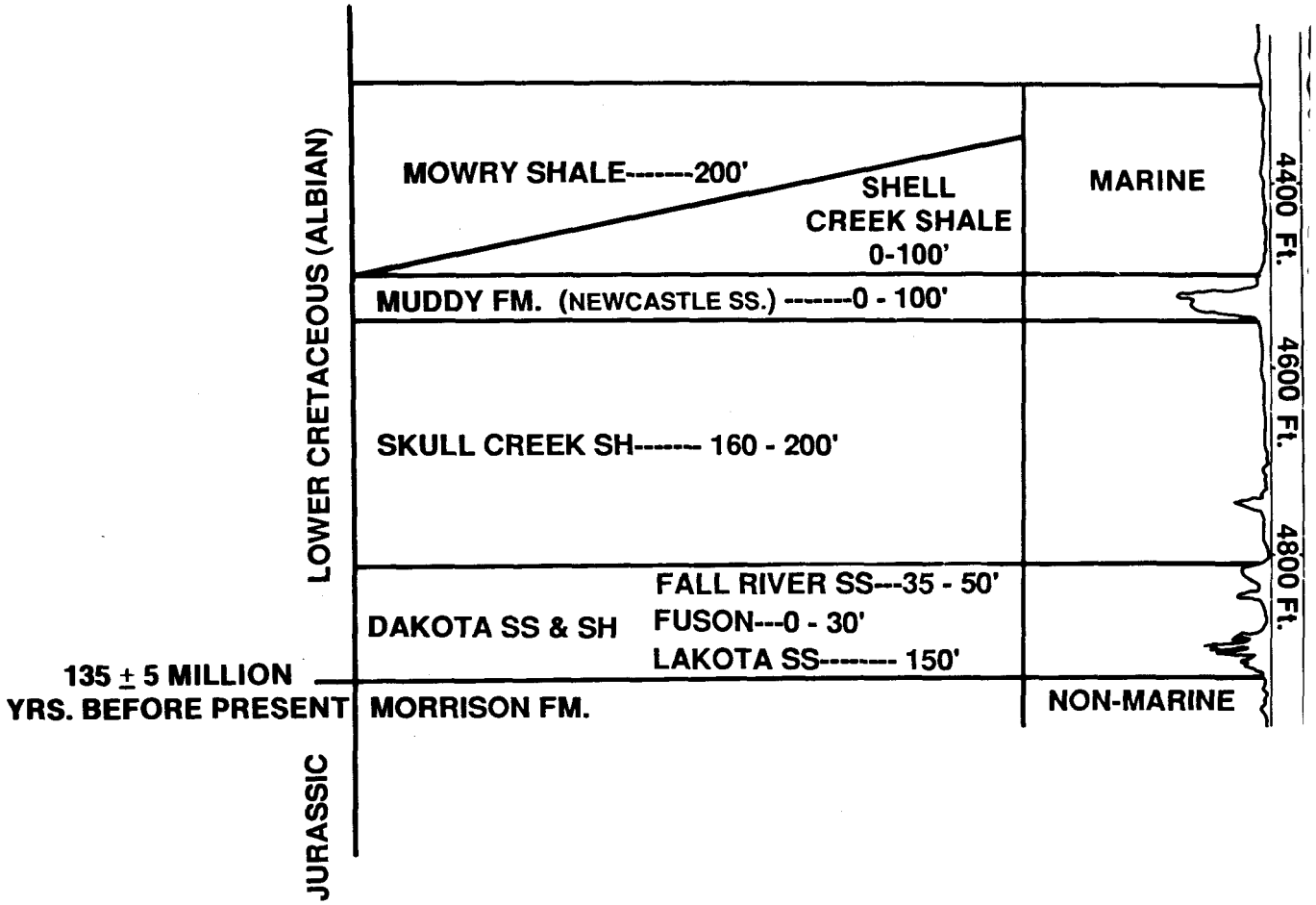


FIGURE 12. - Stratigraphic section showing position of Muddy formation within the Lower Cretaceous.

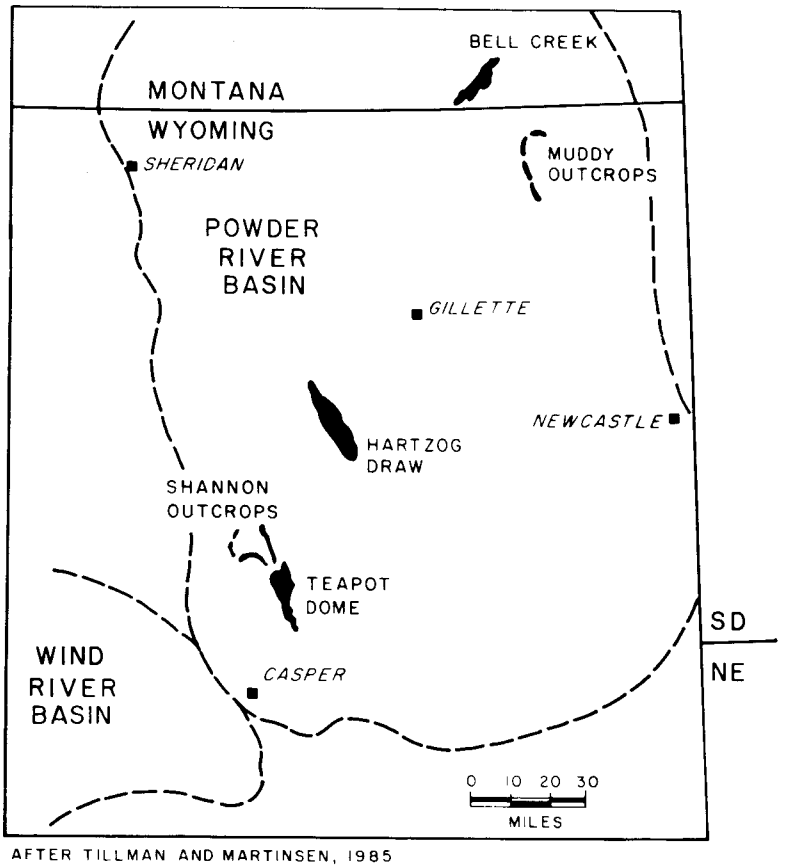


FIGURE 13. - Position of Bell Creek field and Muddy formation outcrops within the Powder River Basin.

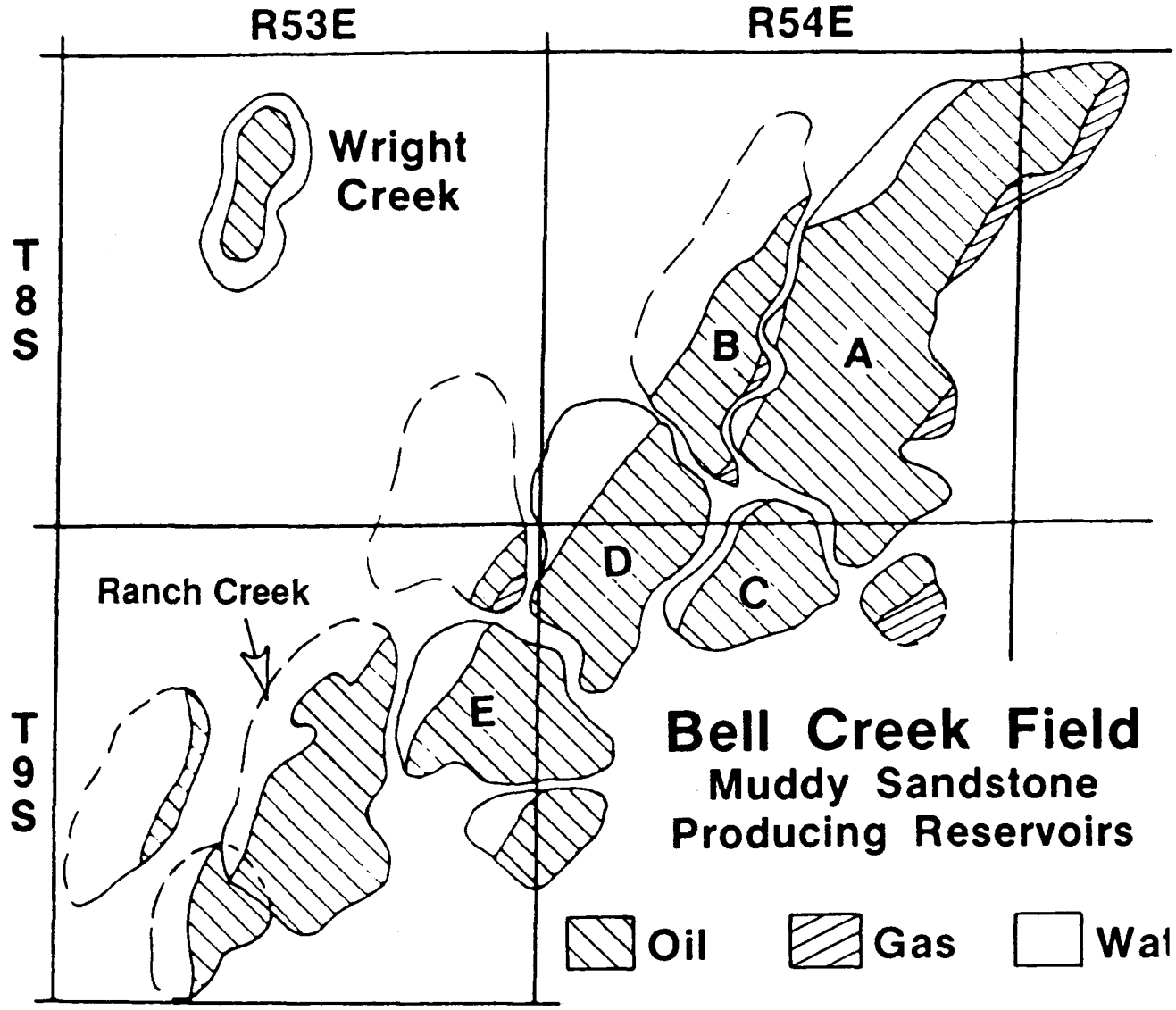


FIGURE 14. - Distribution of formation fluids in production units (A-E) of Bell Creek field and Ranch Creek field (after Jennings, 1986).

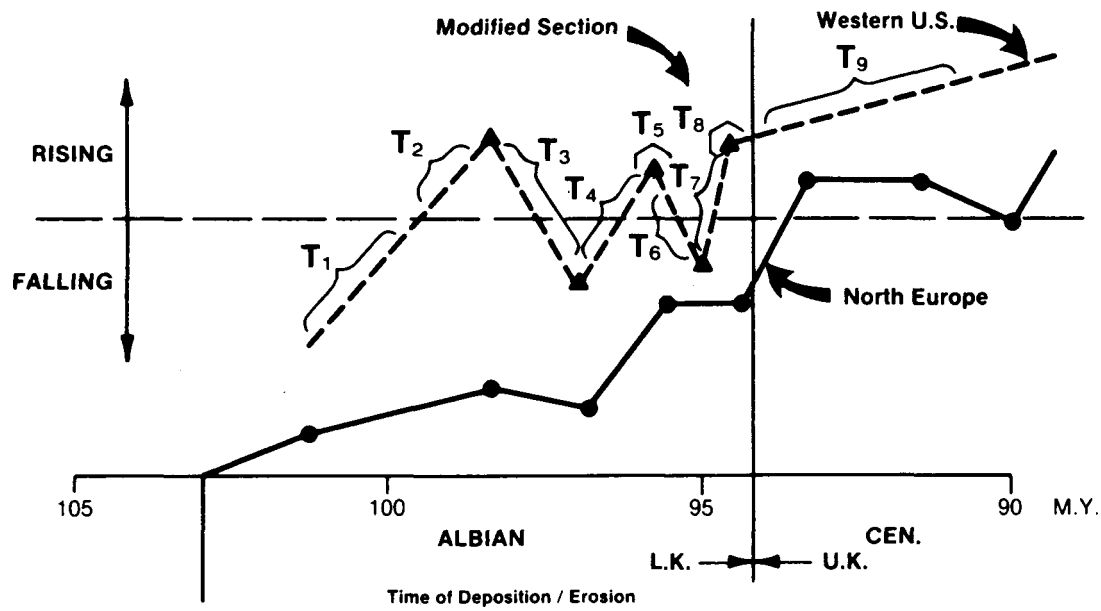


$T_1$ - Inyan Kara Group (Lakota and Fall River Sandstones)

$T_2$ - Skull Creek Shale

$T_3$ - Lower Muddy Valley incisions (in topographic lows)

$T_4$ - Lower Muddy Valley filling (accumulation in topographic lows) (Newcastle Type)

$T_5$ - Barrier Islands formed (Middle Muddy) on topographic highs (Bell Creek, New Haven type)

$T_6$ - Valley incisions into Barrier Islands (Bell Creek, New Haven area)

$T_7$ - Valley infill (Upper Muddy) brackish marine and continental (Bell Creek)

$T_8$ - Shell Creek / Mowry Shale

$T_9$ - Belle Fourche Shale

FIGURE 15. - Relationship of deposition and erosion to inferred sea-level changes during Lower Cretaceous stages in NE Powder River Basin. Based on lithostratigraphy of Muddy formation deposits in Bell Creek field. (Modified from Weimer et al., 1982).

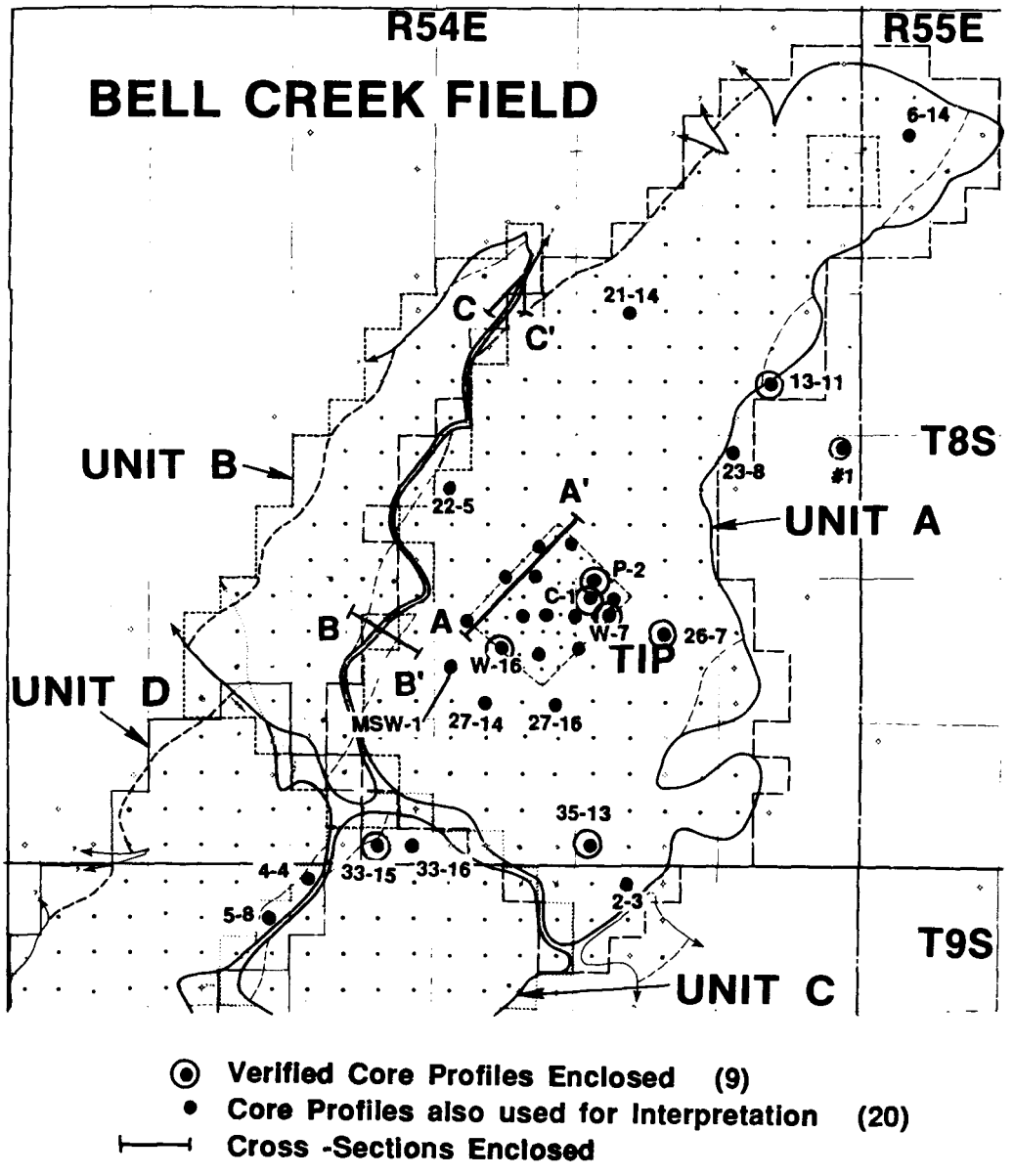


FIGURE 16. - Location of sedimentologically interpreted cores and cross-sections in Bell Creek field (see appendix B for core description).

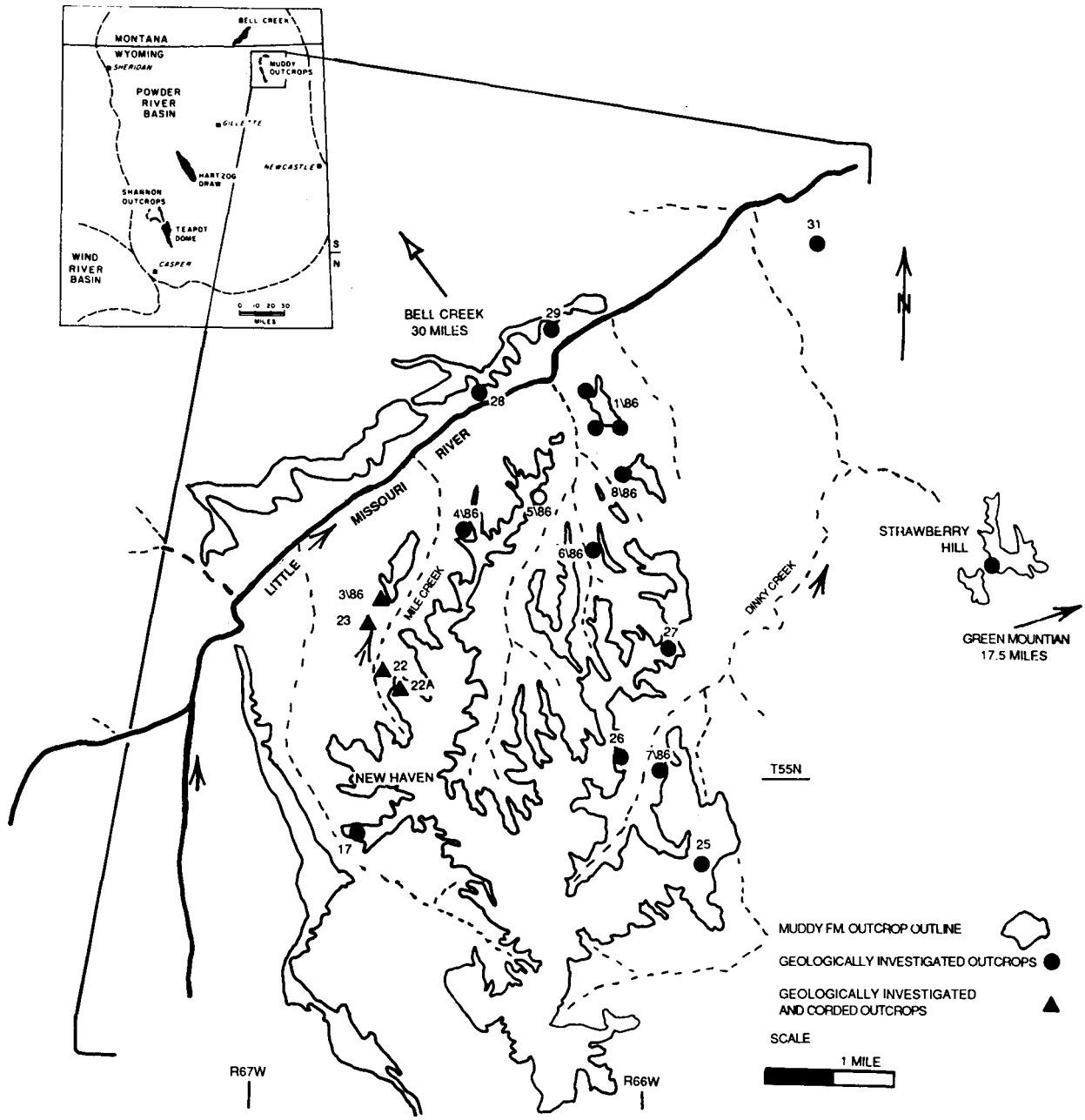


FIGURE 17. - Location of described and interpreted Muddy formation outcrops in New Haven area, NE Wyoming. These outcrops (indicated by triangles) were cored for examination of petrophysical properties.

FIGURE 18. - Muddy formation sandstones, barrier island facies, as seen in outcrops 26 and 27, New Haven area, Wyoming. For location refer to figure 17. A: measured section in outcrop 26 transition sandstones and siltstones (7.8 ft) interbedded with gray shale (1); lower shoreface sandstone (7.7 ft) subhorizontally laminated, 10% shale layers (2); lower section of upper shoreface sandstone (3). B: measured section in outcrop 27 transition sandstone (100 micron) intercolated with silty and sandy shale (1); lower shoreface with trace of shale drapes, hummocky cross-stratification (HCS), and pebbly layer, upper 1.5 feet interbedded with silty shale (2); middle shoreface sandstone, beds 0.5 to 1.5 ft thick (3). C: close up of lower shoreface facies form profile in B. Just above contact with transition facies (1) is hummocky cross-stratified layer (arrow) and pebbly layer (arrows at hammer level) indicating high energy events. D: 3-ft-diameter, highly calcite-cemented patch (arrow) within middle shoreface sandstone. Site located 24 ft east of measured profile at outcrop 23.

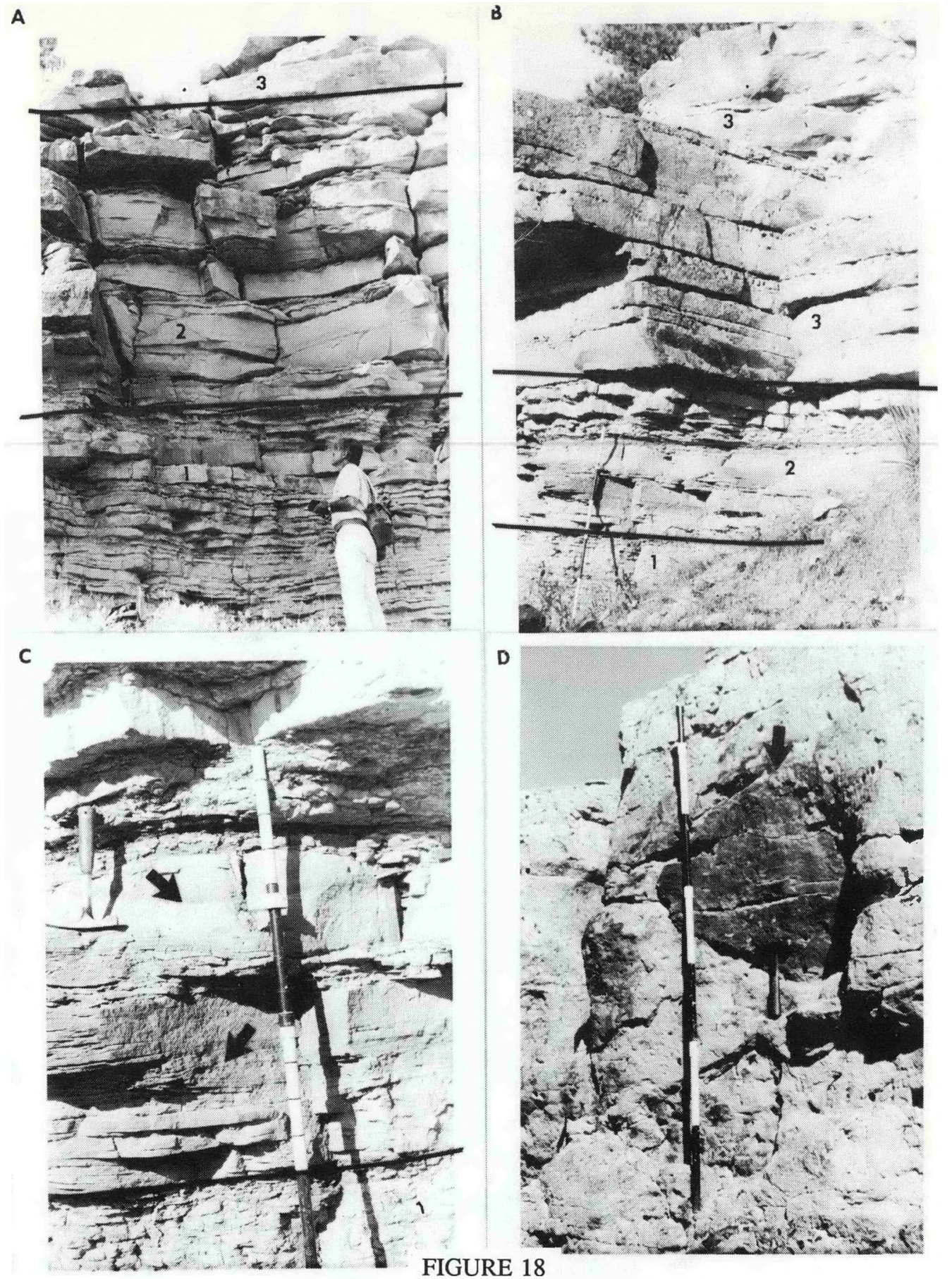


FIGURE 18

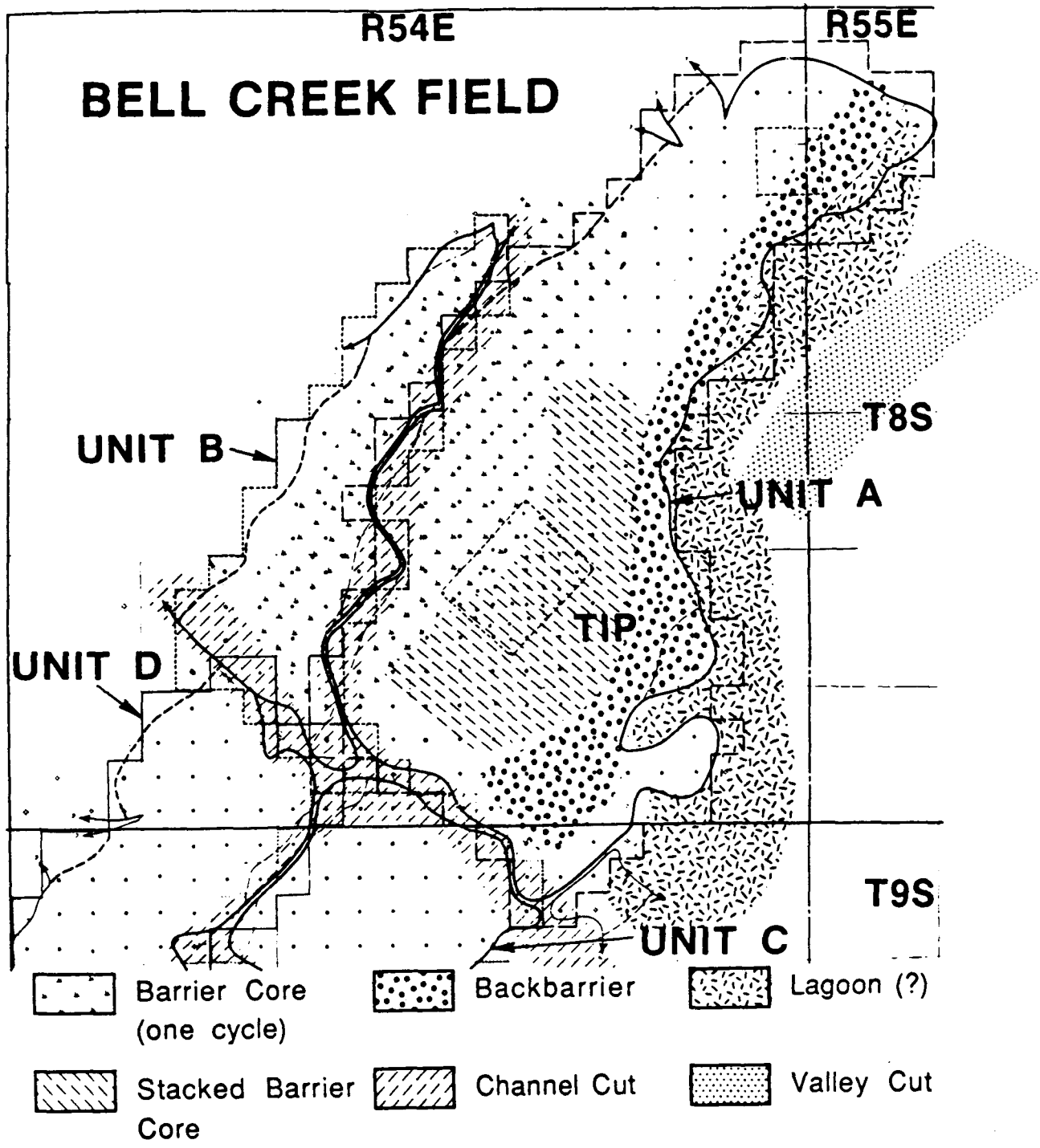


FIGURE 19. - Sketch map of the inferred depositional setting and facies distribution based on geological interpretation of cores and logs in northern part of Bell Creek field. Distribution of cores used to determine facies shown in figure 10.

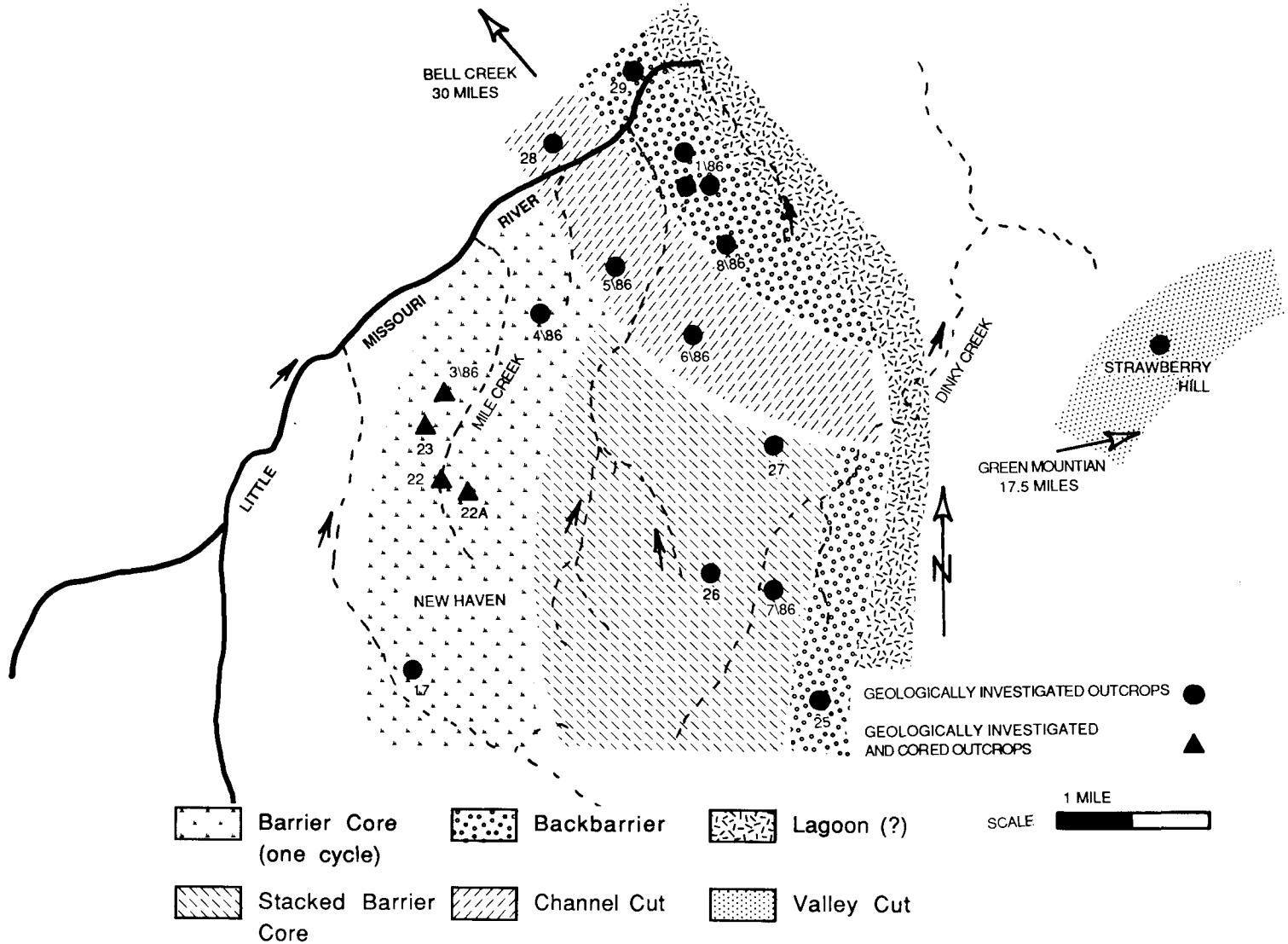


FIGURE 20. - Sketch map of the inferred depositional setting and facies distribution based on geological interpretation of Muddy (Newcastle) formation outcrop profiles in New Haven area, NE Wyoming.

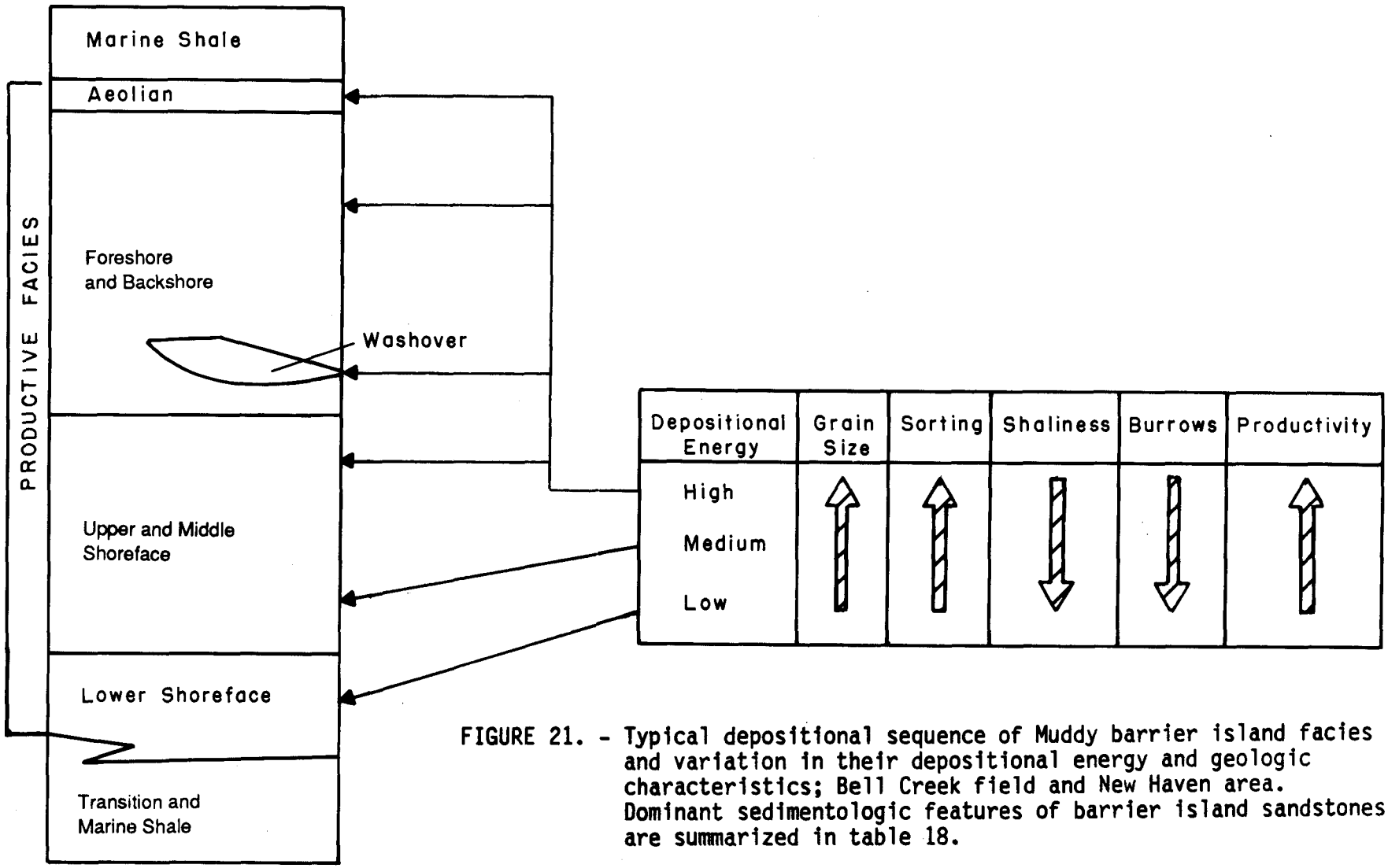


FIGURE 21. - Typical depositional sequence of Muddy barrier island facies and variation in their depositional energy and geologic characteristics; Bell Creek field and New Haven area. Dominant sedimentologic features of barrier island sandstones are summarized in table 18.

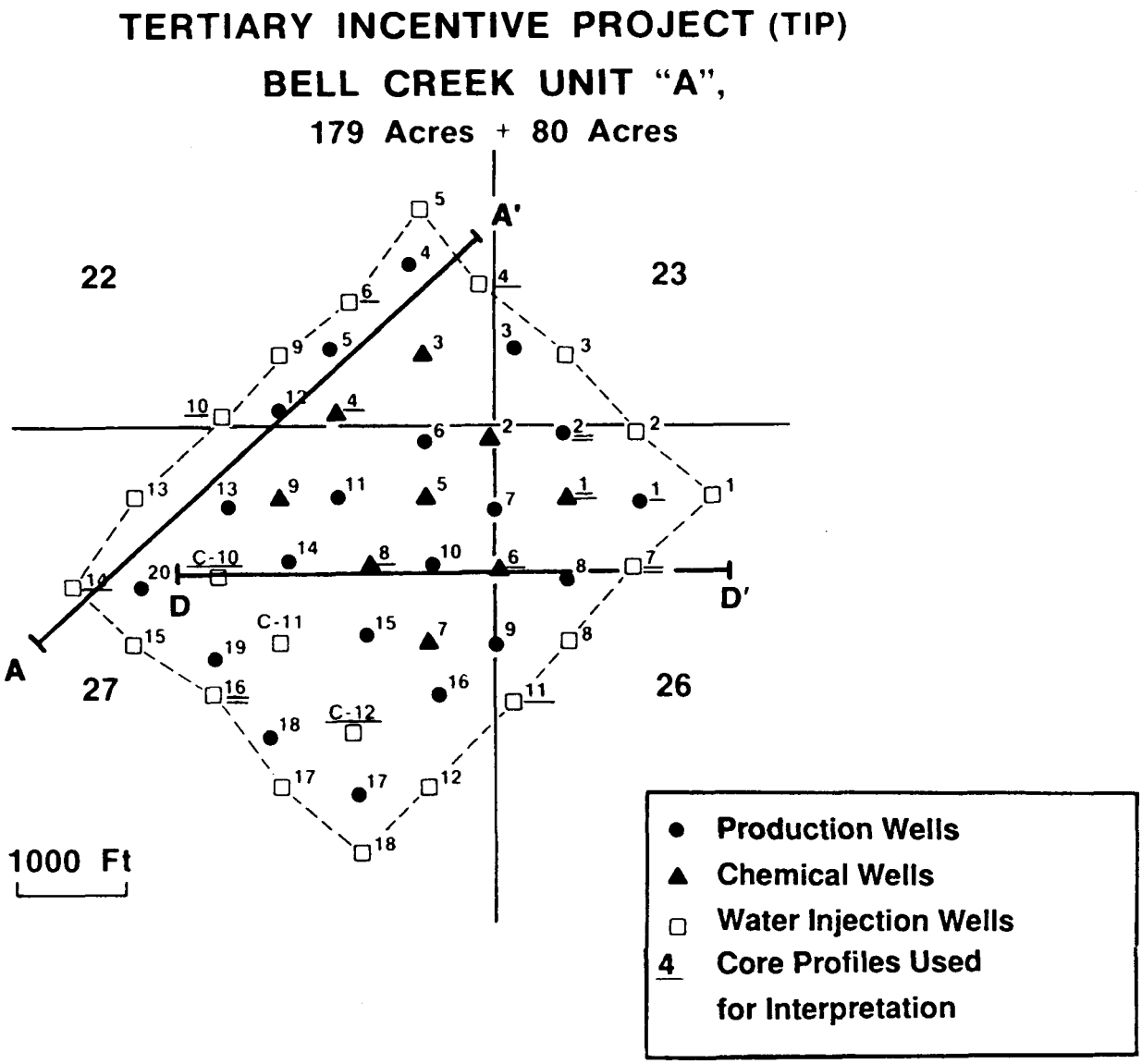


FIGURE 22. - Tertiary incentive project (TIP) area; Bell Creek field, Unit 'A'. Locations of production (P) wells, chemical injection (C) wells and water injection wells (W) are shown as well as location of lithostratigraphic cross-section A-A' (fig. 30) and flow units cross-section A-A' (fig. 100).

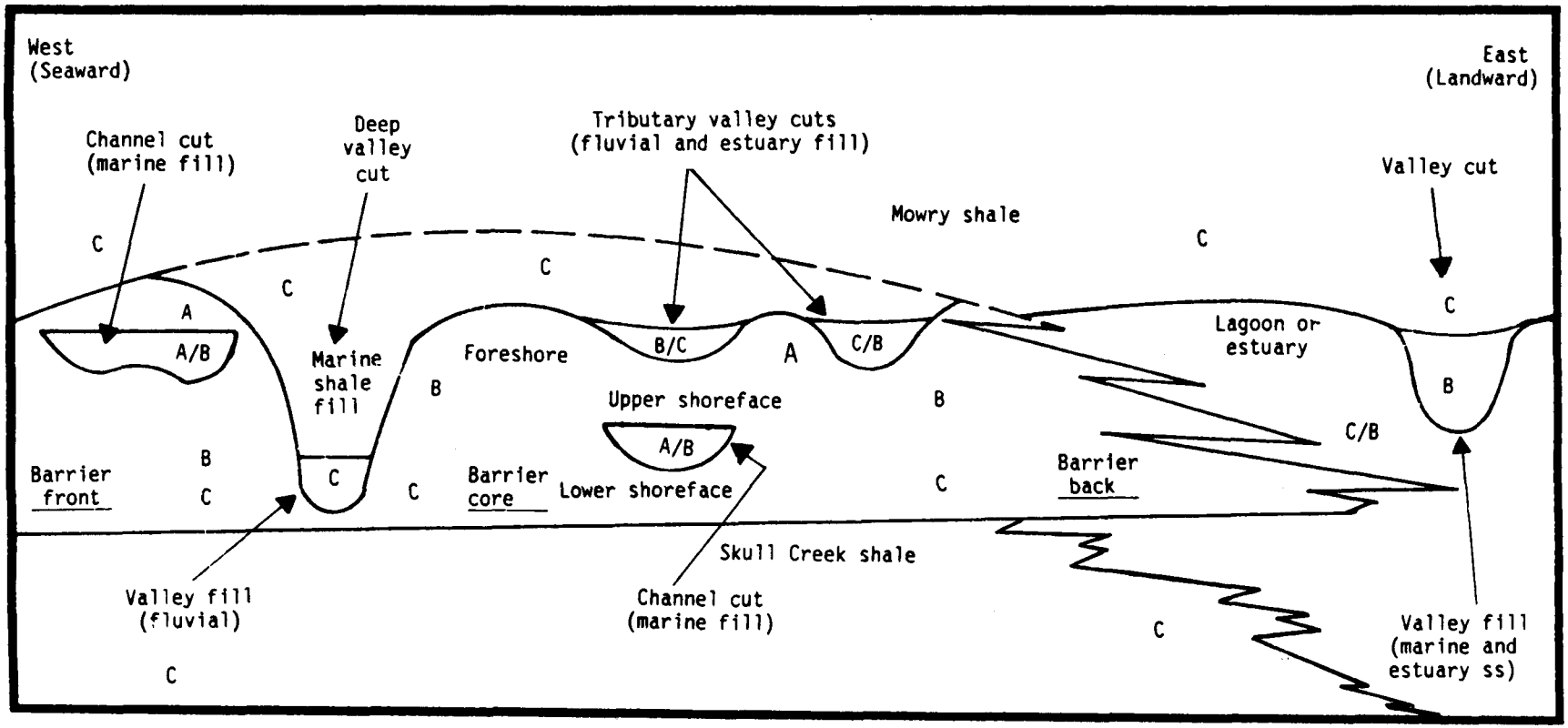


Classification of deposits (A,B,C) as in table 5.
Eroded top of the barrier.
Note details of valley cut infillings.

FIGURE 23. - Conceptual distribution of barrier island and genetically associated nonbarrier facies observed in cores at Bell Creek field. Sedimentologic divisions of typical barrier island sandstones and valley fill sandstones are summarized in tables 18 and 22, respectively. Quality of reservoir rocks indicated as class A, B, and C is indicated in table 20. Note erosion of barrier island top and types of valley cut infilling.

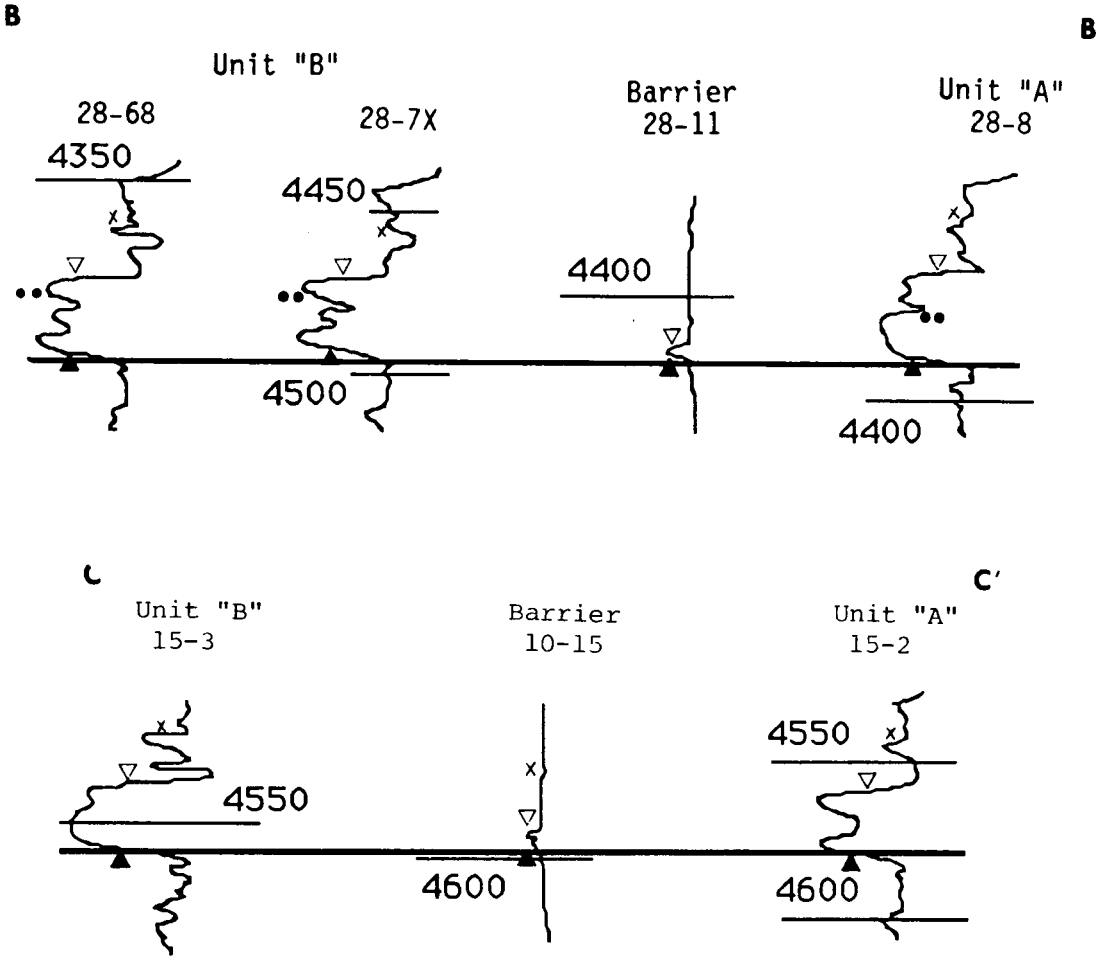


Explanation

- Δ Base of Muddy formation (barrier island sandstones).
- ∇ Top of Muddy sandstone reservoir.
- ... Inferred top of barrier island sandstones.
- x Datum near top of Muddy formation.

FIGURE 24. - Cross-sections B-B' and C-C' (see fig. 16 for location). Gamma ray log responses across hydraulic barrier (channel) dividing production Units 'A' and 'B' in Bell Creek field. Logs indicate deep cuts into Muddy formation barrier island and earlier valley fill which were followed by filling by marine (?) shale. Wells 28-11 and 10-15 are dry holes which are projected into the line of section.

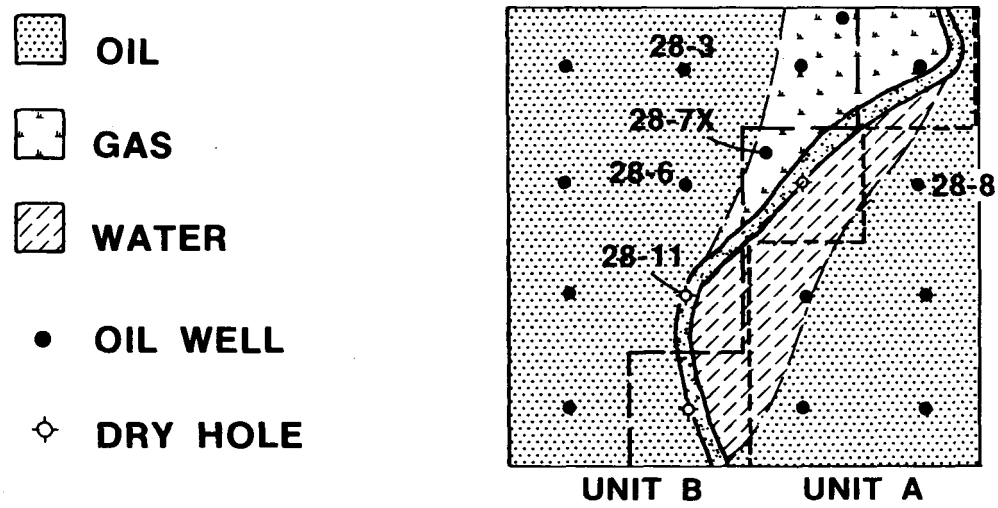


FIGURE 25. - Channel fill comprising hydraulic barrier; western limit of Unit 'A'. Note position of oil, gas, and water contacts on both sides of the barrier. Refer to figure 2 for location within Sec. 28, T8S and R54E.

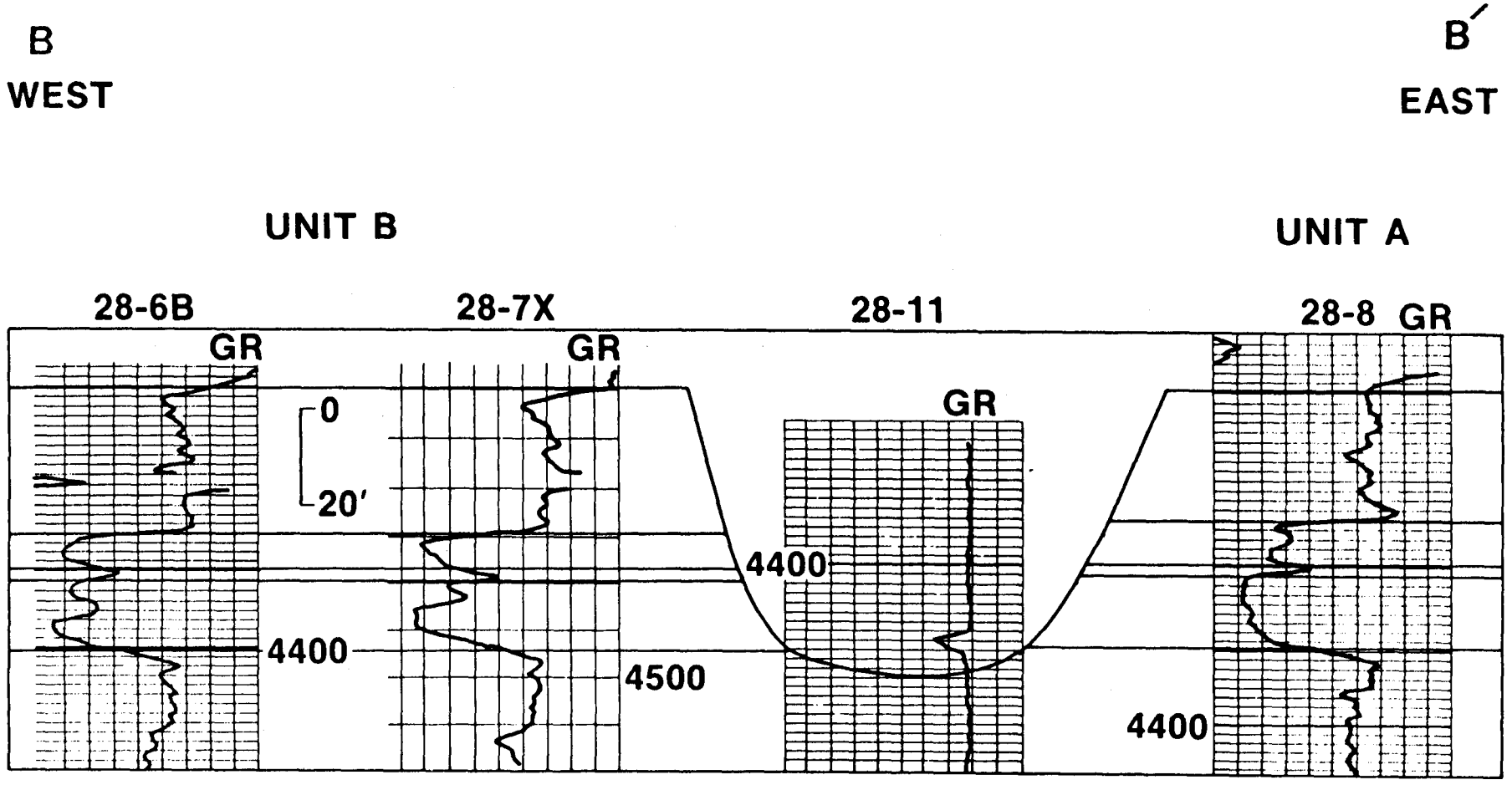


FIGURE 26. - Cross-section B-B' (see fig. 16 for location) showing geometry of deep incision where only 4 feet of possible barrier island sandstone or inlet fill sandstone remain. Thick barrier island sandstone sequences continue on both sides of the erosional cut.

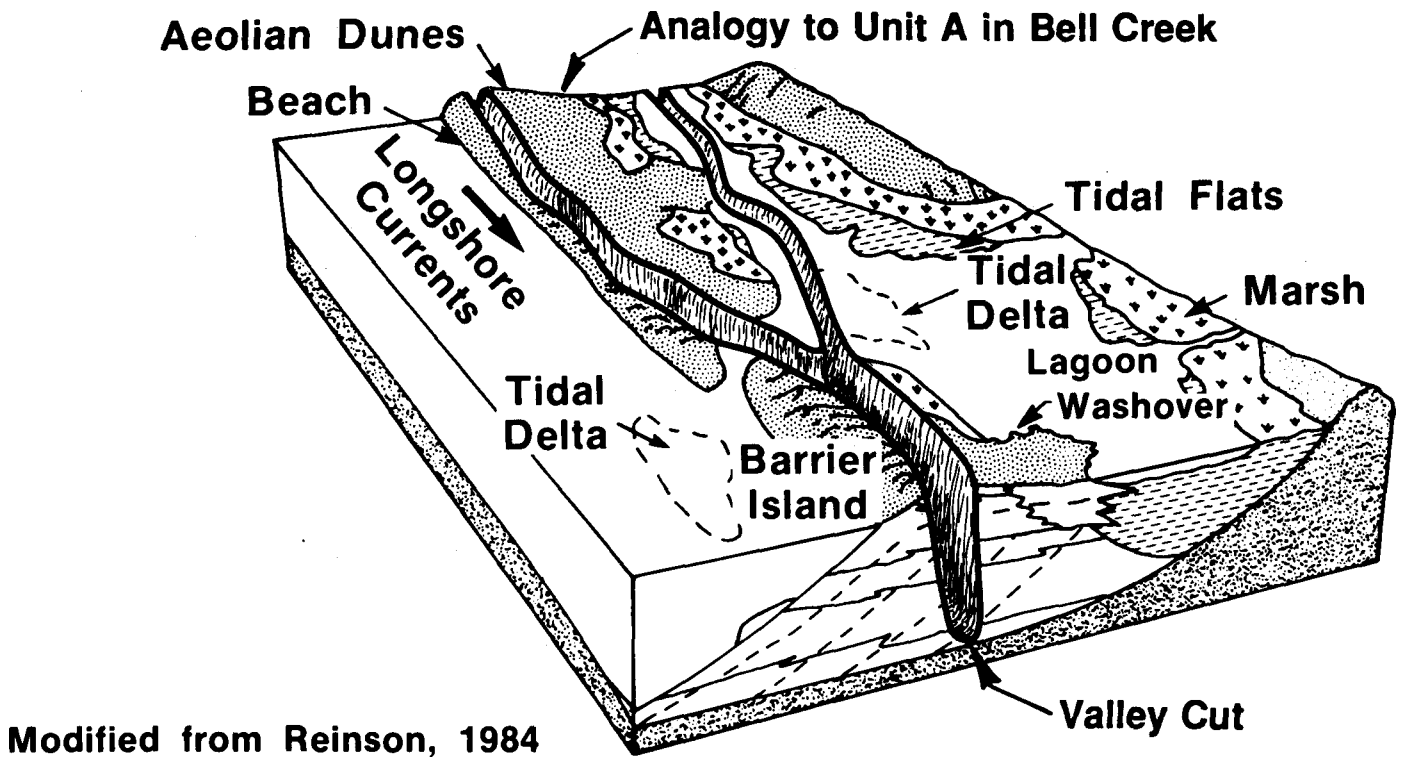


FIGURE 27. - Deep erosional cuts superimposed on diagram of barrier island deposits showing analogy with separation of production Unit 'A' in Bell Creek field from other units.

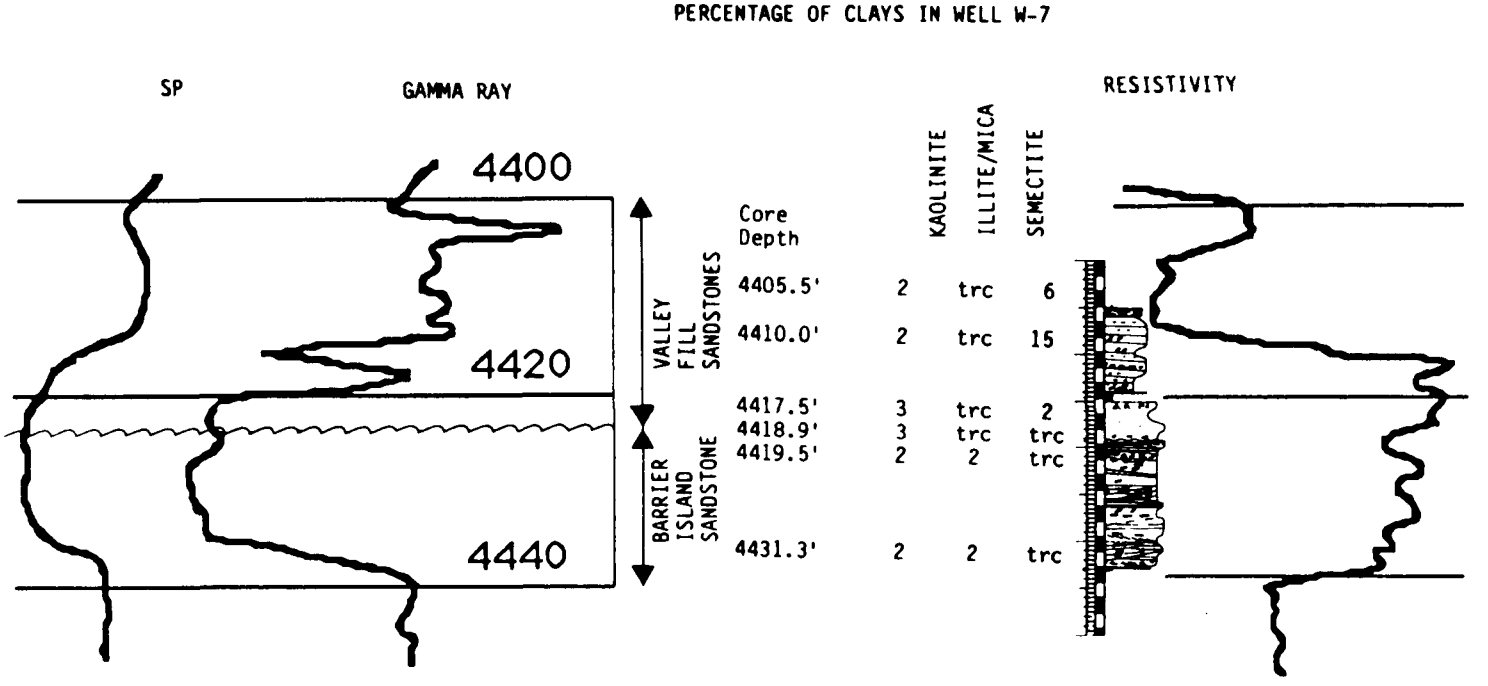


FIGURE 28. - Correlation of core-derived geologic profile with log responses and clay percentages (XRD). High-quality barrier island reservoir sandstones are overlain by valley fill sandstones which have inferior production characteristics. Unconformity between barrier island and valley fill is observed in core at 4,419.3 ft (1,348 m). Note that smectite (mixed layer clay) is significantly more abundant in valley fill deposits. Illite/mica is more abundant in barrier-island sandstone.

FIGURE 29. - Muddy formation, Bell Creek field, Unit 'A'. Upper left-hand photo illustrates depositional disconformity between barrier island and lagoonal sediments at 4,420.2 ft in well P-1 (for location refer to figs. 10 and 22). Permeability of lagoonal silty and shaly sandstones above disconformity (4,439.6 ft) is only 0.78 md. Permeability of backbeach sandstone just below disconformity (4,440.6 ft) is 275 md, while 1 foot deeper (4,441.8 ft) the permeability is nearly 1,000 md. Prominent horizontal line on this photo is an artifact of marking the core at 4,440 ft.

Photos of slabbed core, well W-7 located about 1,000 ft SW of well P-1. Cored interval 4,405.0 ft to 4,433.1 ft. For location refer to figures 10 and 22. Detailed descriptions of cored intervals are available on Open file at NIPER.

| | |
|---|---|
| 4,405.0 - 4,413.0 | Lagoon or estuary (8'+) |
| 4,413.0 - 4,414.0 | Channel fill (1'), unconformity at base. |
| 4,414.0 - 4,415.0 | Swamp (1') |
| 4,415.0 - 4,419.3 | Alluvial channel fill (5'), unconformity at base. |
| 4,419.3 - 4,425.9 | Backshore sandstone (5') |
| 4,425.9 - 4,432.8 | Middle shoreface (9') |
| 4,432.8 - 4,433.1 | Lower shoreface (1'+) |

In this well, permeability of alluvial channel fill immediately above disconfirmity at 4,419.3 ft is 1.7 md. Permeability of backbeach sandstone below disconformity (4,419.5 ft) is 1,730 md, but decreaseds drastically below 4,425 ft (middle shoreface facies) because of clay cementation (lighter-colored part of core). Note that alluvial channel fill is absent in well P-1 (upper left-hand photo) where lagoonal sediments directly overlie the barrier island sandstones.

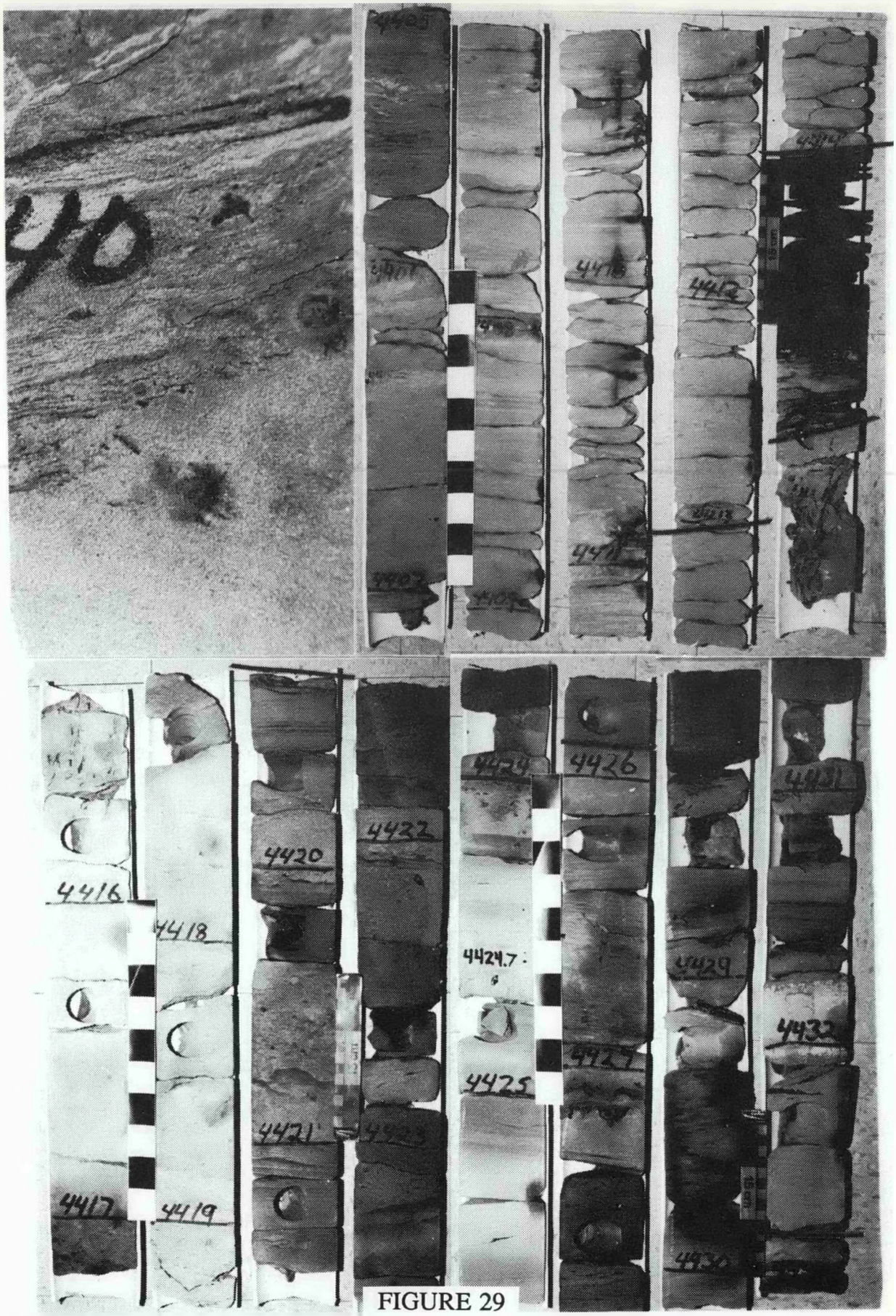
4416
4418
4420
4432
4417
4419
4421
4423
4424.7
4425
4426
4427
4429
4430
4431
4432

FIGURE 29

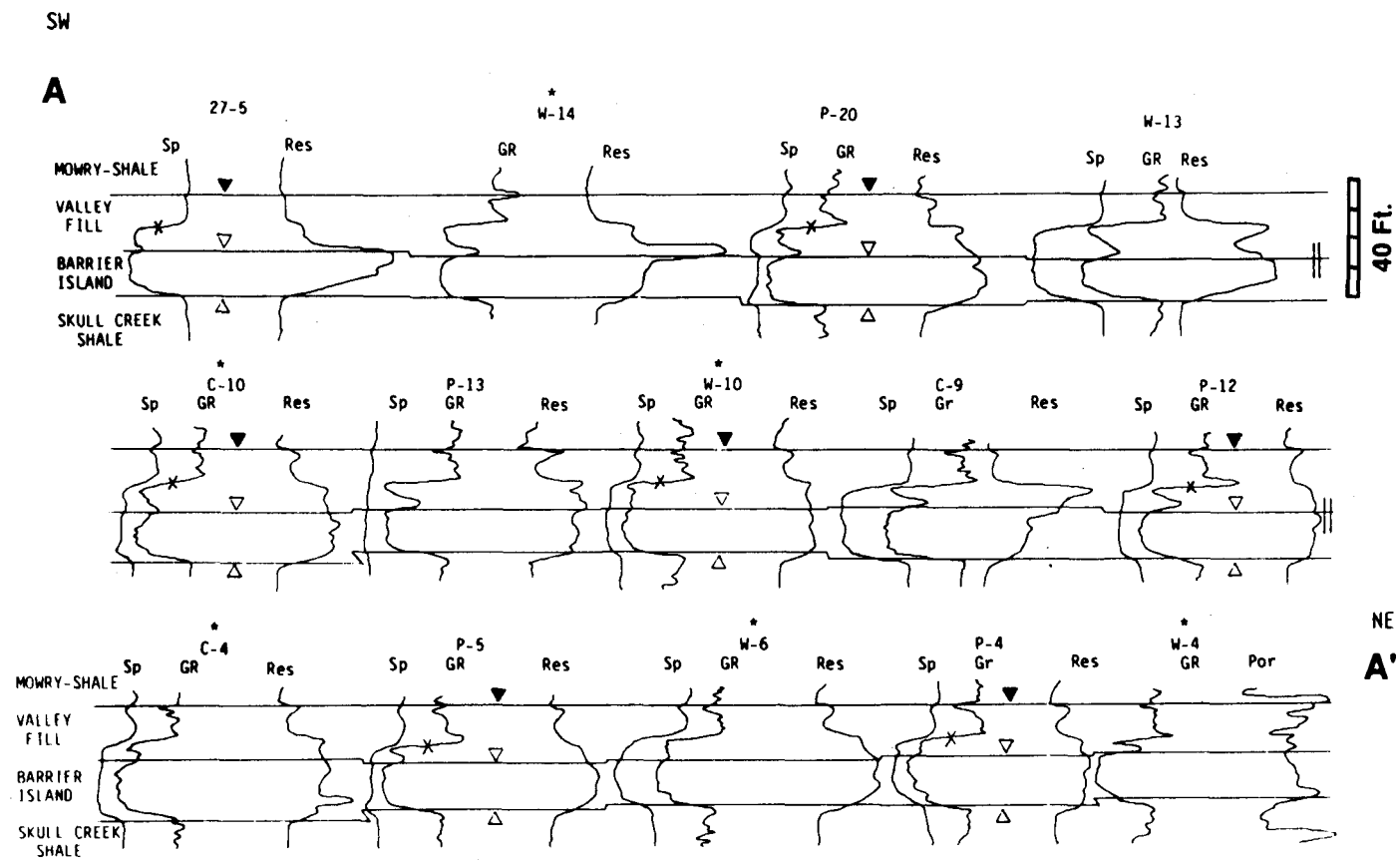


|| break in cross-section
* Core control in these wells.
∆ base of Muddy formation and barrier island unit.
∇ top of barrier island unit.
X top of Muddy sandstones complex (barrier island and valley fill).
▼ top of Muddy formation

FIGURE 30. - Log and core based lithostratigraphic cross-section A-A'. For location see figures 10 and 22. Relationship of major genetic units of Muddy formation in TIP area, Bell Creek field are shown. The datum for the crosssection is the marker near the top of Muddy formation which is constant on SP and gamma ray logs over the area.

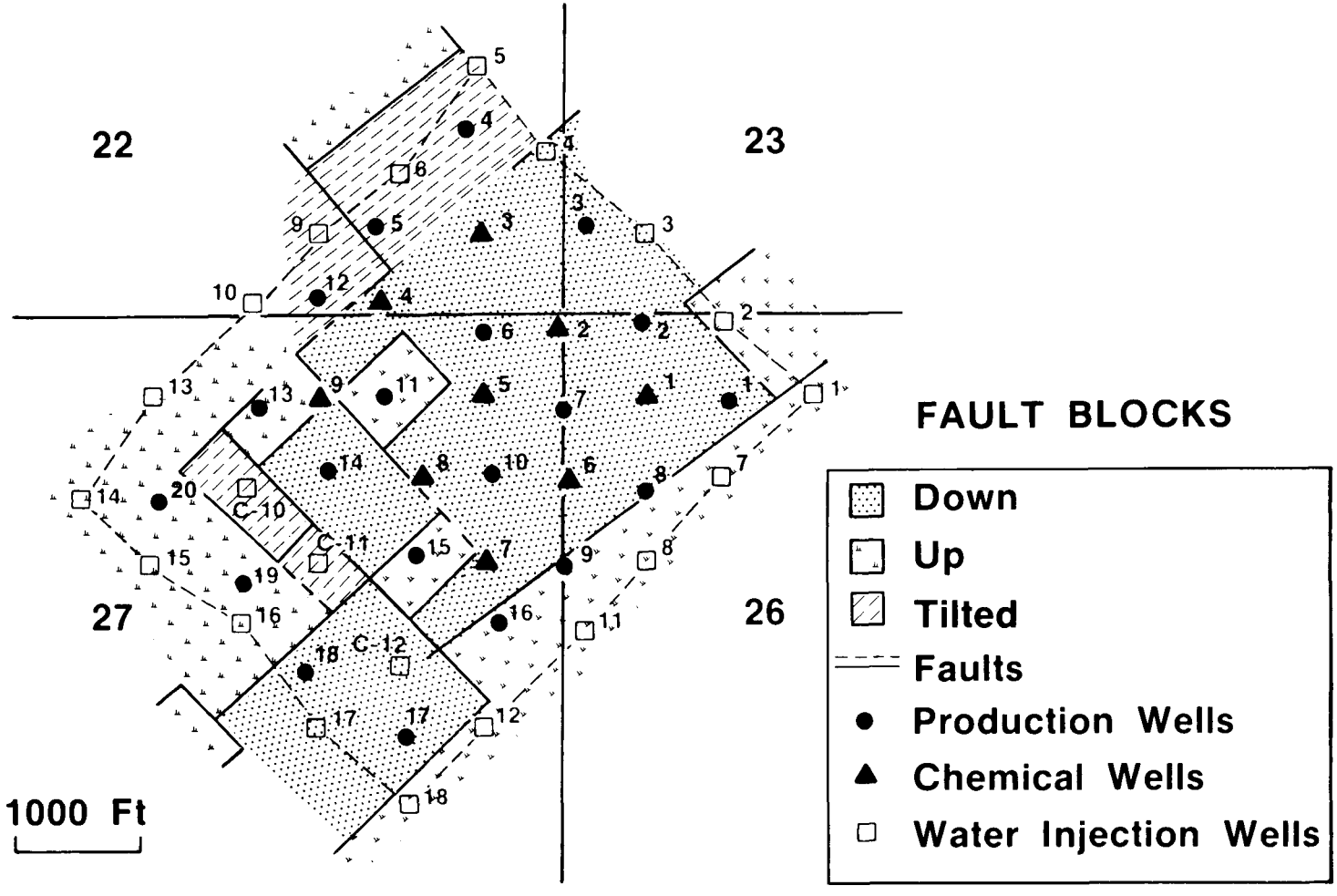


FIGURE 31. - Fault blocks and their relative vertical positions. Tertiary incentive project (TIP) area, Bell Creek field, Unit 'A'.

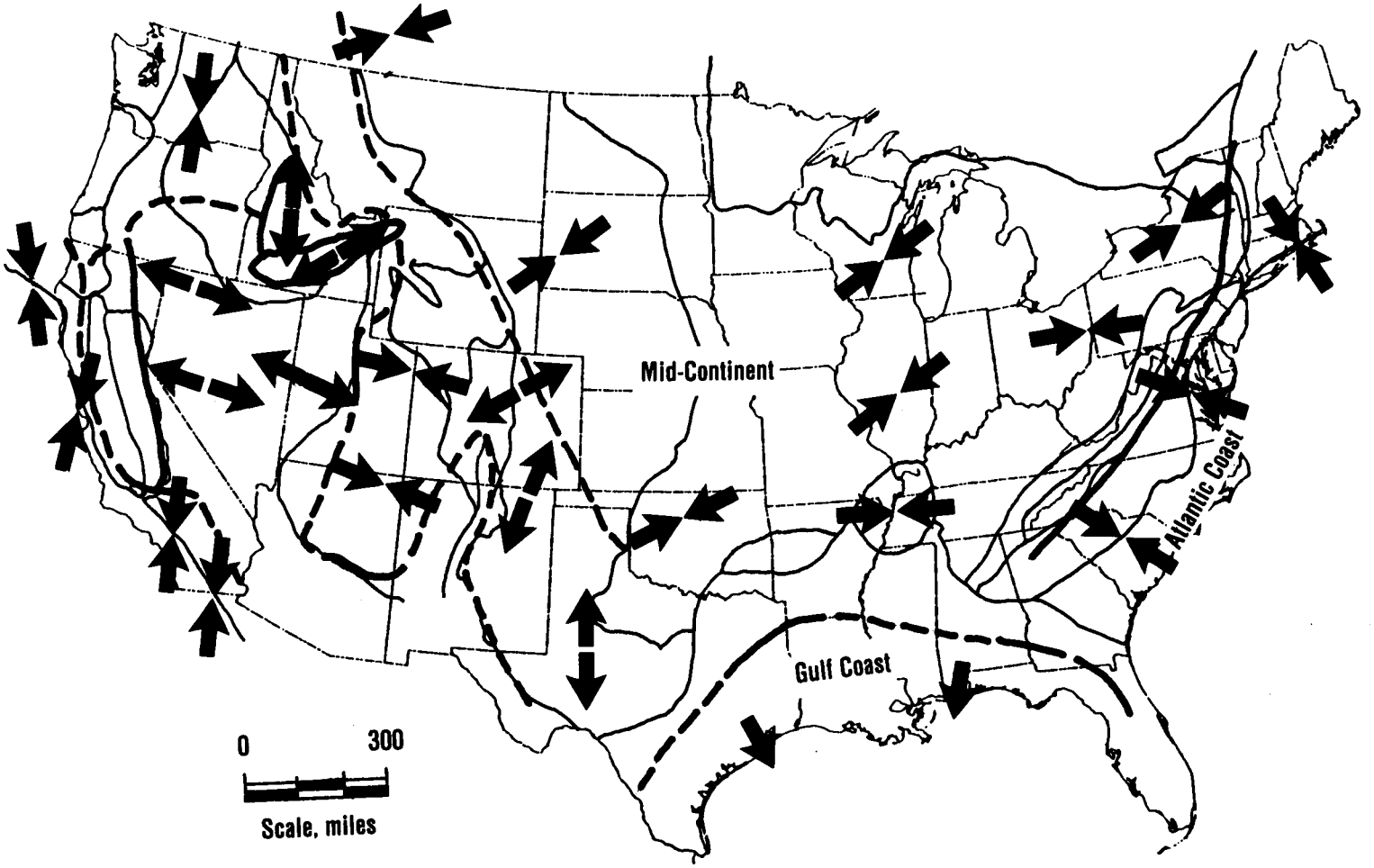


FIGURE 32. - Stress map of the United States (after Zorback and Zorback, 1980). Arrows indicate directions of regional stress.

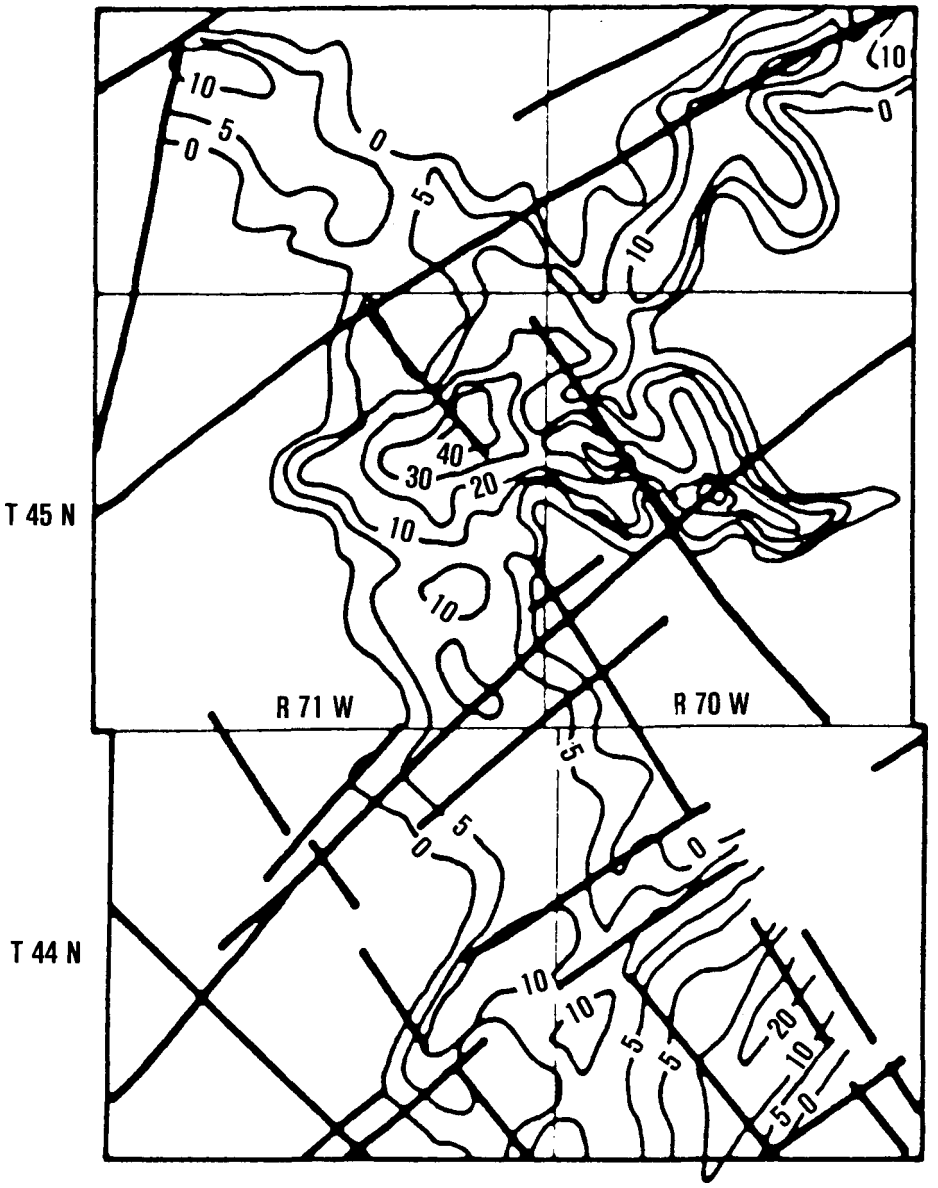


FIGURE 33. - Isopach map of Muddy sandstone in Hilight field, Powder River Basin. Note direction of linear features mapped from Landsat imagery (after Michael and Merin, 1986).

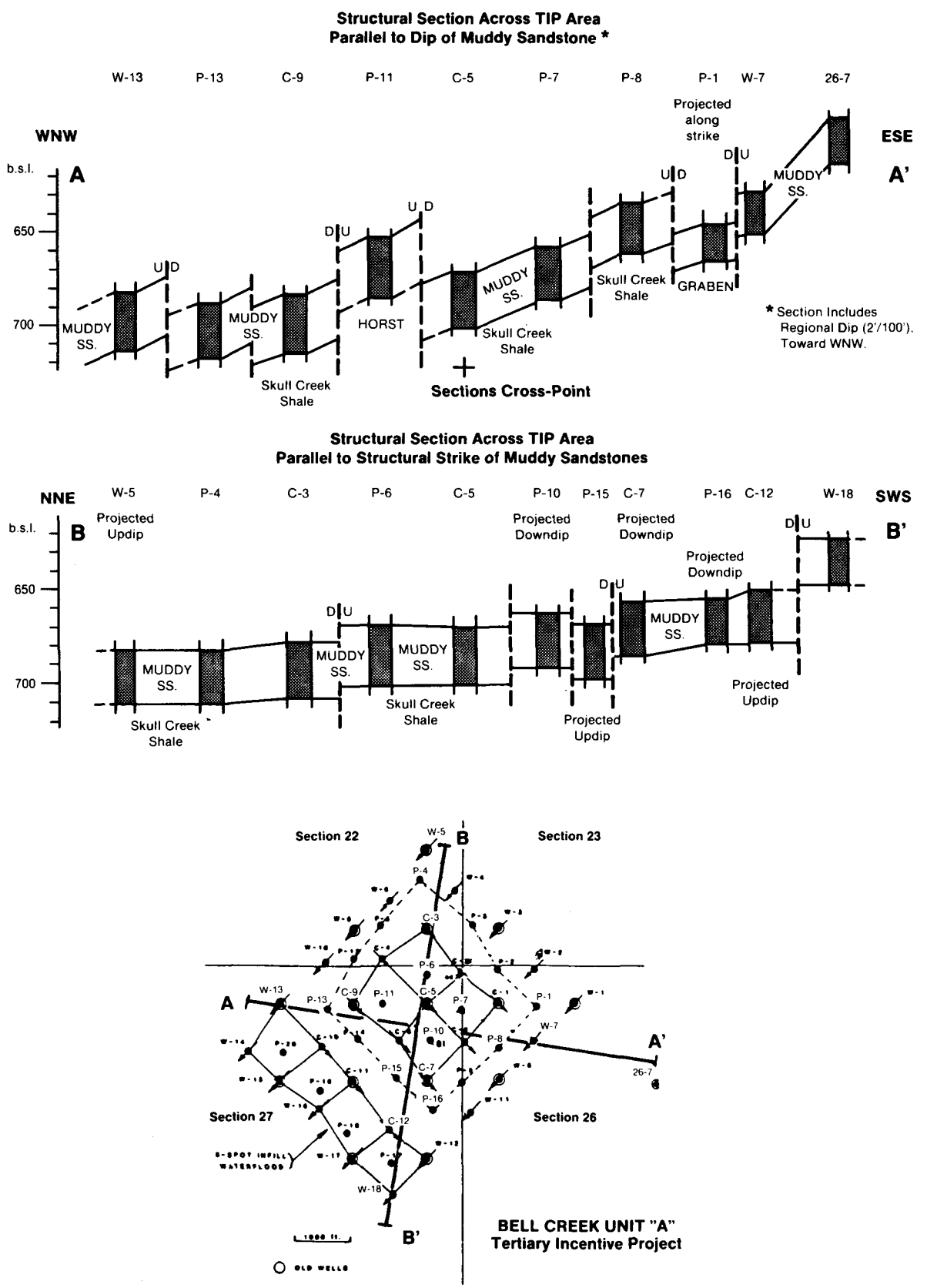


FIGURE 34. - Structural crosssections across TIP area parallel to dip (A-A') and strike (B-B') of Muddy formation. Note vertical displacements and position of wells within fault blocks.

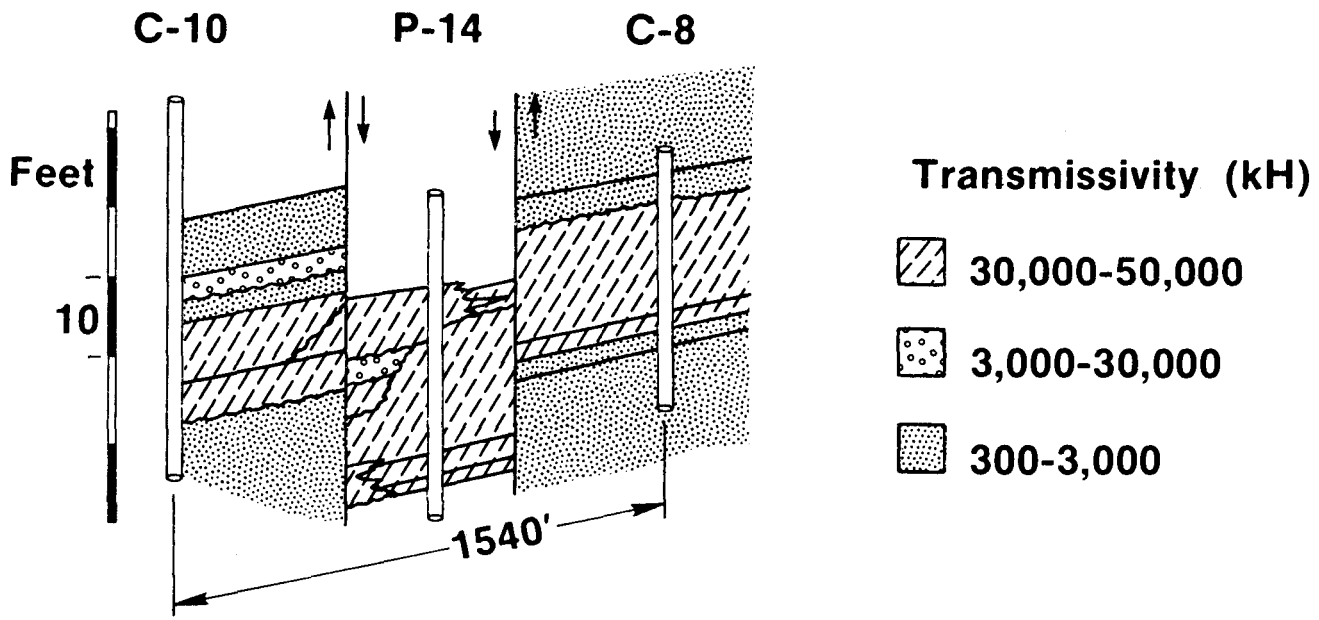


FIGURE 35. - Transmissivity (permeability x net pay) of Muddy sandstones and fault disruption of flow units between production well P-14 and chemical injection wells C-10 and C-8.

FIGURE 36. - Lower shoreface facies with low permeability. Well P-2, 4,437.1 ft (1,353 m). Porosity = 22.5%, permeability = 186 md. A,B. Scanning electron images. Note abundant clay between grains, leached feldspar (arrow in A); plugged throats (arrows in B). Scale bar is 100 microns. C. Thin section photomicrograph; plane polarized light. Oversize pores (OP) in sample contrast with clay-cemented smaller pores. Note quartz overgrowth (arrow); despite presence of oversize pores, most of the rock is moderately compacted. Based on visual estimates about 15% clay cement exists in this sample. Scale bar is 100 microns. D. Scanning electron image of pore cast. Thin plate-like pores are moderately well connected. In this sample, compaction created numerous flattened pores (P) and was responsible for decreased porosity. Scale bar is 100 microns.

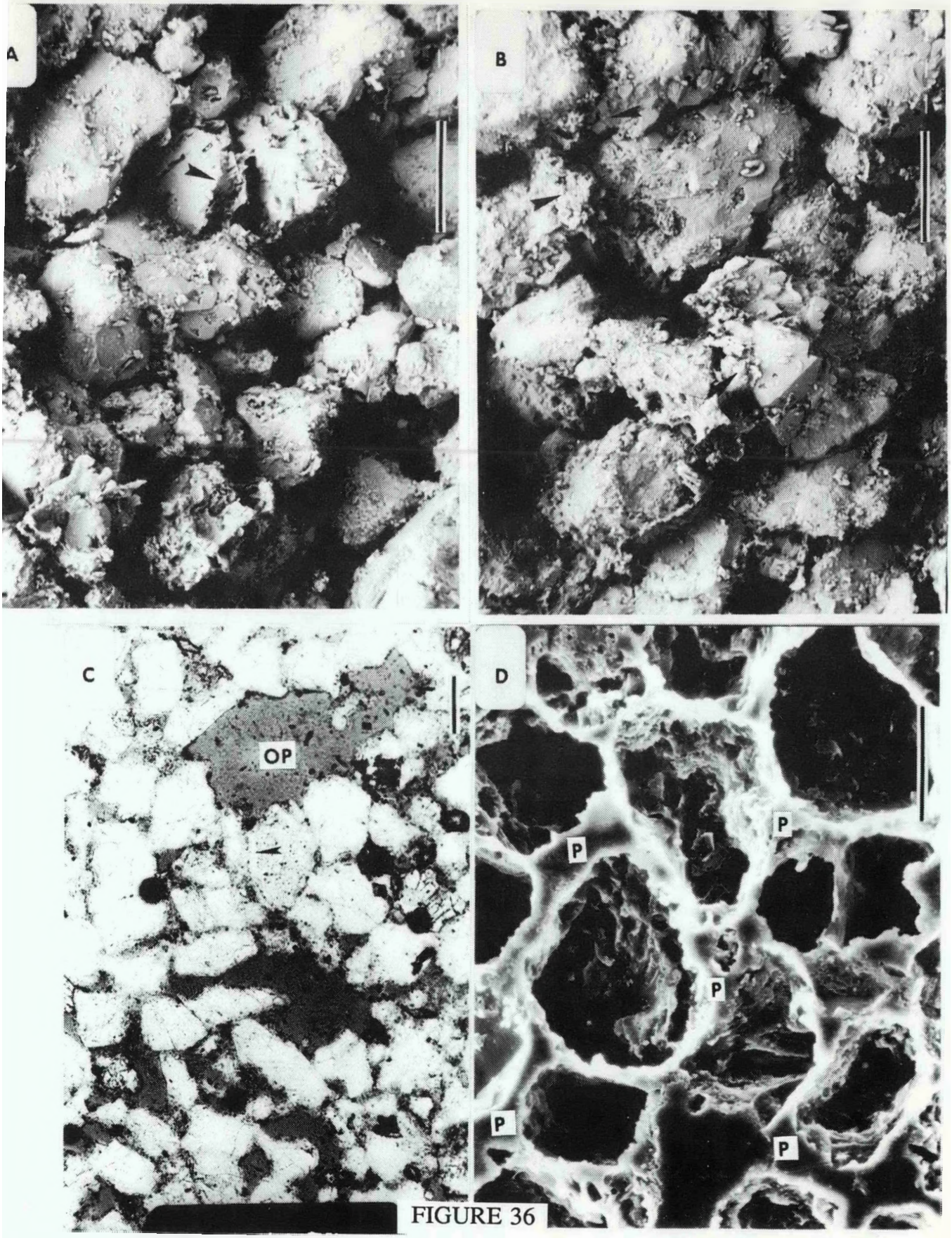


FIGURE 36

FIGURE 37. - Middle shoreface facies with high permeability. Well P-2, 4,430.5 ft (1,351 m). Porosity = 29.3%, permeability = 3,337 md.

A,B. Scanning electron images. Clean, well-sorted quartzose sandstone has virtually no clay cement. Some compaction and quartz overgrowths indicated in B. Scale bar is 100 microns. C. Thin section photomicrograph; plane polarized light. Black is very dark artificial stain in porosity. Feldspar (F) at top of micrograph has been leached along cleavage; polycrystalline quartz (Q), just below center, was strongly leached. Pores are relatively large and open. Less than 2% clay is present in this sample based on visual estimates. Scale bar is 100 microns. D. Scanning electron image of pore cast. Note large and well connected pores. Many pore throats are large, and pores (P) are not divided by fine grains or clay. Scale bar is 100 microns.

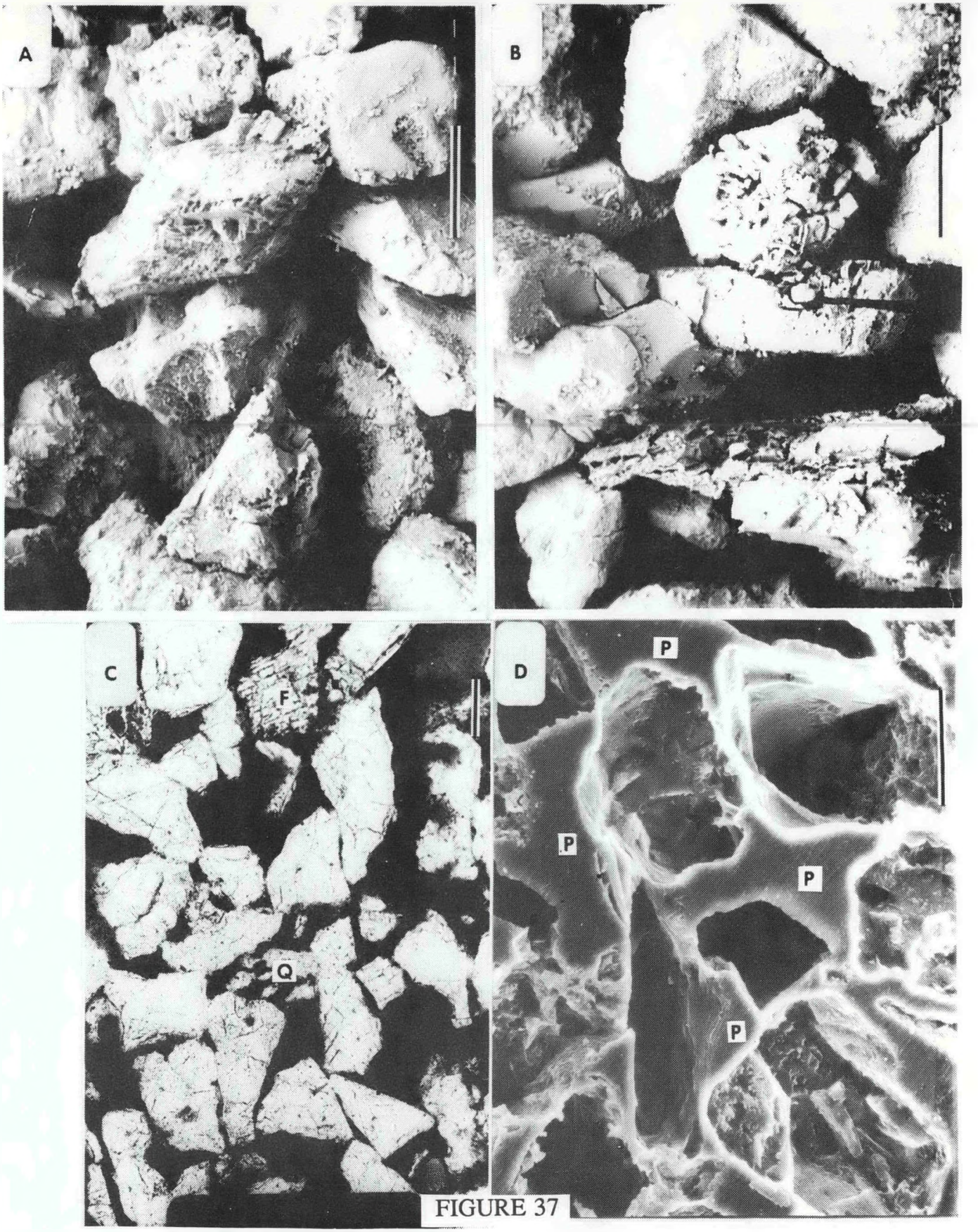


FIGURE 37

FIGURE 38. - Foreshore facies with "lower" permeability. Well W-16, 4,311.6 ft (1,315 m). Porosity = 26.7%, permeability = 1,935 md. A,B. Scanning electron images. Clays block pore throat in A (arrow). Note corroded feldspar (F) near bottom of image. Scale bar is 100 microns. C. Thin section photomicrograph; plane polarized light. This sample contains about 4% clay cement, most of which is concentrated around margins of pores. Note poorly developed clay bridge (arrows) bisects oversize pore and indicates vanished grains. Average grain size is 188 microns based on point counts. Scale bar is 100 microns. D. Scanning electron image of polished pore cast. Wavy margins of pores reflect location of clay cement. Clay lining of pores reduced throat size, and resulted in decreased permeability. Compare with smooth edges of core casts in figure 30 B. Scale bar is 100 microns.

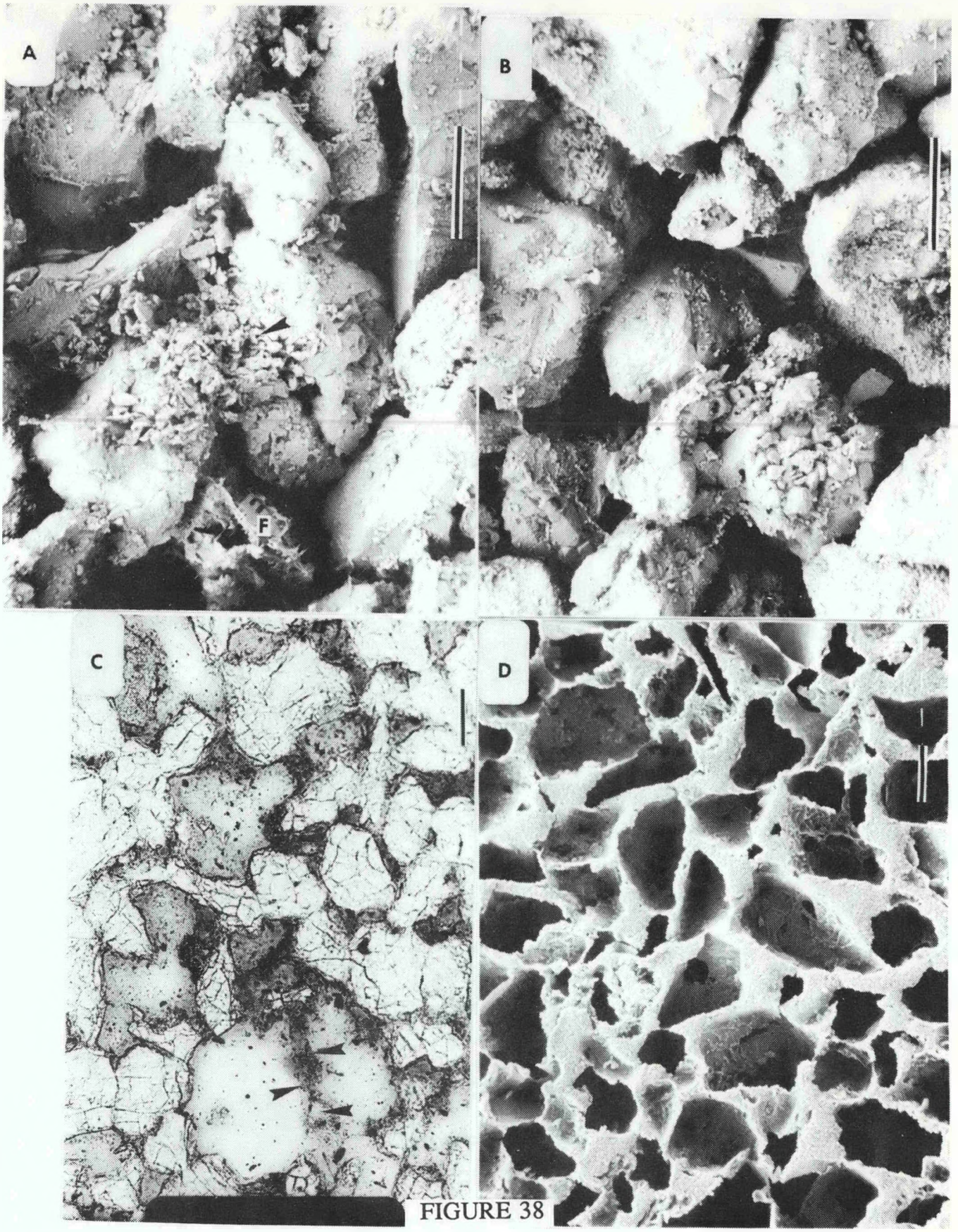


FIGURE 38

FIGURE 39. - Foreshore facies with higher permeability. Well P-2, 4,418.5 ft (1,348 m). Porosity = 28.3%, permeability = 3,186 md. A. Scanning electron image. Intricate corrosion of feldspar and minor "dusting" of clay cement (above center) are evident. Scale bar is 100 microns. B,D. Scanning electron images of pore casts. Because of generally clean fabric (absence of clays) the size contrast between pores and throats is distinct (B). In complex leaching of skeletal feldspar produced convolute secondary porosity which is finely divided. Scale bar in B is 100 microns. In D, bar represents 10 microns. C. Thin-section photomicrograph, plane polarized light. Overall sorting is poor because of included silt-size grains. Based on point counts, average grain size is 201 microns. Less than 1% clay cement is present in this sample, concentrated in smaller pores (dark areas). Higher permeability foreshore samples tend to be slightly coarser, well sorted, and contain very little clay cement. Scale bar is 100 microns.

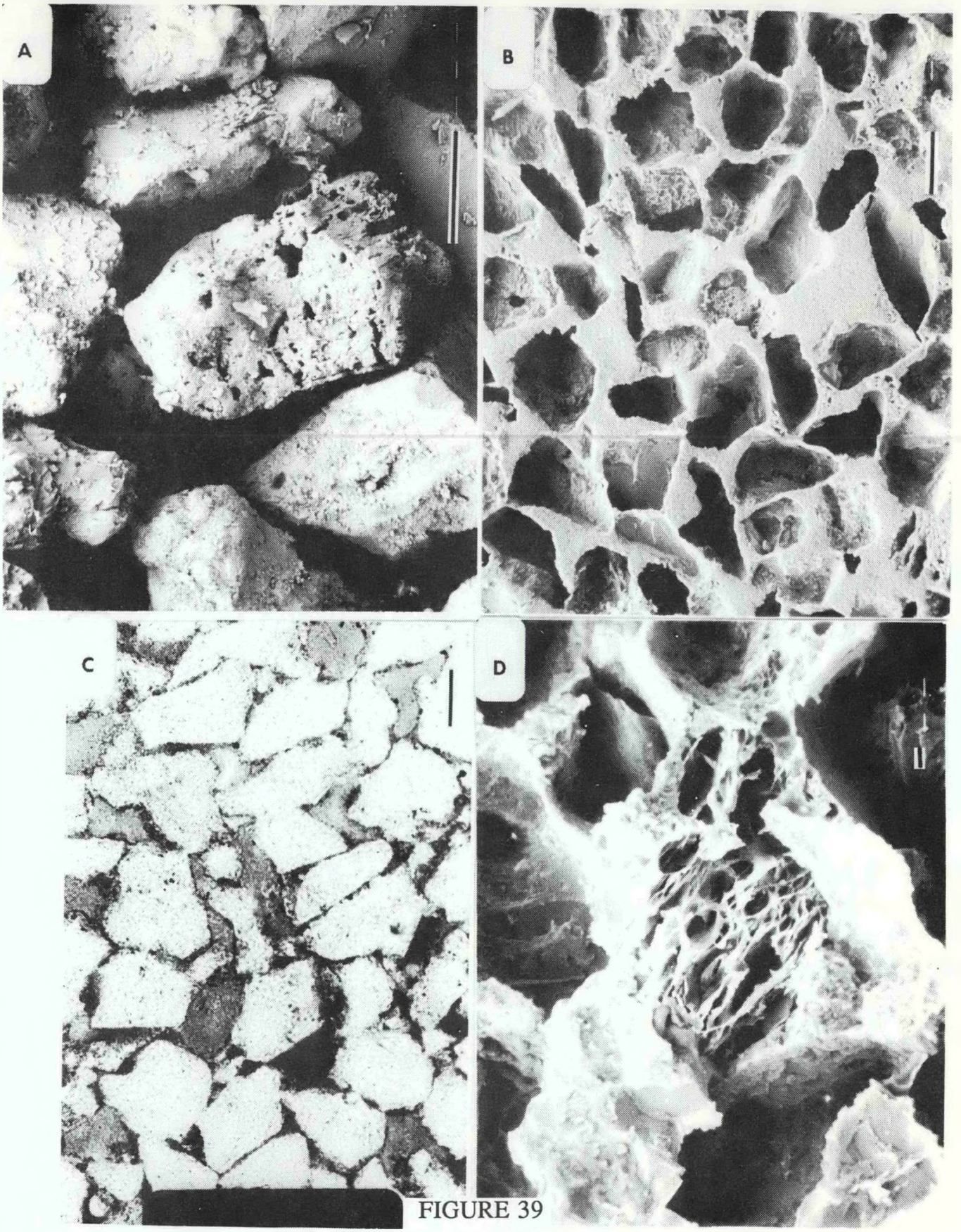


FIGURE 39

FIGURE 40. - Washover facies with lower permeability. Well W-16, 4,301.5 ft (1,312 m). Porosity = 27.3%, permeability = 710 md. A. Scanning electron image. Moderately well-sorted sandstone has 14% total clay based on thin-section analysis. Clay coatings are clearly visible on grains (arrows). Scale bar is 100 microns. B. Scanning electron image. Closeup of pore throat blocking by kaolinite. Scale bar is 10 microns. C. Thin-section photomicrograph, plain polarized light. Interpenetrating grains (arrow) in an otherwise uncompacted fabric indicate that the sample was compacted and then leached. Clay cement (darker parts of pores) is concentrated in smaller pores and around pore throats. Scale bar is 100 microns. D. Scanning electron image of pore cast. Sample was polished prior to acid etching. Note flattened, relatively small pores. Numerous throats (arrows) are particularly small. High clay content caused pour communication between pores and, therefore, reduced permeability relative to clay - pore samples (e.g. fig. 41). Scale bar is 100 microns long.

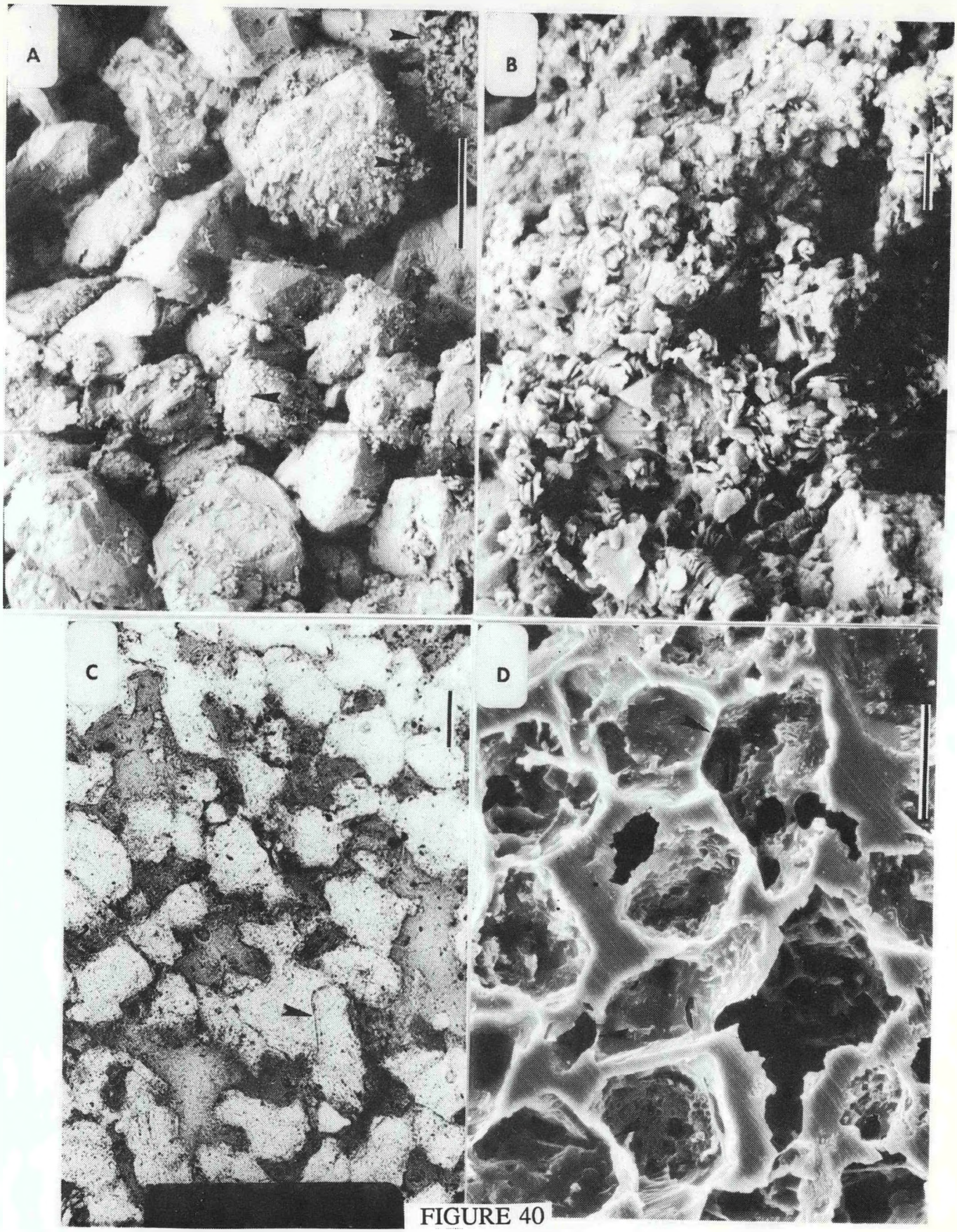


FIGURE 40

FIGURE 41. - Washover facies with high permeability. Well W-16, 4,328.5 ft (1,320 m). Porosity = 28.3%, permeability = 1,382 md. A. Scanning electron image. Well-sorted quartzose sandstone with less than 2% clay cement shows intricately corroded feldspar (F). Scale bar is 100 microns. B, D. Scanning electron images of pore casts. Sample B was polished flat prior to etching. Grains occupied dark areas. Silt size debris (holes in cast) in central pore was probably produced by leaching; hence, this is secondary porosity. D is closeup of complex pore-grain relationship produced dominantly by 5-micron-diameter particles (holes in cast), most of which were remnants of leached grains. Scale bars are 10 microns long. C. Thin-section photomicrograph; plane polarized light. An oversize pore (center) contains a few grain remnants indicating that this is secondary porosity. Oversize pores, a generally undercompacted fabric, leached grain remnants; "floating" and "near floating" grains all emphasize the strong effect that leaching had on this rock. Scale bar is 100 microns.

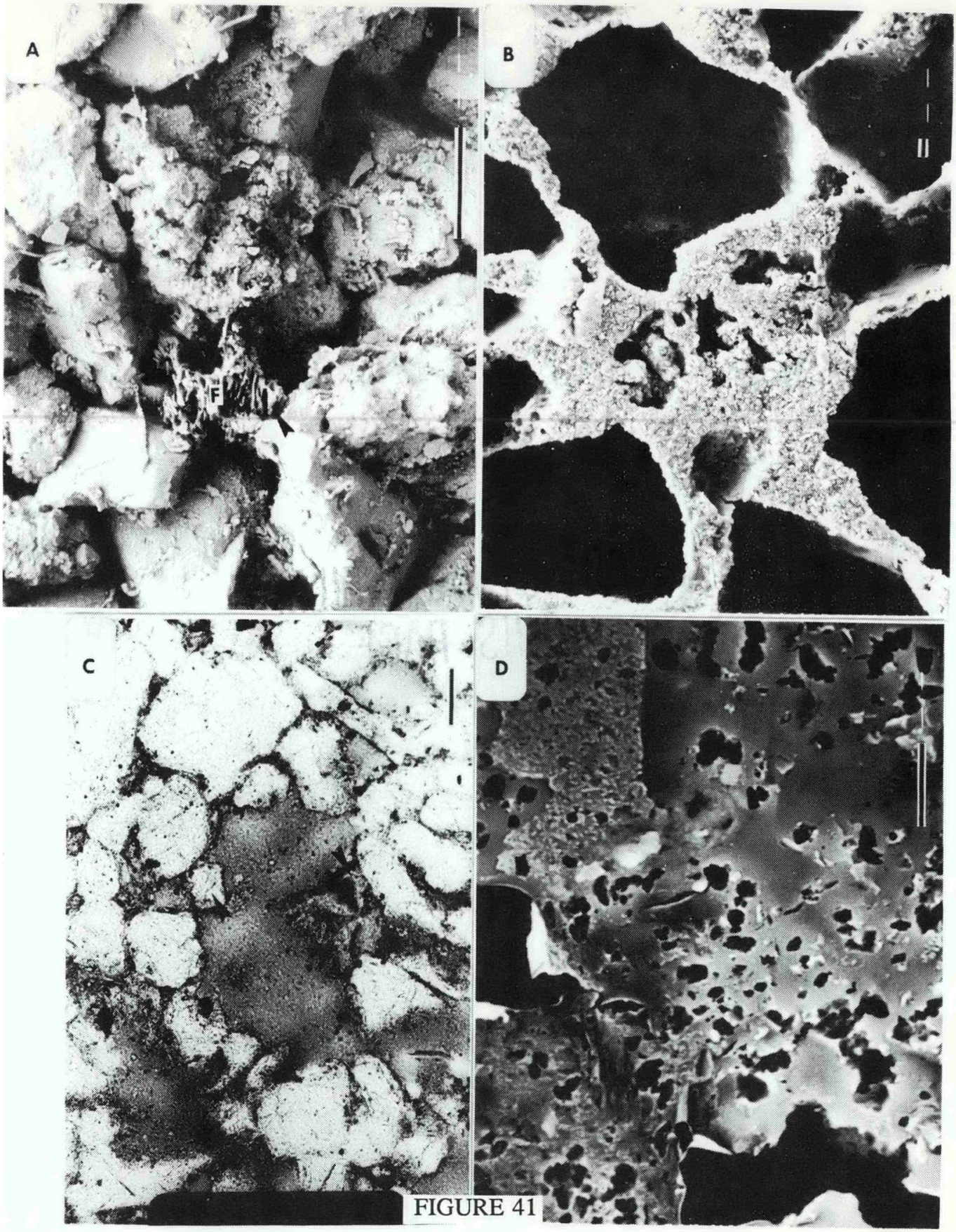


FIGURE 41

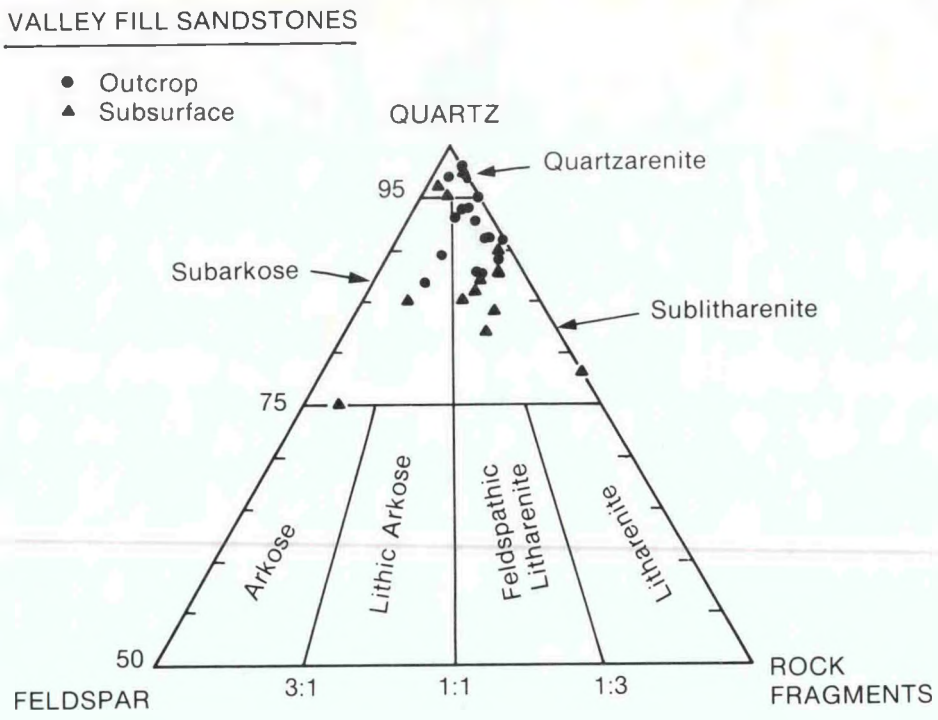


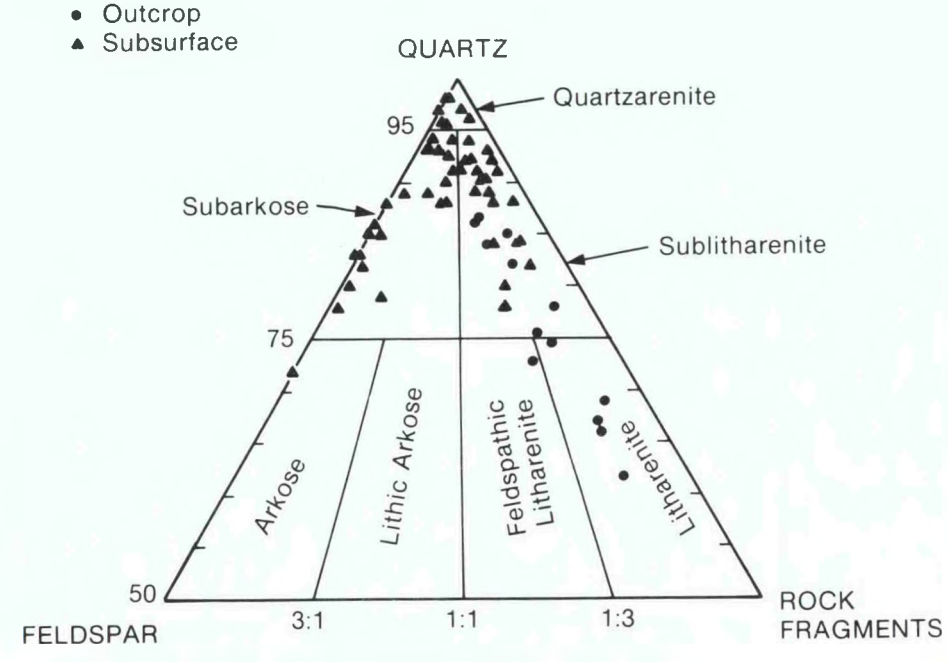


FIGURE 42. - Quartz - feldspar - rock fragment composition and rock type classification (after Folk, 1968) for thin-section samples from valleyfill sandstones and barrier sandstones from the Muddy formation.

FIGURE 43. - Secondary porosity development in reservoir sandstone. (A) Scanning electron image of highly corroded detrital feldspar (F). Well W-7, 4,431.3 ft (1,352 m). B. Scanning electron image of pore cast of partly leached feldspar (F) illustrates connectivity of secondary pore space in leached feldspars. Sample from well P-2, 4,421 ft (1,348 m). C. Surviving silt size remnants (S) of leached grains partly fill primary and secondary pores. Where remnants are absent, secondary oversize pores (O) are clearly distinguished from primary pores. Thin-section photomicrograph; Well W-10, 4,429.5 ft (1,351 m). D. Strong leaching of chert grains (C) created abundant microporosity. Thin-section photomicrograph; sample from well C-8, 4,372.6 ft (1,334 m). Scale bars are 100 microns long.

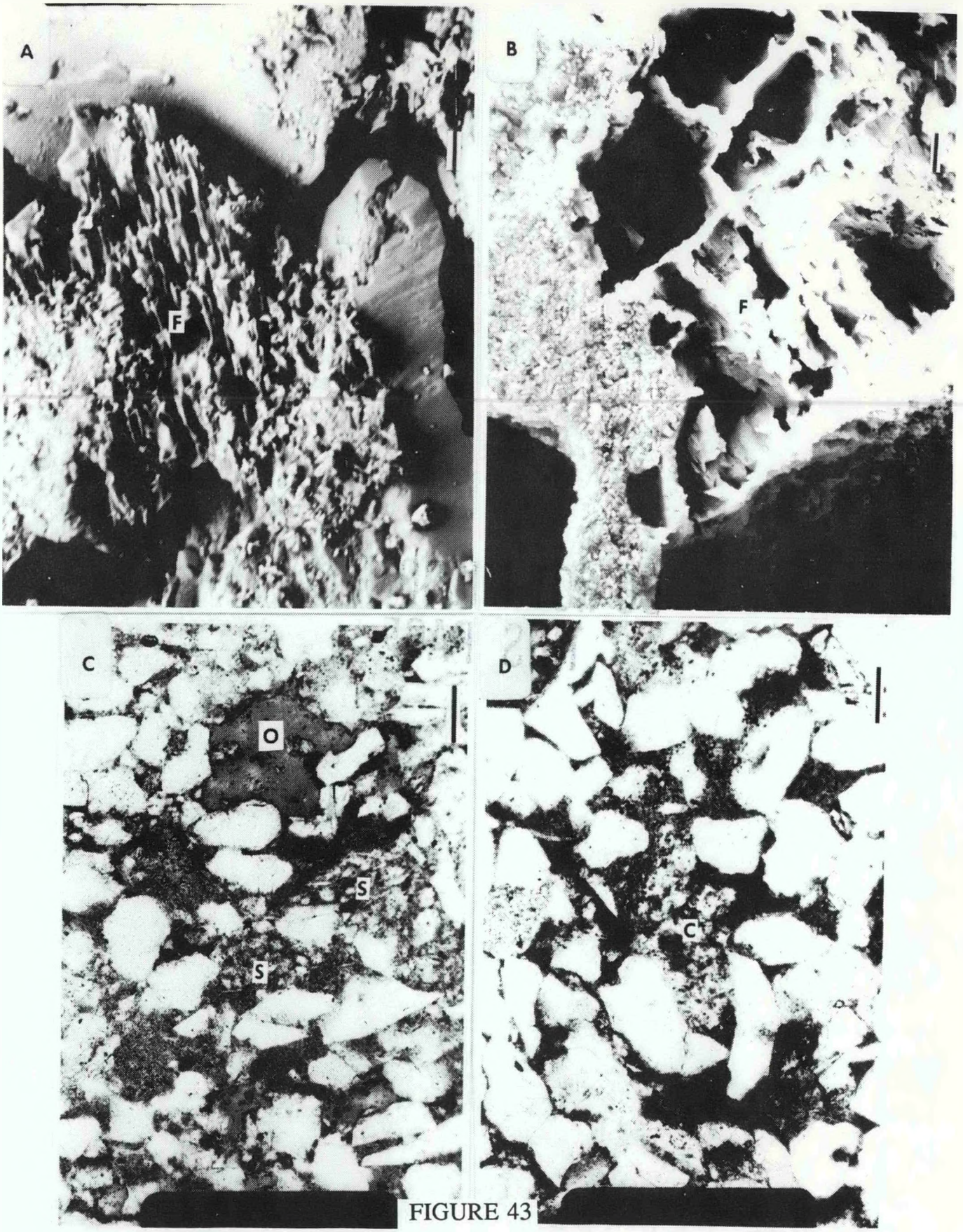


FIGURE 43

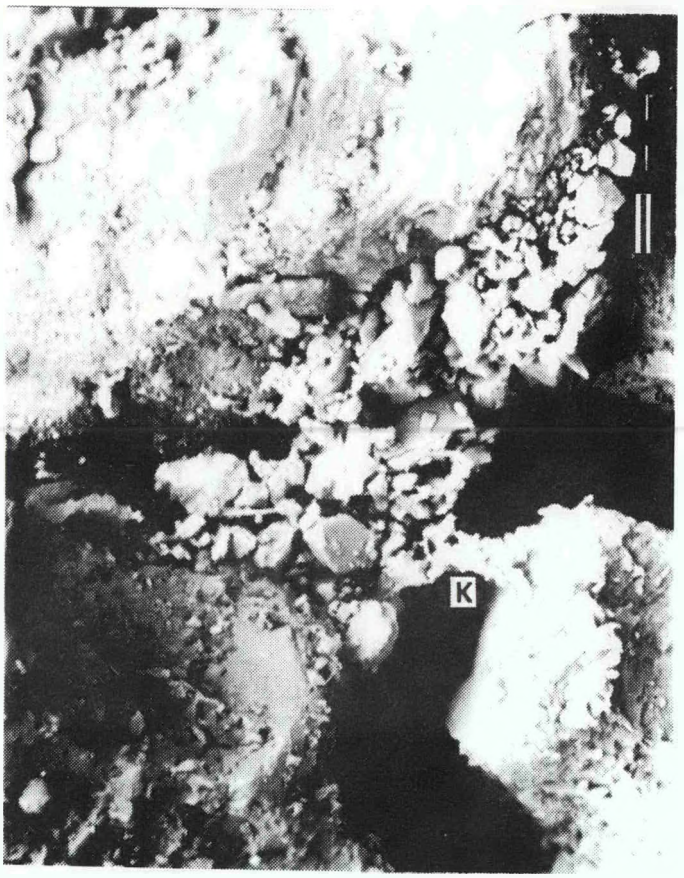


FIGURE 44. - Scanning electron micrograph shows pore and pore throat blocked by kaolinite and fine silt size feldspar particles. Blockage may have been in part created by collapse of kaolinized feldspars. Subsequent authigenic kaolinite (K) creates pore bridges and clay crusts. Samples from well C-6, 4,415.8 ft (1,347 m). Scale bar is 10 microns long.

FIGURE 45. - A. Inclusion-poor quartz, overgrowth predates clay cement (reddish color). Sample from well C-6, 4,409.8 ft (1,345 m). B. Siderite cement (S) and quartz grains have interpretating margins (arrow). Therefore, siderite precipitated prior to compaction. C. Compacted microporous sedimentary rock fragment (RF), oversize pores with preserved leached remnants (in D), and "clean" oversize pores are all the same size in this sample. This observation provides strong evidence that oversize pores originated by leaching of sedimentary rock fragments. Postcompaction creation of oversized pores (as in D) is evidence for late stage leaching. Sample from well P-2, 4,437.1 ft (1,353 m). D. Bimodal size distribution is the result of diagenesis. Silt particles in normal and oversized pores are leached remnants of original framework grains. Sample from well C-8, 4,365.4 ft (1,331 m). E. Pseudomatrix (PS) was created by compaction of sedimentary rock fragments between more rigid framework grains. sample from well C-6, 4,422.6 ft (1,349 m). All scales are 100 microns.

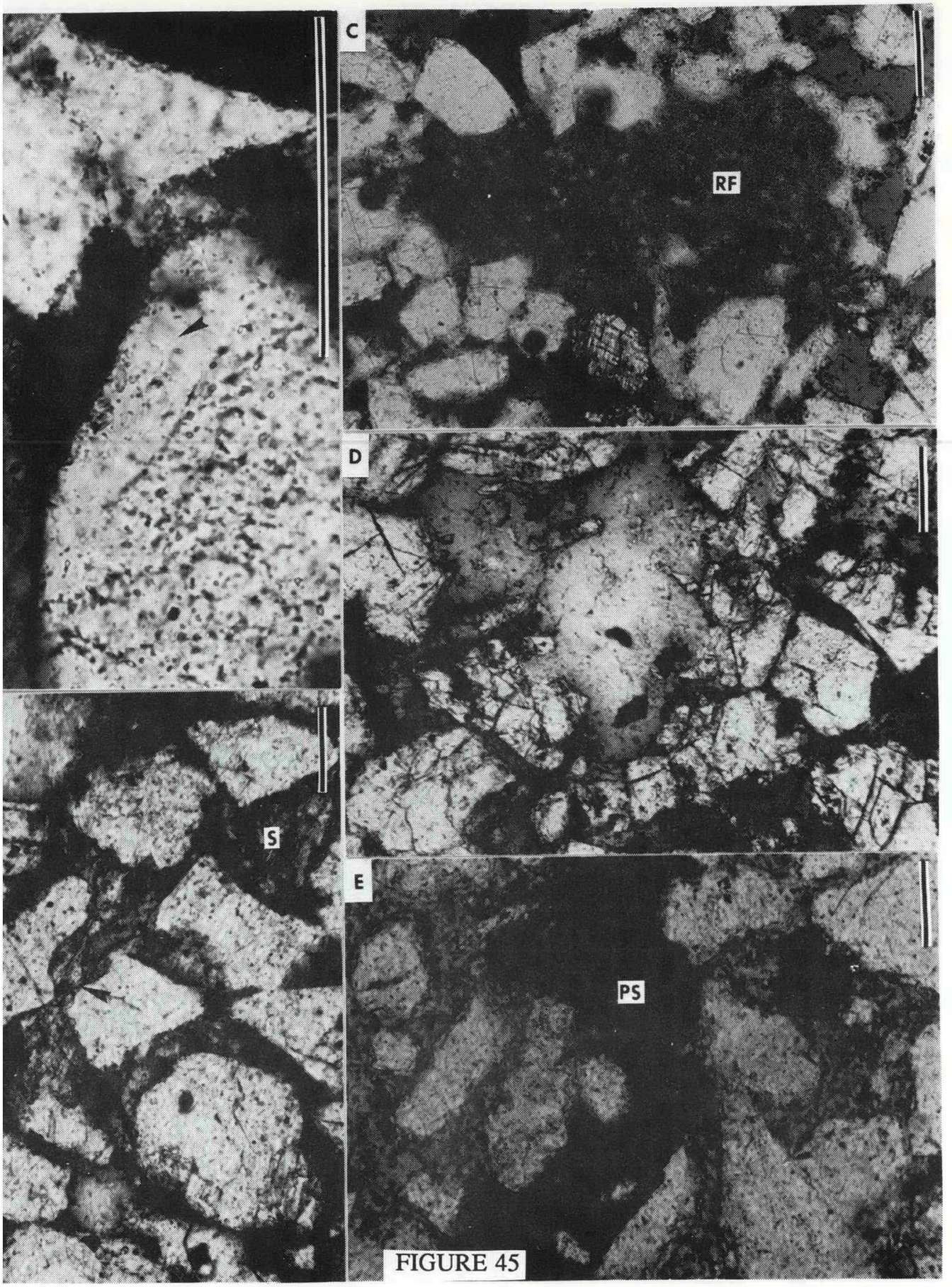


FIGURE 45

FIGURE 46. - Very high permeability reservoir sandstone (foreshore facies). Sample from well C-8, 4,370.5 ft (1,333 m); permeability is 5,498 md, porosity 30.3%. Total clay content is trace only. A,B. Scanning electron images. Traces of kaolinite (K) cement are visible. Despite good porosity and permeability, sorting is only moderate. C. Thin-section photomicrograph; plane polarized light. Oversize pores that contain a few remnants of leached grains (R) provide increased pore space in an otherwise moderately fitted skeletal fabric. D. Scanning electron image of pore cast. Pore cast had been polished flat prior to leaching of grains with hydrofluoric acid. An oversize pore (OP) is partitioned by silt size leach remnants. Scale bars are 100 microns long.

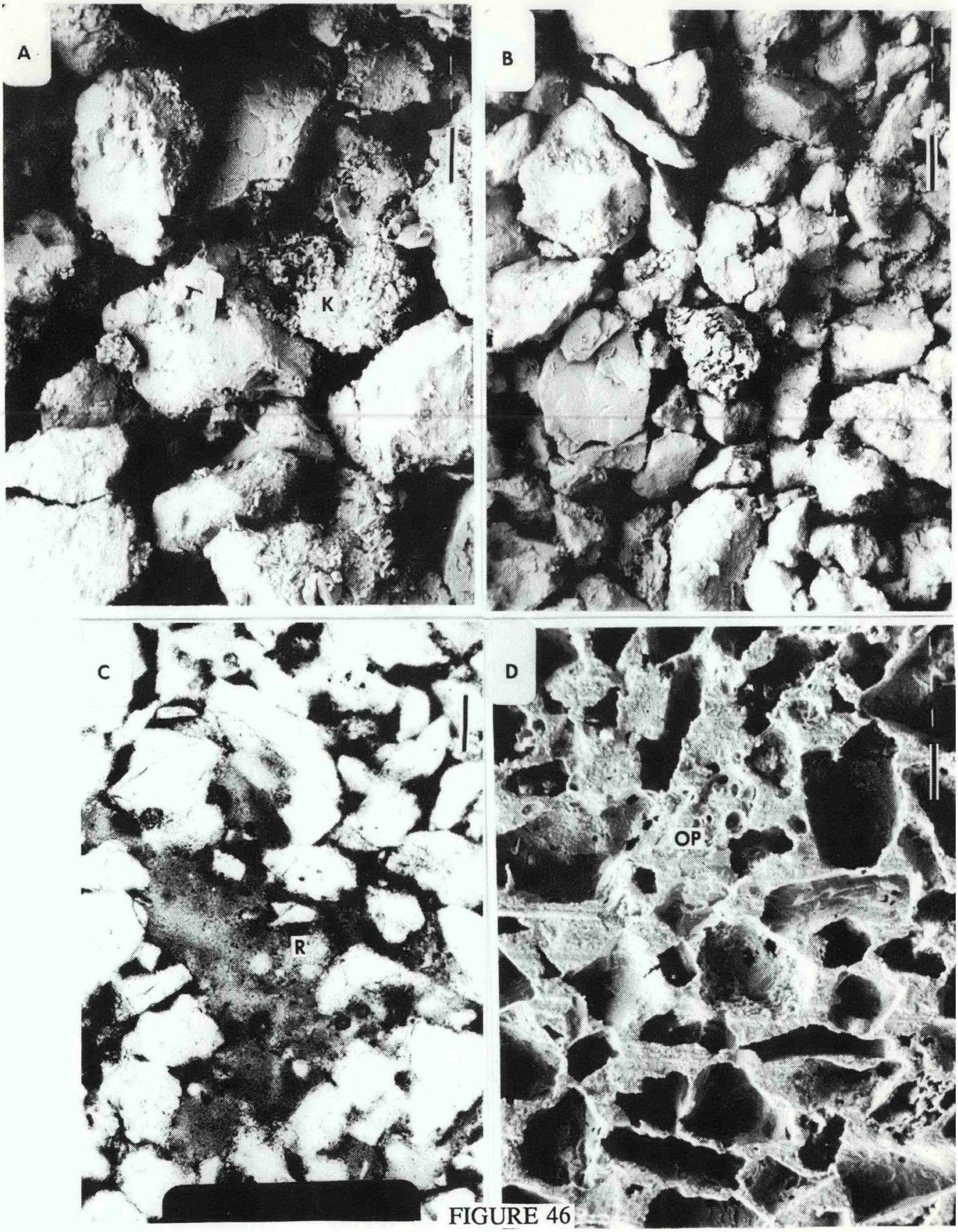


FIGURE 46

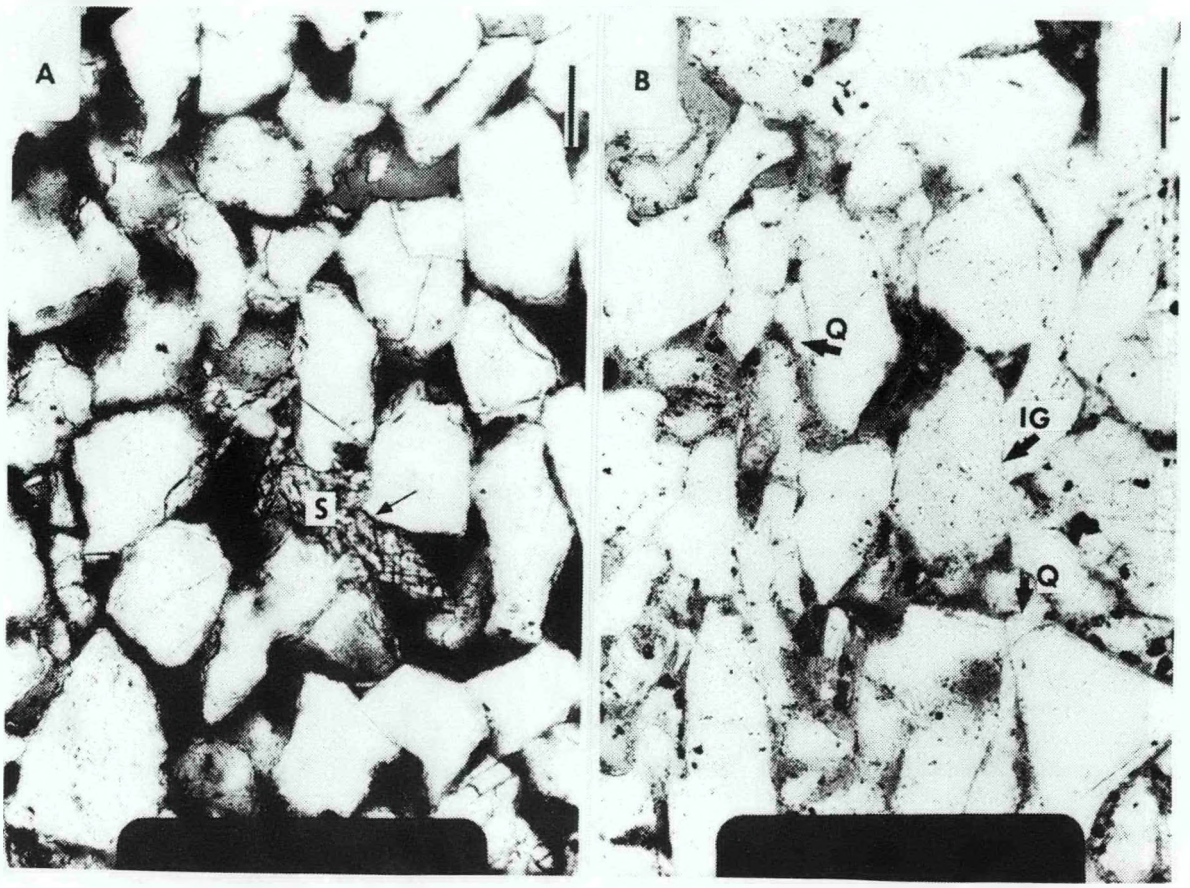


FIGURE 47. - Thin-section photomicrographs. A. The early diagenetic origin of siderite (S) is indicated because it was involved in compaction (arrow). Sample from well C-8, 4,365.4 ft (1,331 m). B. Grain reorientation, long contacts between framework grains, interpenetrating grains (IG) and quartz overgrowths (Q) reflect increased compaction brought about by physical and chemical (solution-reprecipitation) processes significantly reduced average pore size. Sample from well W-14, 4,297.7 ft. Scale bars are 100 microns long.

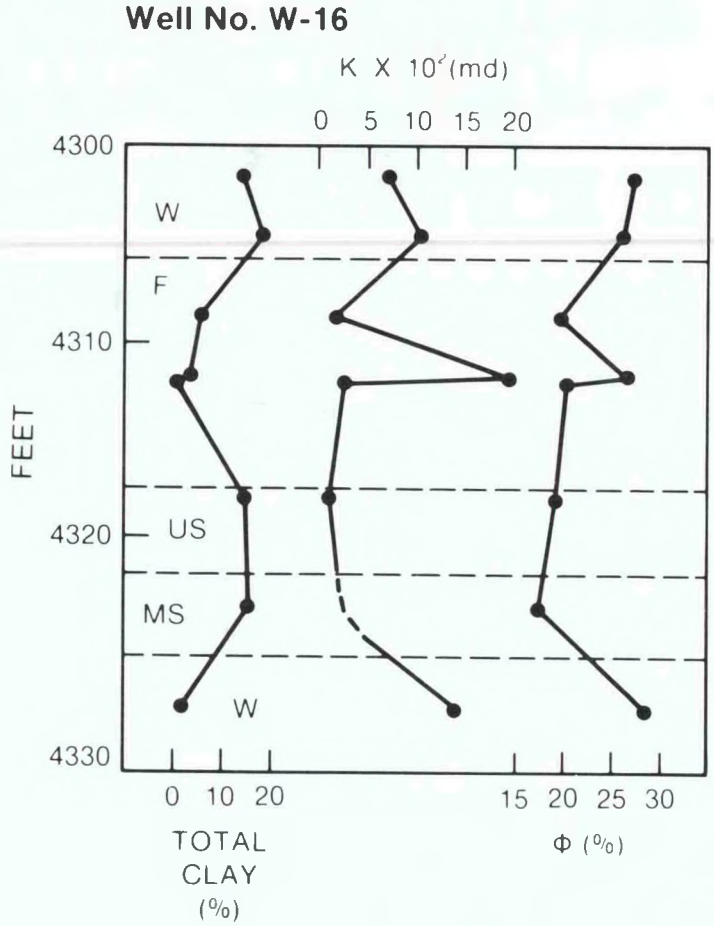


FIGURE 48. - The relationship between porosity, permeability, and total clay percent in well W-16. Based on thin-section analysis, the sandstone samples are quartzarenite and sublitharenite with zero to 2 % clay matrix; they average 9 % clay cement and have moderate sorting. Abbreviations: F, foreshore; MS, middle shoreface; US, upper shoreface; W, washover.

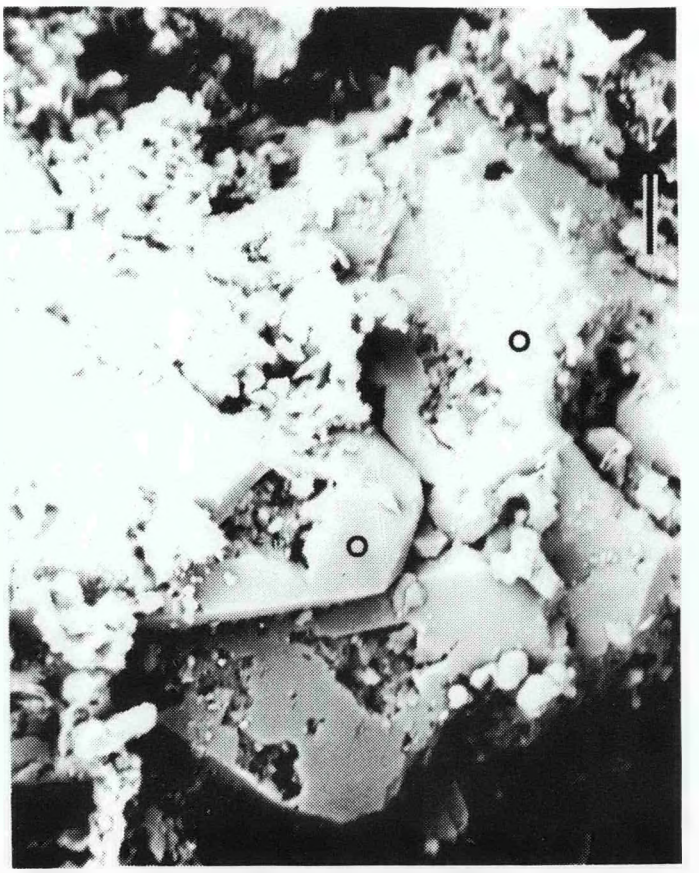

FIGURE 49. - Discontinuous euhedral quartz overgrowths (O) envelop host quartz grain and early kaolinite cement. Although quartz cement generally comprises less than 2 % of the rock, it appears to be the only means of consolidation in many samples.

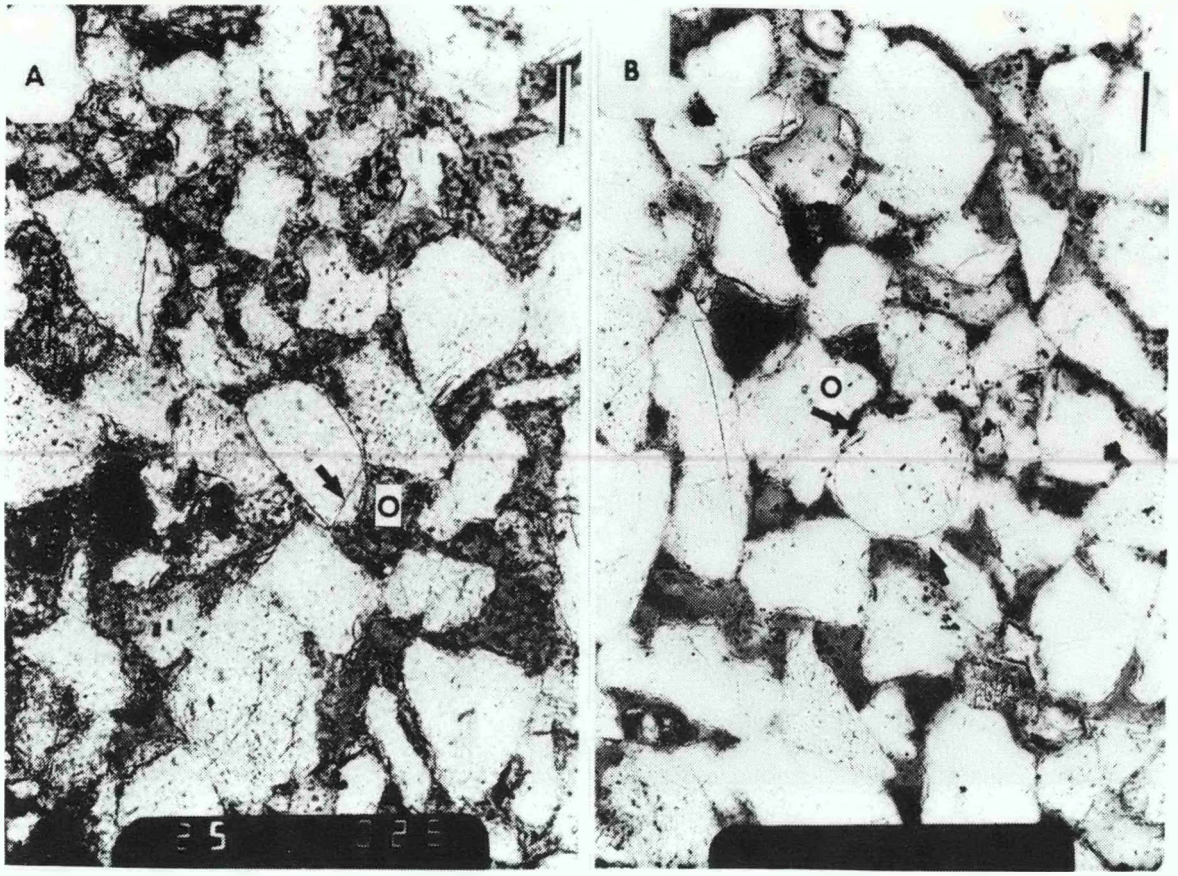


FIGURE 50. - Quartz overgrowths (O) formed before precipitation of most clay cement. "Dust lines" composed of fluid-filled vacuoles and clay particles separate quartz host grains from quartz overgrowths in A and B. A. Sample from well W-7, 4,427.5 ft. B. Sample from well W-14, 4,297.7 ft (1,311 m). Scale bars are 100 microns long.


FIGURE 51. - Scanning electron micrographs of late stage cements. (A) Five percent calcite (C) cement in addition to 3 % clay (K) and 1 % siderite cement are the reason that permeability in this sample is less than 1 millidarcy. Well C-6, 4,422.6 ft (1,349 m). (B) Five- to thirty-micron thick clay cement (arrows) coats reduce an otherwise good reservoir sandstone to 236 md permeability. Sample from W-14, 4,297.7 ft (1,311 m). Scale bars are 100 microns long.

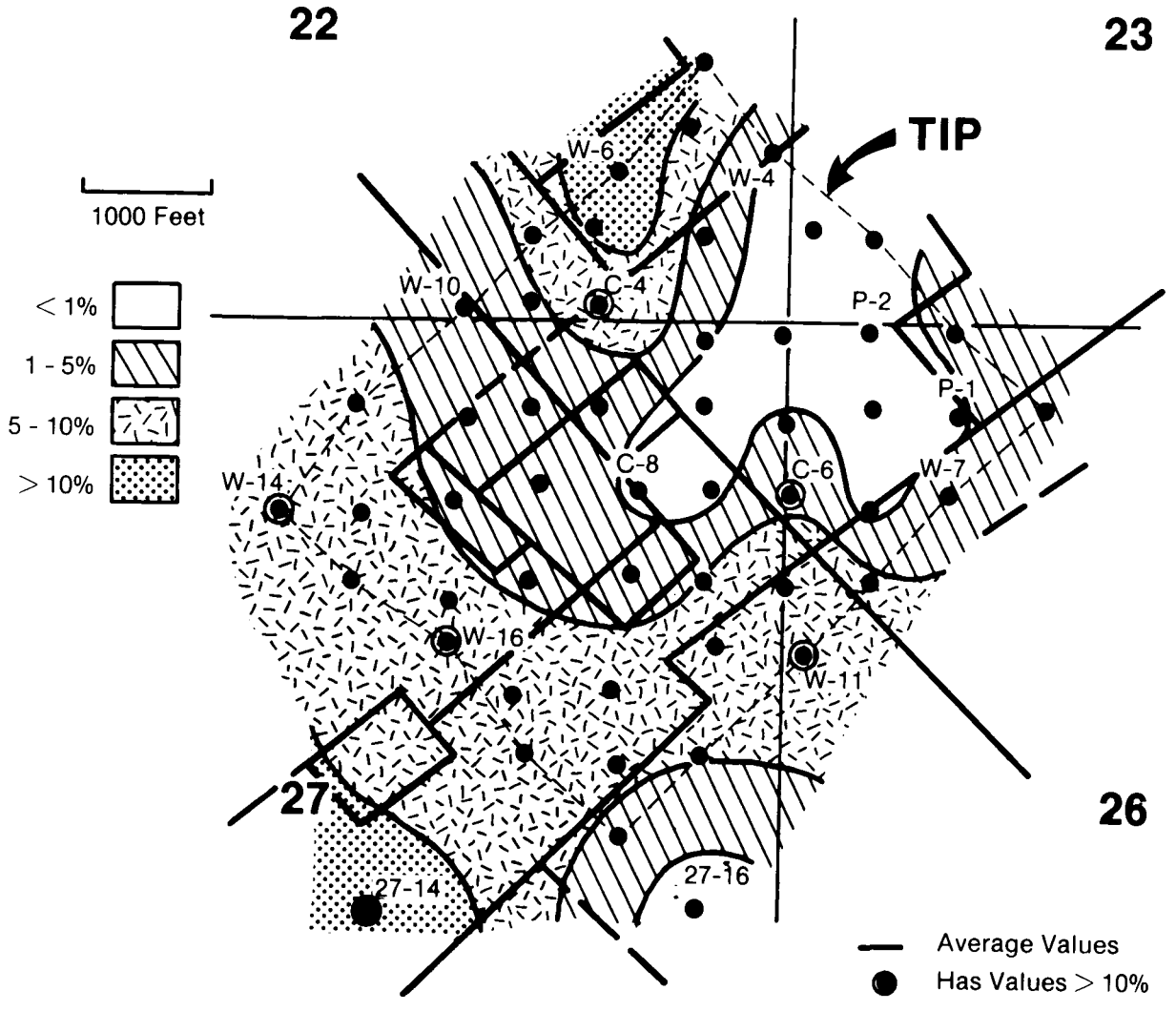


FIGURE 52. - Average percent diagenetic clay in middle and upper shoreface and foreshore facies within barrier island strata. Thin-sections were available from numbered wells. Circled wells have individual values greater than 10% diagenetic clay.

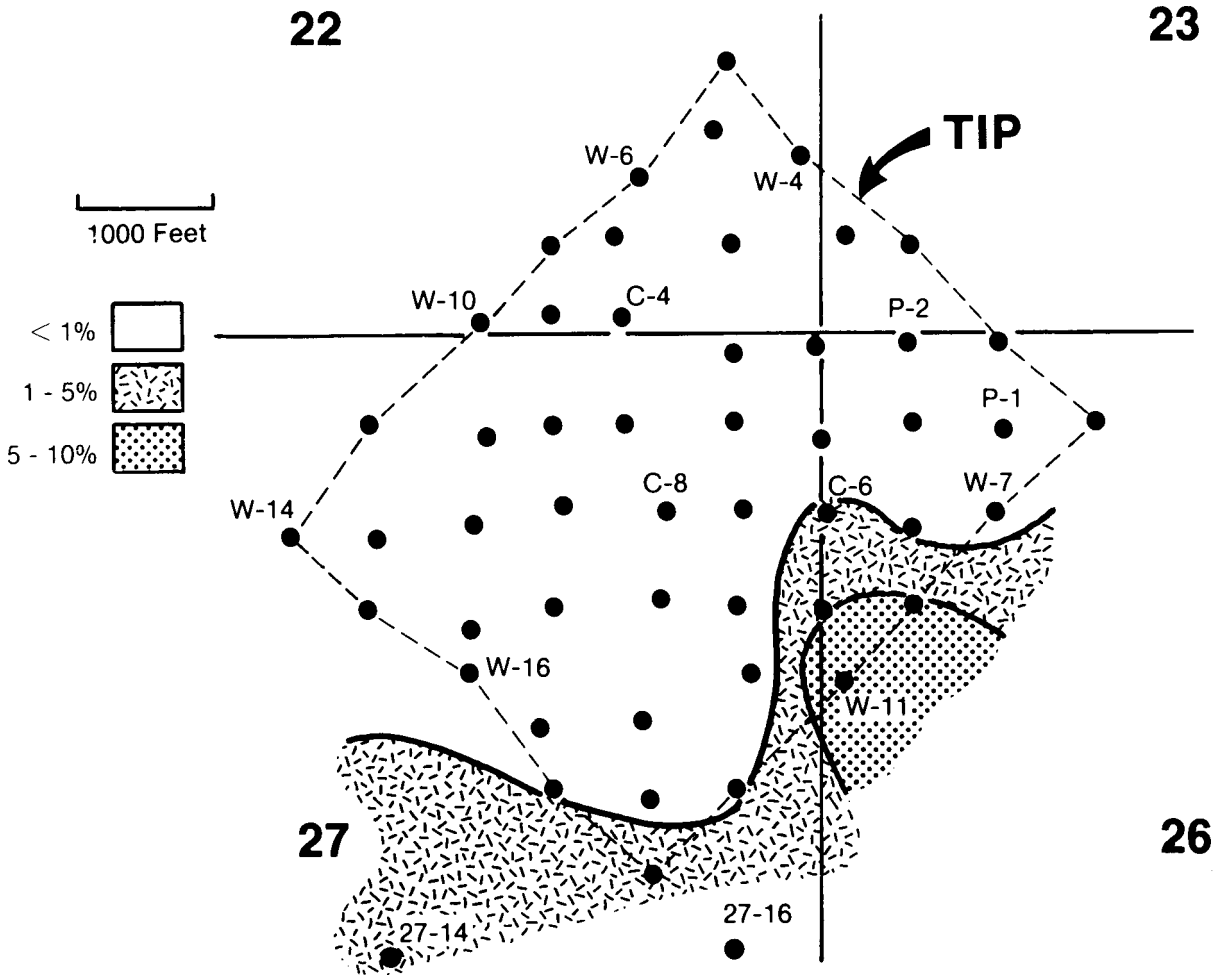


FIGURE 53. - Average percent matrix in middle and upper shoreface and foreshore facies within the barrier island strata. Based on thin-section analysis from numbered wells.

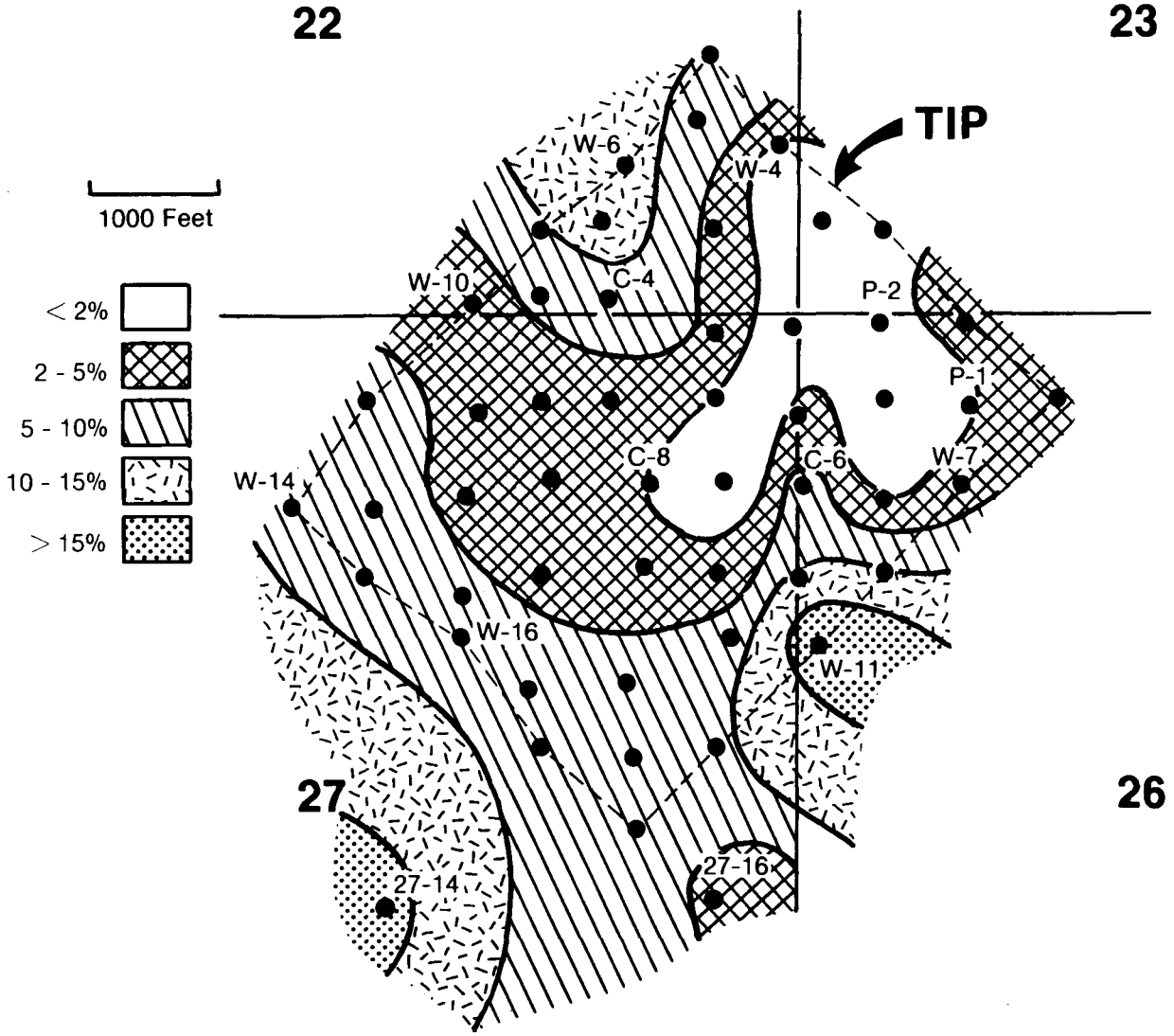


FIGURE 54. - Total clay content, in percent, based on thin-section analysis of numbered wells. From middle and upper shoreface and foreshore facies within the barrier island. Similarity with figure 42 indicates that diagenetic clay content is the dominant control of total clay distribution within barrier island facies.

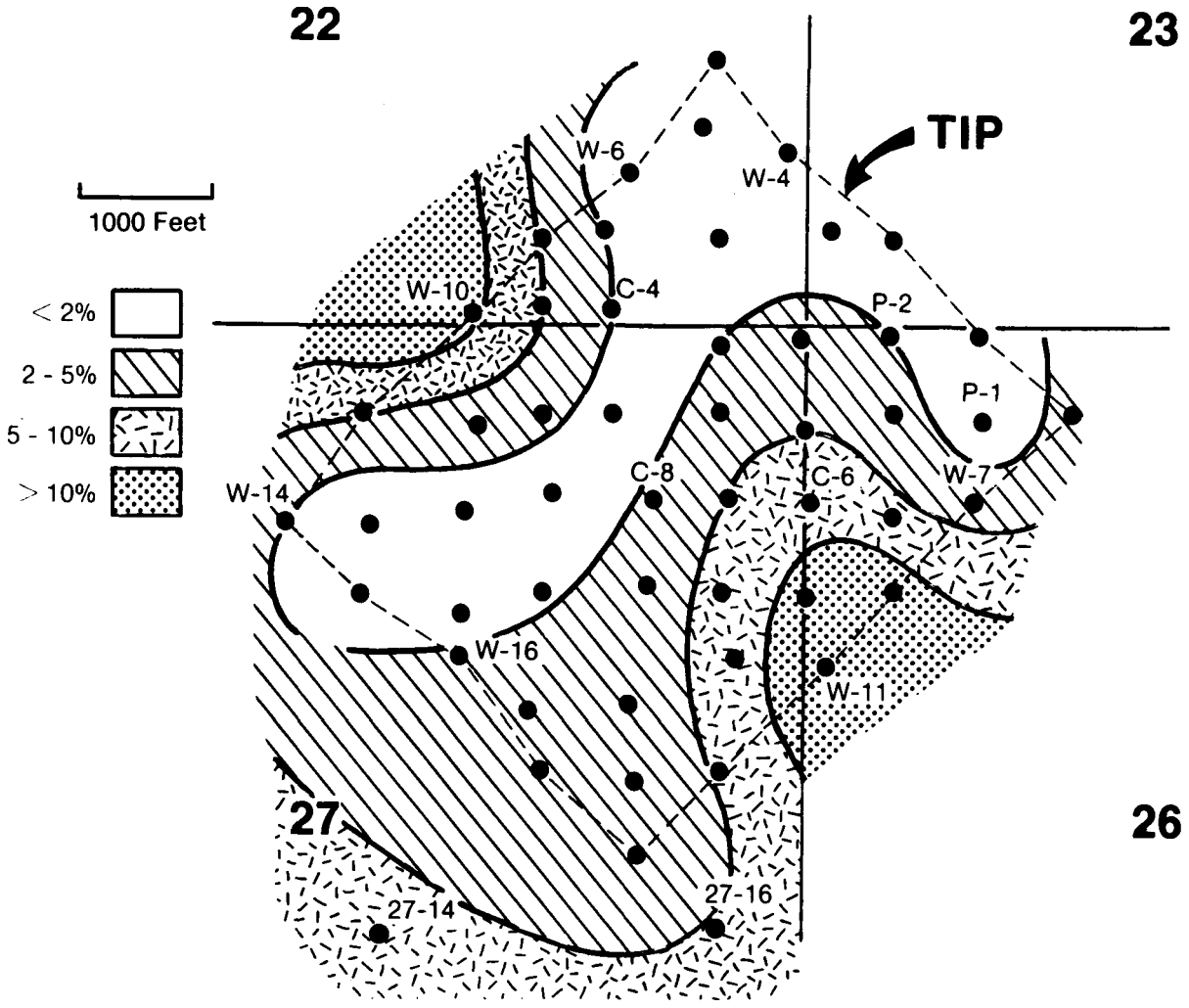


FIGURE 55. - Maximum value for matrix percent in any barrier island facies. Based on thin-section analysis from numbered wells. Map gives an indication of the amount of interbedded nonbarrier sediments within the barrier island sandstones.

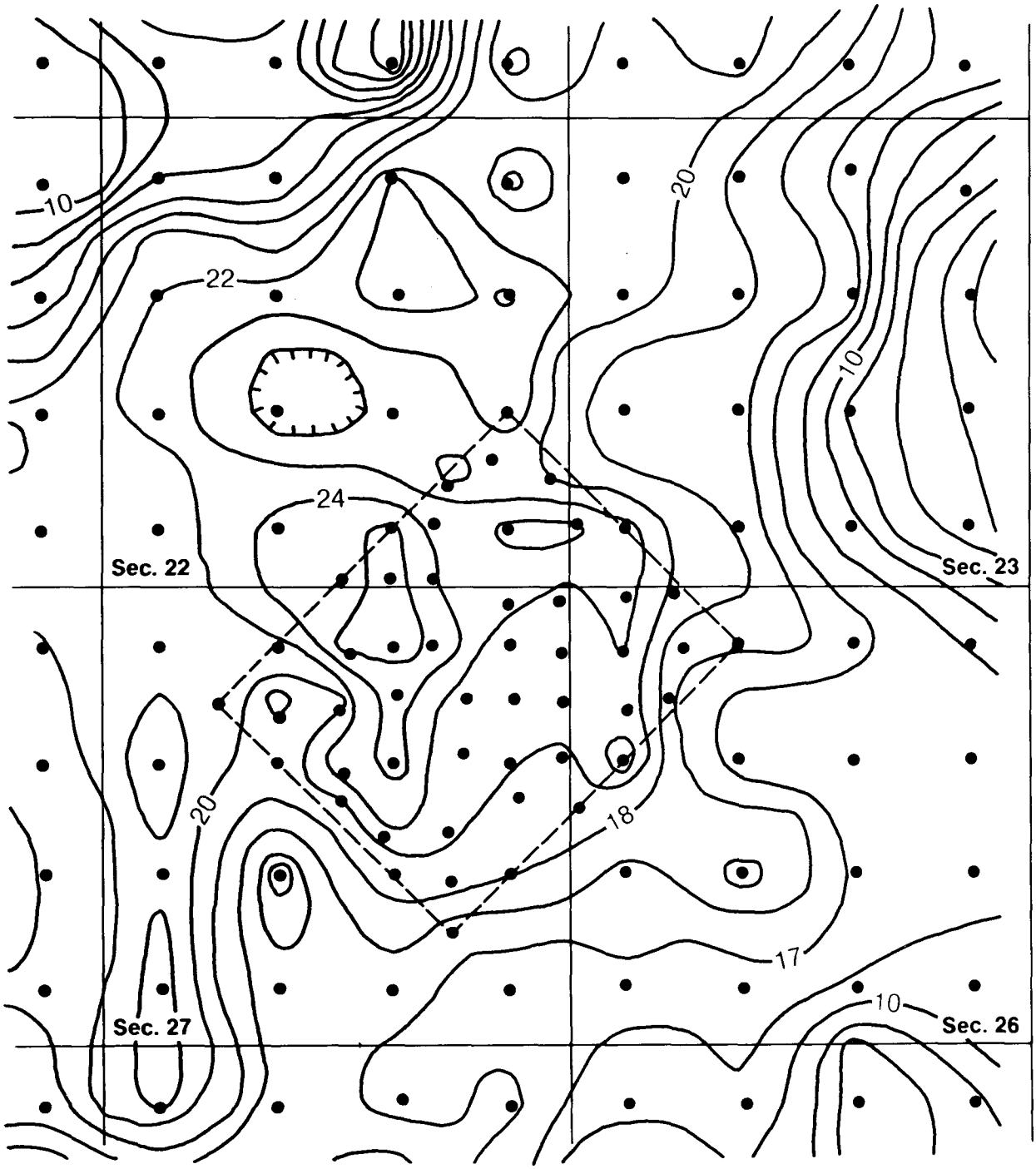


FIGURE 56. - Net pay map of Muddy formation in study area of Unit 'A' of Bell Creek field. Contours are in feet. TIP area indicated by dashed line. Sections are 1 mile across.

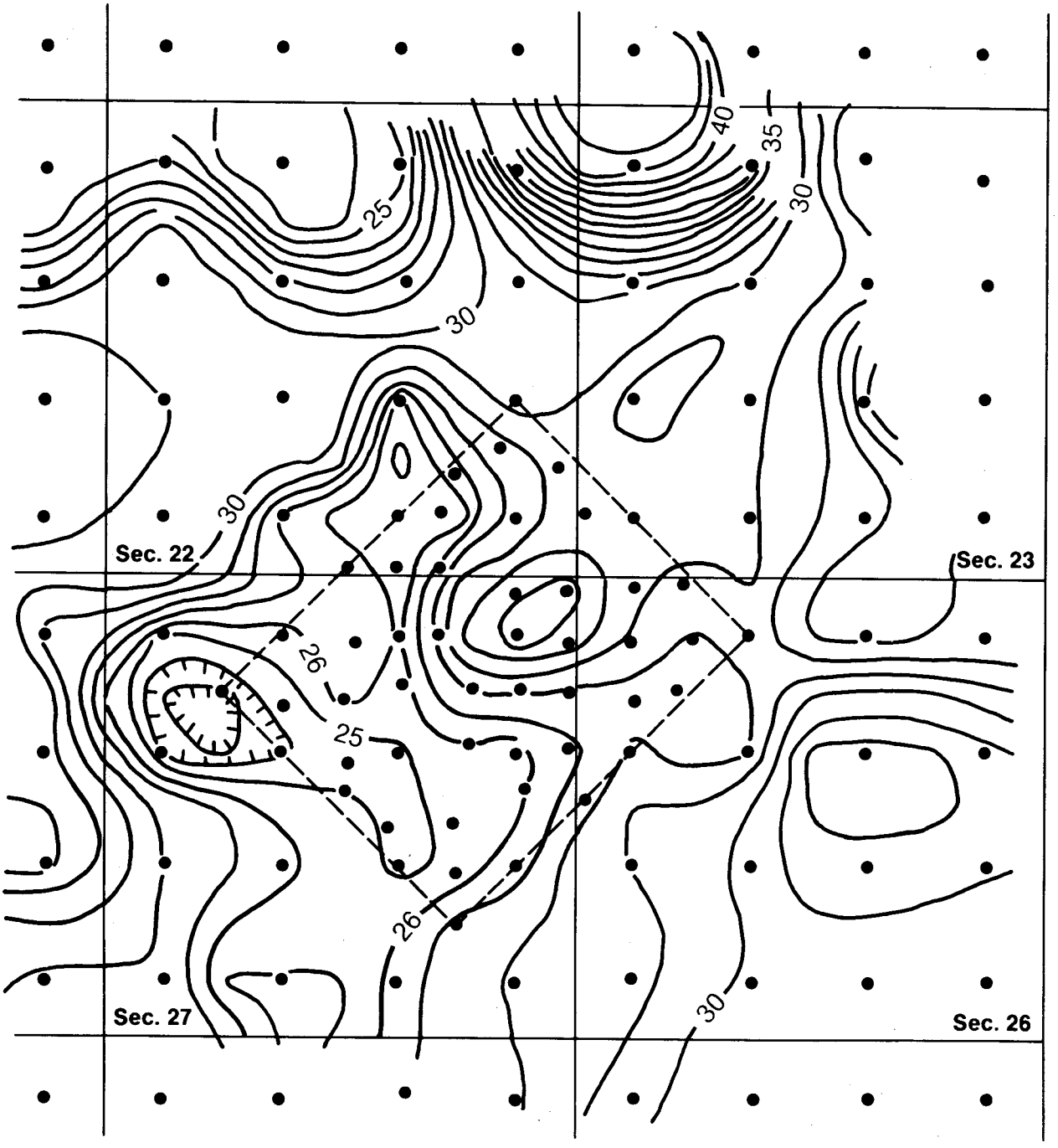


FIGURE 57. - Distribution of core-derived average porosity (barrier island + valley fill) for the study area. Contour intervals in percent.

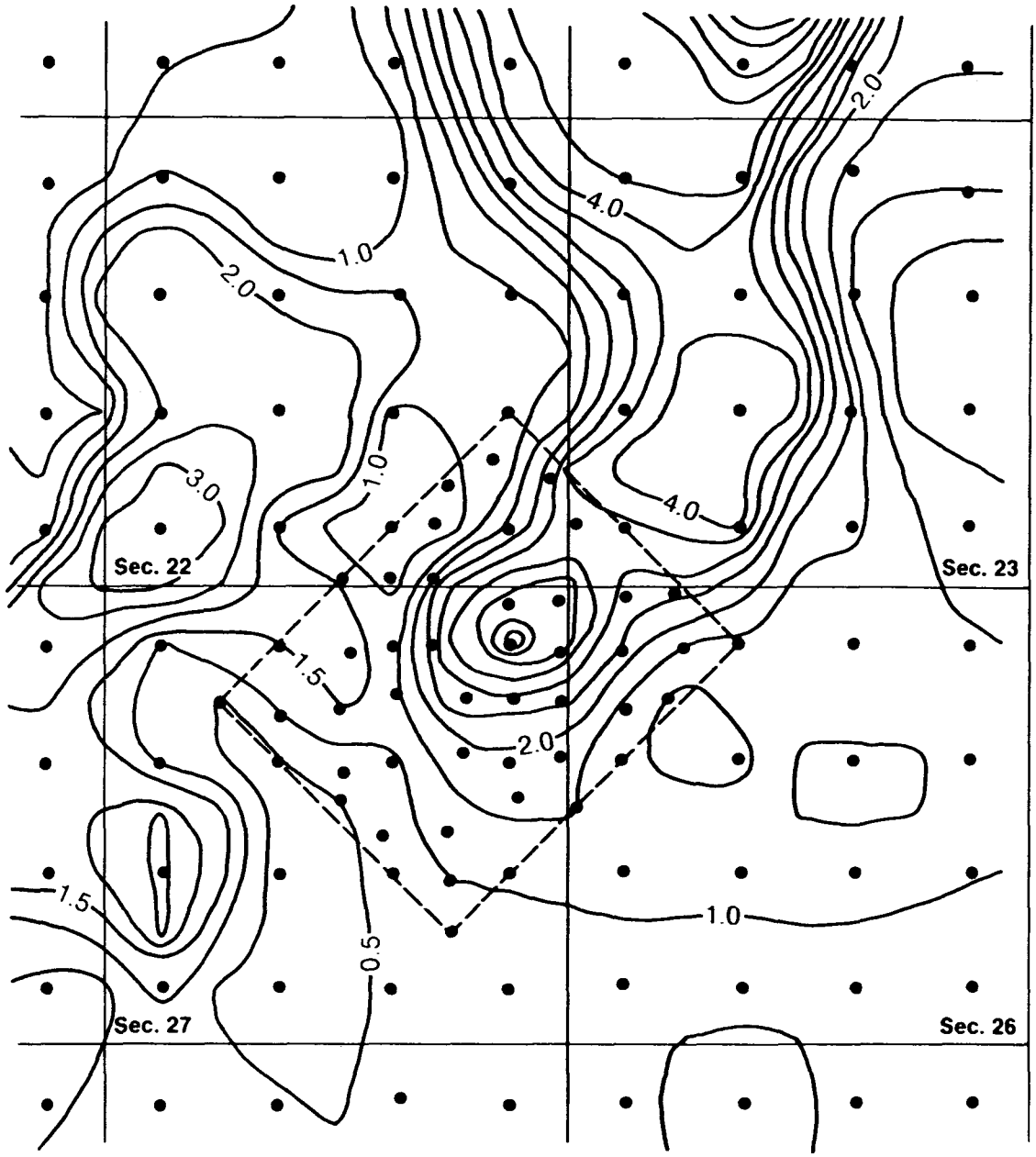


FIGURE 58. - Distribution of average arithmetic horizontal air permeability in Muddy formation (barrier island + valley fill) for study area within Unit 'A', Bell Creek field. Contour interval is 0.5 darcy.

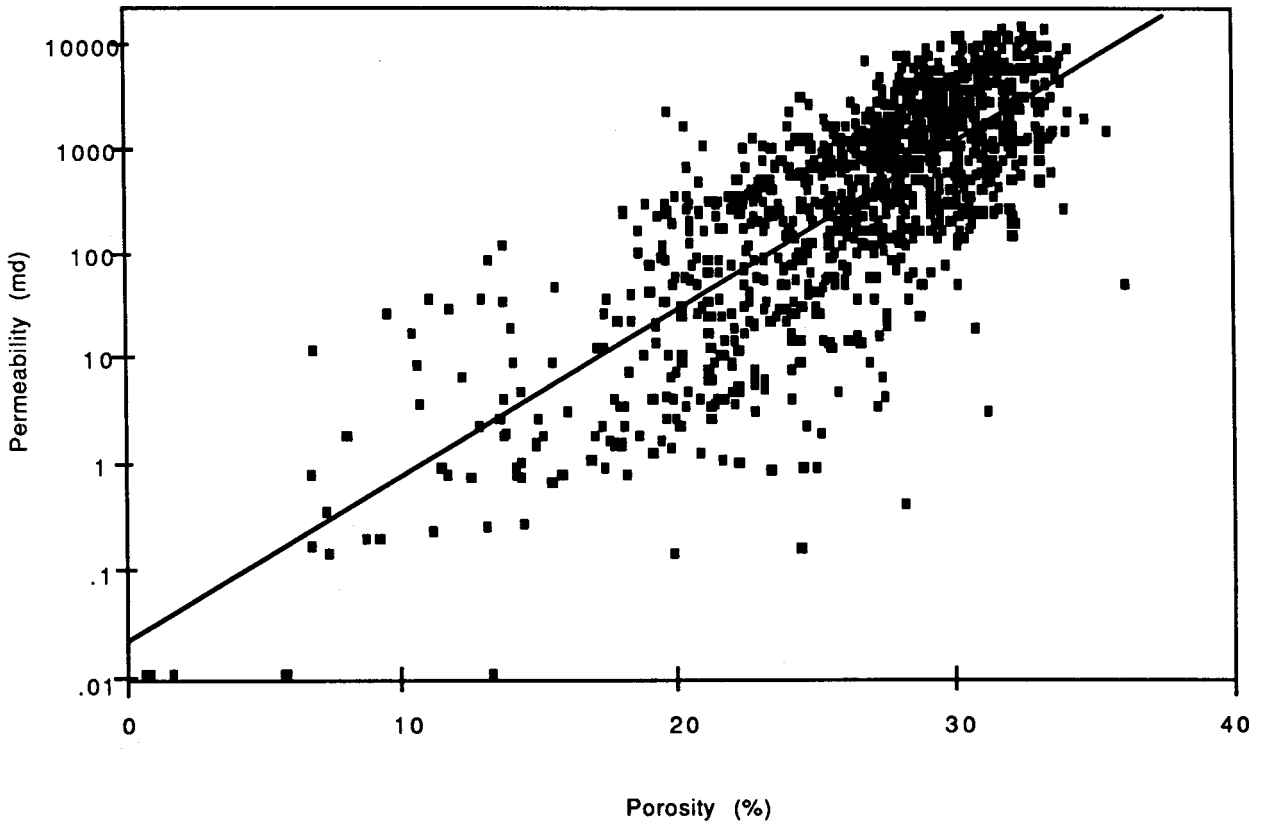


FIGURE 59. - Cross-plot of air permeability versus porosity. No attempt was made to distinguish barrier island and valley fill samples.

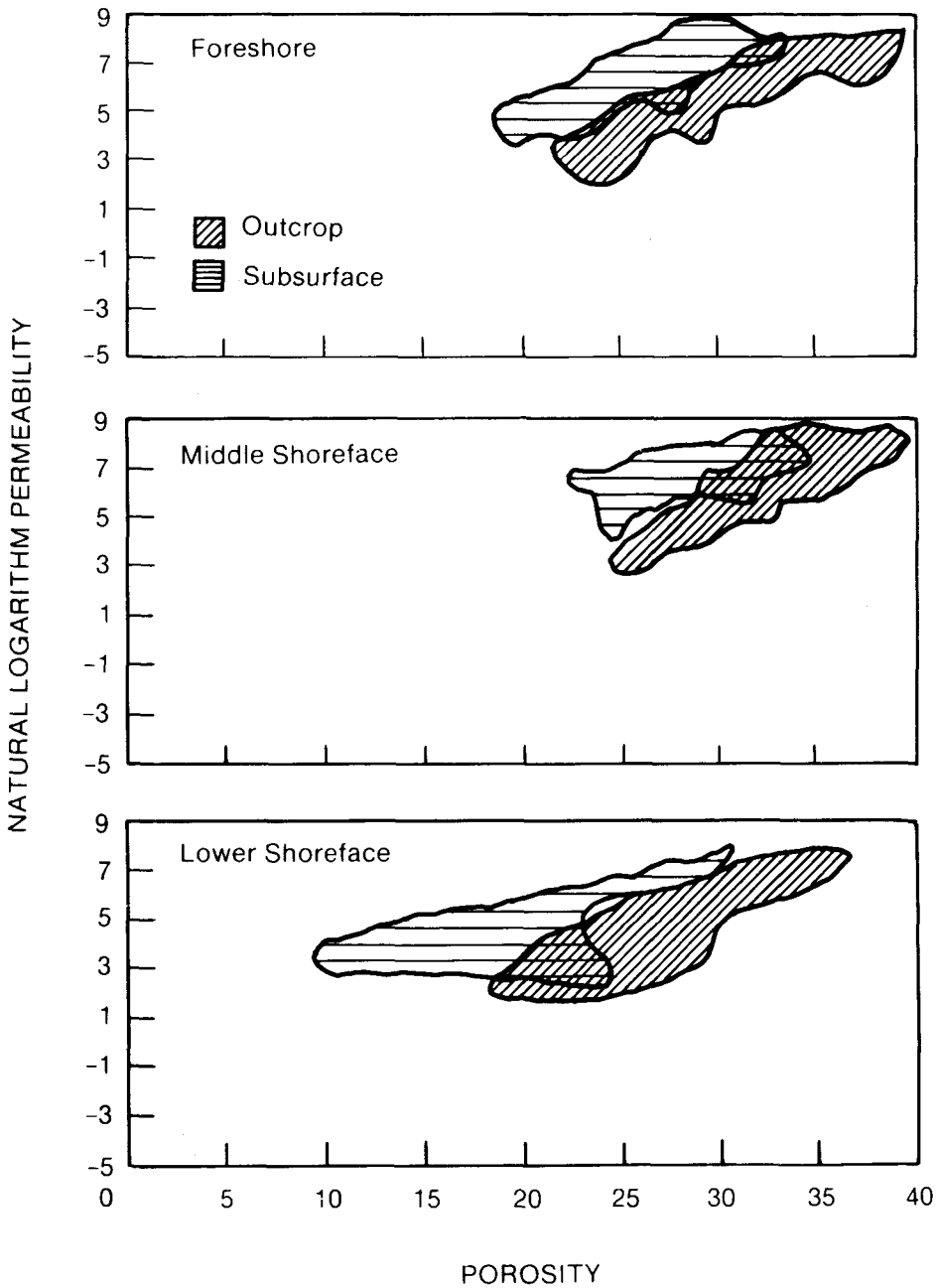


FIGURE 60. - Comparison of natural logarithm permeability versus porosity in outcrop and subsurface barrier island facies. Note shift of porosity in outcrops toward higher values.

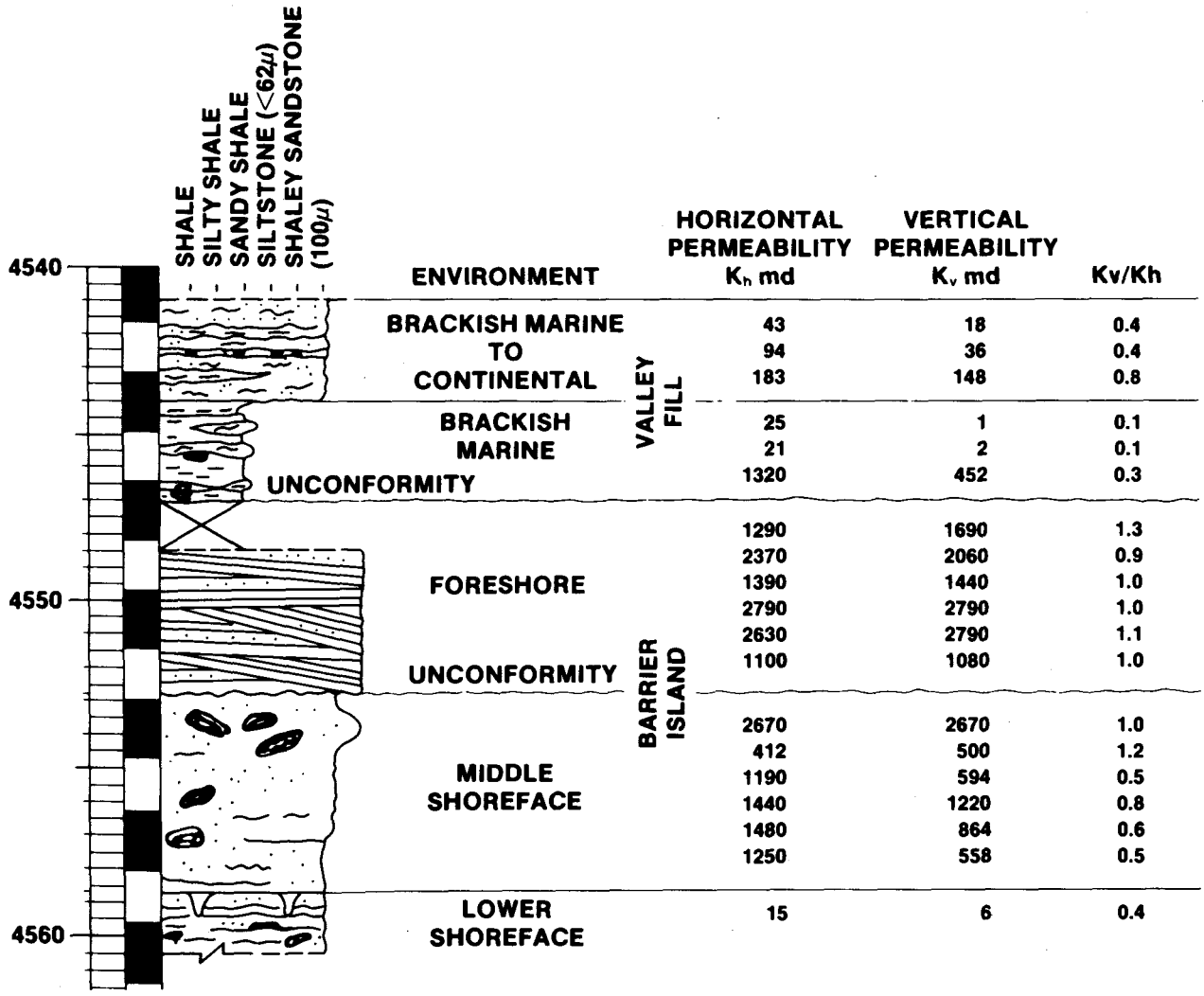


FIGURE 61. - Petrophysical properties of barrier island and nonbarrier facies in stratigraphic profile of well 26-7.

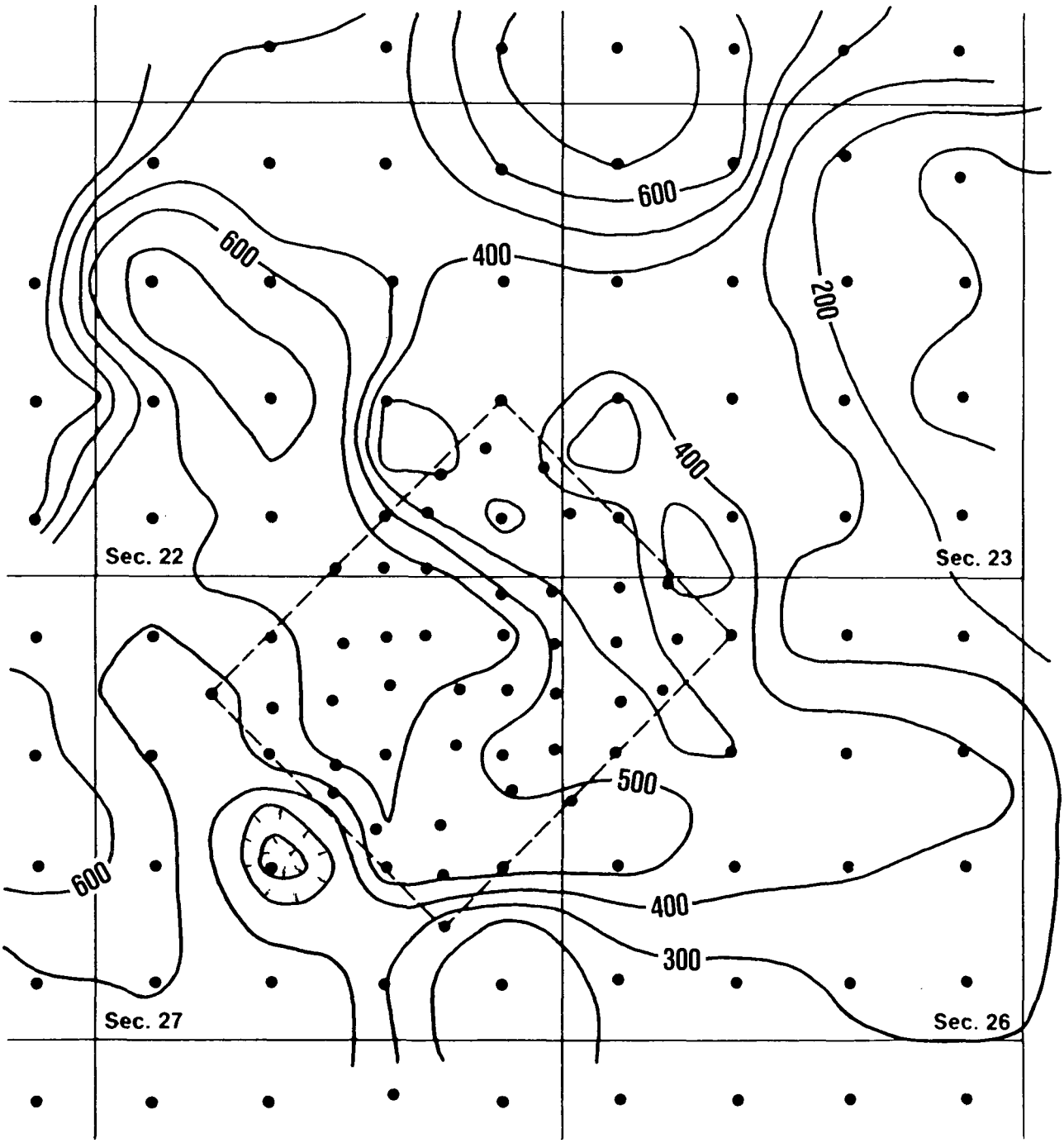


FIGURE 62. - Distribution of Muddy formation storage capacity (product of core porosity and net pay), in %-ft; Bell Creek field, Unit 'A', (barrier island and valley fill facies).

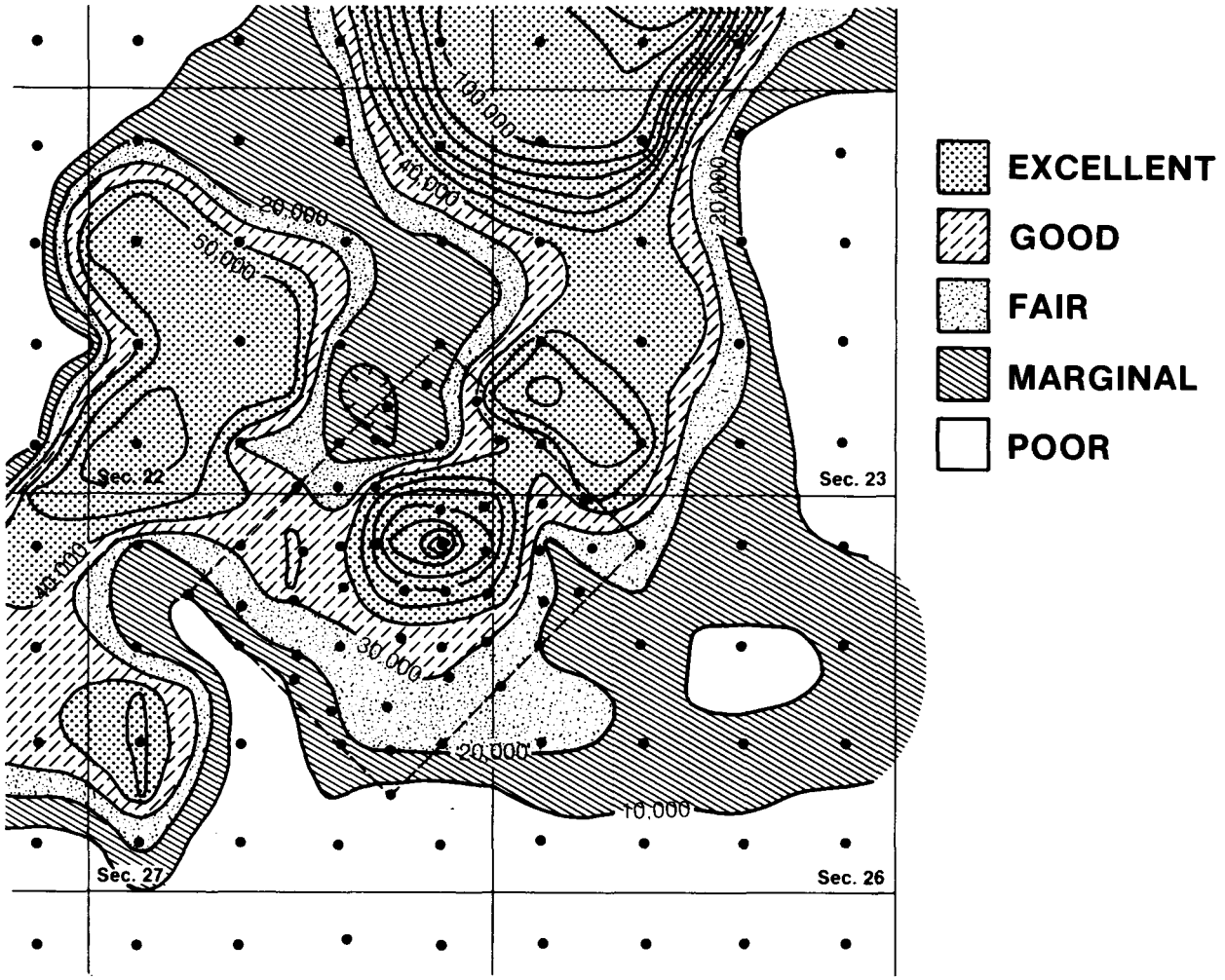


FIGURE 63. - Fluid flow capacity (product of core permeability and net pay) of Muddy formation in md-ft Bell Creek field, Unit 'A' (barrier island and valley fill facies).

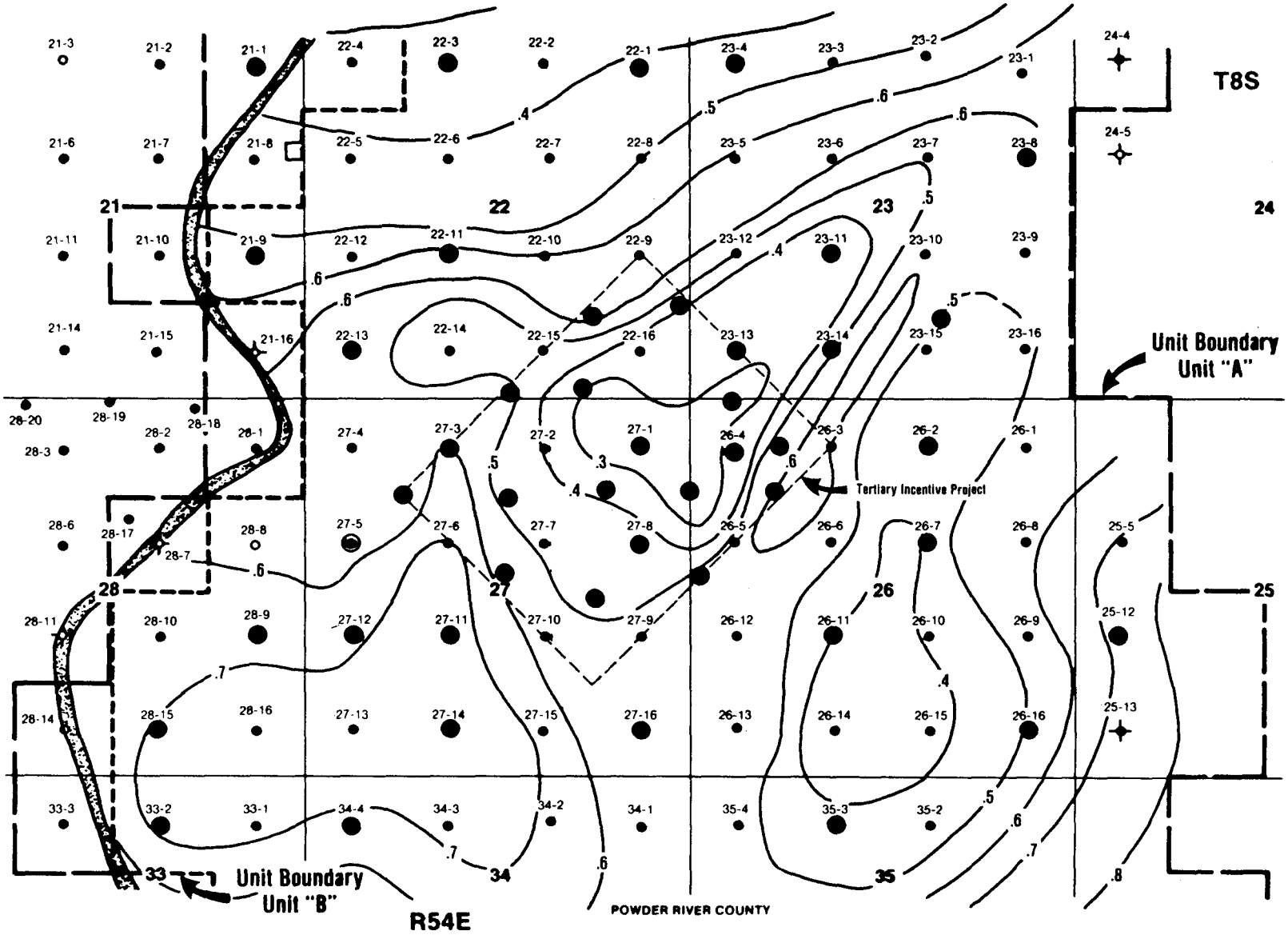


FIGURE 64. - Distribution of Dykstra-Parsons coefficients obtained from air-permeability data in the study area. Wells with permeability data are indicated by large circles.

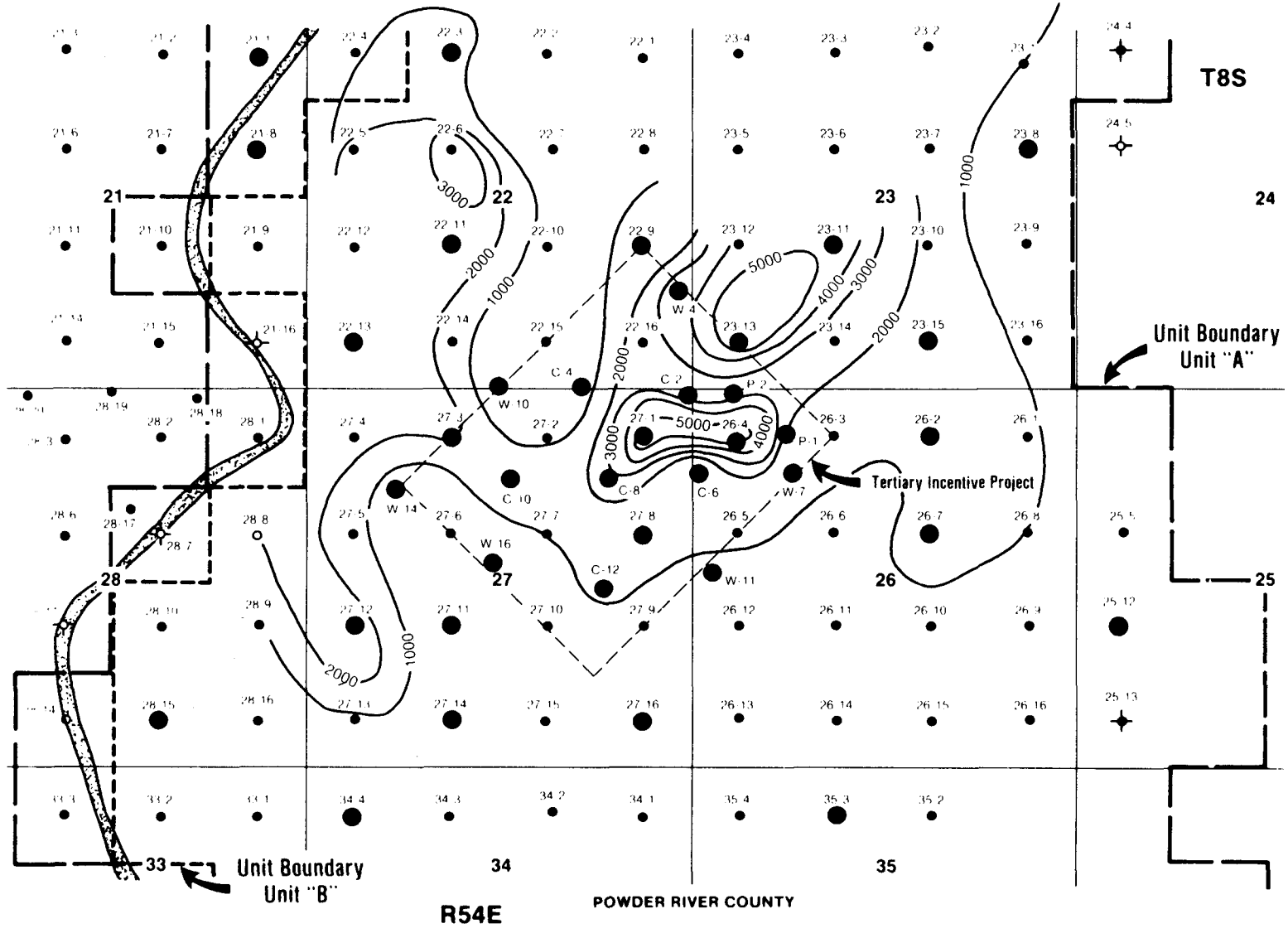


FIGURE 65. - Distribution of geometric means of air permeability data for wells in the study area. C.I. = 1,000 md. Wells with permeability data are indicated by large circles.

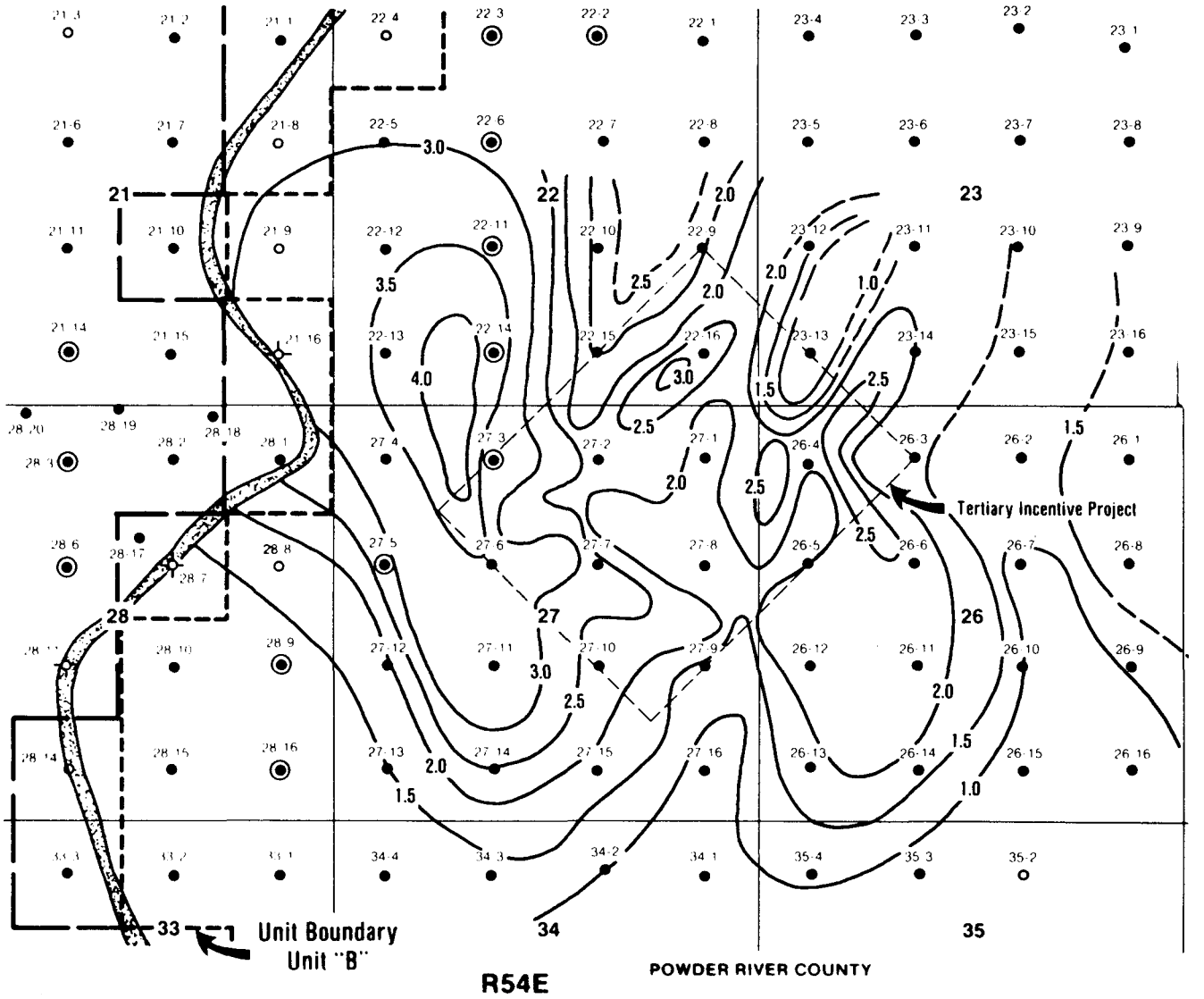


FIGURE 66. - Log-derived heterogeneity index (LHI) of the barrier island sandstones in the study area. Small values of the index indicate relatively cleaner reservoir sandstone.

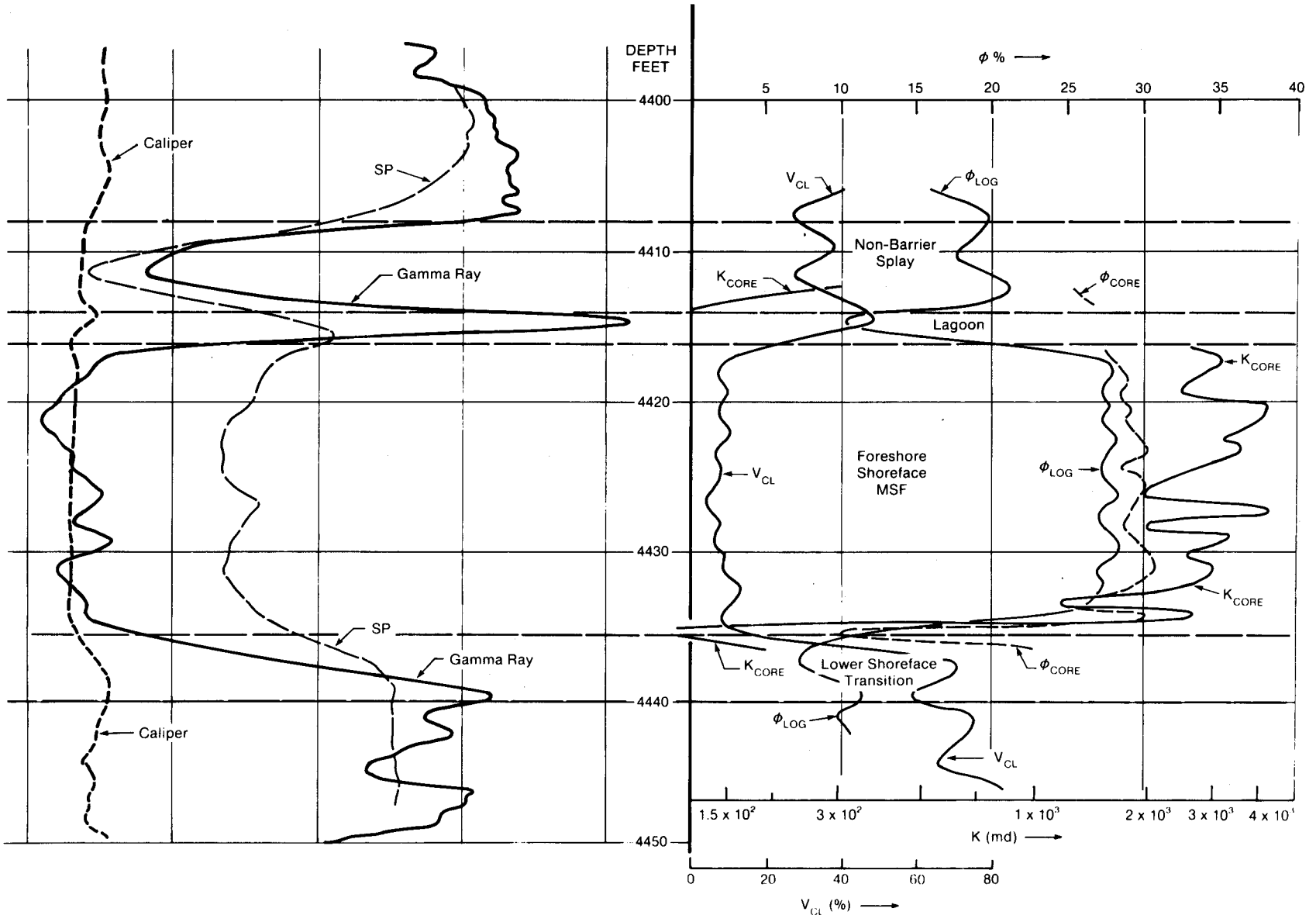


FIGURE 67. - Distribution of permeability, porosity, and clay content index Vcl (percentage of intermatrix porosity) in the various facies of barrier island and nonbarrier sandstones in well P-2. The clay content curve is obtained from interpretaton of sonic and density logs; porosity curves, from core data; and density logs and the permeability curve, from core data. Note good agreement between core and log porosity values in this relatively clay-free barrier island sandstone unit. Facies were identified during sedimentologic analysis of the cored interval from 4,413.0 to 4,438.6 ft.

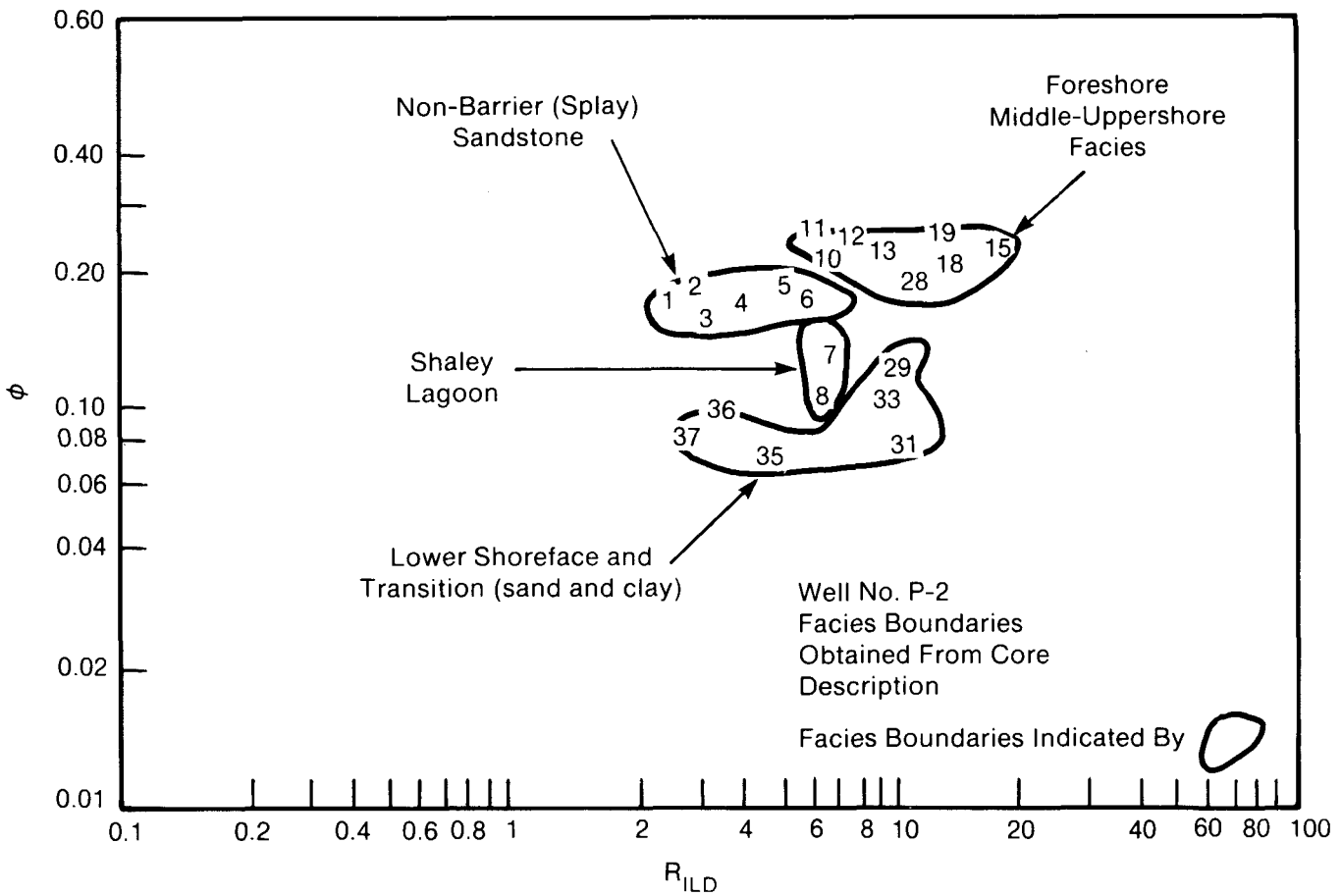


FIGURE 68. - Cross-plot of formation resistivity against density log porosity for well P-2 for distinguishing barrier island from nonbarrier sandstone facies. Numbers within facies boundaries indicated sequences of data points.

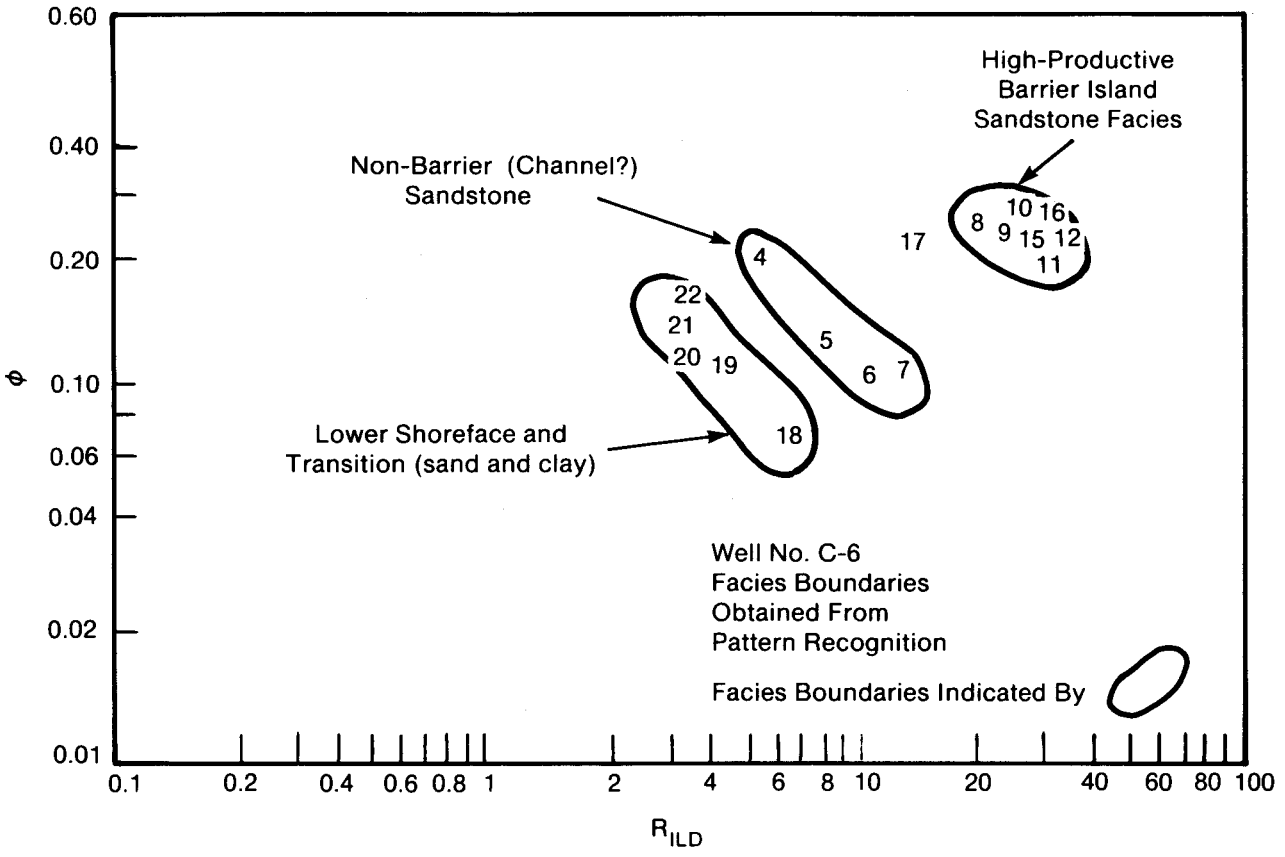


FIGURE 69. - Cross-plot of formation resistivity against density log porosity for well C-6 for distinguishing barrier island from nonbarrier sandstone facies. Numbers within facies boundaries indicate sequences of data points.

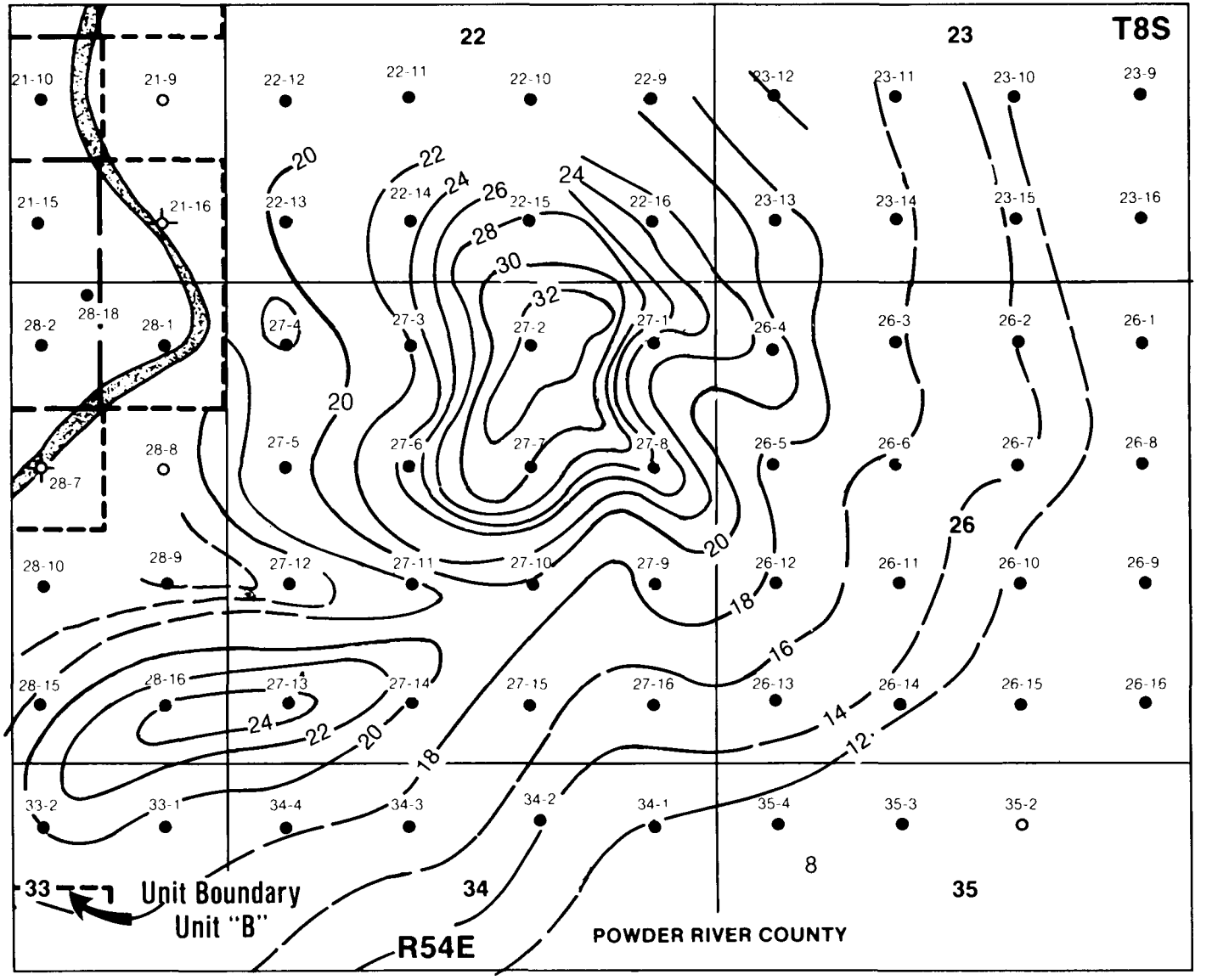


FIGURE 70. - Isopach map of the barrier island sandstones interpreted from logs in the study area. C.I. = 10 ft.

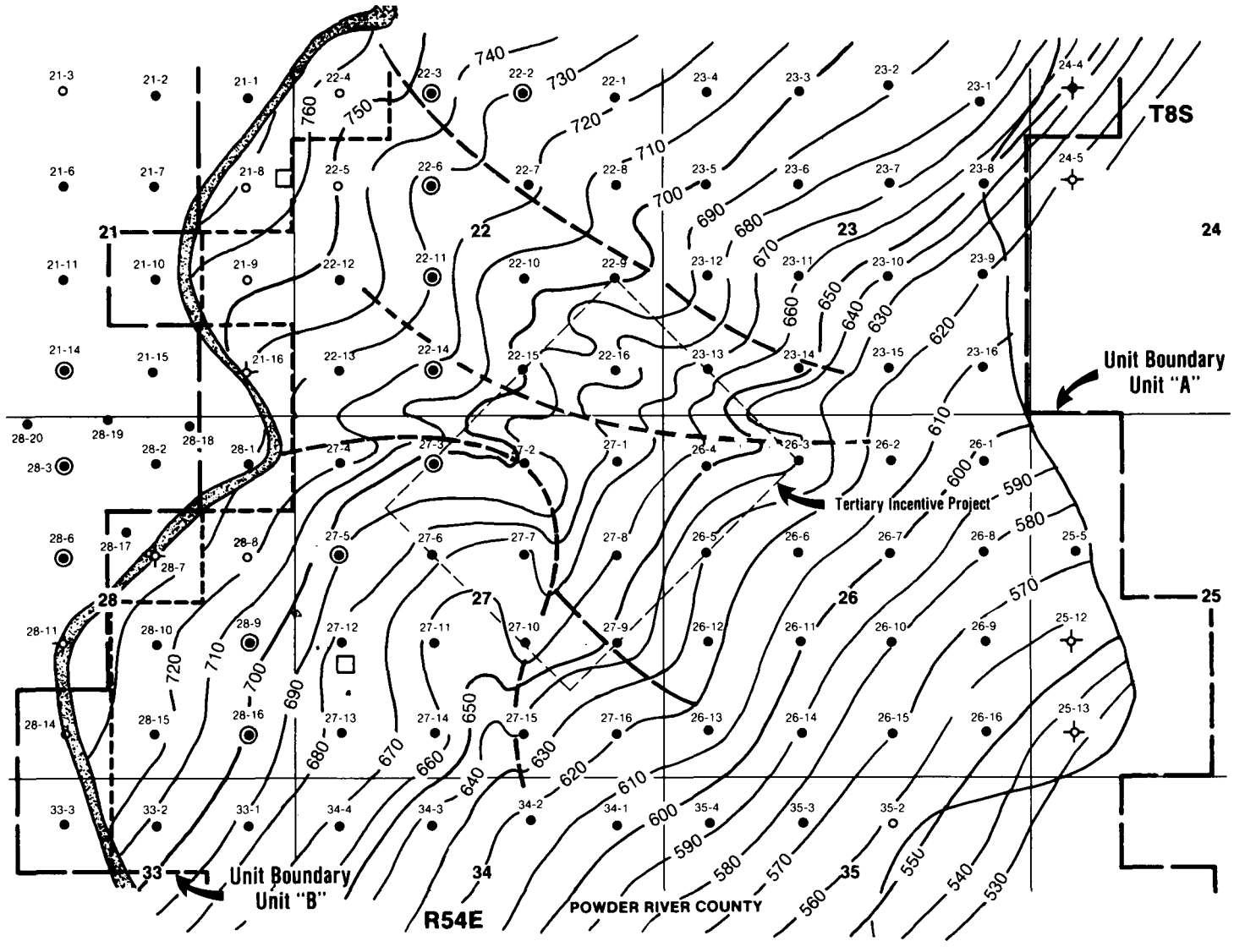


FIGURE 71. - Structural contours (in ft below M.S.L.) on the top of the barrier island sandstones. C.I. = 10 ft. Locations of possible faults and or valley incisions are indicated by dashed lines.

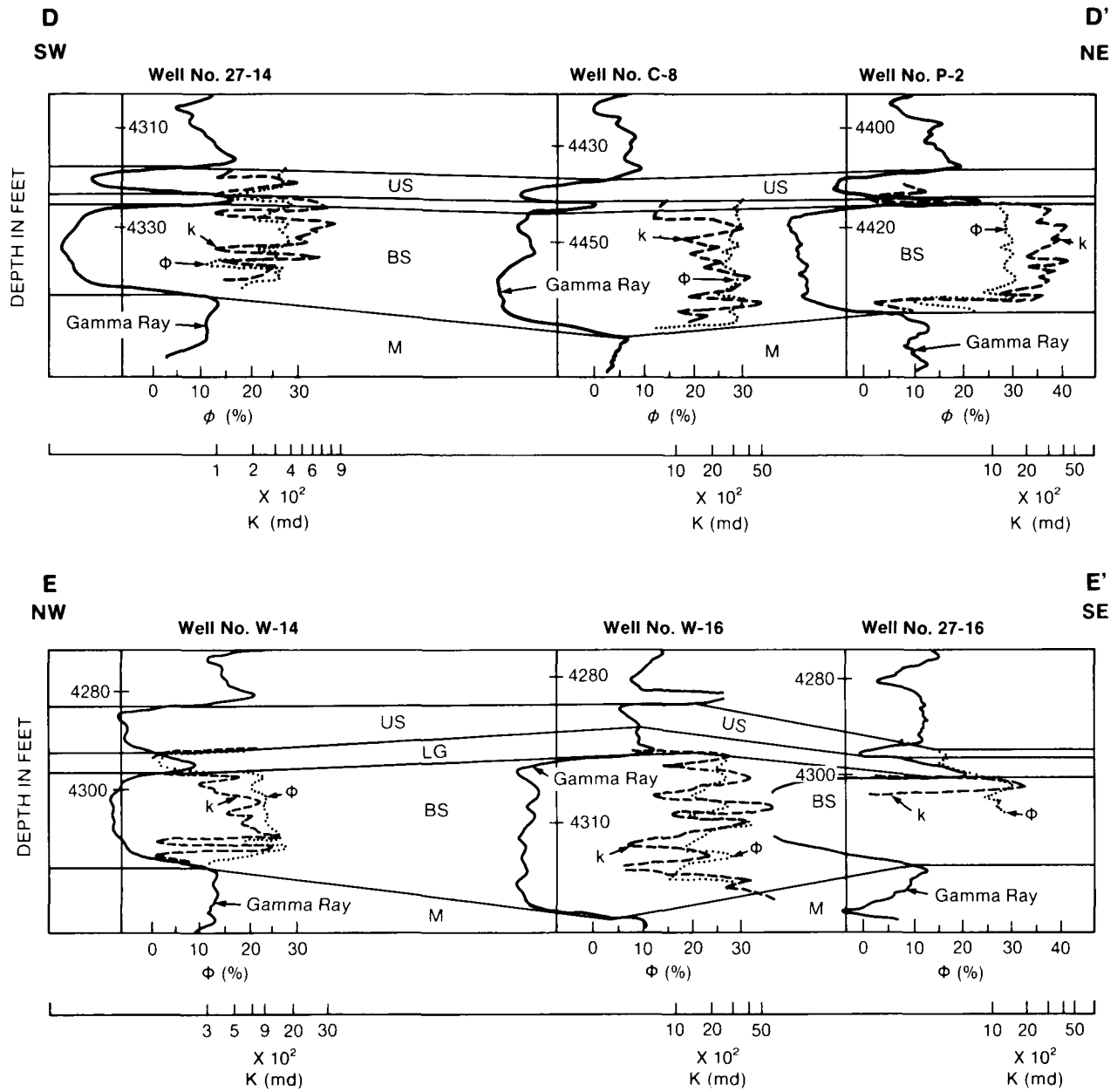


FIGURE 72. - Stratigraphic crosssections parallel (AA') and perpendicular (BB') to the depositional strike of the bar.

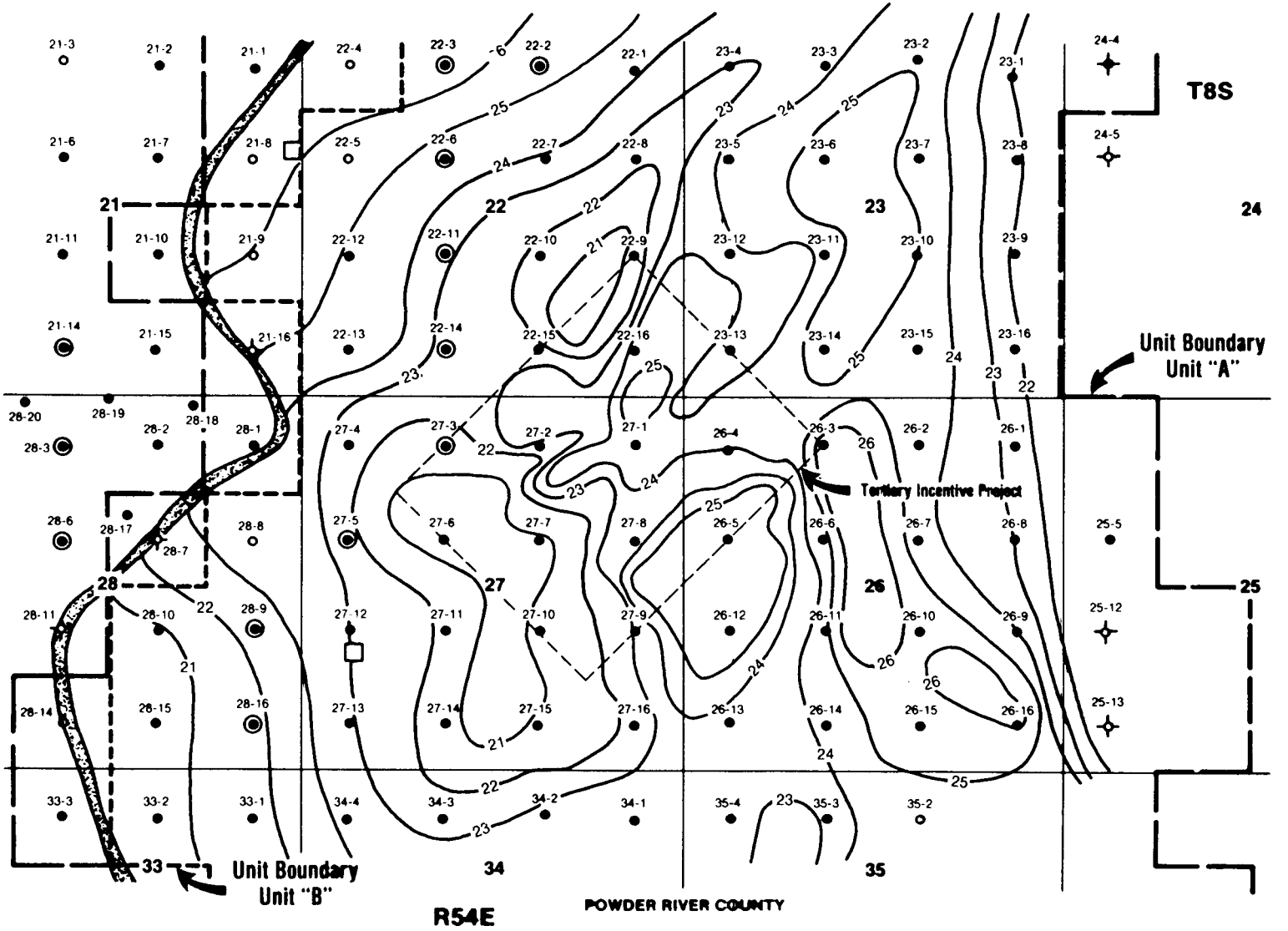


FIGURE 73. - Average log-derived porosities (in percentage of the barrier island sandstones in the study area).

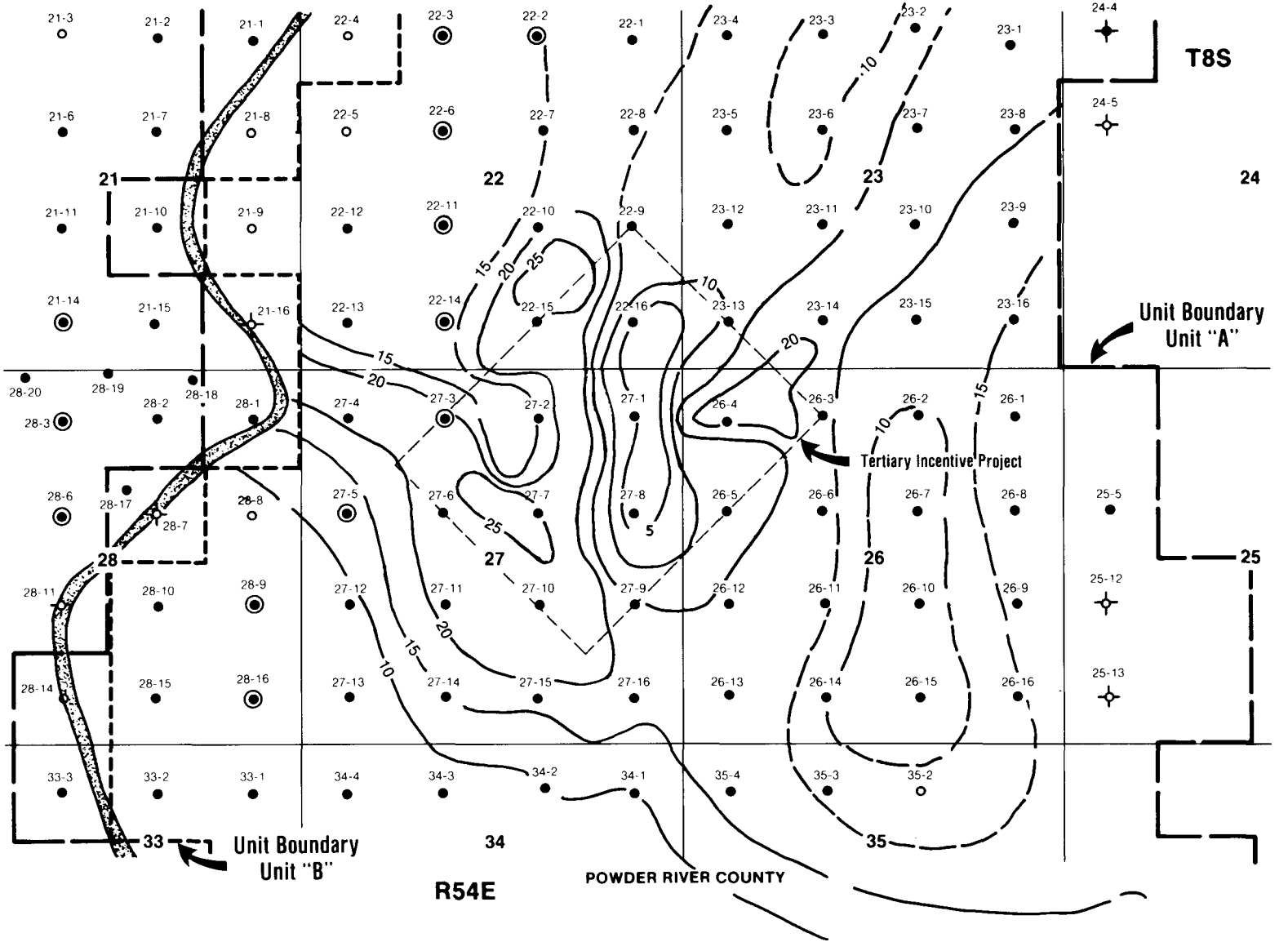


FIGURE 74. - Log-derived clay content index of the barrier island sandstone in the study area. Dotted lines indicate areas of limited data.

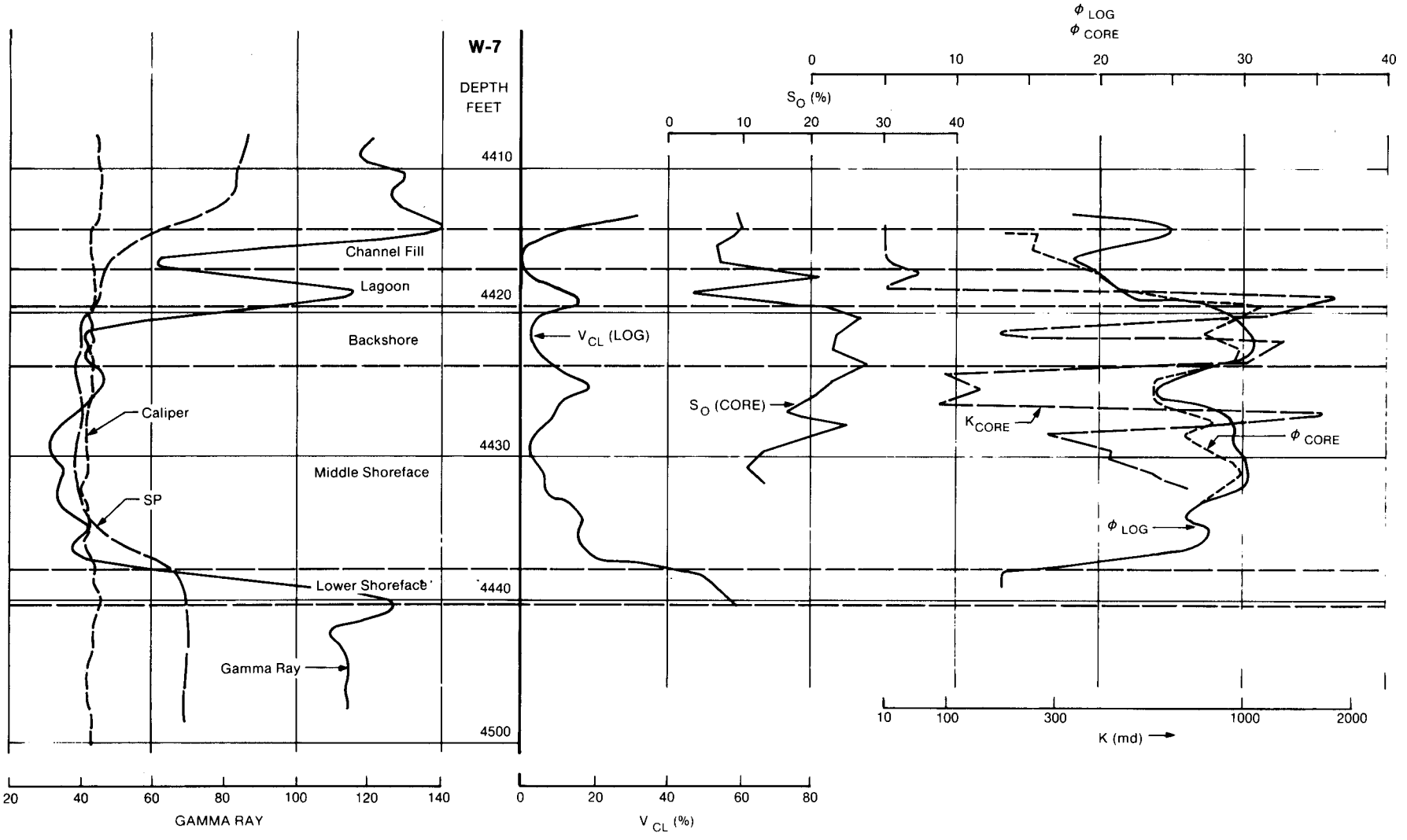


FIGURE 75. - Plots of porosity, permeability, clay content, Vcl, (% of intermatrix porosity), and oil saturation in well W-7 obtained from core and log data. Note higher porosity, permeability stratification in this well due mainly to higher clay content compared to well P-2 (fig. 67). Facies were identified by sedimentologic analysis of the cored interval from 4,405.0 to 4,433.1 ft.

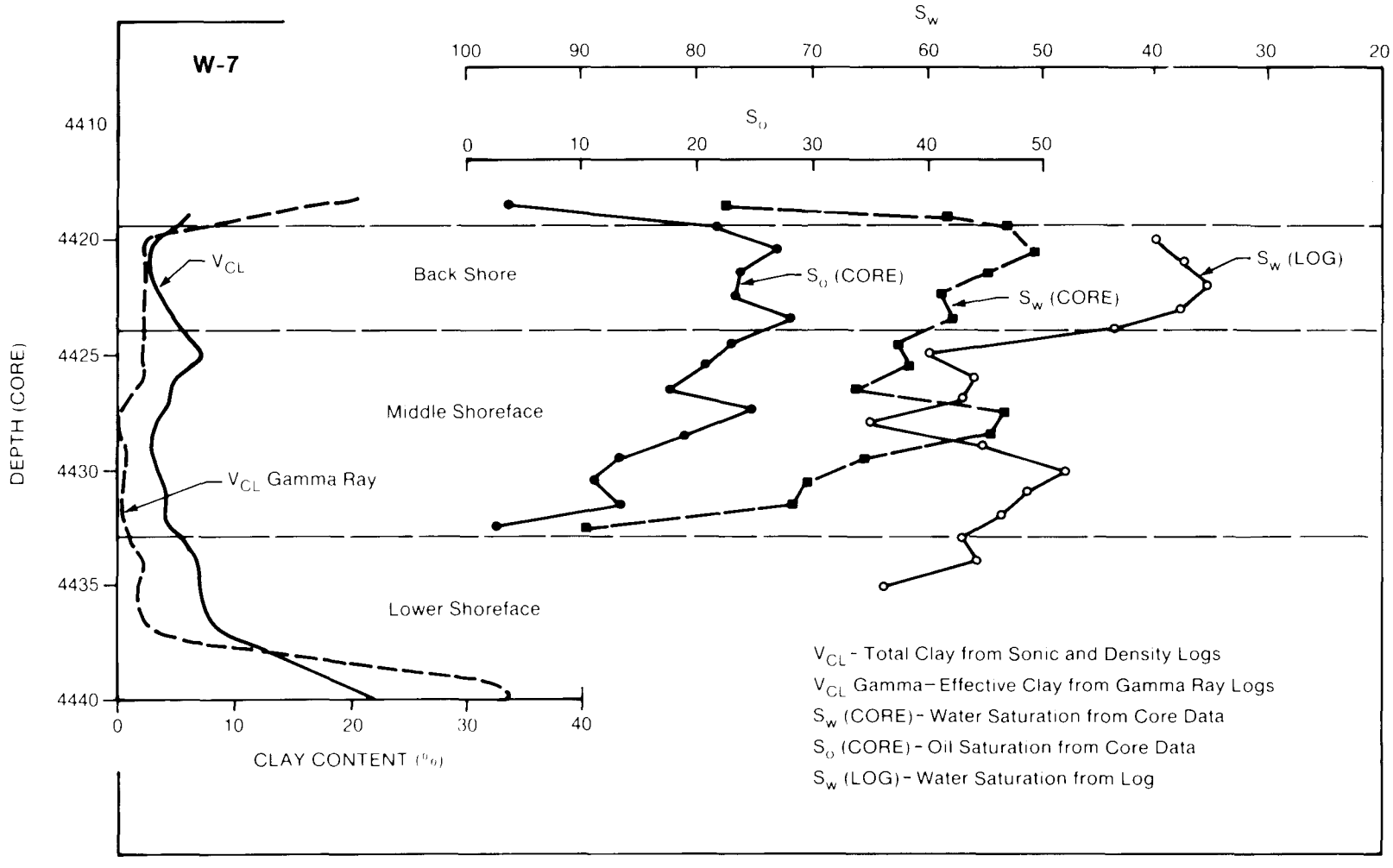


FIGURE 76. - Sw determination in well W-7 by application of Waxman-Smit equation. Effective clay Vcl obtained from gamma Ray log. Total clay from sonic and density logs. Core control was available from 4,405.0 to 4,431.1 ft.

DATA GATHERING AT EACH FIELD DEVELOPMENT STAGE OF AN OIL RESERVOIR

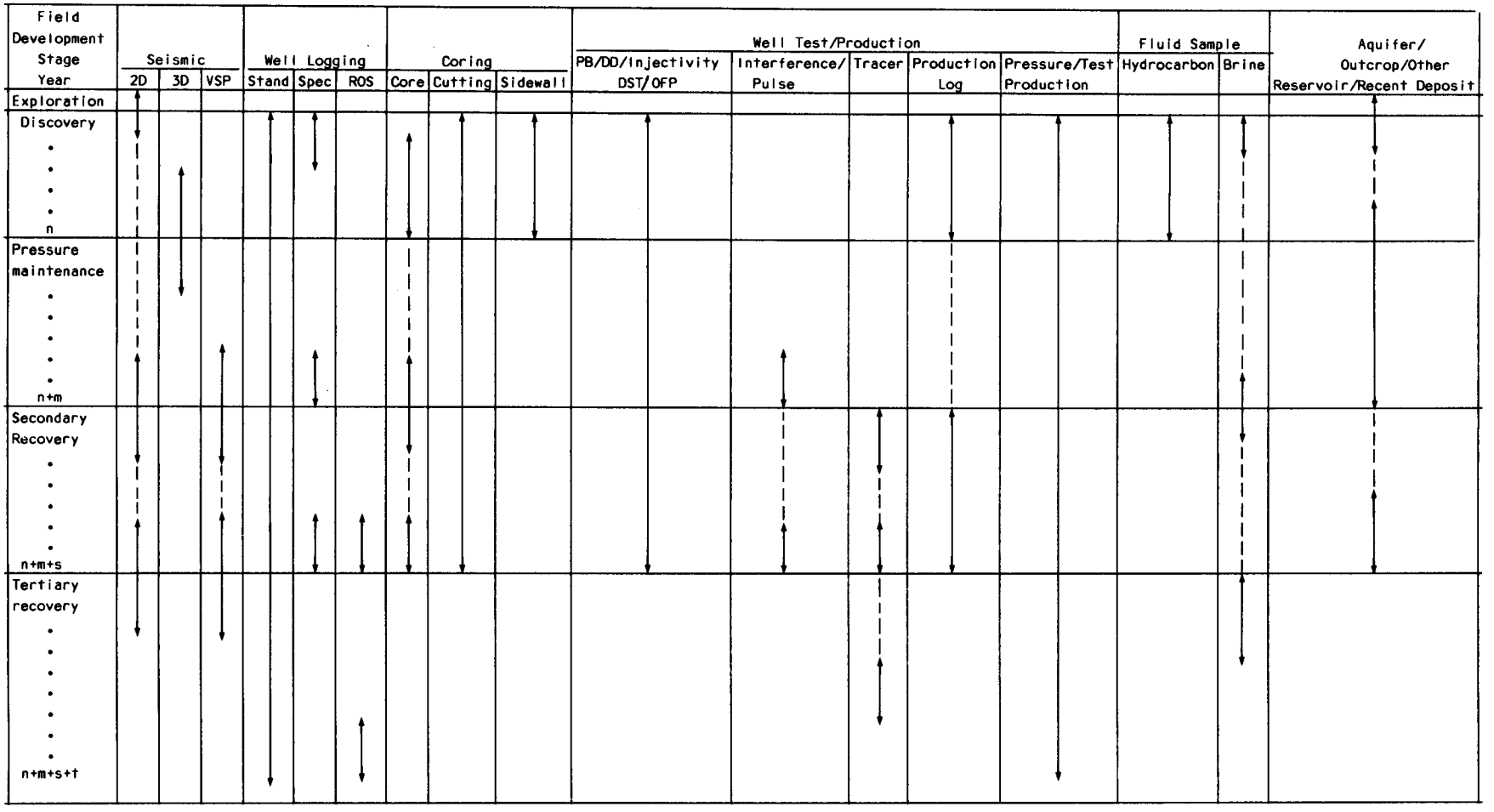


FIGURE 77. - Chronology of data-gathering at each field-development stage of an oil reservoir.

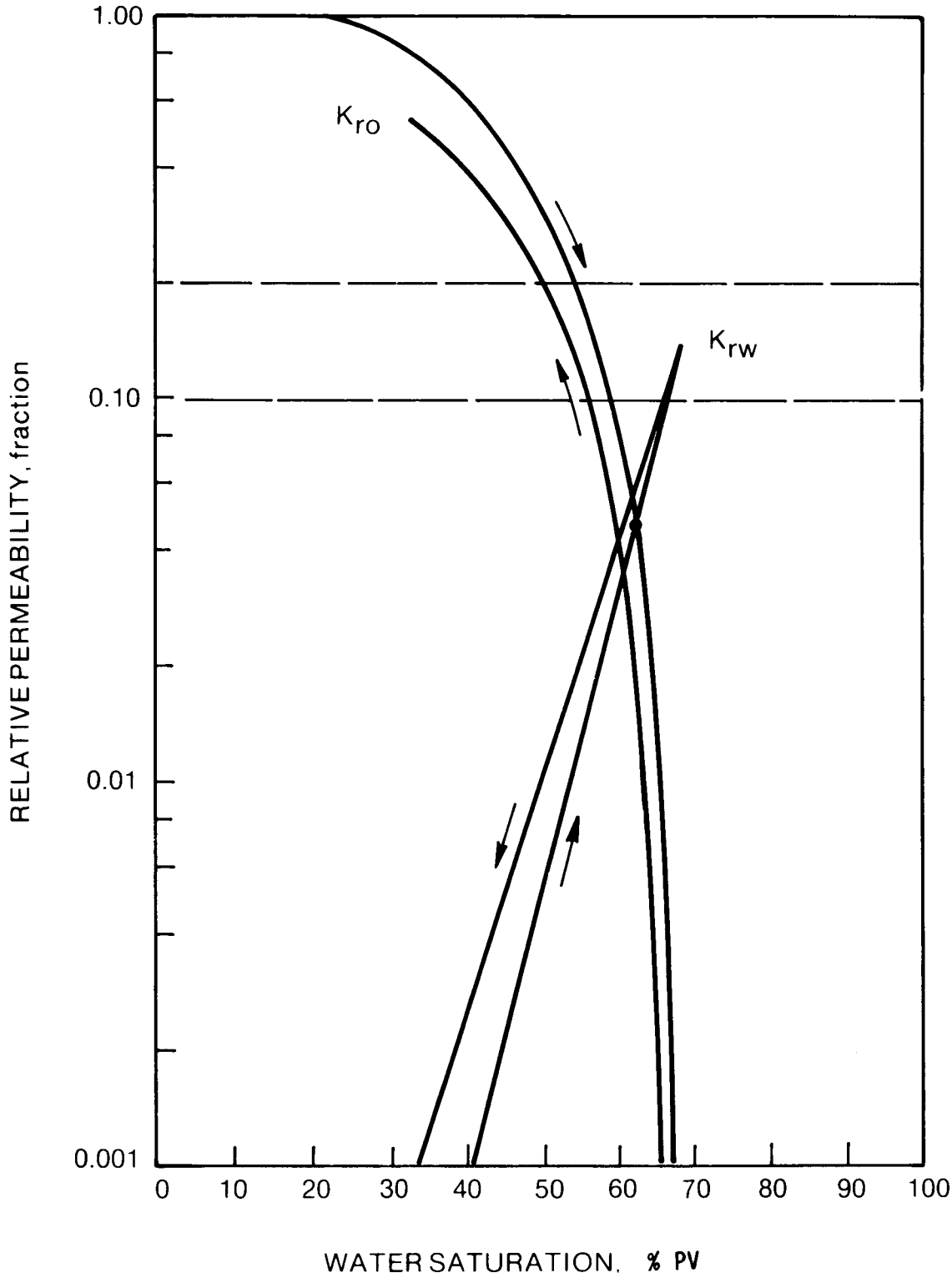


FIGURE 78. - Water-oil relative permeability curves for both imbibition and drainage cycles.

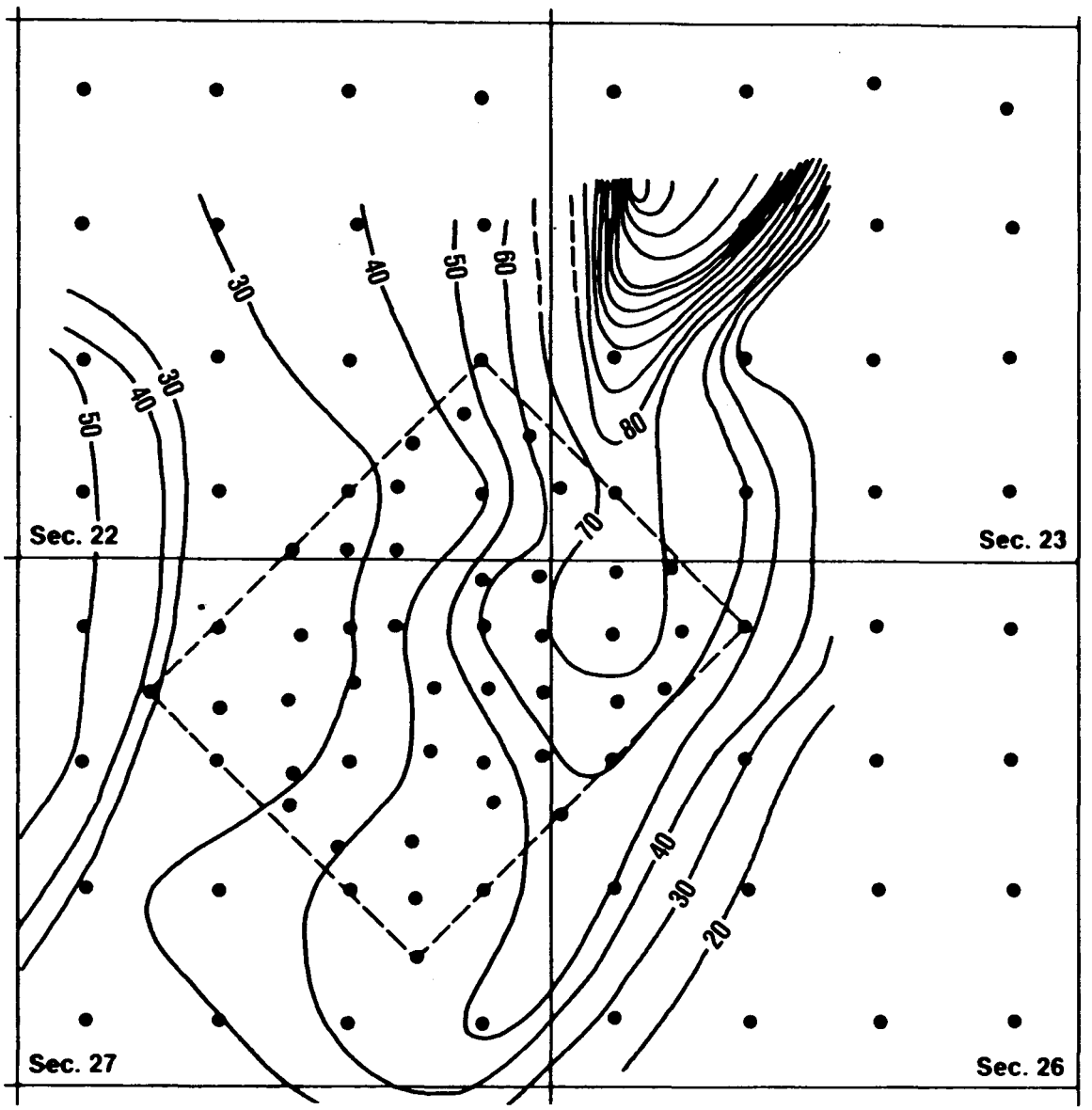


FIGURE 79. - Distribution of initial electrical resistivity values within the study area in Ω-m.

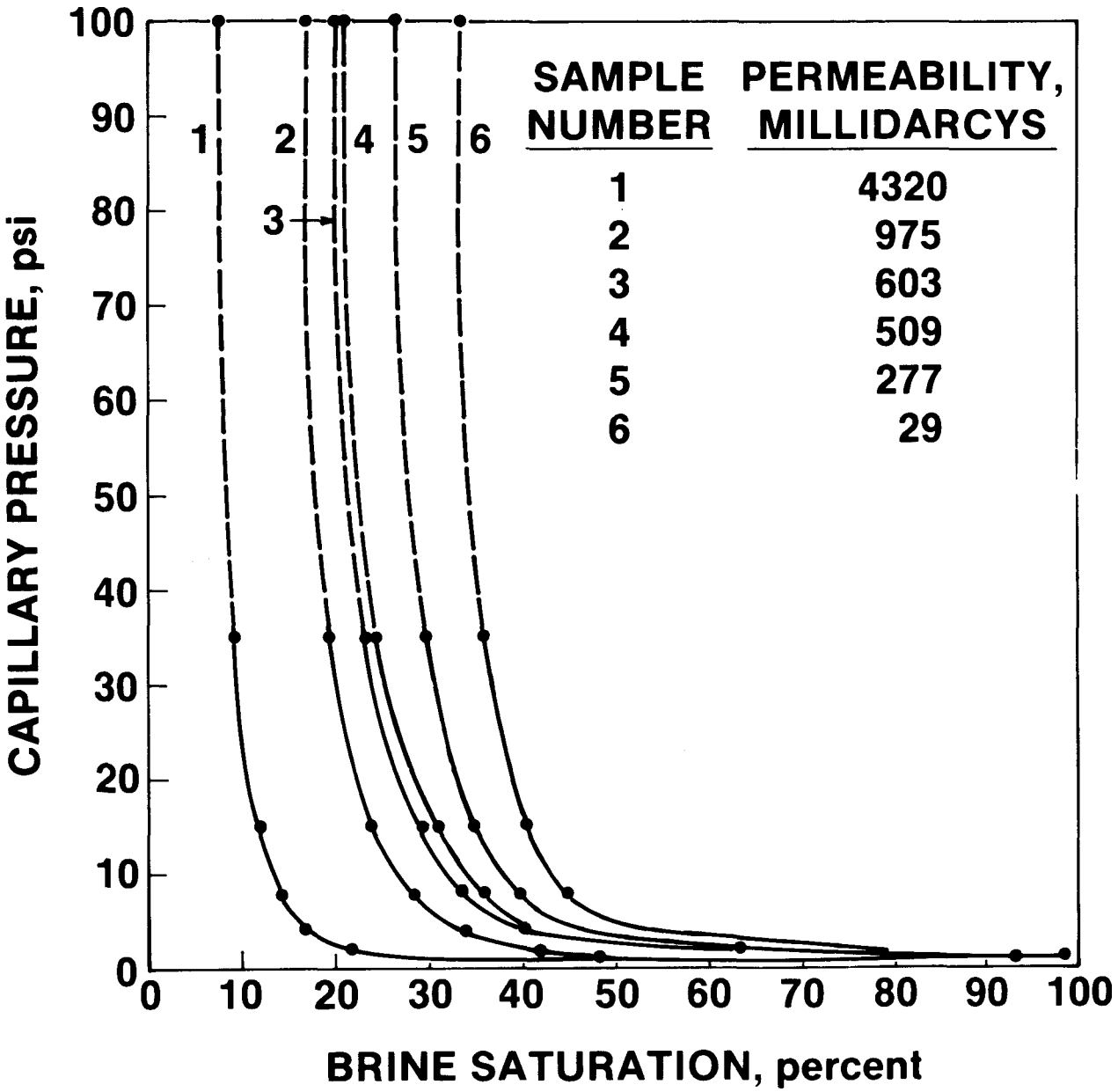


FIGURE 80. - Air-brine capillary pressure curves for six samples from well 22-9.

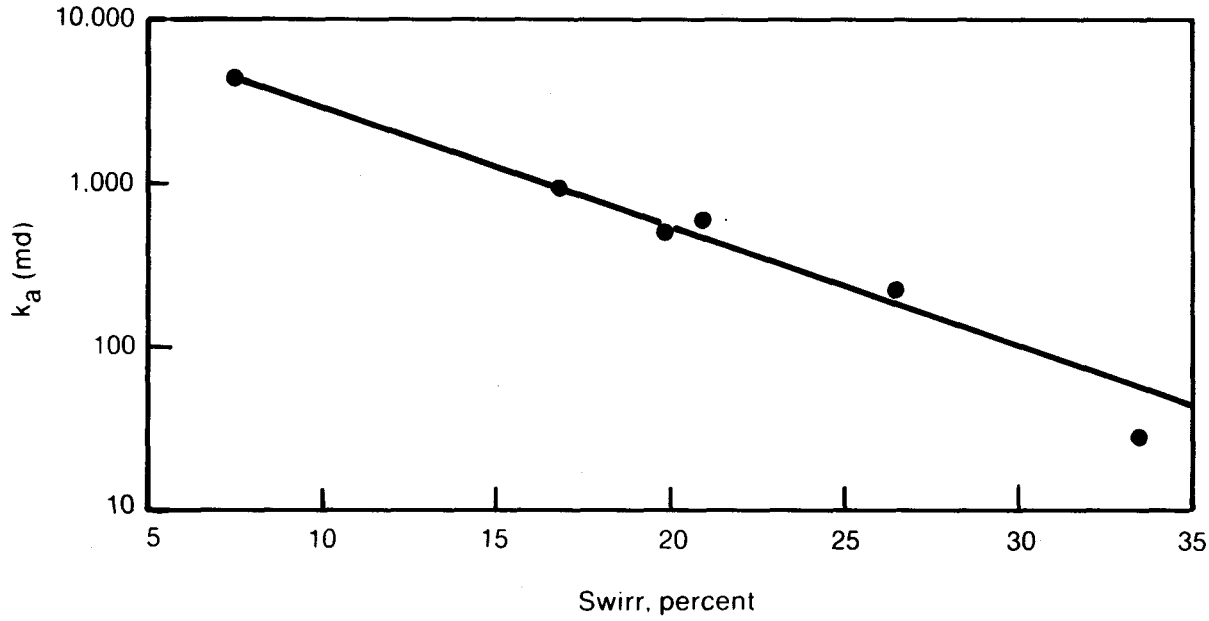


FIGURE 81. - Crossplot of air permeability versus irreducible water saturation. Irreducible water saturation derived from figure 80.

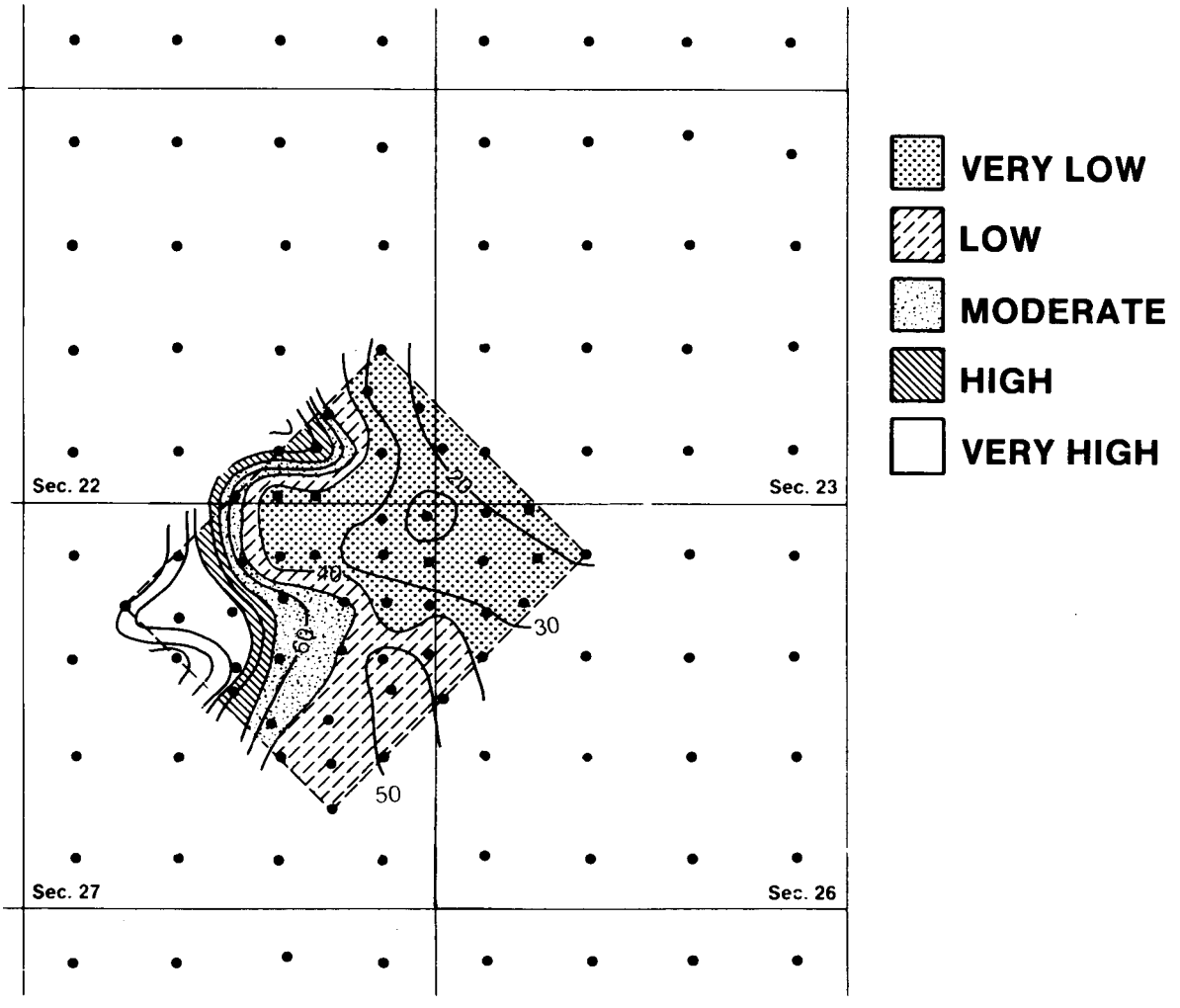


FIGURE 82. - Distribution of the 1980/1967 electrical resistivity ratio within the study area.

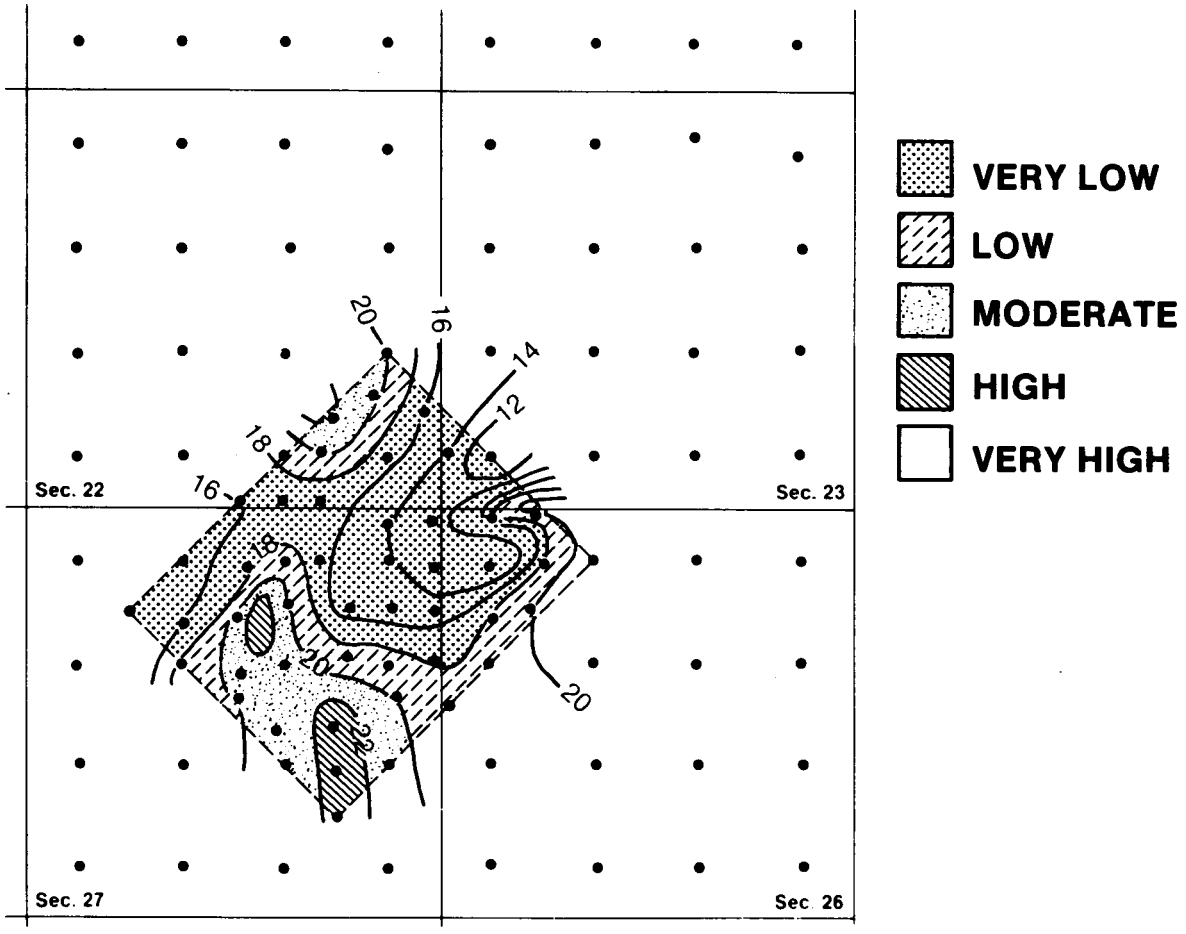


FIGURE 83. - Residual oil saturation distribution in 1980. Data obtained from routine core analysis, in percent.

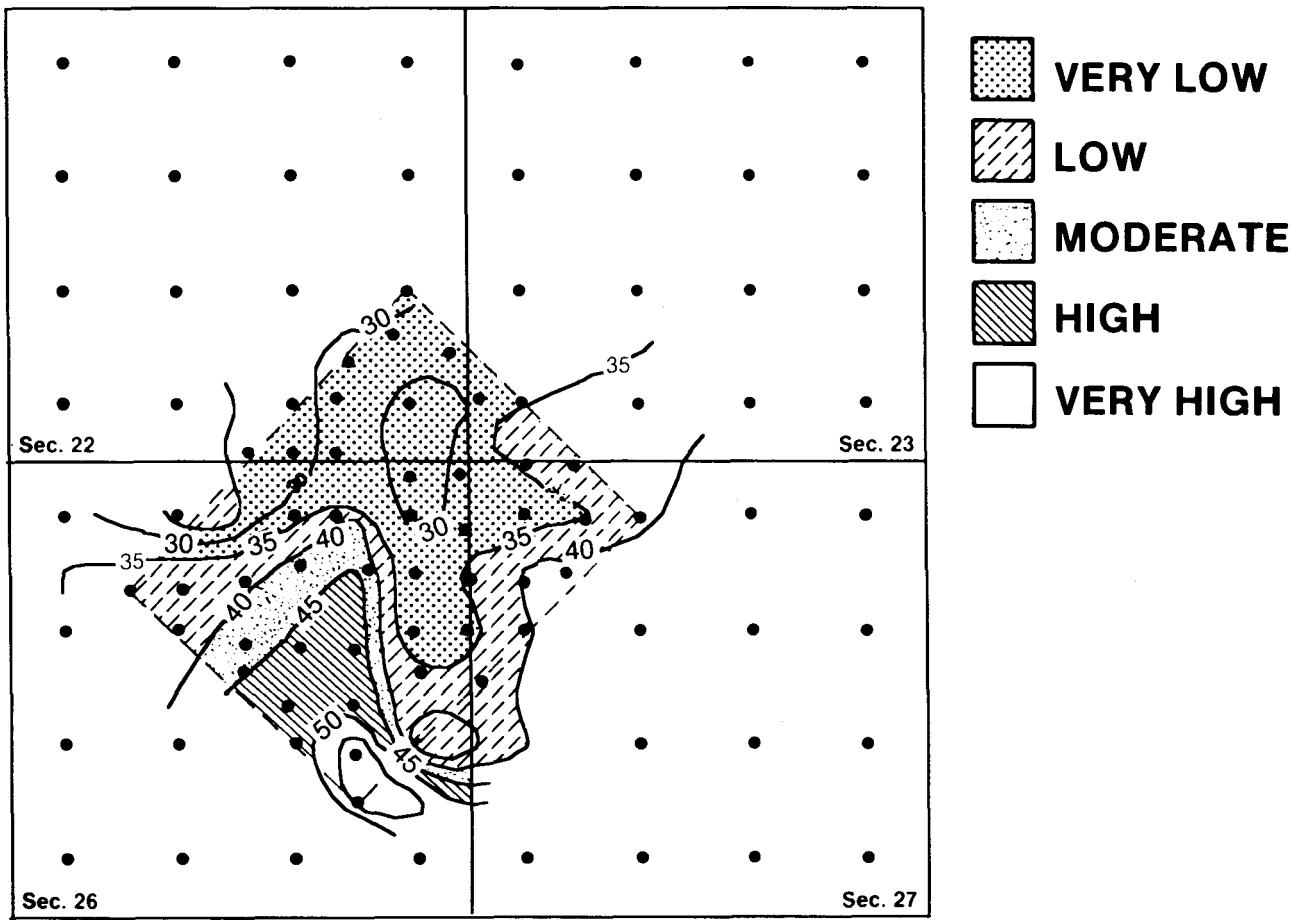


FIGURE 84. - Residual oil saturation distribution in 1980. Data obtained from full-scale areal simulation, in percent.

# CHAPTER 5. APPLICATION OF OUTCROP STUDIES TO QUANTITATIVE RESERVOIR CHARACTERIZATION

## Background

Reservoir simulation requires input of geological data before subdivision of a reservoir into layers and grid blocks and assigning values of critical physical properties to these blocks. Spatial variations of reservoir parameters are quite often ill-defined; therefore, simulator predictions of primary, secondary, and tertiary production are just as often significantly in error. Predictions of primary recovery efficiencies could be substantially improved by using an accurate and detailed geological model to simulate fluid movements on the critical interwell scale. Existing geological depositional models provide a logical starting point for constructing quantitative or engineering models but do not contain the degree of detail necessary to predict the spatial distribution of flow properties on an interwell scale which will enable accurate simulation.

Current geological depositional models are based on geometry, lithology, sedimentary structures, and the sequence of sedimentary structures within a particular depositional environment. Studies of modern environments can be used to determine which processes operate in various environments and which sedimentary structures and lithologies result from these processes.

Because depositional processes are similar, our working hypothesis is that predictable, characteristic properties of critical reservoir parameters exist in reservoirs deposited in similar depositional (geological) environments. Although absolute values of reservoir parameters may not be the same from one deposit to another, general framework, trends, degree of contrasts, and the degree of variability within and between flow units should be comparable.

This hypothesis has been largely substantiated by studies described in this report and other studies which have indicated that (1) lithofacies (depositional units) defined on the basis of lithology and sedimentary structures provide a good approximation of permeability units and layering;[1] (2) permeability classes can be associated with stratification types and other sedimentary structures;[2-5] (3) the length of shales can be related to the environment of deposition;[6] and (4) within a specific channel environment, the area of a shale can be related to the scale of the sedimentary unit with which

it is associated.[7] The correlation of sedimentologic features with petrophysical properties allows the use of geological depositional models to predict the spatial distribution of petrophysical properties.

Depositionally analogous outcrops are an excellent source of quantitative geological information at the level of detail necessary for interwell simulation. Outcrops provide laterally continuous exposures, which enable closely spaced sampling of scales of inches, feet, 10's of feet and 100's of feet, information not readily available from the subsurface. This detailed outcrop information allows definition of the spatial distribution of parameters which are critical to fluid flow on the desired interwell scale.

## Objectives

The objectives for this part of the study were as follows:

(1) to determine the relationship between sedimentologic units and permeability in order to assess the utility of sedimentologic models in predicting the spatial distribution of petrophysical properties, and

(2) to determine similarities and differences between outcrop and reservoir data in order to identify types of outcrop information which can be used to supplement the subsurface data.

## Outcrop Data Collection and Analysis

The data used for this part of the study were primarily from the Upper Cretaceous Muddy formation, a barrier island deposit which produces oil in many fields in the northern Powder River Basin. Data from outcrops in northeastern Wyoming were compared with those from Bell Creek (MT) field, which is located about 40 miles from the outcrops at a depth of 4,500 ft. Results from a preliminary study of the Shannon sandstone, a shelf sand ridge deposit, are included in this report.[2] Information from Shannon outcrops in southwestern Powder River Basin were compared with data from the Shannon in Teapot Dome field, located about 5 miles from the outcrop at a depth of 300 ft (fig. 13).

## Outcrop Selection

The selection of outcrops was based on the following criteria: (1) the location of the outcrops within the barrier island system was similar to that of the Bell Creek pilot area; (2) the lateral extent of accessible outcrop was about 1,300 ft, a lateral distance comparable to 40-acre spacing; (3) the lateral continuity and accessibility allowed vertical profiles to be drilled at approximately 200- to 400-ft intervals and (4) rocks present were representative of the facies of interest.

Candidate outcrop locations were determined from topographic maps and aerial reconnaissance followed by field examination. Nineteen outcrops were examined and described. Facies were identified, and a general paleogeographic reconstruction was made to identify the various parts of the barrier island deposystem. Outcrops 22a, 22, 23, and 386 were selected from among the 19 outcrops as the best candidates for sampling and detailed study (fig. 17). They are located near the central portion of the barrier island deposit, which is similar to the location of the pilot area in Bell Creek field. Outcrops 22a and 22 provide a nearly continuous exposure which extends 2,200 ft and provides data on a 100's-of-feet scale. Outcrops 23 and 386 are located approximately 1/2 mile away and provide data on a 1,000-ft scale.

## Outcrop Sampling

The sampling pattern was designed to allow analyses of lateral variability of reservoir parameters on scales of 1, 10's, 100's and 1,000's of feet over distances comparable to interwell distances on 40-acre spacing. In outcrops 22a and 22, nine vertical profiles were drilled on a 1-ft vertical spacing. The vertical profiles were spaced between 20 and 500 ft apart (fig. 85). Samples were taken horizontally on a 0.5-ft spacing along a few horizons to allow documentation of lateral variability on 1- and 10-ft scales.

One-inch diameter cores 3 to 6 in. long were drilled with a portable, air-cooled drill. Cores were drilled generally parallel to bedding. Detailed geologic descriptions and photographs of the vertical profile in each sampling area were made to document vertical and lateral sedimentologic changes (see appendix C).

Standard techniques for measurements of air permeability and porosity were used. One-inch-long cores were cut from the end of each core sample farthest from the outcrop face to reduce the influence of weathering. These cores were dried overnight at 60°C. Permeability to air was calculated from the average of three flow rates (low, medium, and high) read from two electronic mass flowmeters (0 to 10 and 0 to 200 $cm^3$/min) for Klinkenberg corrections. Pressures were read from manometers--a water-column manometer for low pressures and a mercury-column manometer for high pressures. The apparatus was calibrated with metal calibration plugs, and the calculated error for permeability values was less than ±5%.

Porosity was determined by using Boyle's law porosimeter. To minimize error derived from the noncylindrical shape of some cores, lengths of 2 orthogonal diameters at each end were measured and used in computing the bulk volume of the sample.

## Relationship Between Sedimentologic Units and Permeability

### Permeability Contrasts Among Facies

Facies, which are sedimentologically defined units, were found to provide a good approximation of rock units with similar permeability characteristics, although in some cases different facies could be combined to form one permeability unit.

For permeability data from the Muddy formation facies, Kolmogorov-Smirnoff (K-S) two-sample tests[8] were conducted to determine whether the permeability distributions from one facies were significantly different from those of another facies. The K-S test is a nonparametric test (it does not assume a normal frequency distribution) which calculates the maximum distance between cumulative distribution functions of the two samples. If this distance is large enough, the hypothesis that the distributions are the same is rejected. The K-S test is not very powerful; however, it may indicate which facies can be grouped for permeability layers.

Results of the K-S test suggest at least three distinct permeability groups or distributions in the Muddy formation: one group includes higher energy deposits of the middle shoreface, upper shoreface, foreshore, and washover facies; a second group includes lower energy deposits of lower

shoreface and backshore; and the third group includes the lowest energy lagoon deposit.

Figure 86 presents box-and-whiskers plots of permeabilities from facies in 19 described wells in Unit 'A' of Bell Creek field. In this plot, the box covers the middle 50% of the permeability values, between the lower and upper quartiles. The "whiskers" extend to the extremes (minimum and maximum values), whereas the vertical line within the box is at the median permeability value for that sample. A few values greater than 1.5 times the interquartile range (outliers) are not shown in the diagram.

The vertical arrangement of the facies in figure 86 is typical for progradational cycles in barrier island deposits. The sequence shown in figure 86 is a composite; complete sequences rarely occur in one well. The permeability values reflect the energy of the depositing currents, where middle shoreface, upper shoreface, foreshore, and washover facies are high-energy deposits; lower shoreface and backshore are lower energy deposits; and lagoon facies, the relatively lowest energy deposits.

A generalized, simplistic permeability layer model for progradational barrier island deposits was developed from previously described statistical analysis of permeabilities from Bell Creek (fig. 87). Alluvial valley fill facies and channel deposits are not included here because of the lack of permeability data; however, these facies are an important component of the depositional system and strongly affect the reservoir architecture in the Bell Creek reservoir. This simplistic model is based on data from the progradation units from Muddy sandstone. To obtain a more detailed model, other components such as permeability characteristics of transgressive depositional units, lateral facies changes, diagenetic features, fractures, and faulting must be incorporated.

Another example of sedimentologic units corresponding to permeability units is illustrated by Shannon sandstone permeability data. Except for the high-energy, ridge-margin (HERM) and low-energy, ridge-margin facies (LERM), which overlap and are not statistically different, the central ridge, inter-ridge and bioturbated shelf sandstone facies form distinct permeability groups at the 95% confidence interval (fig. 88). This analysis also illustrates that decreasing permeability corresponds to a decrease in depositional energy going from the top of the sand ridge (central ridge facies) to the base (bioturbated

shelf sand facies) and was found in outcrop samples and those from Hartzog Draw field.

### Permeability Contrasts Among Sedimentary Structures

Stratification types and sedimentary structures can be related to at least two permeability classes in the Shannon sandstone: a higher permeability class associated with cross-bedded sandstone samples and a lower permeability class associated with shaley, rippled, and bioturbated samples (fig. 89). This relationship was found in Shannon sandstone outcrop samples as well as samples from Teapot Dome and Hartzog Draw fields.

Relationships between sedimentary structures and permeability have also been reported for a barrier island deposit,[1] an aeolian (dune) deposit[4-5] and a fluvial deposit.[9]

The grouping of permeabilities according to bedding types indicates a link between sedimentary processes and petrophysical properties. A crossbed is a primary sedimentologic unit which represents one sedimentologic event with essentially constant depositing conditions. The velocity of the currents along with the supply of sediment controls grain size, fabric, sorting, and clay content--all of which are known to affect permeability and porosity. Thus, from a genetic point of view, it follows that similar stratification types within a particular deposit would form a good approximation of permeability groups and, furthermore, that petrophysical properties of bedding-scale features may be the logical units to use for scaling up to larger volumes of the reservoir; e.g. gridblock size. Postdepositional processes such as diagenesis and tectonic features must also be considered, however.

## Comparison of Outcrop and Subsurface Rocks

### Comparison of Sedimentological Features

Outcrop exposures of the Muddy formation documented for this study are sedimentologically similar to the Muddy formation in Unit 'A' of Bell Creek field which is located 40 miles away and produces oil at a depth of 4,500 ft. The similarities include (1) similar barrier and nonbarrier facies characteristics, (2) similar vertical sequence of facies which include

components of both a progradational and a transgressive sequence, (3) similar postbarrier depositional history which consisted of valley incisions into the barrier sands and subsequent deposition of sediments into the valleys.

Facies are distinguished on the basis of grain size, lithology, and sedimentary and biogenic structures. The same criteria used to distinguish facies of the Muddy formation in the subsurface were applicable to the outcrop exposures, suggesting operation of similar depositional processes (table 18). Similar facies characteristics were also found for valley fill facies (table 22).

Frequency distributions of grain sizes calculated by image analysis indicate similar distributions for subsurface upper shoreface facies and outcrop middle shoreface facies (fig. 90). Petrographic analyses of thin sections indicate that the framework mineralogies of barrier island sandstones and valley fill sandstones are similar for outcrop and subsurface samples (fig. 42). These similarities suggest similar depositional conditions for outcrop and reservoir rocks. The similarity in grain size distributions for the subsurface uppershore facies and outcrop middle shoreface facies supports the permeability groupings previously discussed.

Vertical sequences of facies typical for the Muddy formation, both in outcrop exposures and subsurface cores studied, indicate a progradational sequence resulting in deposition of the lower shoreface overlain by middle and upper shoreface, followed by lower and upper foreshore, and often capped by an unconformity overlain by a valley fill or channel fill facies (fig. 21). Aeolian deposits which typically overlay the foreshore and beach facies in modern environments are rarely preserved in examined outcrops and Muddy cores. Transgressive cycles within the Muddy deposition are indicated in outcrop measured section 22 profile 625 and well C-1 where backbarrier lagoon deposits are overlain by lower and upper shoreface facies. (See appendices B and C).

Stacked barrier sequences and single-cycle sequences occur in both the outcrop area studied and in Unit 'A' of Bell Creek, (figs. 19 and 20). Although the outcrop data come primarily from an area of a single-cycle barrier and the subsurface data primarily from a stacked sequence, the thickness of individual facies is similar as are permeability and porosity characteristics.

Valley fill and channel fill deposits were present in both outcrop and subsurface areas studied. This was expected because the formation of valleys in coastal settings is a regional phenomenon.

Few significant sedimentological differences were noted between outcrop exposures and subsurface cores studied. The differences noted were primarily due to diagenetic processes.

## Comparison of Diagenetic Features

Scatter plots of permeability versus visual estimates of total clay (detritial plus diagenetic clay) showed a similar trend of decreasing permeability with increasing total clay content. Large decreases in permeability were associated with small increases of total clay.

Paragenetic sequences for outcrop and subsurface Muddy barrier island facies were found to be similar. Minor differences were found, based on thin section work, such as increased hematite cement and more evidence of late-stage leaching in outcrop samples. Diagenetic differences on a macroscopic scale included laterally extensive calcite cement in the outcrop foreshore facies, which was not found in the subsurface. This cementation was attributed to subaerial exposure of outcrop rocks as the foreshore facies caps the sandstone sequence.

The presence of cement affects the frequency distribution of permeability in both outcrop and subsurface samples. Histograms of permeability from the subsurface foreshore and upper shoreface facies of the Muddy formation indicate two distinct permeability distributions: a relatively sharp-peaked population occurring from 0 to 1,000 md and a broader population from 1,000 to 4,800 md (fig. 91). The samples which comprise the higher permeability are from wells which contain less than 1% clay cement, whereas those samples in the lower permeability population are from wells which contain 1 to 10% clay cement.

Frequency histograms of permeability from the outcrop middle shoreface facies (fig. 92) indicate a permeability distribution similar to that of subsurface samples from the foreshore and upper shoreface facies, in that they contain two permeability populations within ranges similar to subsurface samples (0 to 1,000 md, 1,000 to 4,000 md). Visual examination of outcrop

samples from the lower permeability population indicates that calcite cementation and high amounts of matrix are prevalent, which is similar to that of subsurface lower permeability samples. The presence of two distinct permeability populations within one facies suggests that diagenetic features, when present, mask the primary depositional permeability fabric and underscores the importance of understanding and accounting for the diagenetic processes before predictive permeability models can be developed for Bell Creek field.

## Comparison of Permeability Statistics

A comparison of outcrop and reservoir $k/\phi$ scatter plots indicates a generally close agreement between data from the same facies in outcrop and subsurface, with the subsurface samples exhibiting slightly lower porosities (fig. 59). Table 31 presents the slope and intercept of the regression line calculated for the data.

Permeability distributions from the outcrop middle shoreface and lower shoreface facies are compared with the subsurface foreshore and lower shoreface facies, respectively, in figure 93. Both cumulative frequency distributions (figs. 93a and 93b) and frequency histograms (figs. 93c and 93f) are presented. The Kolmogorov-Smirnoff two-sample test indicated no difference between the two sets of facies.

The comparison of the outcrop middle shoreface to the subsurface foreshore facies is justified in that the subsurface middle shoreface, upper shoreface, and foreshore appear to have similar permeability distributions.

The similarity in permeability statistics in outcrop and subsurface facies encourages the necessary further comparison of additional outcrop and subsurface facies to establish the utility of outcrop petrophysical data to analogous reservoirs.

The distances over which mean permeabilities can be correlated were also compared. Samples were taken from three outcrops spaced about 3,550 ft (0.67 mile) apart in a north-south direction (or parallel to depositional strike). Visual inspection of permeability versus height plots indicates a generally similar pattern which is continuous over 1.3 miles (6,850 ft) (fig. 85). Mean permeability values calculated for all samples within the middle shoreface

facies varied by 25% from outcrop 22 to outcrop 23 and by 3% from outcrop 23 to outcrop 3-86.

In the subsurface, mean permeabilities of the foreshore facies are constant over comparable distances of 2,000 and 1,650 ft. in wells C-8, P2, and W4 (also oriented parallel to depositional strike).

The distances over which mean permeabilities are similar may be used as a guide for appropriate grid block sizes for reservoir simulation, but effects of smaller scale permeability fluctuations on fluid flow remain to be determined. This similarity also indicates the potential for determining the scale of permeability fluctuations from outcrops before infill drilling, which may prevent drilling unnecessary or misplaced wells.

## Summary and Conclusions

**1. Sedimentological units and permeability.** Sedimentologically defined units provide a good approximation of rock units with similar permeability characteristics. This was found in the study of outcrop and reservoir rocks of both the Muddy formation, a barrier-island deposit, and the Shannon sandstone, a shelf sand ridge deposit. In some cases, however, different facies did not have statistically different permeability frequency distributions and could be grouped together in one permeability unit.

**2. Stratification types and permeability.** Stratification types and sedimentary structures are related to permeability classes in both outcrop and subsurface rocks of the Shannon sandstone, a shelf sand ridge deposit. Similar relationships have also been reported for a barrier island deposit, an aeolian (dune) deposit, and a fluvial deposit.

**3. Vertical sequence of facies and permeability profiles.** Comparison of geologically described cores and outcrops indicates that similar vertical sequences of facies of comparable thickness are present in the subsurface and at sampled outcrops in the Muddy formation.

Permeability trends for the vertical sequence are frequently similar for comparable vertical successions of facies in outcrop and subsurface, with permeability decreasing through generally the same sequence of facies and stratification types and decreasing permeability corresponds to decreasing depositional energy. Similar vertical profiles of permeability in comparable

sequences in outcrop and subsurface rocks were also reported for a barrier-island sandstone and a carbonate formation.[10]

**4. Grain size distribution and mineralogy.** Point count and image analysis of thin sections of the Muddy formation indicate that grain size distribution is similar for outcrop middle shoreface and subsurface upper and middle shoreface foreshore facies. Also, barrier island sandstone framework mineralogy is similar for outcrop and subsurface samples. Likewise, the valley fill sandstone framework mineralogy is very similar for outcrop and subsurface samples.

**5. Critical heterogeneities.** Similar critical heterogeneities have been identified in the subsurface and in studied outcrops. Comparable critical depositional heterogeneities in the Muddy formation include the presence and magnitude of erosion-valley filling episodes and changes of facies succession within and between barrier cycles. Critical diagenetic heterogeneities include the type of clay cement, changes in total clay percent, and variations in compaction. Critical structural heterogeneities include the direction, amount of offset, and block size created by faulting.

**6. Paragenetic sequence.** The paragenetic sequence for outcrop and subsurface barrier island facies is essentially the same. Minor differences were found based on thin section work, such as increased hematite cement and more evident late-stage leaching in outcrop samples. However, the sequence and overall effect of diagenetic processes are not significantly different between sampled outcrops and subsurface barrier island sandstones.

**7. Permeability versus total clay content.** Scatter plots of permeability versus total clay content show similar trends for outcrop and subsurface data sets and indicate a drastic decrease in permeability with small increases of total clay.

**8. Permeability/porosity relationships.** Scatter plots of reservoir and outcrop permeability/porosity data indicate parallel trends for the same facies, with the outcrop samples having about 4% greater porosity.

**9. Permeability frequency histograms for similar facies.** Statistical analysis and comparison of permeability populations of outcrop and subsurface facies indicate similar frequency distributions for depositionally analogous facies. Similarities were found for the Muddy formation outcrop middle

shoreface and the subsurface foreshore and the outcrop lower shoreface and the subsurface lower shoreface facies. Similarities in the frequency distributions of outcrop and subsurface permeabilities were also found to occur in the same facies within the Shannon sandstone.

**10. Scale of permeability changes.** Subsurface maps and continuous outcrop data both indicate that the average permeability of facies and the permeability profile of the entire barrier section remain constant over considerable distances along a depositional strike. Changes in average permeability occur on a scale of miles in both outcrop and subsurface rocks.

**11. Differences between outcrop and subsurface rocks.** Differences found between outcrop and subsurface rocks consisted mainly of diagenetic differences due to atmospheric weathering. In the Muddy formation, this consisted of a minor increase of hematite cement and slightly more late-stage leaching in outcrop samples, which resulted in slightly higher porosities. Laterally extensive calcite cement present in the outcrop foreshore facies was not identified in the subsurface.

## REFERENCES


1. Stalkup, F. E. and W. J. Ebanks, Jr. Permeability Variation in a Sandstone Barrier Island-Tidal Channel-Tidal Delta Complex, Ferron Sandstone (Lower Cretaceous), Central Utah. Pres. at the 61st SPE Ann. Tech. Conf. and Exhib., New Orleans, Oct. 5-8, 1986. SPE paper 15532.

2. Jackson, S. R., M. Szpakiewicz, and L. Tomutsa. Relation of Sedimentological Features and Reservoir Quality in a Shelf Ridge Sandstone Deposit - Comparison of Outcrop and Subsurface Properties. Pres. at the AAPG Ann. Conv., Los Angeles, June 1987.

3. Tomutsa, L., S. R. Jackson, M. Szpakiewicz, and I. Palmer. Geostatistical Characterization and Comparison of Outcrop and Subsurface Facies: Shannon Shelf-Sand Ridges. Pres. at the 56th SPE Tech. Conf. and Exhib., Oakland, Apr. 2-4, 1986. SPE paper 15127.

4. Goggins, D. J., M. A. Chandler, G. A. Kocurek, and L. W. Lake. Patterns of Permeability in Eolian Deposits. Pres. at the SPE/DOE Fifth Symp. on Enhanced Oil Recovery, Tulsa, Apr. 20-23, 1986. SPE/DOE paper 14893.

5. Chandler, Mark A. Depositional Controls on Permeability in an Eolian Sandstone Sequence, Page Sandstone, Northern Arizona. Pres. at the AAPG Ann. Conv., Los Angeles, June 1987.

6. Zeito, G. A. Interbedding of Shale Breaks and Reservoir Heterogeneities. J. Pet. Tech., October 1965, pp. 1223-1228.

7. Miall, Andrew D. Reservoir Heterogeneities in Fluvial Sandstones. Lessons from Outcrop Studies. AAPG Bull. v. 72, No. 6, June 1988, pp. 682-697.

8. Davis, John C. Statistics and Data Analysis in Geology, John Wiley and Sons, New York, 1973, p. 276.

9. Jones, J. R. Jr., A. J. Scott, and L. W. Lake. Reservoir Characterizaton for Numerical Simulation of Mesaverde Meanderbelt Sandstone, Northwestern Colorado. Pres. at the 59th SPE Ann. Tech. Conf. and Exhib. Houston, Sept. 16-19, 1984. SPE paper 13052.

10. Hinrich, P. D., F. J. Lucia, and R. L. Mathis. Permeability Distribution and Reservoir Continuity in Permian San Andres Shelf Carbonates, Guadalupe Mountains, New Mexico. Permian Basin Section, Society of Economic Paloentologists and Mineralogists Publication 86-26, 1986.

TABLE 31. - Comparison of slope and intercept of natural logarithm permeability versus porosity plots in outcrop and subsurface facies

| Facies | Outcrop | | Subsurface | |
|---|---|---|---|---|
| | Slope | Intercept | Slope | Intercept |
| Foreshore | 0.299 | -2.97 | 0.18 | -2.2 |
| Upper shoreface | 0.370 | -5.00 | 0.41 | -4.5 |
| Middle shoreface | 0.280 | -2.00 | 0.25 | -0.9 |
| Lower shoreface | 0.320 | -4.20 | 0.22 | 0.4 |

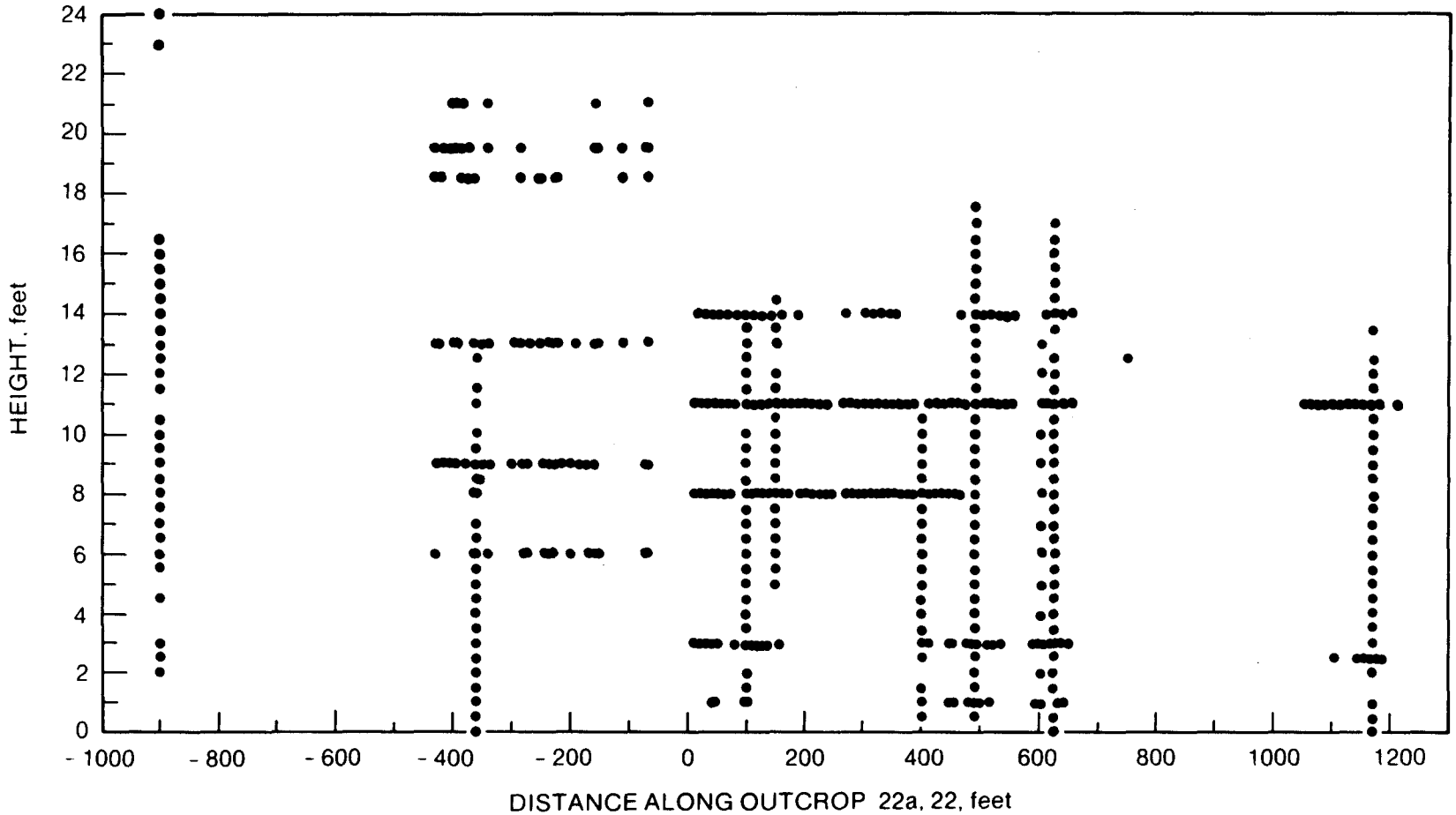


FIGURE 85. - Outcrops 22 and 22a sample locations. See figure 17 for outcrop locations.

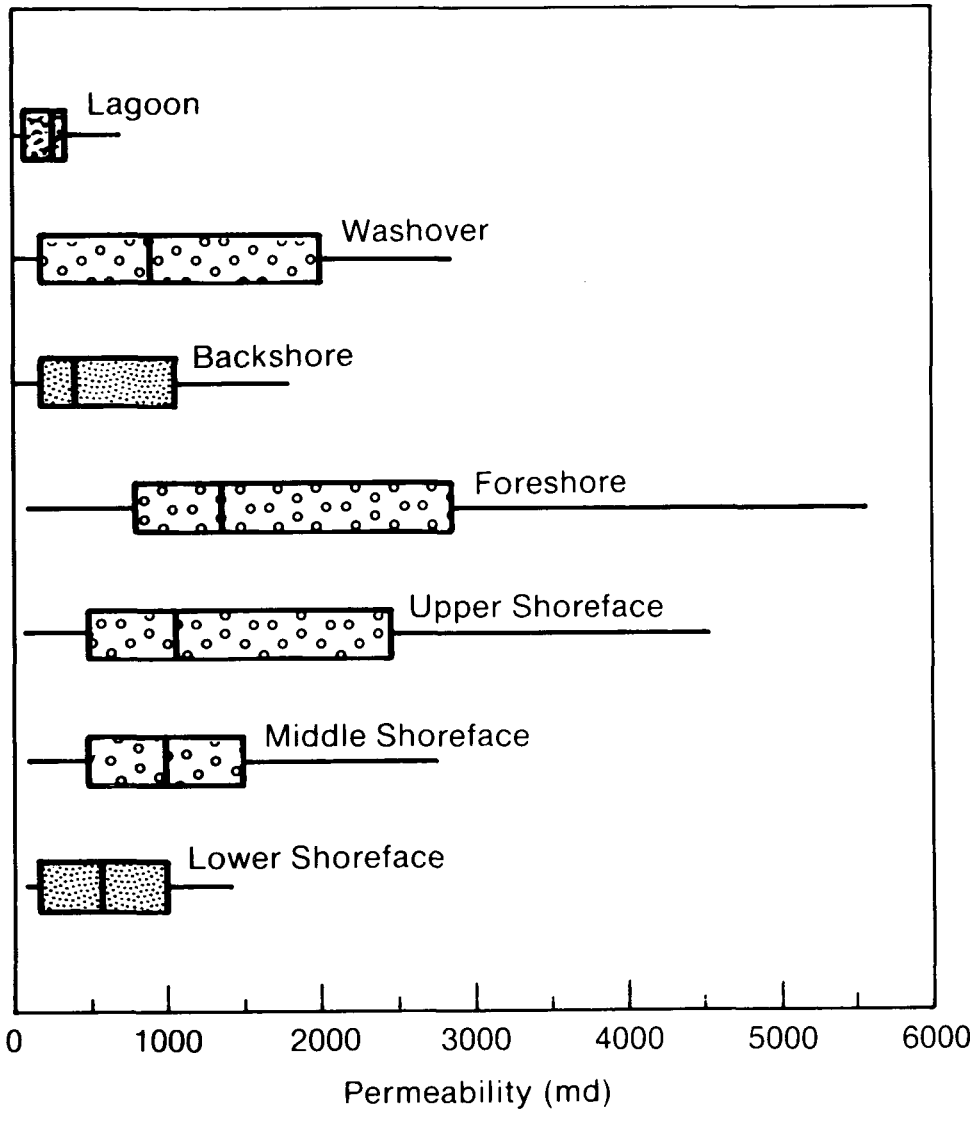


FIGURE 86. - Box-and-whiskers plot of facies permeability values in Unit 'A' of Bell Creek field. The box covers the middle 50% of the permeability values, while the "whiskers" extend to 1.5 times the box (or interquartile range). The few values which are greater than this are considered outliers and are excluded from the diagram.

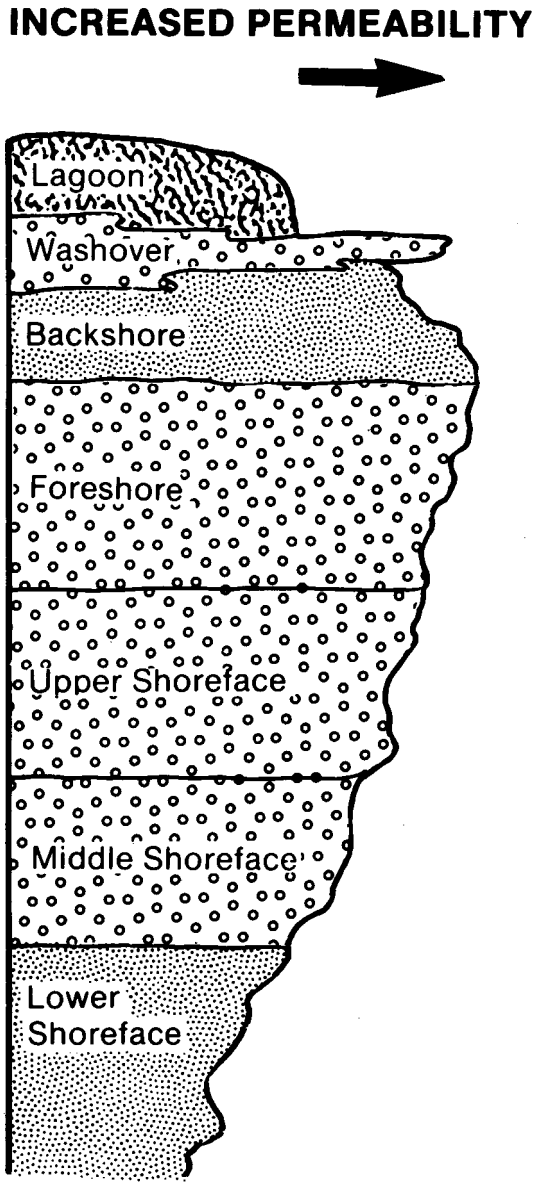


FIGURE 87. - Generalized permeability layer model for a progradational barrier island deposit based on permeability data from Unit 'A' of Bell Creek field.

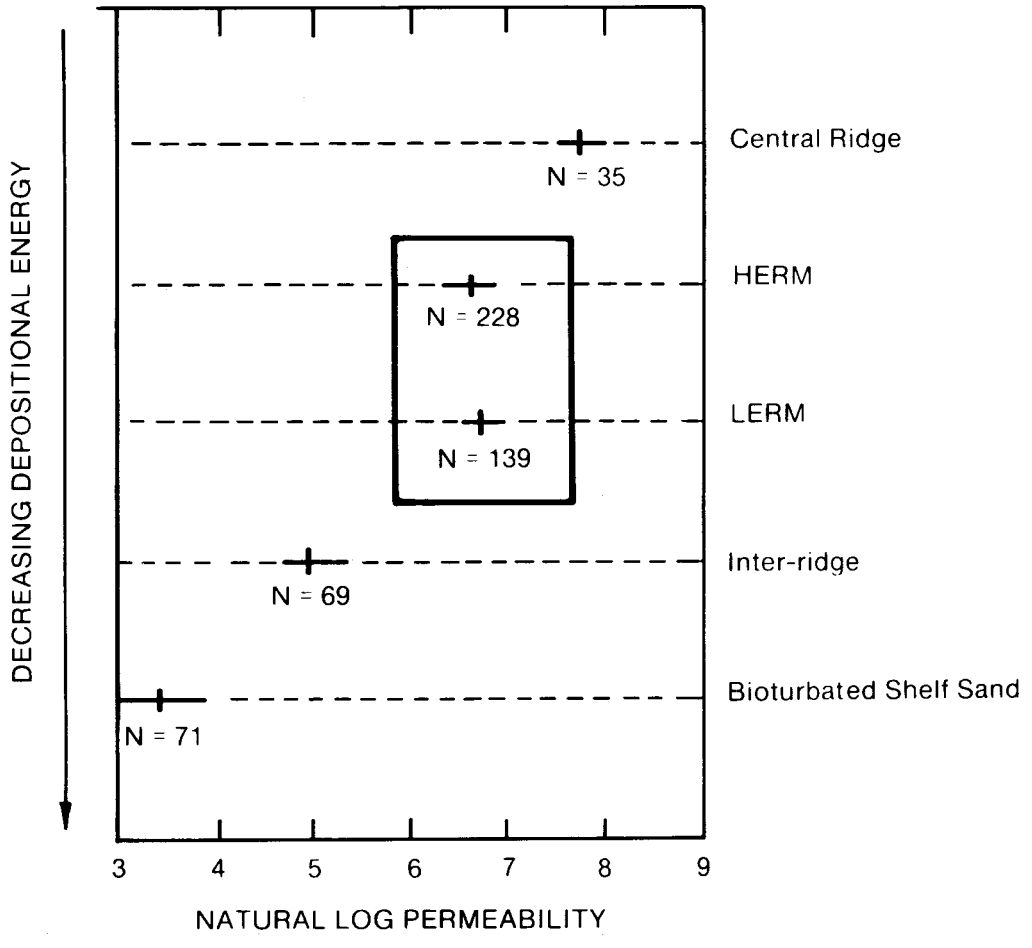


FIGURE 88. - Permeability contrasts among Shannon sandstone outcrop facies. The short vertical bars are mean permeability values, horizontal bars are the 95% confidence interval of the mean (calculated) by dividing the standard deviation by the number of samples. N = numbers of samples.

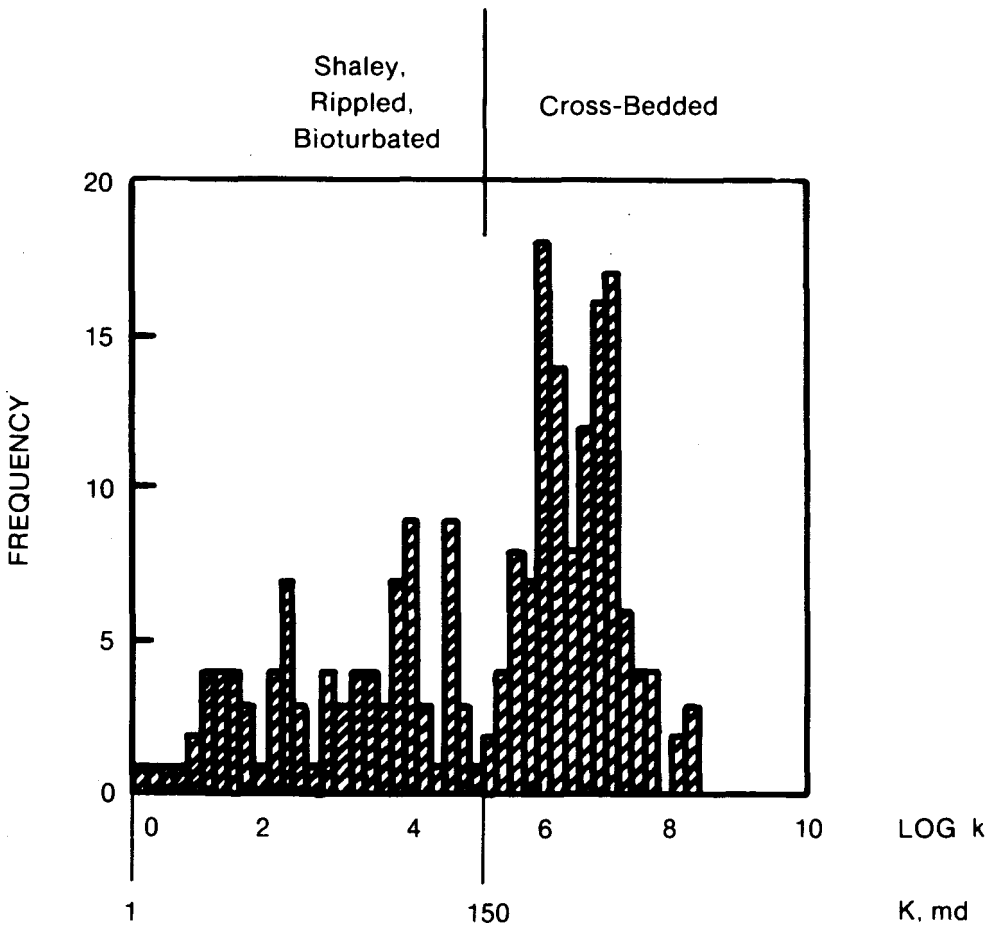


FIGURE 89. - Frequency histogram of natural logarithm of permeability of outcrop samples from the Shannon sandstone high-energy ridge-margin facies. Samples from crossbedded zones are in the higher permeability class (150 to 3,500 md) while those from shaley, rippled, and bioturbated zones are in the lower permeability class (0.1 to 150 md).

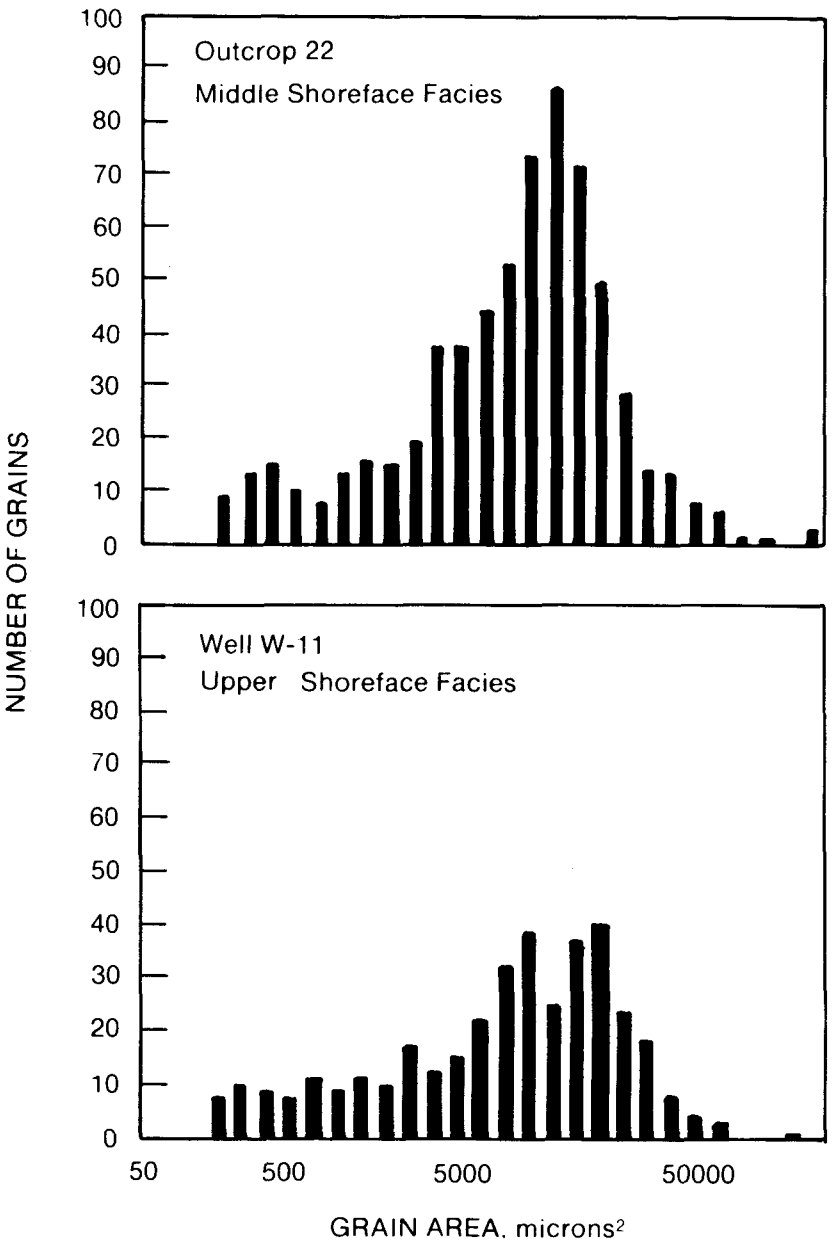


FIGURE 90. - Frequency distributions of grain sizes calculated by image analysis of thin sections. Note that the outcrop middle shoreface facies and subsurface upper shoreface facies have similar distributions.

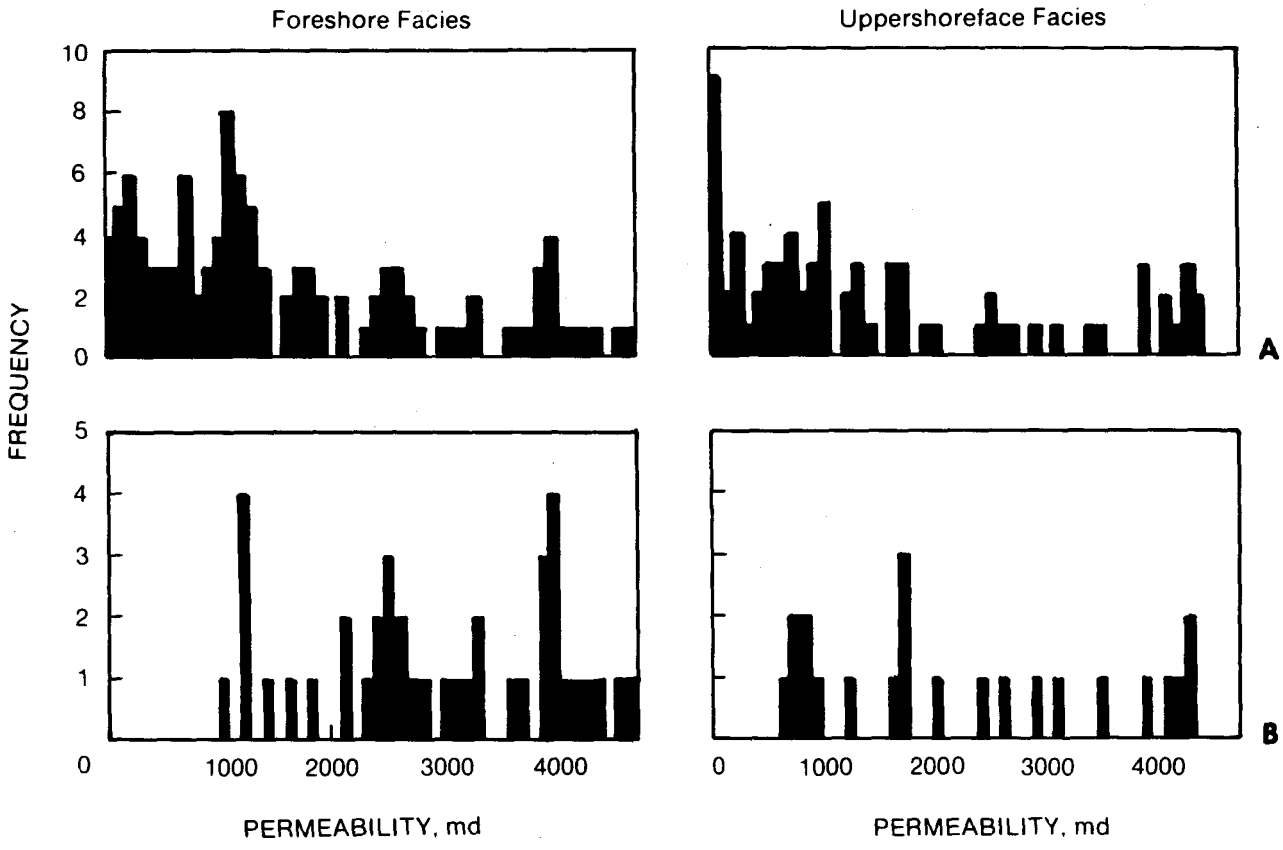


FIGURE 91. - Frequency histograms of permeability in foreshore and upper foreshore facies in (a) all described wells from Bell Creek TIP pilot area and (b) wells which contain less than 1% cement and 3% matrix as determined by petrographic analysis.

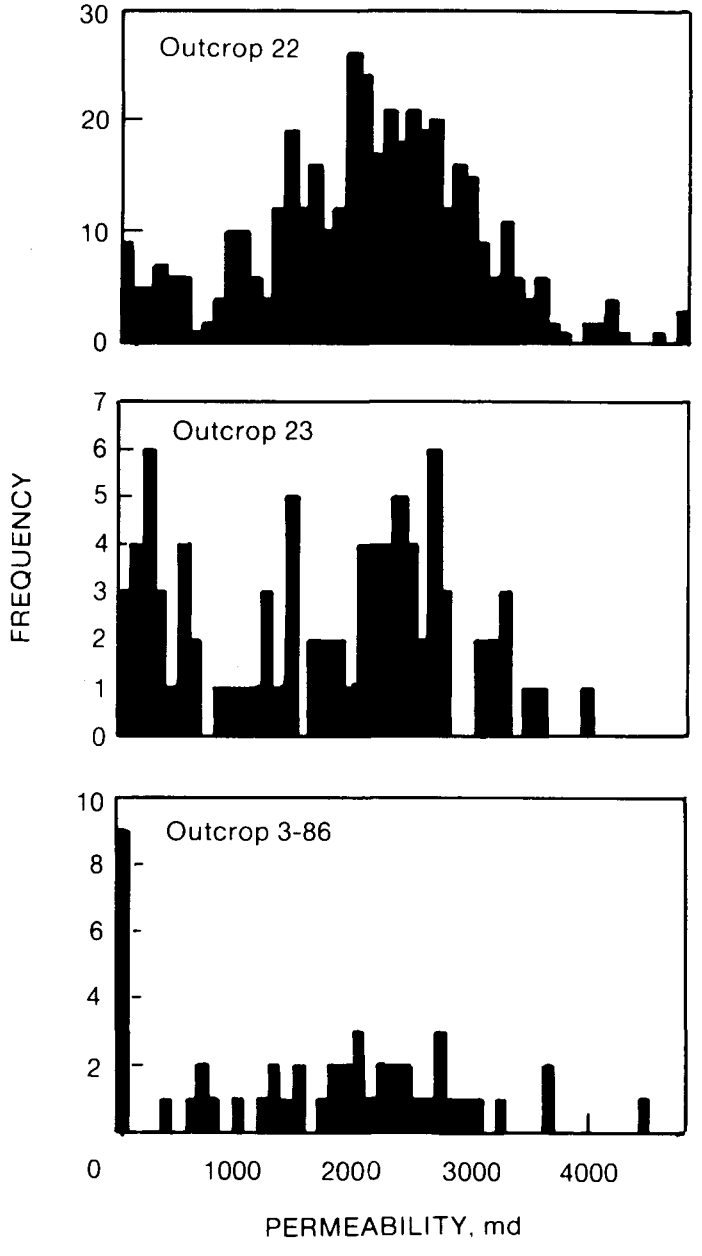


FIGURE 92. - Frequency histograms of permeability from the middle shoreface facies in the three outcrops samples. Distance between outcrops is approximately 0.7 miles.

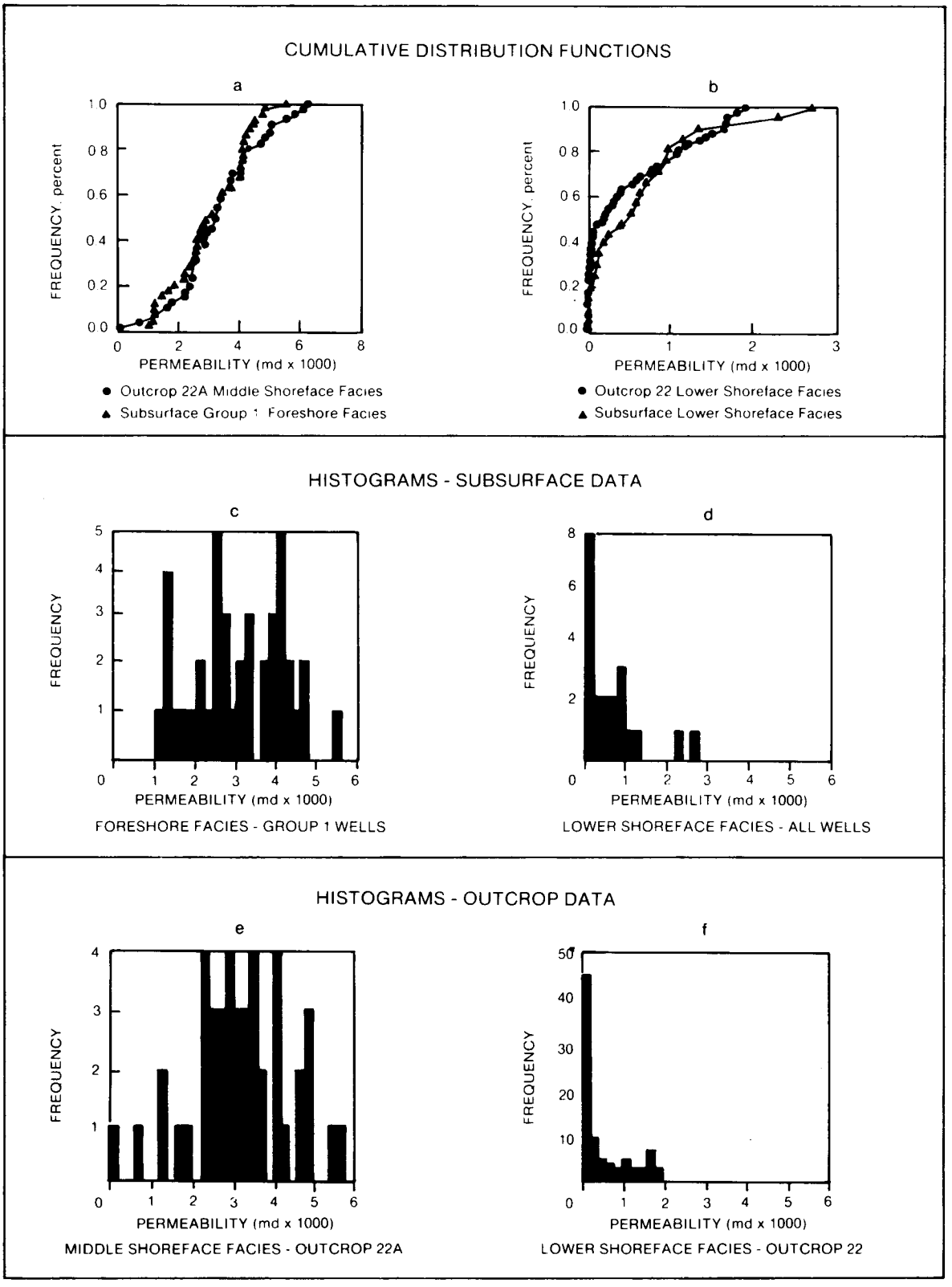


**FIGURE 93. - Comparison of subsurface and outcrop facies permeability frequency distributions, including comparison of cumulative distribution functions (a and b), and frequency histograms (c-f).**

# CHAPTER 6. DEVELOPMENT OF GEOLOGICAL AND ENGINEERING MODEL OF BELL CREEK FIELD

## Primary Production Analysis

### Primary Production Rate Potential--Dykstra Parsons Coefficient Correlation

Primary production potential rate distribution (fig. 94) was based on the daily initial production of the wells in the four-section area enclosing the Tertiary Incentive Project (TIP) area. The initial production rate potential should reflect geological heterogeneities since all wells were completed in similar fashion.

Dykstra-Parsons coefficients calculated from core data provided a general impression of the magnitude of vertical variations in permeabilities. Superimposed Dykstra-Parsons coefficients and the primary production potential rate map (fig. 94) exhibit as good visual correlation. The "homogeneous" sandstone consists of foreshore and middle and upper shoreface facies which characteristically have high porosity and permeability values unless severely affected by diagenesis and consequently a very high primary production rate potential. The coefficients assume higher values both toward lagoonal and toward the basinward side of the buildup as well as in areas where facies variations are common. In these settings, the resulting high degree of permeability variations is due to complex depositional changes. Localized regions of high Dykstra-Parsons values are believed to have been created by diagenetic alterations which resulted in cementation. Higher values of Dykstra-Parsons coefficients correspond with regions of low initial production rate potential. The primary production rate declined exponentially with a decline rate of 0.1/month. A typical production decline curve of a well in Unit 'A' is shown in figure 95.

The general correlation of primary production rate potential with Dykstra-Parsons coefficients indicates layering due to (1) changes in bar facies stacking, (2) intercolation of barrier or nonbarrier facies, and (3) diagenesis which results in higher coefficient values, and almost always corresponds to lower productivity. This means that Dykstra-Parsons coefficients are an indicator of heterogeneity that directly influences the

initial production potential of wells in a barrier bar deposystem. The primary oil production rate in the study area was also restricted to some degree by nongeological factors such as paraffin deposition, sand production, stimulation practices, and completion practices, as well as state regulations; therefore, the primary production rate was kept much lower than the well production rate potential.

### Cumulative Primary Production and Primary Reserve

The primary production mechanism was solution-gas depletion drive. Recovery/efficiency of more than 17% was accomplished in less than 3 years of primary production before reservoir pressure dropped by 1,000 psi. Primary reserves of all producing wells in sections 22, 23, 26, and 27 of Unit 'A' were mapped based on a decline analysis extrapolated to 1 STB/d per well. The primary reserves map (fig. 96a) shows that the highest primary reserves occurred in two, north-south trends near the central part of the area of investigation.[1-2]

The initial production rate potential (fig. 96b) of all wells in the study area was mapped. Production anomalies caused by the presence of reservoir heterogeneities are apparent around wells 22-8, 23-5, 23-14, and 26-3. In addition, the primary reserves map (fig. 96a) generally coincides with the highest permeability regions. Cumulative primary production distribution was also mapped (fig. 96c) and is very similar to the map for primary reserves distribution. Low primary reserves, low initial production potential, and low cumulative primary production are evident because of lower net pay, lower porosity, and lower permeability toward the lagoonal (eastern) part of this barrier island reservoir. Low primary reserves and cumulative production also were noted in the region around wells 26-6 and 26-11.

Wide variations in primary reserves, cumulative production, and initial primary production potential were observed along the western edges of sections 22 and 27 close to deep erosional cuts into the barrier subdividing production Units 'A' and 'B' where reservoir heterogeneities include layering and diagenetic clay (in the S.W. of section 27). The region of highest primary production potential, cumulative production, and reserves corresponds to the areas of highest overall transmissivities, lowest Dykstra-Parsons coefficient, and low clay content. This was also evident from the analysis of pulse tests

performed in this region. Results of drillstem tests from wells 23-1, 23-9, and 27-13 confirm the initial primary rate potential distribution indicated in figure 96b.

The influence of large- and medium-scale geological heterogeneities on cumulative primary performance in the TIP and immediate vicinity was studied and ranked (table 32). Depositional heterogeneities as a result of the stratigraphy and geometry of barrier island and genetically associated facies showed dominant influence on primary cumulative production of wells in the TIP region. Diagenetic effects manifested mainly as clay cementation moderately influenced overall production performance, but faulting was determined to have little effect on primary production in the study area.

## Secondary Production Analysis

Waterflooding was begun in August 1970 and proved to be an efficient recovery mechanism in Bell Creek field. An oil bank was formed, maintained, and moved at an excellent rate (up to 14 ft/d) by using a downdip-located, linedrive injection system. The initial injection rate ranged from 20 to 200 BWPD per foot of sand at surface injection pressures of 1,470 to 0 psig. In 1986, the injection rate ranged from 1 to 100 BWPD per foot of sand at a surface injection pressure of 1,800 to 1,300 psig. Although, linedrive is less efficient than patterned waterflood, in terms of total injectivity, the required investment for a linedrive flood is approximately one-fourth of what it would be for a five-spot pattern.[1-2]

### Cumulative Secondary Production

A cumulative waterflood production distribution map, through September 1986, with water cuts exceeding the 90% level for most parts of the study area, is shown in figure 96d. Initially, injection wells were located in the western part of sections 1, 12, 15, 22, 27, 28, 33, and 34. Additional injectors were later completed toward the eastern part of Unit 'A'. In 1978, a line of injectors that extends northward into section 14 was located in section 23. Waterflooding of Unit 'A' recovered more than 35% of the OOIP, which was twice as much as the cumulative primary oil production. The waterflood performed best in the middle of section 23 and northern half of section 26, as reflected by the secondary cumulative production map

(fig. 96d). The injected water generally pushed the oil into the thin updip part of the barrier which interfingers with backbarrier and lagoonal facies where reservoir properties deteriorated. However, the presence of heterogeneities around wells 26-3, 26-6, 26-10, and 26-11 interrupted the high waterflood recovery trend in the middle of section 26. A north-south trend of low transmissivity between sections 22 and 23, and sections 26 and 27, is indicated on the cumulative waterflood production map. (fig. 96d). This region associated with the neighboring north-south high transmisivity trend caused oil and water diversion southward. As a result, oil was pushed into areas with lower quality reservoir rocks. Wells near 27-15 and 27-16 produced more oil than their reserve figures would predict and may have caused more oil to be trapped and become inaccessible for recovery. Linedrive waterflood recovery might have been improved if additional injectors had been carefully placed so as to prevent oil movement into depositionally and diagenetically inferior regions. Similar oil trapping took place near the eastern termination of the barrier island facies in the back barrier/lagoonal facies. The presence of an anomaly in the primary production rate potential around wells 22-8, 23-5, and 23-6 (fig. 97b) is also reflected in decreased secondary recovery in this region.

## Secondary Waterfront Movement Analysis

Water-cut information for Unit 'A' of Bell Creek field was analyzed and mapped. The advance of the 20 and 70% water-cut production front from the initiation of linedrive water injection in the western part of the field through January 1981 is illustrated in figures 97 and 98.

The waterfront movement in the four-section area which contains the TIP ranges from 0 to 14 ft/d in a NW-SE direction.

A comparison of 20 and 70% water-cut movement maps (figs. 97 and 98) shows that the presence of low horizontal permeabilities in the western part of the north-east and south-east quadrants of section 22 (fig. 58) have retarded water movement. A west-east trending, high-permeability channel starts at well 22-8 and continues toward well 23-5 (fig. 97). This region has low productivity, as is shown in the initial potential map (fig 96b). In the southern part of section 22, the reduction of permeability from west to east has retarded normal fluid movements (fig. 97). Also, the presence of faults

(fig. 99) around wells 22-13 and 22-14 (fig. 2) has influenced the high horizontal permeability region adversely.

The presence of faults between wells W-16 and P-16 (fig. 99) has also retarded fluid movement drastically. The presence of faults between wells 27-14 and 27-15 has retarded the rate of water-cut advancement, as indicated on the 70% water-cut map (fig. 98).

In section 23, the front movements were rapid. A significant amount of water moved southward from the southwest part of section 14 (fig. 97) because of the presence of high $k_h$ in this region. In the area around well 23-10, the front veered once again to the east because of a region with uniform permeability, as reflected in the high initial production map (70% map, fig. 98). The waterfront movement is retarded in the vicinity of well 23-5 due to heterogeneous layering/channeling and low productivity near this well.

The deterioration of permeability because of the presence of clay-filled zones (see figs. 52, 54) clearly retarded fluid movement in the north-west quarter of section 26 (fig. 100). Fluid movement was generally from northwest to southeast. Movement of fluids slowed as it approached the eastern portion of the field due to the deterioration of reservoir properties.

Secondary production performance was highly influenced by the structural dip of the reservoir. Wells located updip of the water injection linedrive pattern showed increasingly higher cumulative production eastward.

The presence of a north-south oriented diagenetic semibarrier located near the western boundary of section 26 prevented fluid flow in an eastward direction and diverted fluid flow (figs. 96, 97, 98).

The preceding results have been confirmed by full-scale areal simulations of the reservoir for the 1967-1980 period. The advance of the 70% water-cut production from the simulation matched well with the waterfront movement obtained from field data.

Diagenesis strongly detoriated petrophysical properties of otherwise favorable development of barrier island facies in the southwestern corner of the TIP area. This effect was magnified by the downdip position of wells in this region resulting in lower-than-expected cumulative secondary production. A similar diagenetic effect combined with significant removal of barrier facies by a valley incision occurred southeast of the TIP area.

However, the productivity of this area was greatly enhanced by the updip position of the reservoir in this region.

The presence of high-permeability regions in the western parts of sections 23 and 26 (in the range of several darcies) resulted in extremely rapid front advancement (as much as 14 ft/d) which may have adversely affected the volumetric and displacement efficiencies. The influence of the rate of front advancement on oil trapping is an area for future investigation. It may be concluded that even though the magnitude of cumulative secondary production was strongly influenced by the position of the producing wells with respect to water injectors, the structural position and diagenetic imprint had decisive effect on secondary production performance. The overall influence of the depositional factor was moderate during waterflooding (table 33).

Areal simulations of primary and secondary production of sections 14 through 35 were performed. The predicted waterfront movement agreed well with the field data. The simulation confirmed the presence of geological heterogeneities in the form of low-permeability, high clay areas, faults, and high-permeability joint-related channels (fig. 102).

## Pressure Transient Testing Analysis

Several pressure-pulse tests and falloff tests were conducted in the TIP area before the initiation of micellar-polymer flooding. The pulse test results showed the variation of flow capacity ($k_w h$) in various directions. Based on pressure transient information superimposed on the fault map (fig. 99), flow capacity was reduced between wells C-4 and P-12 and between C-4 and P-11. The reduced flow capacity was probably caused by the presence of small faults. The limited transmissivities indicate that the faults did not completely sever fluid communication between the wells mentioned above.

The transmissivity between wells C-10 and P-13, P-14, P-19, and P-20 was also limited by the presence of faults as well as sedimentary stratifications and diagenetic alterations. In addition, a fault was responsible for reduced transmissivity between wells C-3 and P-3 (fig. 99). Indications are that the flow capacity was reduced at the flow boundary between sections 22 and 23 and between sections 27 and 26. The best flow capacity in the TIP area was measured around wells C-8.

Petrographic analysis of cores from well C-6 indicated the presence of diagenetic clays and poor sorting which were both absent in well C-8. Diagenetic clay and poor sorting reduced reservoir quality in the immediate vicinity of well C-6. This detoriation did not affect the waterflow capacity in the drainage area of the well. However, the low-quality reservoir rock around well C-6 created a very high skin factor.[3]

## Tertiary Production Analysis

Based on production data, it was expected that total primary and secondary recovery would produce 55% of the original oil-in-place (OOIP) in Unit 'A', leaving 55 million bbl of oil as a tertiary target. The first 160-acre, micellar-polymer pilot project was implemented in the northern portion of Unit 'A' using Union Oil Company's Uniflood™. This project had recovered 28 to 34% of the oil-in-place (OIP) at the beginning of the tertiary preflush in February 1979. The second micellar-polymer flood, installed under the DOE Tertiary Incentive Program (TIP), encompassed 179 acres and was initiated in February 1981 in Unit 'A', 3.6 miles to the south of the first pilot. The Uniflood™ process was again used in nine injector-centered, 20-acre, five-spot patterns. The entire area was surrounded by 16 water-confinement wells to prevent the escape of injected chemicals and mobilized crude oil. Four five-spot, 20-acre patterns were created in the southwestern part of the TIP area to study the performance of patterned waterflooding.[3-4]

Table 34 summarizes the combination of deposition factors (quality of facies and their stacking), diagenetic alterations (amount and type of clays and cementing materials), and structural factors (faulting) in the TIP area. These factors influenced the patterned waterflood and chemical recovery performance of producing wells by altering the transmissivity and continuity of the formation to various degrees. These factors were also responsible for fluid flow performance and residual oil saturation distribution during the waterflood recovery before the initation of the micellar-polymer project in the TIP region.

Pattern waterflooding resulting from infill drilling and reduction of well spacing from 40 to 20 acres showed that it was possible to recover a large portion of the residual oil in the TIP area (where it was totally watered out) by overcoming some of the intermediate-scale geological heterogeneities

between wells and by mobilizing some of the trapped oil. Pattern waterflooding was more effective in areas of high residual oil saturation (figs. 84 and 96e).

The micellar-polymer flood appeared to be most effective in areas where reservoir quality was superior and geological heterogeneities were absent (wells P-6, P-10, and P-11) or where the presence of the heterogeneities favored EOR. For example, a more favorable structure for oil accumulation resulted from the uplift of well P-15 area by faulting.

A comparison of the TIP oil recovery map (fig. 96e) with the resistivity ratio map (fig. 82) and the 1980 residual oil saturation distribution map (fig. 83) indicates that the regions that had better sweep efficiency due to their superior reservoir quality performed better during the tertiary recovery process.

The presence of interwell geological heterogeneities that do not conform to the regular grid of injection and production wells locally drastically reduced well performance.

## Summary of Geological and Engineering Integration

It may be concluded (table 35) that in the barrier island and genetically associated environment type of reservoirs where the mobility ratio is favorable, the role of depositional heterogeneities is very important in terms of production and injection performance. In addition, site-specific diagenetic effects may moderately or highly deteriorate reservoir properties and may locally influence production performance drastically. The geologic structure of the reservoir (site-specific) plays a different role, depending on the stage of production. Faulting could disrupt the continuity of flow units and adversely affect fluid movement (sweep and displacement efficiencies). However in uplifted tectonic blocks, higher oil accumulation result in better production performance. Structural dip of this type of reservoir would be important for improving production performance in areas where the oil bank would be moved by linedrive flooding updip against a stratigraphic pinchout of the barrier island sandstone.

## RESULTS AND CONCLUSIONS

1. A detailed geological-engineering model of the barrier island complex of Unit 'A' of Bell Creek field was constructed based on core, log, petrophysical, and petrographical analyses; well tests results; production/injection performance; and simulations. Rigorous identification of facies and sedimentary contacts (unconformities) was a fundamental prerequisite for calibration of logs in uncored areas and was also required for spatial interpretation of stratigraphy, geometry, and continuity of dominant flow units in interwell areas.

2. Formation heterogeneities influencing production were identified and ranked with regard to primary, secondary, and tertiary production:

a. Primary production was dominantly influenced by large-scale depositional heterogeneities and moderately by medium-scale diagenetic heterogeneities, whereas the influence of structural heterogeneities (regional dipping and faulting) was low or negligible.

b. Secondary production was dominantly influenced by large-scale structural factors (structural dip but not faulting), moderately or dominantly influenced by medium-scale diagenetic heterogeneities, and moderately influenced by large- to medium-scale depositional heterogeneities.

c. Tertiary production was dominantly influenced by large-, medium-, and small-scale depositional heterogeneities; highly or locally very highly by medium- to small-scale diagenetic heterogeneities; and moderately to locally highly by medium- to small-scale tectonics (faulting).

3. Good correlation of initial primary production rate potential with Dykstra-Parsons coefficients indicated that permeability stratification due to depositional and diagenetic factors adversely influenced primary production performance.

4. Water injection front tracking proved to be a useful tool in identification of preferential water paths dictated by large- to medium-scale geological heterogeneities.

5. Depositional and diagenetic heterogeneities were responsible for diversion of the general movement of the oil bank up the structure. Overall influences of these heterogeneities combined with the injection pattern resulted in movement of large volumes of oil into lower quality parts of the reservoir.

6. Monitoring of changes in electrical resistivity provides a good indication of volumetric sweep and displacement efficiencies during the depletion of reservoirs.

7. Reservoir simulation combined with core analysis data and electrical resistivity measurements proved to be valuable complementary tools for mapping the ROS prior to EOR implementation.

8. Pressure-pulse and falloff tests were indicative of reservoir quality and continuity (flow capacity) in the interwell scale. These tests proved to be viable elements which improved the construction of the geological/ engineering model of the barrier island reservoir. Pulse and falloff test results are particularily valuable in confirming the presence of various geological heterogeneities in interwell regions where core data are not available.

9. The best tertiary performance in the TIP area took place in areas of favorable development of barrier island sandstones, negligible diagenetic imprint, favorable depositional and structural continuity, and unrestricted and balanced sweeping by the surrounding chemical injectors.

10. Improved reservoir evaluation is obtainable through multi-disciplinary intergration of conventional reservoir data if updated knowledge of heterogeneities is provided and thorough analysis is performed.

## REFERENCES

1. Burt, R. A., F. A. Haddenhorst, and J. D. Harthoad. Review of Bell Creek Waterflood Performance -- Powder River, Montana. Pres. at SPE Ann. Fall Meeting, Dallas, Sept. 28-Oct. 1, 1975. SPE paper 5070.

2. Hartshorne, J. M. and J. S. Nikonchik. Micellar-Polymer Flood Success in Bell Creek Field. Pres. at SPE Ann. Tech. Conf. and Exhibition, Houston, Sept. 6-9, 1984. SPE paper 13122.

3. Gary-Williams Oil Producers, Inc. Bell Creek Unit 'A' Tertiary Incentive Project Update. Gary Operating Co., Denver, 1985.

4. Goldburg, A. and C. Morgenthaler. Enhanced Oil Recovery Incentives (and disincentives) From A Producers Standpoint. Pres. at 2nd SPE/DOE Symp. on Enhanced Oil Recovery, Tulsa, Apr. 5-8, 1981. SPE/DOE paper 9827.

**TABLE 32. - Influence of geological heterogeneities on primary production in TIP area**

| Location | Depositional (facies & stacking) | Diagenetic (clay cement) | Structural (faulting) | Average primary production |
|---|---|---|---|---|
| Central part of TIP | VF | N | N | High |
| SW portion of TIP | F | VU | VU | Moderate |
| SE of TIP | U | VU | N | Low |
| Over all influence | Very High | Moderate | Low | |

VF = very favorable; F = favorable; N = negligible;
U = unfavorable; VU = very unfavorable

TABLE 33. Influence of geological heterogeneities on secondary production in TIP area

| Location | Depositional (facies & stacking) | Diagenetic (clay cement) | Structural (faults) | Structural (dip) | Average secondary production |
|---|---|---|---|---|---|
| Western Edge | F | VU | N | VU | Very Low |
| Western Part North | F | VU | F | U | Low |
| South | F | VU | N | U | Low |
| Central Part North | F | N-U[1] | N | M | Low |
| South | VF-F | N-U[1] | N | M | High-Medium |
| Eastern Part | F | N-U[1] | N | F | Very High |
| Eastern Edge | F | VU | N | VF | High |
| Overall Influence | Moderate | Moderate to Very High | Low | Very High | |

[1]Diagenetic semibarrier diverted oil to southern part of TIP.

## TABLE 34. - Influence of geological heterogeneities and engineering factors in the drainage area of wells on TIP production

| Production Well Number | Depositional (facies and stacking) | Diagenetic (clay cement) | Structural (Fault) | Produced sulfunate volume | Number of waterflood/chemical injectors surrounding | Tertiary Cum. oil production |
|---|---|---|---|---|---|---|
| P-1 | F[1] | N | U[2] | Moderate | 3/1 | High |
| P-2 | VF[1] | U[2] | U[2] | High | 2/2 | Moderate |
| P-3 | F[1] | U[1,2] | N | Low | 2/2 | Low |
| P-4 | U[1] | U[1] | U[2] | Low | 3/1 | Low |
| P-5 | U[1] | U[1] | U[2] | Low | 2/2 | Low |
| P-6 | VF[1] | N/U[1,2] | N | High | 0/4 | Highest |
| P-7 | F[1] | U[1,2] | N | High | 0/4 | Moderate |
| P-8 | F[1] | U[1,2] | U[2] | High | 2/2 | High |
| P-9 | U[1] | U[1,2] | U[2] | High | 2/2 | Moderate |
| P-10 | F[1] | U[1,2] | F | Very High | 0/4 | High |
| P-11 | F[1] | U[1,2] | F | High | 0/4 | High |
| P-12 | F[1] | U[1] | U[2] | Moderate | 2/2 | Moderate |
| P-13 | U[1,2] | U[1,2] | U[2] | Moderate | 3/1 | Low |
| P-14 | U[1,2] | N | U[2] | Low | 2/2 | Moderate |
| P-15 | F[1,2] | U[1] | F | Moderate | 2/2 | High |
| P-16 | U[1,2] | U[1,2] | U[2] | Low | 3/1 | Moderate |
| P-17 | U[1,2] | U[1,2] | U[2] | None | 4/0 | Moderate |
| P-18 | F[1,2] | VU[1,2] | U[2] | None | 4/0 | Low |
| P-19 | F[1,2] | VU[1,2] | U[2] | None | 4/0 | Low |
| P-20 | F[1,2] | VU[1,2] | U[2] | None | 4/0 | Low |
| Overall Influence | Very high | High, Locally Very High | Moderate, Locally High | | | |

[1] Influencing kxh.
[2] Influencing continuity.
For abbreviations see table 32.

TABLE 35. - Summary of reservoir heterogeneities in cores and fluid samples from Unit 'A' of Bell Creek field. Muddy formation (barrier island and valley fill)

| | SCALE[1] |
|---|---|
| **A. DEPOSITIONAL HETEROGENEITIES** | |
| (1) Laterally changing facies patterns: | L/M |
| - within one complete barrier sedimentary cycle | L |
| - between stacked incomplete sedimentary barrier-cycles | M |
| (2) Variation in petrophysical (log) properties and net pay caused by: | M |
| - distribution of sedimentary structures (bedding types, bioturbation, clay laminations) | M/S |
| - variation of grain size and sorting | L/M |
| - variation of detrital clay content and type | L/M |
| - variation of sandstone mineralogy | M |
| - position of sand-shale boundaries | L |
| (3) Modification of reservoir geometry and net pay by erosion of barrier island deposits: | L |
| - variation in depths of cuts | M |
| - variation widths of cuts | L/M |
| - variation in petrophysical properties of infills (sandstones, siltstones and shales) | M |
| **B. DIAGENETIC HETEROGENEITIES** | |
| (4) Distribution of diagenetic clays: | M |
| - kaolinite "cement" dominant | M/S |
| - coatings on framework grains and blocking pore throats | M |
| - amplified by compaction | S |
| - control of $\phi$ and k in barrier sandstone | L/M |
| (5) Undercompacted zones: | S/M |
| - process poorly understood; diagenetic origin explains 1-2 foot thick intervals with as much as 11,000 md permeability; lateral extent not yet documented | U |
| - can reverse expected $\phi$ and k trends | S |
| (6) Non-clay cementation | S/M |
| - thin calcite-cemented zones provide local and interwell blockage of fluid flow | S/M |
| - dolomite, quartz overgrowths create local hindrances to fluid flow | S |
| **C. STRUCTURAL (TECTONIC) HETEROGENEITIES** | |
| (7) Influence of faulting offset along faults causes decrease or cessation of fluid flow between wells | U/M |
| - different vertical displacement and filting of tectonic blocks | M |
| - decrease in offset of faults over a short distance | M/S |
| - fault-related fracturing of Muddy reservoir | U |
| **D. FLUID HETEROGENEITIES** | |
| (8) Lateral changes in oil gravity | L |
| (9) Variable wettability | U |
| (10) Variable characteristics of formation fluids | L |
| (11) Variable reservoir pressure | L |
| (12) Position of water/oil and oil/gas contacts | L/M |

[1] L - Large scale-affect large areas of field or productive unit (in miles).
M - Medium scale-affect predominately the interwell areas among a group of wells (hundreds of thousands of feet).
S - Small scale affecting local fluid flow pattern in interwell area (in feet or tens of feet).
U - Unknown scale, to date.

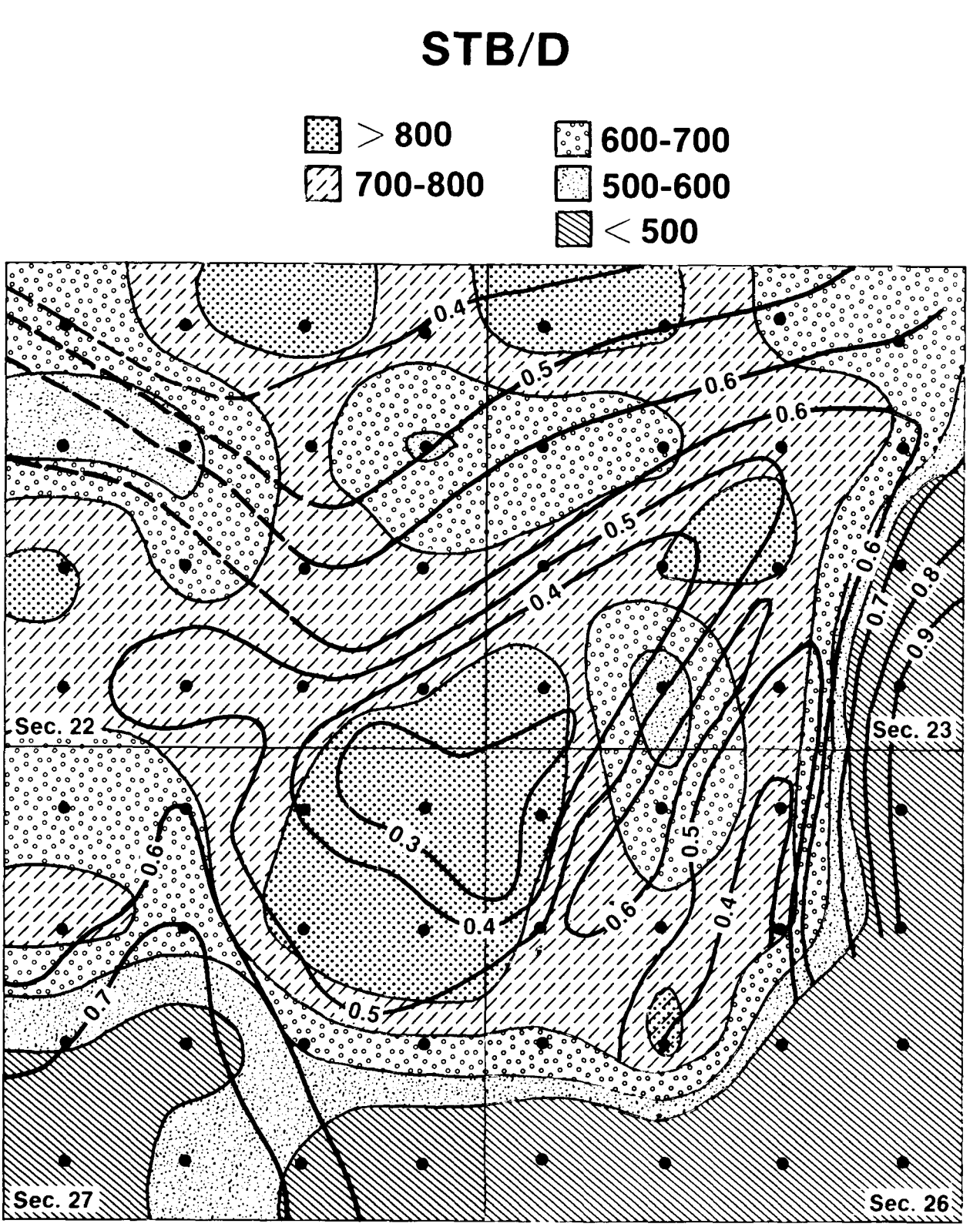


FIGURE 94. - Initial production rate potential (shaded, in STB/d) superimposed on Dykstra-Parsons coefficient distribution.

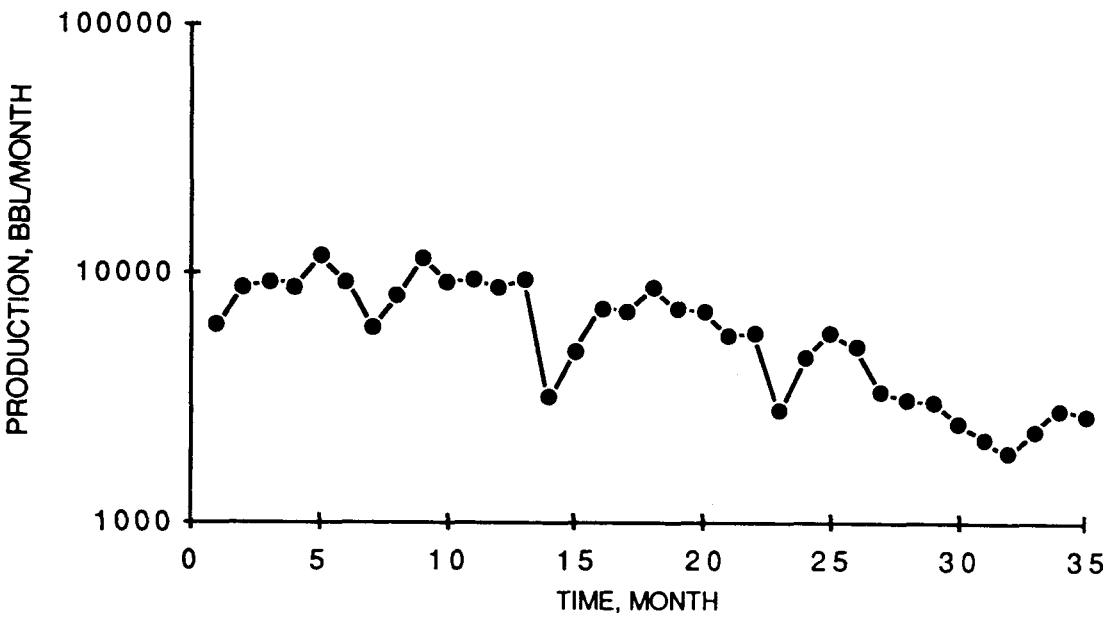


FIGURE 95. - A typical production decline curve in Unit 'A', Bell Creek field.

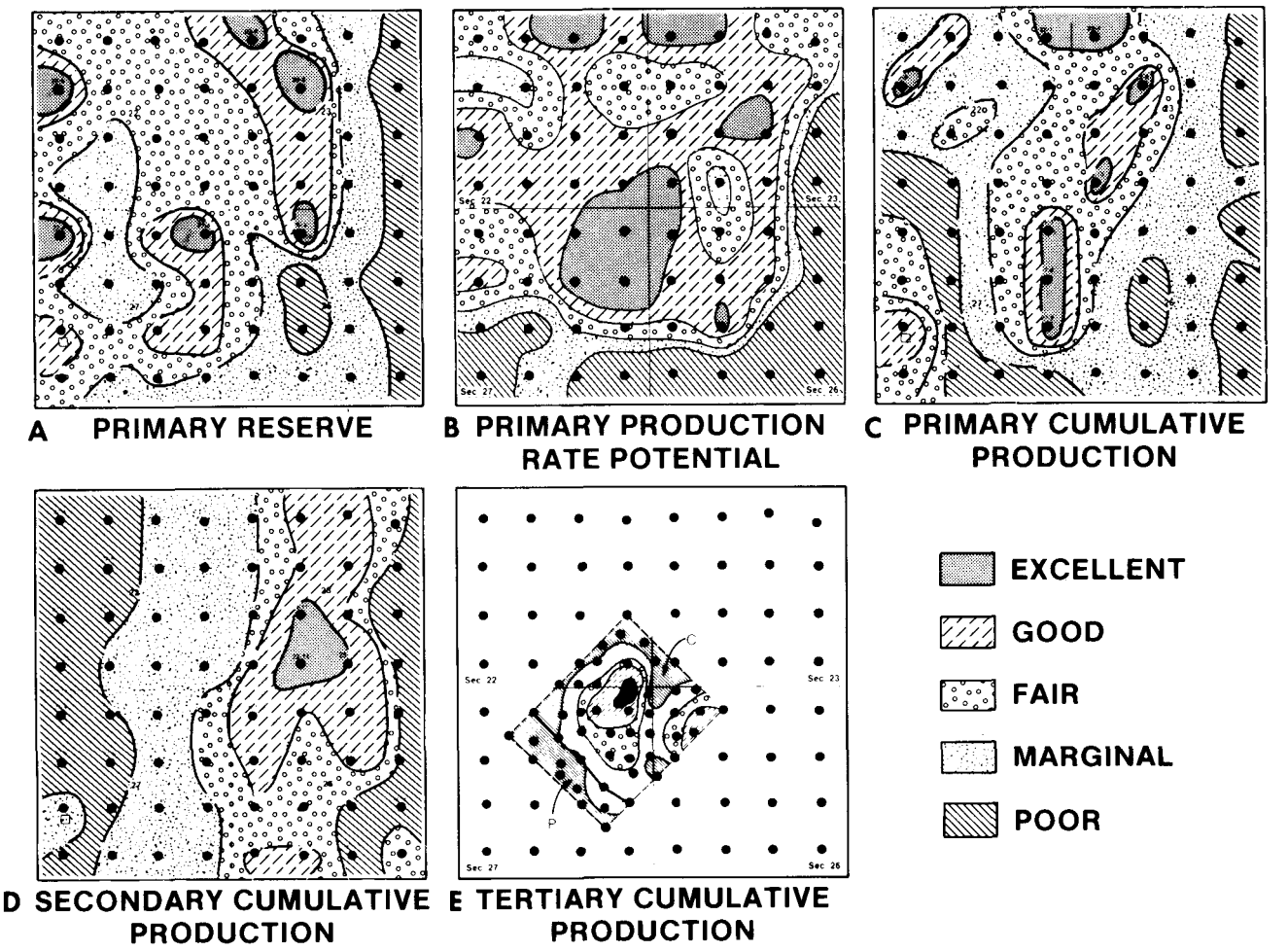


FIGURE 96. - Summary of A, primary reserves; B, primary production rate potential; and primary, waterflood, and tertiary production (C, D, E, respectively) in the study area in Bell Creek field. The TIP area in E is divided into a patterned waterflood region (P), and an area where polymers were injected (C).

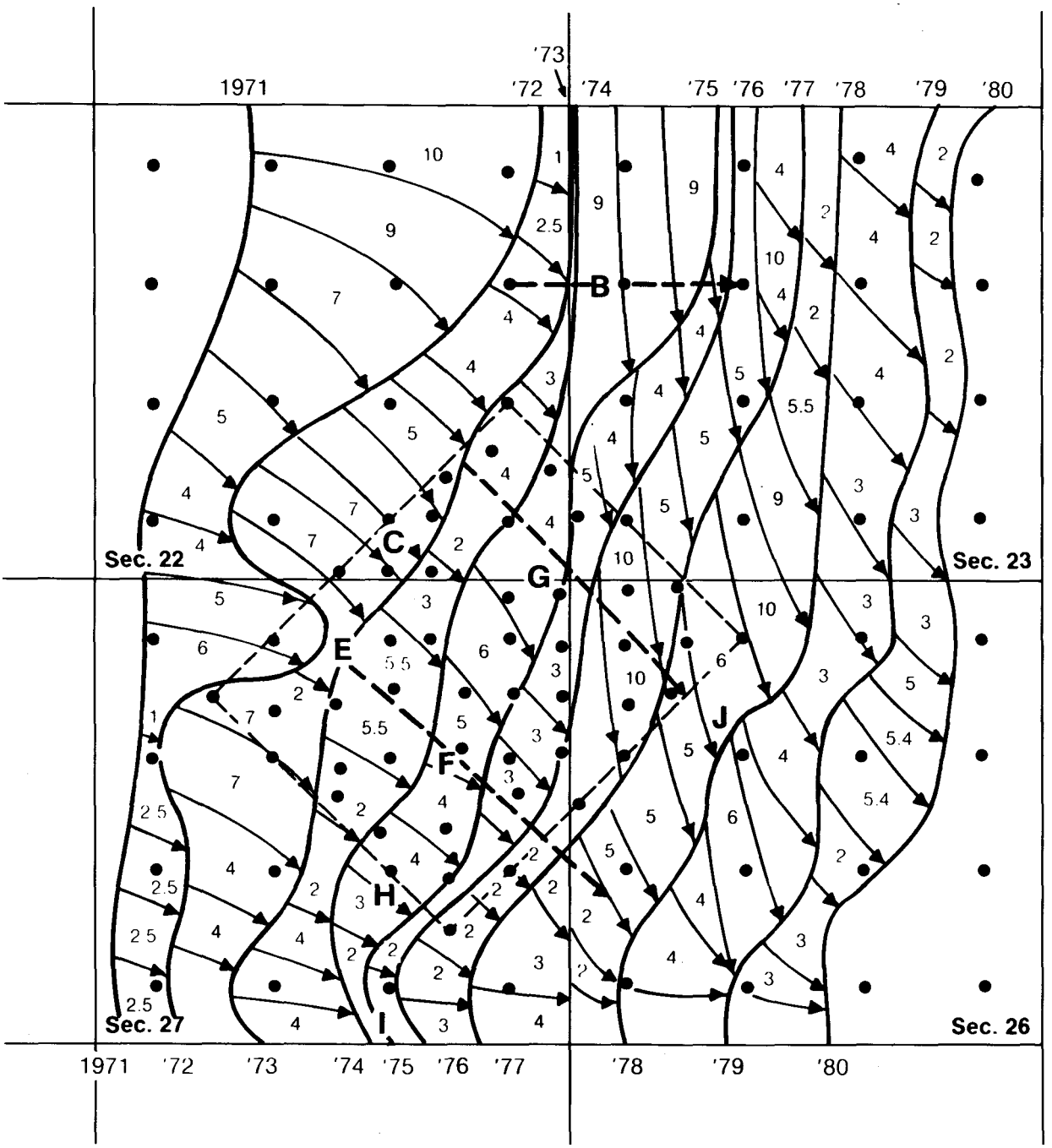


FIGURE 97. - 20% water-cut advancement within the study area. Small numbers indicate fluid rate movement in ft/d; arrows show direction of fluid movement. Dashed arrows represent direction of less than 20% rapid water movement.

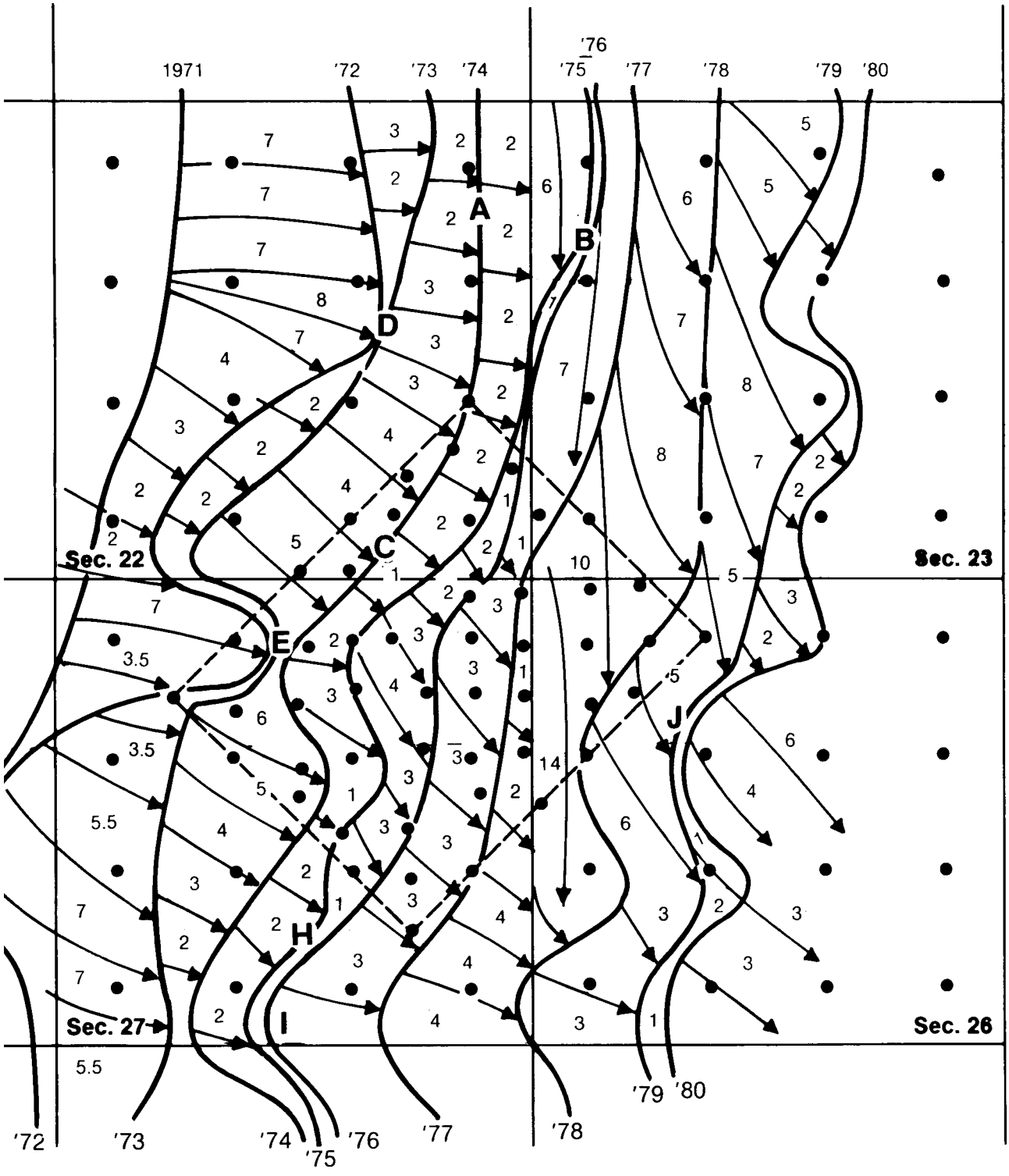


FIGURE 98. - 70% water-cut advancement within the study area. Small numbers indicate fluid rate movement in ft/d; arrows show direction of fluid movement.

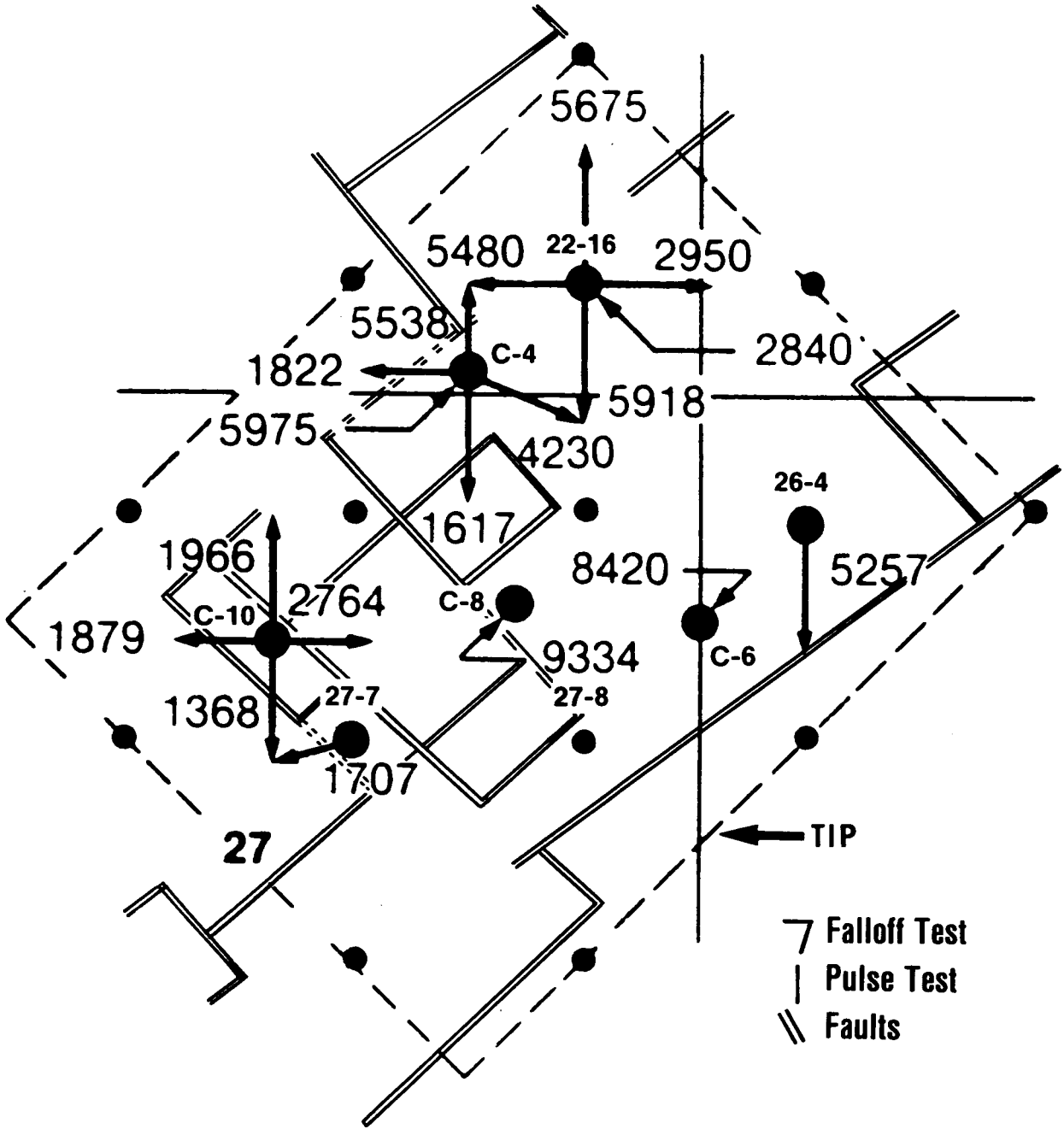


FIGURE 99. - Pressure-pulse and falloff test results prior to initiation of chemical flooding. The large numbers beside an arrow indicate water flow capacity (kwh) in the indicated direction. Numbers indicated on the side of straight arrows represent pulse test results, while numbers next to the bent arrows represent falloff test results.

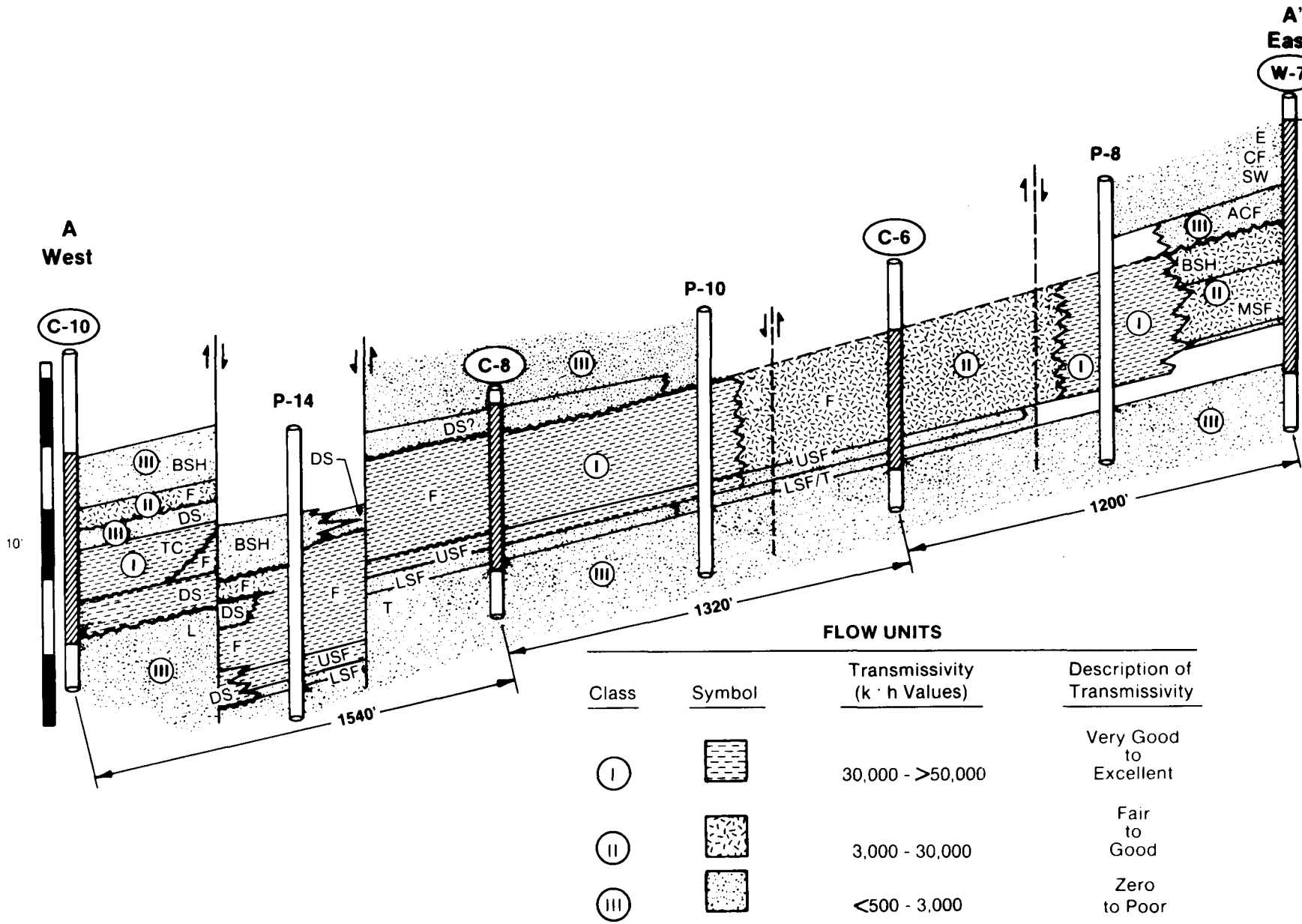


FIGURE 100. - Cross section A-A' showing geology and flow units across central part of TIP. For location of the cross section see figure 16.

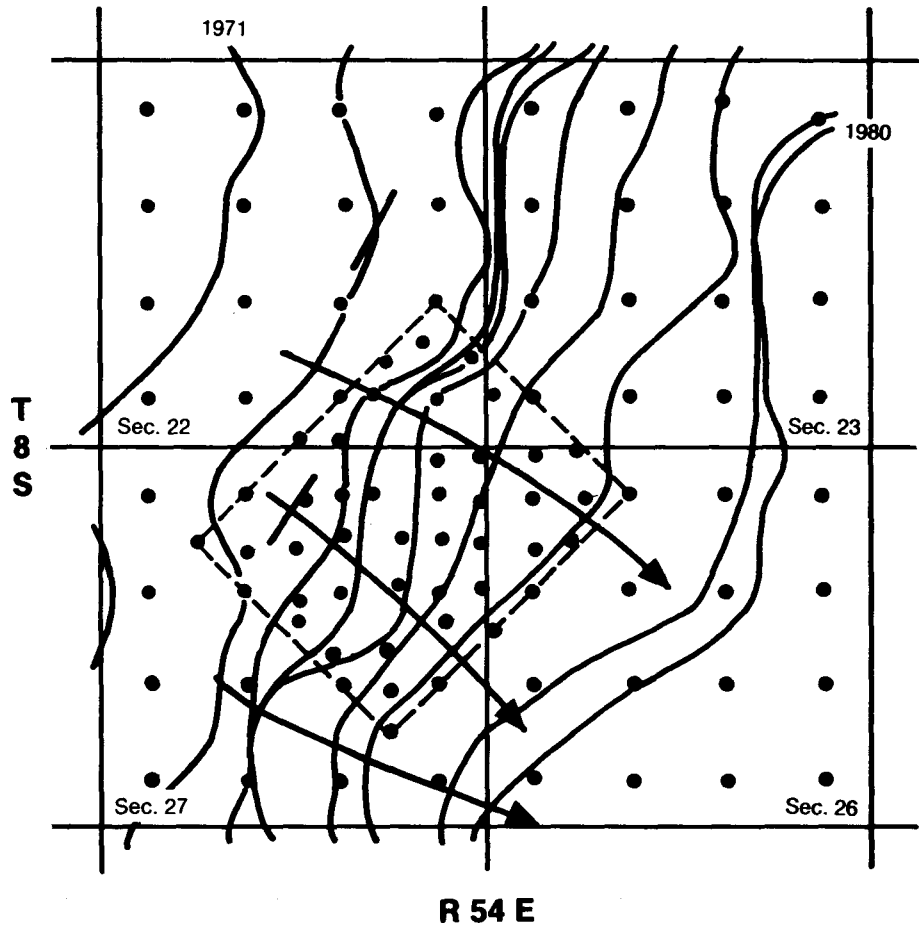


FIGURE 101. - Simulated 70% water-cut advancement within the study area. Arrows shows regions where the simulated waterfront advancement was slower than the actual case. The reason is because the simulation did not include the presence of faults and associated fractures.

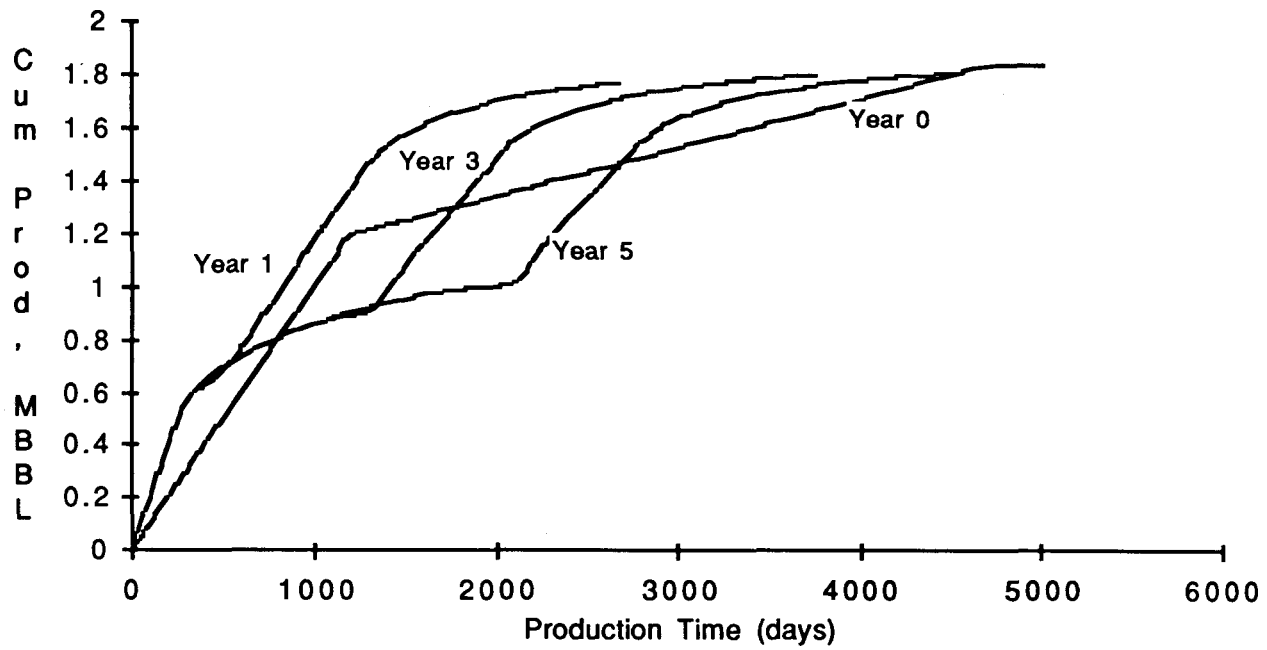


FIGURE 102. - Cumulative oil production at four waterflooding initiation times (1,500 md, 35° API, 40 acres, and 1,000 BPD well capacity).

# CHAPTER 7. SENSITIVITY STUDIES AND NUMERICAL SIMULATION OF WATERFLOOD AND CHEMICAL FLOOD OF BELL CREEK FIELD

## Secondary Production Sensitivity Studies

Simulations were performed to study the capability of a modified version of the black oil simulator BOAST to handle reservoir heterogeneities of the type encountered in the barrier bar depositional system studied in the geoscience research program being performed for the Department of Energy as Project BE1. Cases studied consisted of two-dimensional and three-dimensional simulations of layered reservoirs with different permeability contrasts between the layers, different vertical permeability-horizontal permeability ratios, and continuous and discontinuous shale layers. The details of this work were published in 1987.[1]

To understand the effect of heterogeneities on residual oil location, software was developed to show graphically the residual oil saturation (ROS) in reservoir gridblocks at selected time intervals during the simulation. BOAST was modified for ROS displays as well as for graphical displays of production rates and cumulative production of oil, water, and gas.

It was found that BOAST could adequately handle the type and range of permeability variations and contrasts studied; however, the increase in run time/simulation limited the number of gridblocks that could be processed to less than 2,000 when the Microvax II computer was used. To reduce the computation time, thin layers with permeability ratios of 2 or less or with vertical permeability to horizontal permeability ratios larger than 4 could be combined into single layers with only a small effect on residual oil distribution and oil production rates. High-permeability contrasts in transgressive or regressive sequences caused early water breakthrough and low cumulative oil production, with the transgressive permeability cases being worse. A single, discontinuous layer of shale did not significantly affect simulation results.

The purpose of this work was as follows:

1. To review the previous work concerning reservoir heterogeneity effects on waterflood and chemical flood simulations;[1]

2. To conduct sensitivity studies with emphasis on ROS (using a simulator readily available to NIPER) for heterogeneities of the type present in the barrier island deposystem selected for study in the reservoir characterization project; and

3. To make recommendations concerning the degree of detail necessary to adequately describe reservoirs for waterflooding or chemical flooding.

To simulate accurately on a large scale the movement and retention of fluids in a petroleum reservoir, accurate descriptions of properties of reservoir rocks, reservoir fluids, and their microscopic interactions are required.

For black oil waterflood simulation, the following reservoir parameters are needed: reservoir depth; thickness; permeability vector (or tensor); porosity; transmissibility vector (or tensor) between gridblocks; rock compressibility; oil, water, and gas relative permeabilities; and capillary pressures.

The following fluid PVT properties should be specified:

1. Oil PVT properties -- initial bubblepoint pressure; tables of variation of oil viscosity with pressure, oil formation volume factor and solution gas-oil ratio for undersaturated oil; and tables of variation of viscosity with pressure, formation volume factor, and solution gas-oil ratio for the saturated oil.

2. Water PVT properties -- tables of variation of viscosity with pressure, formation volume factor, and solution gas-water ratio.

3. Gas PVT properties -- tables of variation of viscosity with pressure and formation volume factor.

4. Stock tank fluid densities for oil and water; initial pressure; oil, water, and gas saturation distributions; and well information data (location of injectors and producers, flow rates or bottomhole flowing pressures, completion depth and interval, and the productivity index).

The simulation output consists of fluid flow rates, cumulative fluid production, water-oil and gas-oil ratios for each layer, and totals for each well. The output also contains the spatial distribution in the reservoir of the pressure, water saturation, residual oil saturation, and gas saturation.

For chemical flood simulation, other data should be added to the above, for example:

1. salinity of the reservoir brine, preflush, and chemical (and/or polymer) slug;
2. injection rates and duration of the preflush, chemical, and/or polymer slug;
3. phase behavior of the chemical slug with oil versus the salinity and chemical concentration;
4. viscosity of the chemical slug and the polymer slug;
5. adsorption coefficient of the surfactant and polymer;
6. cation exchange capacity; and
7. interfacial tension data as a function of salinity.

Reservoir heterogeneities are described by variations in rock-related parameters throughout the reservoir: permeability, porosity, relative permeability, capillary pressure, and rock compressibility.

Rock parameters are often measured on much smaller volumes than simulator gridblocks. Furthermore, measurements are obtained only at well locations throughout the reservoir. Therefore, mathematical methods which consider the type of flow process and the spatial distribution of different rock types in the reservoir must be used to predict values of these parameters for simulator gridblock volumes (scaleup process) and at locations where no samples are taken (interpolation process). Depending upon the rock distribution, either deterministic or statistical methods are used in scaleup and interpolation processes.

## Summary of Sensitivity Studies

Based on results of the simulations performed, the following conclusions were made:

1. The graphical display of residual oil saturations developed at NIPER is an essential tool for studying how various heterogeneities affect the displacement of oil from a reservoir.

2. BOAST handles adequately the range of permeability variations and contrasts typical for the depositional system studied in the geoscience base programs.

3. The effect of oil trapping in low-permeability layers and oil and water channeling in high-permeability layers is shown both in ROS graphical displays and in cumulative oil production curves. The presence of a thin (less than one-third of reservoir thickness) high- or low-permeability layer in a reservoir does not have a significant effect on the oil recovery unless the permeability ratio between it and the rest of the reservoir is larger than 2.

4. The effect of variation in vertical permeability on oil saturation and oil production is highly significant for $k_h/k_z$ ratios smaller than 4. Once the ratio becomes greater than 4, its variation affects only very slightly the oil production (essentially the reservoir presents more of a one-dimensional (1-D) flow for a 2-D reservoir model or a 2-D flow for a 3-D reservoir model).

5. Shale layers have a strong effect on ROS distribution (for $k_z = k_h/10$) only if they are essentially continuous. When a continuous shale layer separates two zones of different permeabilities, even a small permeability contrast (permeability ratio = 2) between the two zones can have a marked effect on the ROS in both zones.

6. The higher the permeability contrasts between the layers, the earlier the water breakthrough takes place and the lower the cumulative oil production. Gradual vertical variations in permeability compound the effect of gravity in producing an earlier water breakthrough when the higher permeability is at the bottom of the reservoir. The vertical variation in permeability counteracts the action of gravity when the higher permeability is at the top of the reservoir. Thus, a permeability ratio of 5 between top and bottom layers and a permeability ratio of 1 (homogeneous case) give mirror-

image ROS distributions and almost identical oil production curves. For smaller ratios, with higher top permeability, the oil displacement is more pistonlike, which is a desirable effect.

7. The computation time increases as the vertical permeability increases and as the permeability contrast between layers is increased. Models with 2,000 gridblocks and moderate heterogeneity are expected to require CPU times on the Microvax in the 10- to 20-hour range.

8. The simulator should be adapted to accept different relative permeability and capillary pressure curves for different layers as it is expected that different types of reservoir rock will have different absolute permeabilities, relative permeabilities, and capillary pressures. Sensitivity studies for variations in relative permeability should also be performed.

9. At present, the productivity index (PID), is determined empirically from history matching and well tests. Since it has a very strong effect on the oil production from a given well, it is important to have the PID value determined accurately for actual field studies. The formula for the initial PID value given in the BOAST manual gives only the initial estimate of the PID.

10. Simulation runs of reservoirs containing heterogeneities studied in this work should also be performed with other simulators, such as adaptive implicit simulators.

11. Simulation runs on small heterogeneity models should be performed on the improved Chem 3D model.

## Field Simulation of Primary and Secondary Production

Mathematical simulations were conducted to determine the postwaterflooding ROS distribution in Bell Creek field, Unit 'A'. The distributions of porosity, permeability, initial oil/water saturation, formation (oil-zone) thickness, and formation depth were derived from a mapping package based on controlled values measured from each well. A total of 125 production/injection wells were simulated to match primary and waterflooding productions from June 1967 to August 1980 for 13 years and 2 months. Bottomhole pressures of about 150 psi were assigned to production wells, and water injection rates from field records were used in the history match.

Calculated oil and water production rates were monitored to make necessary adjustments on relative permeabilities of oil, water, and gas.

Simulations were performed on a model dimensioned at 20x33x1 gridblocks with grid size of 660 ft in both x and y directions. Zero transmissibility was assigned to the reservoir boundary and where the faults were located. A well production file from each well and distribution maps of fluid saturations were generated for monitoring. The well production or injection was initiated or shut in during the simulation according to the field data.

BOAST, a black oil applied simulation tool, was used in this field simulation study. Certain modifications were made to enhance its input and output capability.

## History Match

Relative permeability curves from core measurements were initially used in the production history match of Bell Creek field, Unit 'A'. Calculated oil and water productions were found to be sensitive to values of the relative permeability used. High gas relative permeability could reduce reservoir driving force through high gas production. A low value of gas relative permeability was obtained from the simulation to match the liquid production during the primary production period.

A rate constraint was imposed on certain production wells which were near injection wells during waterflooding. Without a limitation on the flow capacity for such producers, the large driving force from close injectors would cause an unrealistic calculation of water production. The simulation showed the difficulty in matching the production from wells in all of the area. Because of different rock properties in the southern part of the simulated area, it was decided that more than one set of relative permeability values should be used in the simulation. BOAST was modified so that more than one set of relative permeability values could be taken and a different set of values could be assigned to different areas.

Compared to the results of a laboratory test, the oil relative permeability obtained from a production match showed lower values at high oil saturations and higher values at lower oil saturations. Calculated residual oil saturations after waterflooding showed a trend similar to that determined

from resistivity logs. The quantitative distribution of ROS from a simulation provided invaluable information for the decision of infill drilling or EOR operations. These results indicated that a two-dimensional simulation study could provide a good history match on a reservoir model of a well-defined barrier island formation.

### Sensitivity Study on Reservoir and Production Parameters

Reservoir and production parameters were varied to investigate the effects of such parameters on production. The parameters studied included formation dip angle, permeability distribution, initial formation pressure, and initiation time of waterflooding. The base case for comparison was the reservoir model used in the history match with 3° formation dip, arithmetically averaged permeability distribution, and an initial formation pressure of 1,200 psi. Results of the sensitivity study are listed in table 36.

A 3° formation dip showed no significant effect on either primary or secondary production. This indicated a minor gravity force compared to a good viscous driving force at a formation permeability over 1 darcy. The permeability distribution averaged geometrically from different wells provided a low fluid production in the simulation. The reduction in oil/water production was more pronounced in the simulation of waterflooding than in that of primary production. This was due to a generally low intrawell permeability value calculated by the geometrical averaging. A high initial formation pressure, doubled from 1,200 to 2,400 psi, showed a high production rate, as had been expected. The calculated improvement in oil production was 21% due to the increase in the initial formation pressure.

### Summary of Linedrive Field Simulation

The reservoir performance was studied by initiating water injection at the beginning of production using the same well configuration of waterflooding in the base case. The results showed that the entire field production life could be reduced to fewer than 5 years, or less than 50% of the base case at an additional 10% increase in oil production. This observation induced a further study of waterflooding initiation time and other reservoir parameters from a five-spot pattern simulation.

## Five-Spot Pattern Simulation

Mathematical simulations were performed for five-spot well patterns with typical reservoir and fluid properties of Bell Creek field, Unit 'A'. Effects of various formation parameters and production strategies on fluid production were evaluated from these simulation studies. Sensitivity runs were conducted by varying the following parameters: waterflooding initiation time, maximum production/injection rate, formation permeability, oil gravity, and well spacing. For each studied case, the waterflooding initiation time was evaluated at 0, 1, 3, and 5 years after the discovery time. Primary production was assumed for all wells in the 5-spot pattern until water injection started.

Two-dimensional areal simulations were performed with 9x9x1 gridblocks. The simulated five wells were located at the central and four corner gridblocks, respectively. The productivity/injectivity indices of corner wells were adjusted so that they could produce/inject fluid at one-fourth the rate of the central well.

All wells were kept active all of the time in the 5-spot simulations. Four corner producers were converted to injectors when waterflooding was begun. Both restrictions of maximum flow rate and maximum wellbore pressure were assigned. The simulations were terminated when the water cut reached 98%.

### Effects of Waterflooding Initialization Time

Typical reservoir and production parameters representative of Bell Creek field were used in this study. These parameters are 1,500 md average permeability, 35° API oil gravity, 40-acre well spacing, and maximum production rate of 1,000 bbl/d per well. Relative permeability values from a field production history match were used in the reservoir model.

Figure 102 shows the cumulative oil production at four different water flooding initiation times: year 0, year 1, year 3, and year 5. All four cases produced about the same cumulative oil production in their entire field lives, but the case of year 1 showed the fastest oil recovery because of the early waterflood initiation time and keeping the existing producers during their high primary oil production period. The year-3 case took 2 years longer,

whereas the year 5-case took 4 years longer to recover the secondary oil, compared to the year-1 case. Figure 103 shows that the reservoir pressures of the year-3 and year-5 cases were almost depleted after the first year of oil production. The fast oil recovery of the year-1 case was, therefore, due to the avoidance of unnecessary delay in water injection when reservoir pressure was depleted. Initiation of a water injection program at the beginning of field production, as indicated in the case of year 0 in figure 103, did not provide the fastest recovery of oil because some of the potential producers were converted to injectors. In the year-0 case, the four corner wells produced no oil and were used as injectors. Figure 104 shows oil production rates for these four different water injection initiation times. When water injection was initiated in the year-0 case, oil was produced at a maximum rate of 1,000 bbl/d until 1,157 days later when water breakthrough occurred. Then, the rate dropped sharply and leveled at 180 bbl/d for the remainder of the field life. The oil production rate of the other three cases did not drop after 7 months of production at the assigned rate of 1,000 STB/d per well. However, pressures of the other three cases dropped drastically during the first year of oil production and continued to drop until the initiation of water injection. All of the latter three cases showed that oil production rates did not increase until 3 to 5 months after the initiation of water injection. The water about time was approximately 3 years and corresponded with a sharp decline in production.

## Effects of Well Flow Capacity

Reservoir performances were studied at two other well production capacities, 300 and 3,000 STB/d, in addition to the 1,000 STB/d that was previously discussed.

Figure 105 shows the cumulative oil production from the 3,000-STB/d well for four water initiation times (0, 1, 3, and 5 years). The year-0 case showed the fastest oil recovery after the first 300 days of oil production. Production from high-capacity wells depleted the reservoir energy faster than that from low-capacity wells. The immediate supply of injection water in the case of year 0 at a maximum allowable 3,000 STB/d production/injection rate kept the oil rate above 2,000 STB/d during most of the first 500 days of oil production, as shown in figure 106. The entire production lives were reduced

from about 2,700 to 5,000 days at 1,000 STB/d per well to 2,500 to 3,800 days at 3,000 STB/d per well. The recoverable oil at four water injection initiation times was about the same (1.8 million STB or 70% of the initial oil-in-place).

The cumulative oil production at a maximum allowable rate of 300 STB/d per well and four different water injection initiation times is shown in figure 107. Because of a low allowable production rate and good formation permeability of the reservoir, oil could have been produced at 300 STB/d for 3 years. Therefore, oil production from year 3 and year 5 showed faster oil recovery than the other two cases. The recoverable oil at 300 STB/d was about equal to that of 1,000 or 3,000 STB/d production rates. However, field production lives were prolonged from 6,000 to 20,000 days.

This study indicates that a high maximum allowable rate can reduce the production life at about the same total oil production, but the higher the maximum allowable rate, the sooner water injection should be initiated.

### Effects of Oil Gravity

Reservoir production performances were studied for 25°, 35° and 45° API gravity oils. Figure 108 shows the cumulative production from a 45° API gravity oil reservoir. Higher oil production rates were sustained due to higher solution gas of higher API gravity oil and therefore higher cumulative oil production at a given time as compared to lower API gravity oil cases.

Figure 109 shows cumulative oil production for 25° API gravity oil at four different water injection initiation times. Both cases of year 0 and year 1 produced a total of 1.2 million bbl of oil within 1,300 days, but in all cases, ultimate production of less than 1.5 million STB was achieved. For the 45° API as well as the 35° API gravity oil, the year-1 case showed the fastest recovery. However, the 35° API gravity oil showed 11% higher cumulative oil production than that of the 45° API gravity case. The low solution-gas-oil ratio of 25° API gravity oil did extend the field life to 13,000 days for similar recovery efficiency.

Figures 110, 111, and 112 show the effect of oil gravity on cumulative oil production at three water injection initiation times. Oil production rates were about the same for different oil gravities until water breakthrough took

place for the year-0 case. Afterward, the production of the high API gravity oil was higher than that of all others. A similar effect of oil gravity on oil production is shown in figures 112 and 113. The higher API gravity oil showed earlier recovery. Oil production rates generally increased after water injection began and decreased after water breakthrough. Figure 113 shows oil rates at three oil gravities when water injection was initiated after 1 year of primary production.

### Effects of Well Spacing

Oil production for 20-acre well spacing was compared to that from 40-acre well spacing. Figure 114 shows the cumulative oil production from a reservoir with 20-acre well spacing at four water injection initiation times. Cumulative oil production per unit volume from 20-acre well spacing was just about the same as that from 40-acre drainage areas. However, the total production period for the 20-acre spacing was two-thirds of that of the 40-acre spacing. The year-1 water injection case appeared to be the best choice among the four cases studied. These studies assumed a homogeneous formation.

### Effects of Formation Permeability

Bell Creek field has an average permeability of 1,500 md. The oil production performance was investigated for a 150-md case, and other reservoir parameters were kept constant. Field production was significantly delayed when the average permeability was reduced to 150 md (figs. 102 and 115). Injection and production rates were substantially lower (fig. 116), whereas the response time for production due to water injection was much longer. The recoverable oil from the 150-md formation was lower than that from the 1,500-md formation. Cumulative oil production for the year-0 and year-3 cases coincided at 2,000 days of oil production. The year-0 case showed higher cumulative oil production beyond 2,000 days of production.

### Summary of Five-Spot Pattern Simulation

The effects of the following formation parameters have been examined:

1. Waterflood initiation time: Initiation of waterflood 1 year after discovery provided the fastest oil recovery rate; however, initiation time did not affect cumulative production.

2. Well flow capacity: High maximum allowable rates of production/injection can reduce production life but have little effect on cumulative production if waterflood injection is begun as soon as possible.

3. Oil gravity: Generally, recovery efficiency and recovery rates should be greater for higher API gravity oils.

4. Well spacing: Cumulative oil production on a per unit volume basis is approximately the same for 20- and 40-acre spacings, assuming a homogeneous formation.

5. Formation permeability: Production rates were significantly reduced by lower permeability rocks, and the recoverable oil was less than that of high-permeability formations.

## NUMERICAL SIMULATION OF A FIVE-SPOT CHEMICAL FLOOD IN THE TIP AREA OF BELL CREEK FIELD

Simulation of the micellar-polymer flood in the TIP area was performed using the chemical simulator UTECHEM developed at the University of Texas. The geological/engineering model developed in the project was used in the development of the numerical model.

The following steps were followed in this simulation task: (1) perform a streamline simulation of the TIP to allocate the injection rate from each injector to its four surrounding producers; (2) perform history match of the available corefloods (from the Bell Creek cost-shared project) to determine key process parameters for the Uniflood process; and (3) perform field simulations on a five-spot pattern in the TIP area.

### Streamline Simulation

Since only part of the TIP area was simulated, the fraction of the fluid for each injector entering the selected five-spot had to be estimated. This was estimated by performing a streamline calculation of the TIP area.

A unit mobility streamline model was used. This model identified any location in the TIP area by x and y coordinates. For each of these locations, the velocities $V_x$ and $V_y$ were calculated using Darcy's law. The computed velocities were used in determining the location of the injected fluid front at a certain period of time. An analysis of the streamlines showed that the

pattern was unbalanced. The unbalance apparently resulted from high water injection rates in wells limiting the TIP area in the NE and SE boundaries. Figure 117 shows the streamline distribution during preflush injections. This situation became very serious during the micellar-polymer slug injection since chemical injection rates were lower at the time (fig. 118).

## Numerical Simulation of Soluble Oil CoreFlood Experiments

Four soluble oil coreflood experiments [2-3] were numerically simulated to evaluate the soluble oil design for the Bell Creek micellar-polymer demonstration project. The purpose of this simulation study was to estimate various input parameters needed to use UTCHEM for the field simulation.

## Simulation Input Parameters

The initial conditions of the coreflood experiments described in references 2 and 3 are listed in table 37. The initial anion and divalent cation concentrations of the coreflood experiments were not reported; therefore, the average anion and divalent cation concentrations produced from the five wells in the pilot area, as reported in table 8 of reference 2, were used in these simulations. One-dimensional simulations were performed using 40 gridblocks.

Compositions of the slugs injected are given in table 38. The effects of high pH and silicate reactions of the preflush were not simulated directly. However, their effect on the cation exchange capacity (CEC) of the cores was taken into account. As previously noted, four coreflood experiments were simulated with slug sizes of 0.040, 0.030, 0.0225, and 0.0150 PV. The same injected compositions were used for all four coreflood simulations; only the surfactant slug size was changed accordingly.

Physical property input parameters were estimated from extremely limited data and are therefore highly uncertain. Thus, most of the input was obtained from history matching of the oil recovery only. Because of the salinity gradient set by the preflush, surfactant slug, and polymer drive, the oil recovery efficiency was found to be very sensitive to the lower and upper limits of effective salinity for the middle phase microemulsion (Type III). If the lower limit was chosen so that the surfactant slug did not reach the Type III environment, the recovery was very low. However, when limits were

chosen so that the slug traveled in the Type III region, there was no strong sensitivity to these values.

The longitudinal dispersivity was set to 0.05 ft, a typical value for a 4-ft-long Berea sandstone core. Surfactant adsorption parameters were adjusted to give a reasonable match of the oil recovery of the four coreflood experiments. Actually, because of the favorable salinity gradient present in these experiments, there was not a high degree of sensitivity to cation exchange capacity (CEC). A CEC value of 0.02 meq/mL of PV was used, but reducing this value to zero did not appreciably affect the results.

## Simulation Results

A comparison of experimental and simulated oil recoveries for the four coreflood experiments showed that the experimental oil bank was smaller but had an oil cut about 20% higher than the simulated initial oil cut, which caused oil recovery curves to be different even though the final oil recovery was about the same. This difference was the greatest for the 0.040 and 0.015 PV slugs. Experimental and simulated oil breakthroughs for all of the slug sizes were in good agreement. Figure 119 shows the results obtained when a 0.030-PV slug was injected. A comparison of experimental and simulated oil recoveries with slug sizes is shown in figure 120. The simulated effective salinity increased more than the optimum due to the high salinity of the preflush, then it crossed the Type III phase environment to reach the lower salinity of the drive. The salinity wave traveled with the remaining surfactant, and at least a small but important part of the slug traveled as a middle-phase microemulsion.

Simulated co-solvent and surfactant breakthroughs were about 0.066 and 1.05 PV, respectively. Peak concentrations for the co-solvent and surfactant were 7 and 12% of the injected values. Surfactant retention was 0.0015 meq/mL of PV or 0.67 lb/bbl of PV (0.14 mg/g of rock). Polymer breakthrough was noted at about 0.7 PV. The polymer retention was about 0.01 lb/bbl of PV or 2.1 μg/g of rock. This is a very small retention value but is in agreement with reported values. The simulated surfactant slug to oil bank mobility ratio ($M_{c/ob}$) was 0.3, and the polymer-drive to surfactant slug mobility ratio ($M_{d/c}$) was 0.5. The overall mobility ratio, polymer drive to oil bank

mobility ratio ($M_{d/ob}$) was 0.15. These values indicated that these experiments had stable displacements and good sweep efficiencies.

## Summary of Coreflood Simulation

Results of coreflood simulations were not the best matches of experimental results; however, the lack of physical property data for the surfactant-solvent formulation and the lack of effluent histories for the surfactant, polymer, co-solvent, calcium, chloride, and pressure drop made the simulation matching process difficult and more uncertain than usual. Nonetheless, oil recovery and breakthrough times of the four corefloods were successfully matched. Important physical property parameters were determined, and the sensitivity of the results to these parameters was studied. A better match of the oil cuts could almost certainly be achieved by adjusting the relative permeability curves, but this would accomplish little since these curves are different for the Muddy sand Unit 'A' of the Bell Creek TIP project and do not apply to the simulation of the field process. However, the other process parameters, such as those describing phase behavior, interfacial tension, and viscosity, should be applicable, at least approximately, and should reduce the even greater uncertainty associated with the field-scale simulation of the TIP project.

## Field Simulation of a Five-Spot in the TIP Area

The ultimate objective of the proposed field simulation in this project was to use the simulation outcome in developing strategies for future developments of a barrier island reservoir.

Based on the geological model of the TIP area, three five-spots were selected for history-matching simulation. The work presented here involved preliminary sensitivity analyses and preliminary history matches performed for the five-spot containing producer well P-10 and the four chemical injectors C-5, C-6, C-7, and C-8. This five-spot was selected because it contains four chemical injectors and the geology of the area is not as complex as that of other areas of the TIP. The presence of four chemical injectors is desirable when evaluating a micellar-polymer process.

Actual field data and supporting physical property data were used as much as possible to estimate simulator input parameters. First, the description of

the input data and the performed sensitivity analysis were presented. The sensitivity analysis was only performed for the preflush period. Preliminary simulation results and a comparison with field results are discussed, and results from a 4-year waterflood simulation are analyzed further in this report.

A description of preliminary field simulation results is presented in the next three sections. Only some of the input parameters are described. A complete description is given in appendix D.

## Field Simulation Input Data

An area of 1,075.2 ft x 921.6 ft, or 22.75 acres was simulated with a 7x6x3 grid ($\Delta X$ = 153.6 ft and $\Delta Y$ = 153.6 ft). Three layers were simulated with the following thicknesses: 17.02 ft for the top layer, 2.16 ft for the middle layer, and 4.00 ft for the bottom layer. A core analysis of well C-6 (fig. 10) showed the presence of diagenetic clays and poor sorting which were both absent in well C-8. The permeability and porosity of part of the simulated area deteriorated because of the presence of the clay-filled zones. The vertical-horizontal permeability ratio was considered to be 0.1. A dip angle of 3 degrees in the northwest direction was simulated.

Based on the injection data, the initial reservoir pressure was estimated to be 3,167 psi at well C-5. The four injectors in the five-spot were kept under rate constraints, whereas the producer was kept at a constant pressure of about 3,100 psi. Injection rates were allocated according to streamline results.

Most of the engineering data were obtained from Gary Williams Bell Creek reports. The geological data were obtained from NIPER's Bell Creek Unit 'A' geological model, and the other engineering data were obtained from an analysis of Bell Creek field tests. The oil saturation at the start of the preflush was assumed to be 33%, based on a waterflood simulation study performed at NIPER.[1]

In the absence of information on the injected fluid composition for the TIP, the injected fluids composition of the Uniflood micellar-polymer design used for the cost-shared project in Bell Creek field was assumed for the TIP. Some information about the application of the process in the TIP was

obtained from Union[4] and Gary Williams Oil Producers,[5] and only a few changes in the pilot design were made. The slug sequence was obtained from Hartshorne and Nikonchik.[6]

Most of the physical properties determined by the coreflooding history match were used in this preliminary field simulation. The residual oil saturation was estimated by a sensitivity analysis performed during the preflush period. The end point water relative permeability at high interfacial tension ($k_{rlw}$) was determined from well test data. Finally, the longitudinal dispersivity ($\alpha_L$) was found by considering the $\Delta X/\alpha_L<2$ constraint, where $\Delta X$ is a typical gridblock dimension and transverse dispersivity $\alpha_T$ was assumed to be 1/30 of the longitudinal dispersivity.[7]

## Sensitivity Analysis During Preflush Period

The input data previously described were considered as the base case. Considerable uncertainty existed in the published data; therefore, a sensitivity analysis of the oil cut and the fraction of oil recovery (FORC) during the preflush period was performed. Most of the micellar physical property input parameters were not considered in this analysis. Furthermore, the analysis was not extended to the complete micellar-polymer injection period, which was 4 years. Consequently, only a preliminary analysis of the sensitivity study will be presented here. Future work will include a detailed sensitivity analysis to the process parameters[8] and reservoir heterogeneities.[9]

Many fluid and reservoir parameters--relative permeability (end points, exponents, and residual saturation), fluid injection rates (balanced pattern versus unbalanced), initial reservoir pressure, initial oil saturation, reservoir dip, fluid dispersivities, rock and liquids compressibilities, rock permeability, flowing bottomhole pressure, and location of the diagenetic region--were varied considerably during this history match. The results showed that oil cut and FORC were dependent on mobile oil saturation, end point oil relative permeability at high interfacial tension, relative permeability exponent for the oleic phase at high interfacial tension, and reservoir dip, while other parameters showed almost no effect. Some of these results are supported by Datta-Gupta, Pope et al.[9]

Based on this sensitivity study of the preflush period, the estimate of the residual oil after waterflooding was revised to be 32% since a better history match of the oil cut and the FORC was obtained with this value. The other data were used as presented in the previous section (base case).

### Comparison of Simulated Results With Field Data

Preliminary simulated and field oil recoveries (as a fraction of initial oil-in-place) versus pore volumes injected are shown in figure 121. A comparison of simulated and field oil cuts is shown in figure 122. Field and simulated oil breakthrough times and oil recoveries were almost the same. The field oil recovery was 26.4%, whereas the simulated oil recovery was 23.2%, or about 3% lower. These simulated results were obtained by assuming balanced injection rates. The oil breakthrough, with unbalanced rates obtained from the streamline calculation, was about 0.1 PV ahead of the field breakthrough time. The simulated oil production was only 1% higher than that of the field (27.4%). It is obvious that the shape of the oil-cut curve has not been matched. A possible explanation may be that in the simulated run, oil was arriving to the producer at almost the same time from each layer.

A preliminary qualitative analysis of the field and simulated produced surfactant indicated that surfactant retention was simulated closely. The field and simulated surfactant breakthrough times did not match. Chloride-, polymer-, and cation-produced concentration histories were also analyzed. The chloride concentration was too high, and the cation concentration was too low. The simulated polymer adsorption was also too high. These results indicate that further work is needed to evaluate the Bell Creek micellar-polymer flood performance.

To determine the amount of oil that would have been produced by waterflood alone, preflush fluid was injected for 4 years. Assuming an unbalanced injection rate, an oil recovery of 1.9% would have been obtained after injection of 0.37 PV of water. Contrarily, 2.3% oil recovery would have been obtained after injection of 0.42 PV of water, assuming a balanced injection rate.

## Summary of Coreflood and Field Simulations

Results of coreflood simulations did not exactly match experimental results; however, the lack of physical property data for the surfactant-solvent formulation and the lack of effluent histories for the surfactant, polymer, co-solvent, calcium, and chloride, and pressure-drop made the simulation matching process difficult and more uncertain. Nonetheless, oil recovery and breakthrough times of the four corefloods were successfully matched. Important physical property parameters were determined, and the sensitivity of results to those parameters was studied. A better match of oil cuts could almost certainly have been achieved by adjusting relative permeability curves, but this would have accomplished little since these curves were different for the Muddy sand Unit 'A' of the Bell Creek TIP project and did not apply to the simulation of the field process. However, the other process parameters, such as those describing phase behavior, interfacial tension, and viscosity, should be applicable, at least approximately, and should reduce the even greater uncertainty associated with the field-scale simulation of the TIP project.

The oil cut and fraction of oil recovery during the preflush period were sensitive to the mobile oil, the end point relative permeability of oil displaced by water at high interfacial tension, and the phase relative permeability exponent for oleic phase at high interfacial tension and reservoir dip.

Preliminary field simulation runs showed good agreement between field and simulated oil recoveries and oil breakthough time; although the oil cut did not show good agreement. The field oil recovery was 26.4%, whereas the simulated oil recovery was only about 3% lower -- 23.2% when assuming a balanced injection rate. A waterflood simulation showed that infill drilling would have recovered less than 3% of the oil-in-place.

Oil cut and fraction of oil recovery should be history-matched, but concentration histories, pressure drop, dispersion, and adsorption are other factors that should be considered. These factors will be considered in future simulations. A sensitivity study of field results to physical property field parameters will also be performed to adjust some of the parameters determined through coreflood history matches.

## REFERENCES

1. Tomutsa, L. and J. Knight. Effect of Reservoir Heterogeneities on Waterflood and EOR Chemical Flood Performance. Dept. of Energy Report No. NIPER-235, 1987, p 82.

2. Bhuyan, D., L. W. Lake, and G. A. Pope. Mathematical Modeling of High-pH Chemical Flooding. Pres. at the SPE/DOE Symp. on Enhanced Oil Recovery, Tulsa, OK., Apr. 17-20, 1988. SPE/DOE paper 17398.

3. Camilleri, D., S. Engelsen, L. W. Lake, E. C. Lin, T. Ohno, G. A. Pope, and K. Sepehrnoori. Description of an Improved Compositional Micellar/Polymer Simulator. SPE Reservoir Engineering, 1987.

4. Robertson, S. D. Personal Communication, 1988.

5. Nikonchik, J. Personal Communication, 1988.

6. Hartshorne, J. M. and J. S. Nikonchik. Micellar/Polymer Flow Shows Success in Bell Creek Field. Pres. at the 1984 SPE Ann. Tech. Conf. and Exhib., Houston, sept. 16-19. SPE paper 13122.

7. Saad, N., G. A. Pope, and K. Sepehrnoori. Simulation of Big Muddy Surfactant Pilot. SPE paper 17549 to be published in SPE Reservoir Engineering.

8. Pope, G. A., B. Wang, and K. Tsaur. A Sensitivity Study of Micellar/Polymer Flooding. Soc. of Pet. Eng. J., Dec. 1979, pp. 357-368.

9. Datta-Gupta, A., G. A. Pope, K. Sepehrnoori, and M. Shook. Effects of Reservoir Heterogeneity on Chemical Enhanced Oil Recovery. SPE Reservoir Engineering, May 1988, pp. 479-488.

TABLE 36. - Study of sensitivity of Bell Creek field Unit 'A' production performance with different reservoir parameters and production/injection strategies

| | Oil | | Water | |
|---|---|---|---|---|
| | Mbbl | % Change | Mbbl | % Change |
| A. Primary production | | | | |
| Base (3° dip, arithmetically average permeability distribution, initial formation pressure 1,200 psi) | 15.4 | -- | 1.3 | -- |
| No dip | 15.4 | < 1 | 1.3 | < 1 |
| Geometric averaged permeability | 14.1 | -8 | 1.1 | -15 |
| Initial formation pressure, 2,400 psi | 18.6 | 21 | 1.4 | 8 |
| B. Waterflooding | | | | |
| Base | 38.0 | -- | 45.5 | -- |
| No dip | 39.3 | 1 | 44.0 | -3 |
| Geometric averaging permeability | 30.1 | -21 | 31.1 | -31 |
| C. Pressure maintenance by waterflood from the beginning of oil production | | | | |
| Base (primary and waterflooding) | 53.4 | -- | 46.8 | -- |
| Water-injection pressure maintenance | 58.7 | 10 | 25.8 | -45 |

TABLE 37. - Initial condition - coreflood simulation

| | |
|---|---|
| Core dimensions, ft | 4 x 0.125 x 0.125 |
| Porosity, fraction | 0.2 |
| Permeability, md | 500 |
| Initial water saturation, fraction | 0.65 |
| Initial oil saturation, fraction | 0.35 |
| Initial anion concentration, meq/mL | 0.06581 |
| Initial calcium concentration, meq/mL | 0.001406 |
| Oil viscosity, reservoir cond., cP | 4.8 |
| Water viscosity, reservoir cond., cP | 0.63 |
| Reservoir temperature, ° F | 110 |
| Constant injection rate, $ft^3/d$ | 0.003125 |

TABLE 38. - Injected composition - coreflood simulation

| | Preflush | Surfactant slug | Polymer frive | Post flush |
|---|---|---|---|---|
| Slug Size, PV | 0.10 | 0.03 | 0.70 | 0.37 |
| Water, vol. fr. | 1.000 | 0.524 | 1.000 | 1.000 |
| Oil[1], vol. fr. | 0.000 | 0.400 | 0.000 | 0.000 |
| Surfactant[2], vol. fr. | 0.000 | 0.070 | 0.000 | 0.000 |
| Polymer[3], wt % | 0.000 | 0.000 | 0.095 | 0.000 |
| Anions, meq/mL | 0.18310 | 0.10920 | 0.03083 | 0.07912 |
| Calcium, meq/mL | 0.000514 | 0.000514 | 0.000399 | 0.000848 |
| Co-solvent[4], vol. fr. | 0.000 | 0.006 | 0.000 | 0.000 |

[1] Bell Creek crude oil.
[2] Mostly Stepan Petrostep™ 465.
[3] Cyanatrol WF950S.
[4] Butyl cellosolve.

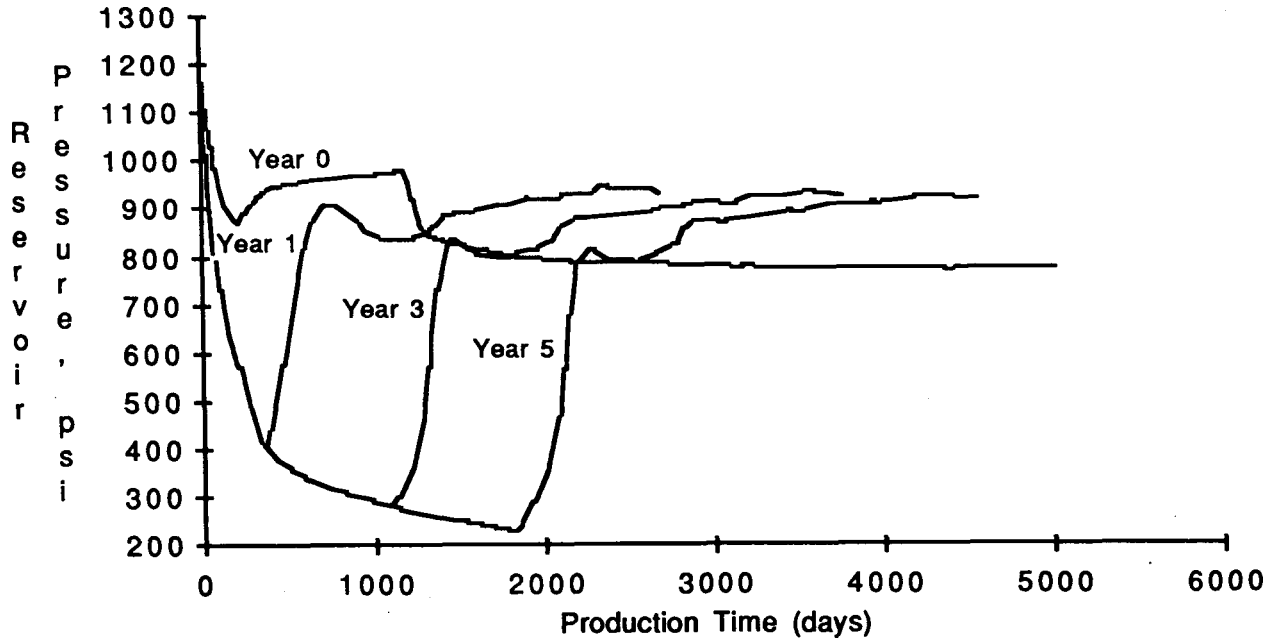


FIGURE 103. - Average reservoir pressure at four waterflooding initiation times (1,500 md, 35° API, 40 acres, and 1,000 BPD well capacity).

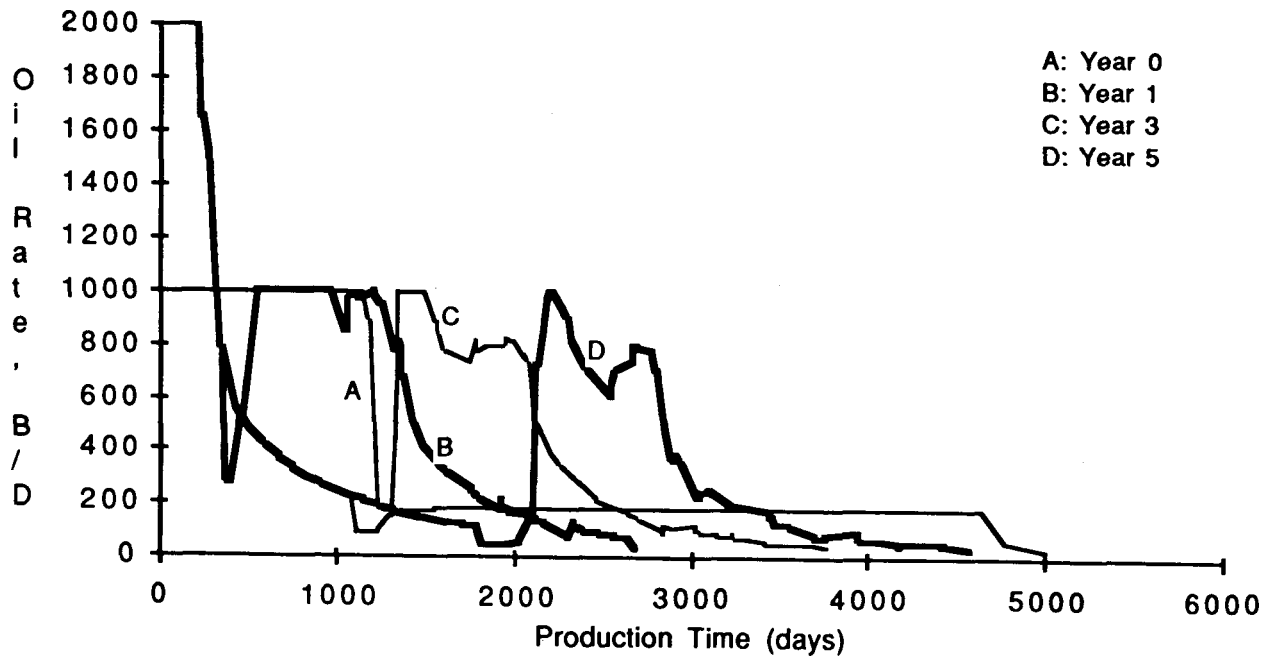


FIGURE 104. - Oil production rates at four waterflooding initiation times (1,500 md, 35° API, 40 acres, and 3,000 BPD well capacity).

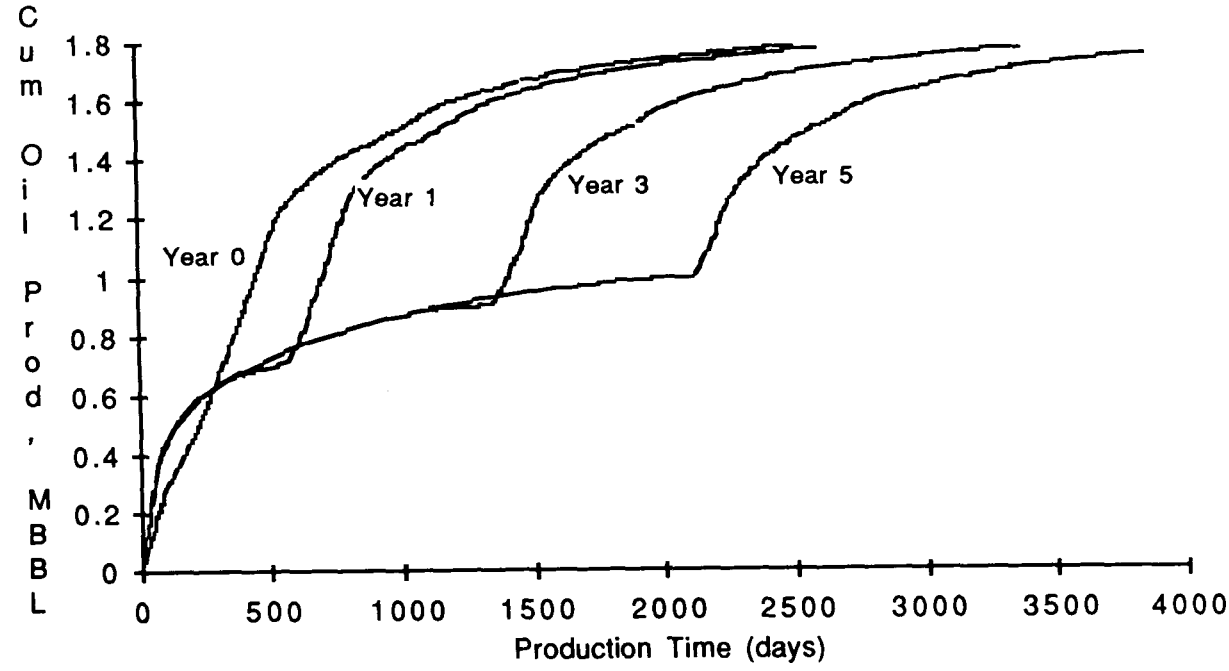


FIGURE 105. - Cumulative oil productions at four waterflooding initiation times (1,500 md, 35° API, 40 acres, and 3,000 BPD well capacity).

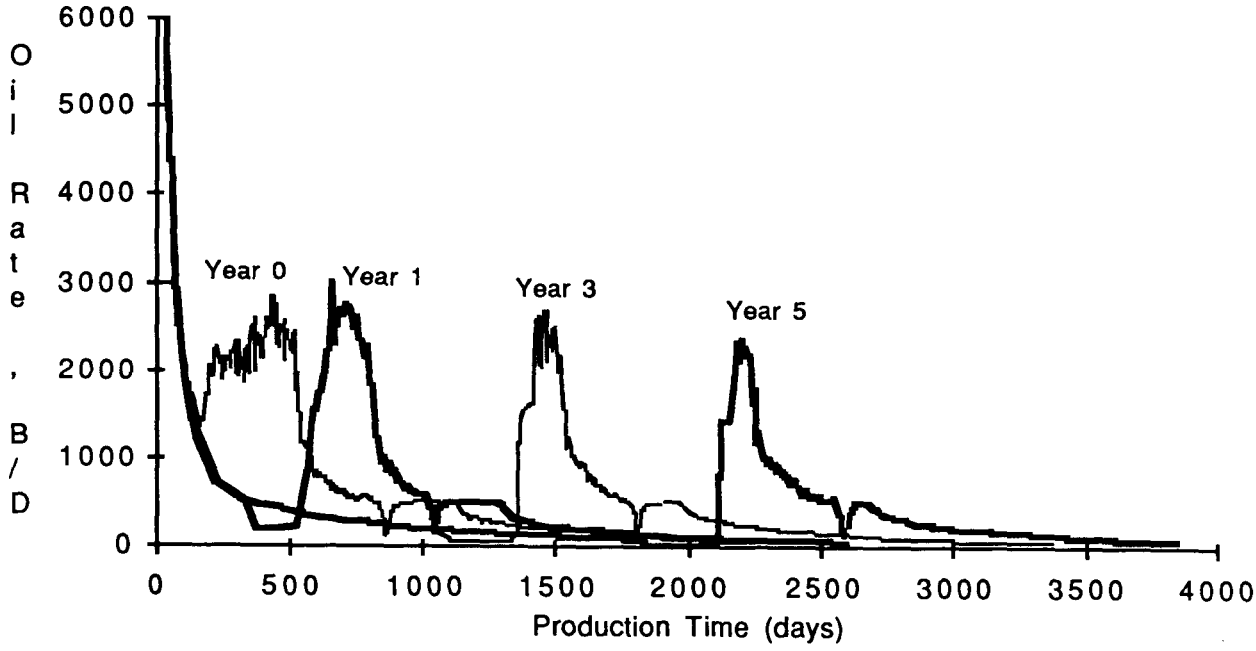


FIGURE 106. - Oil production rates at four waterflooding initiation times (1,500 md, 35° API, 40 acres, and 3,000 BPD well capacity).

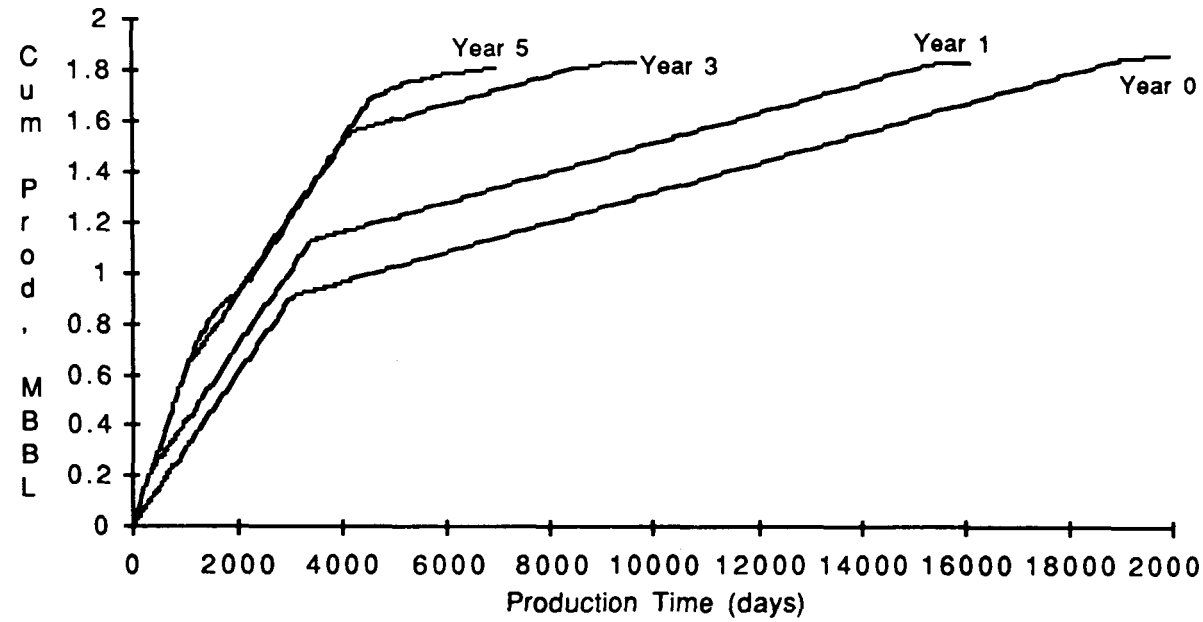


FIGURE 107. - Cumulative oil productions at four waterflooding initiation times (1,500 md, 35° API, 40 acres, and 300 BPD well capacity).

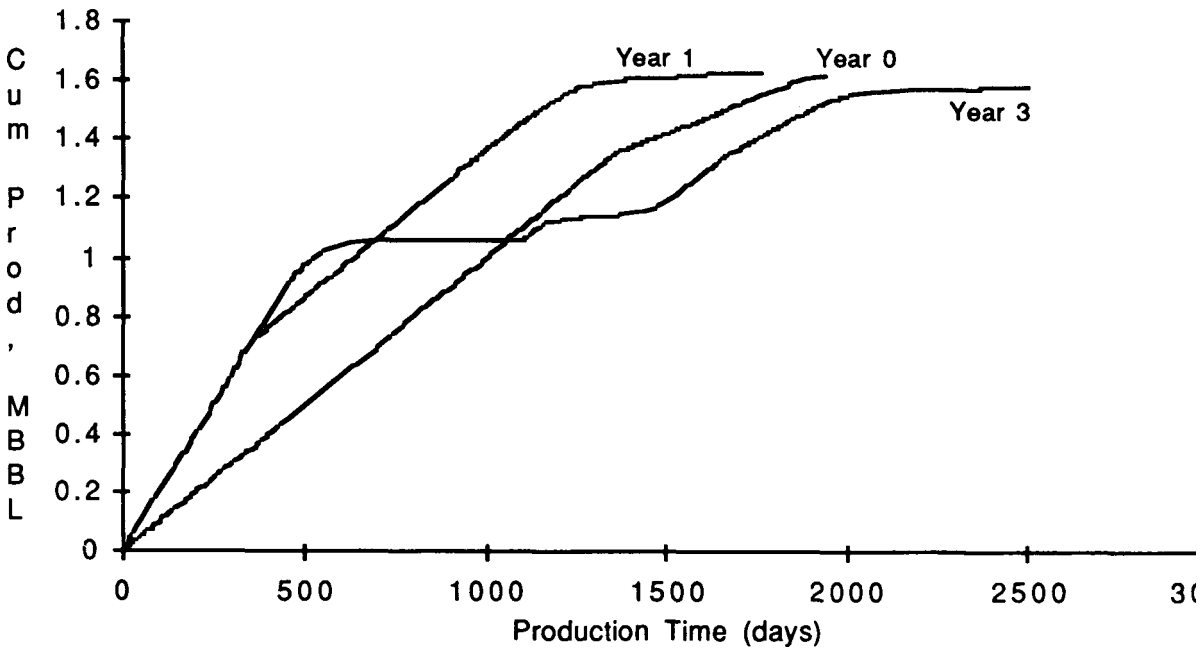


FIGURE 108. - Cumulative oil productions at four waterflooding initiation times (1,500 md, 45° API, 40 acres, and 1,000 BPD well capacity).

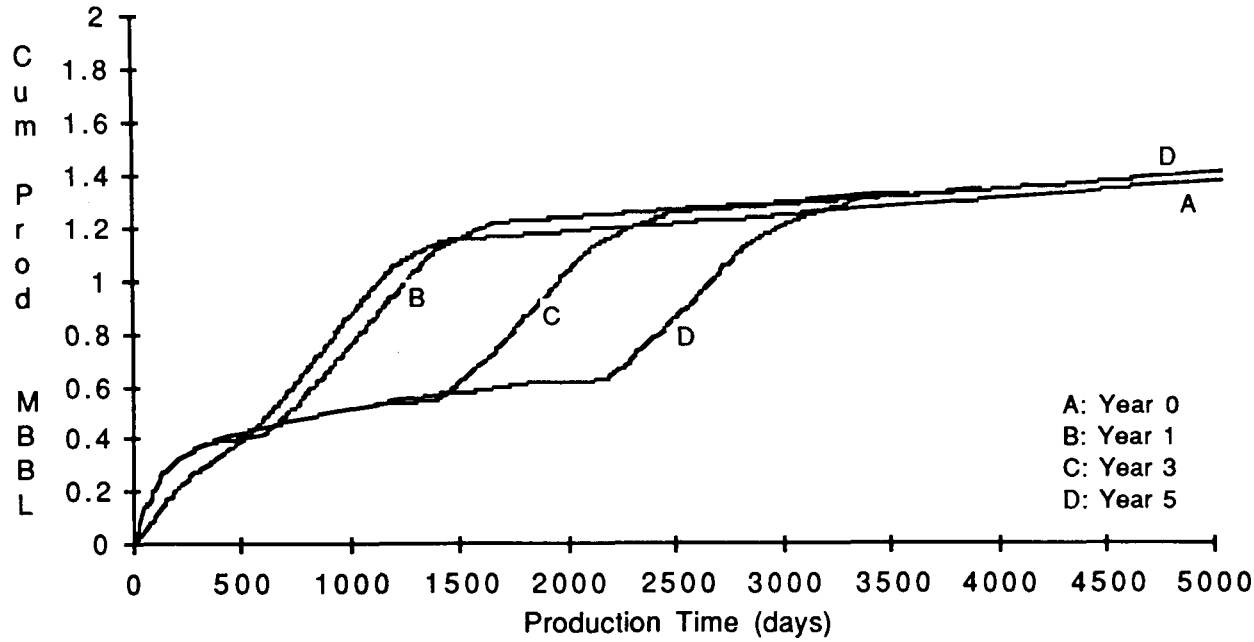


FIGURE 109. - Cumulative oil productions at four waterflooding initiation times (1,500 md, 25° API, 40 acres, and 1,000 BPD well capacity.

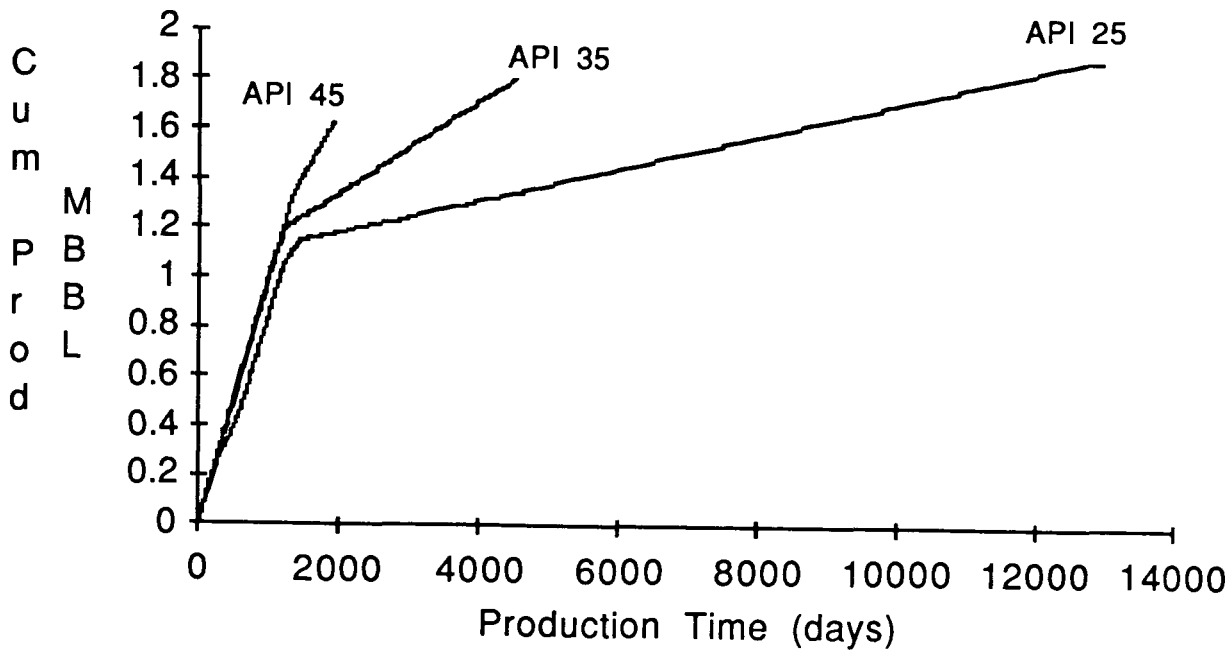


FIGURE 110. - Cumulative production of oil of three API gravities when water flooding was being initiated at year 0.

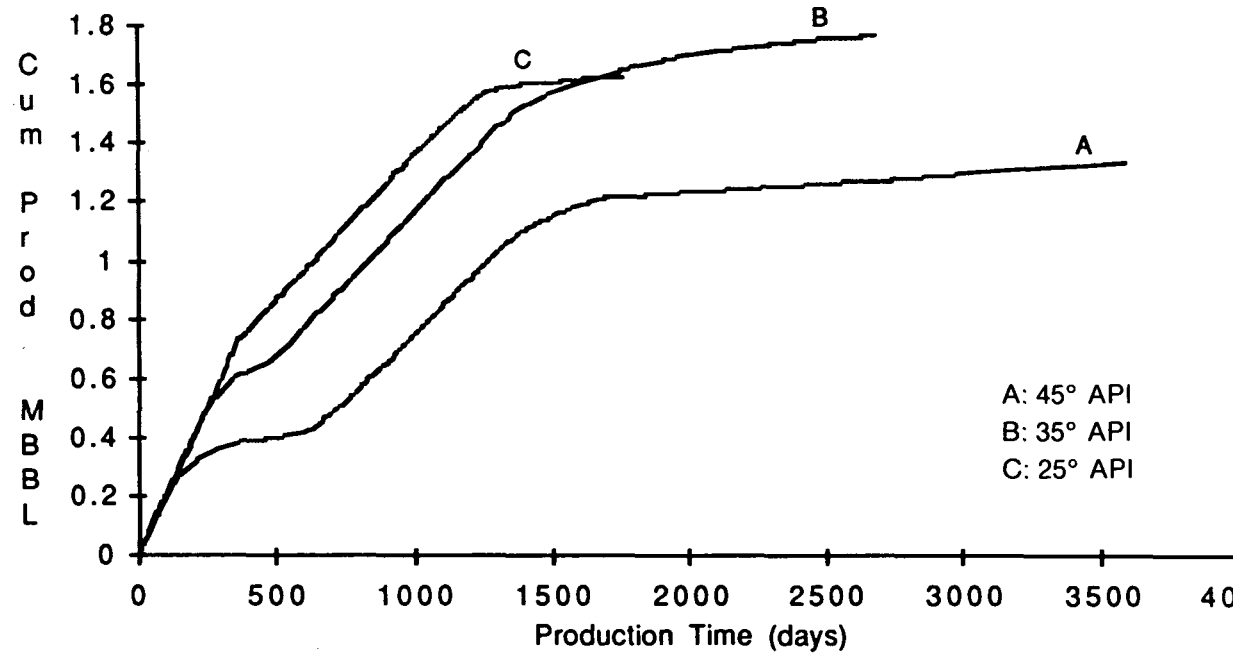


FIGURE 111. - Cumulative production of oil of three API gravities when wate flooding was being initiated at year 1.

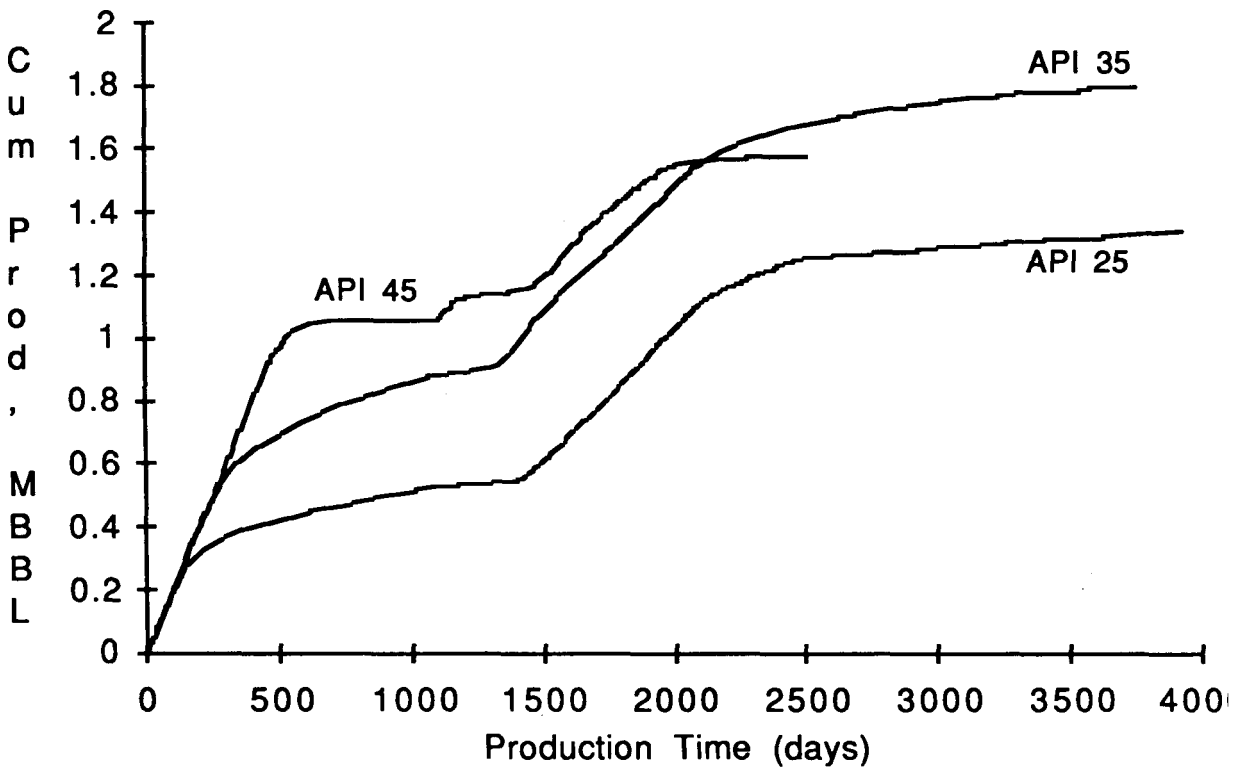


FIGURE 112. - Cumulative production of oil of three API gravities when waterflooding was being initiated at year 3.

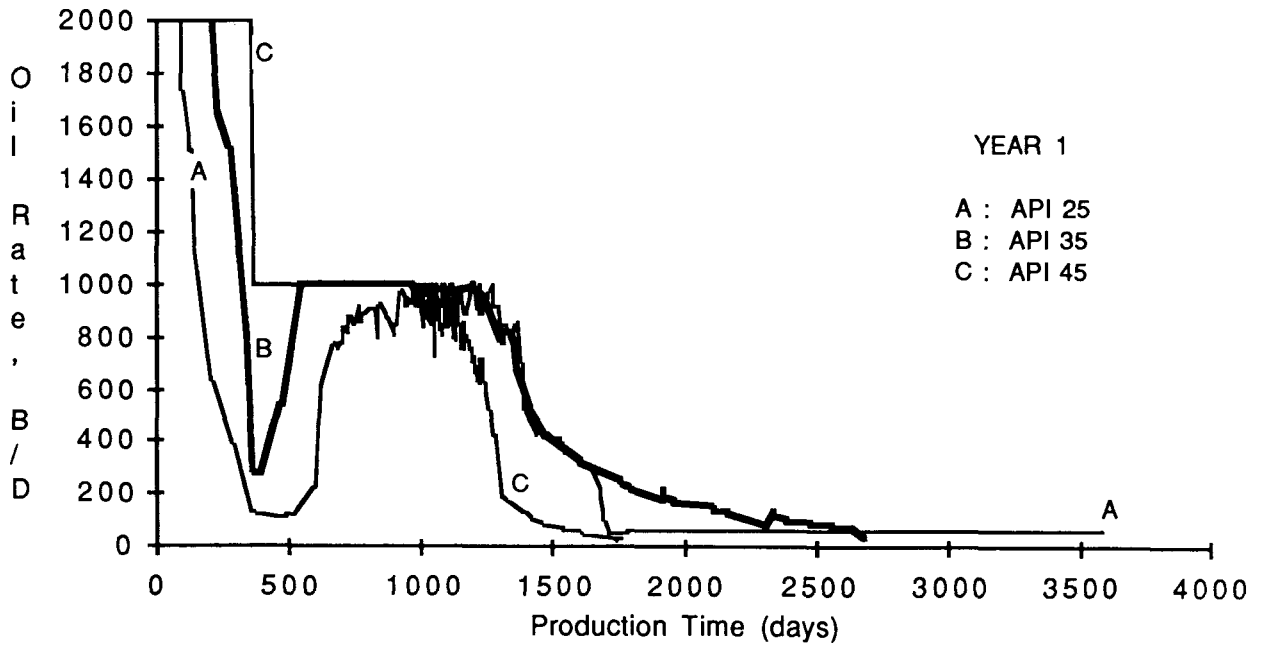


FIGURE 113. - Production rates of oil of three API gravities when waterflooding was being initiated at year 1.

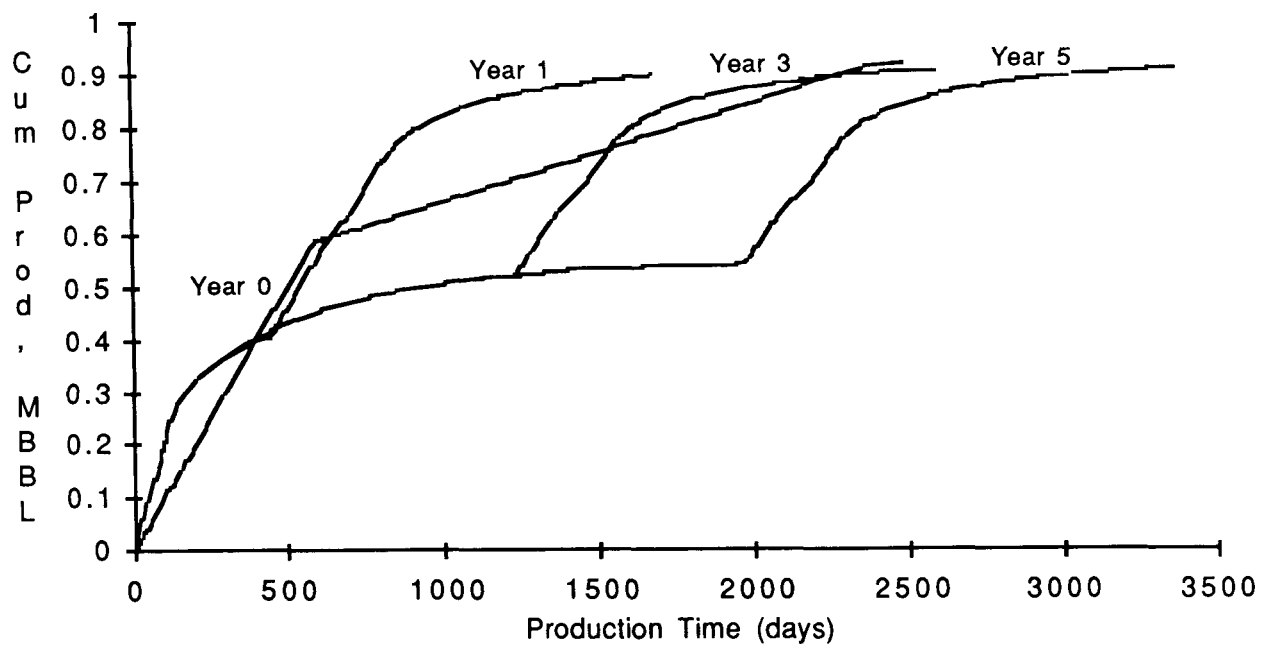


FIGURE 114. - Cumulative oil productions at four waterflooding initiation times (1,500 md, 35° API, 20 acres, and 1,000 BPD well capacity).

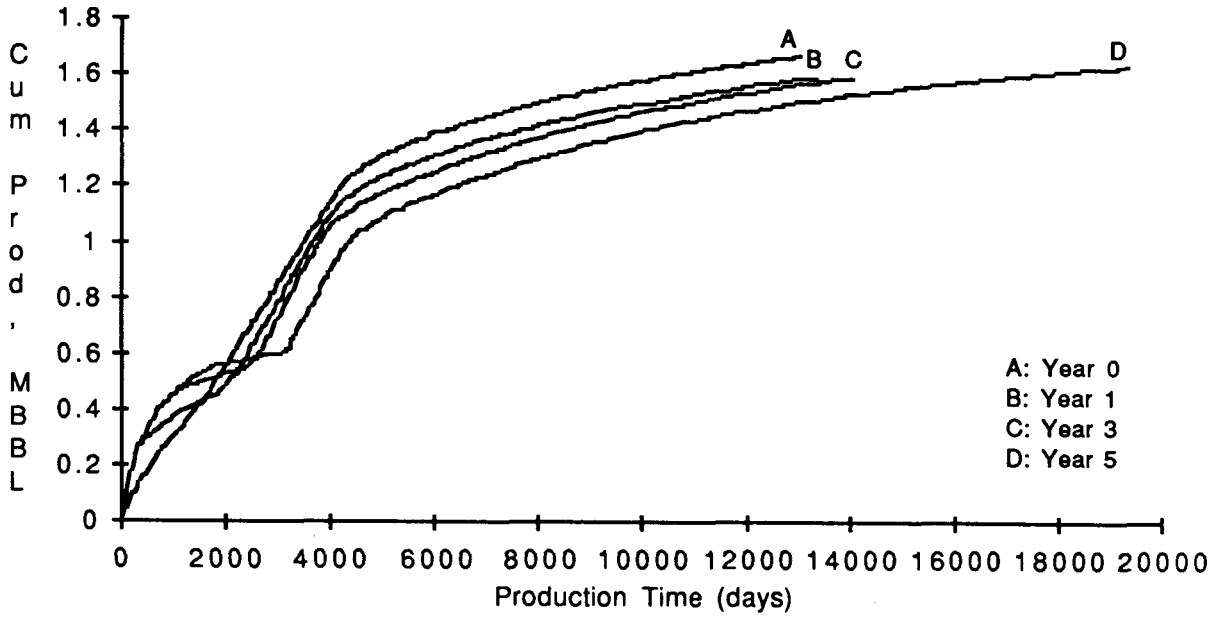


FIGURE 115. - Cumulative oil productions at four waterflooding initiation times (150 md, 35° API, 40 acres, and 1,000 BPD well capacity).

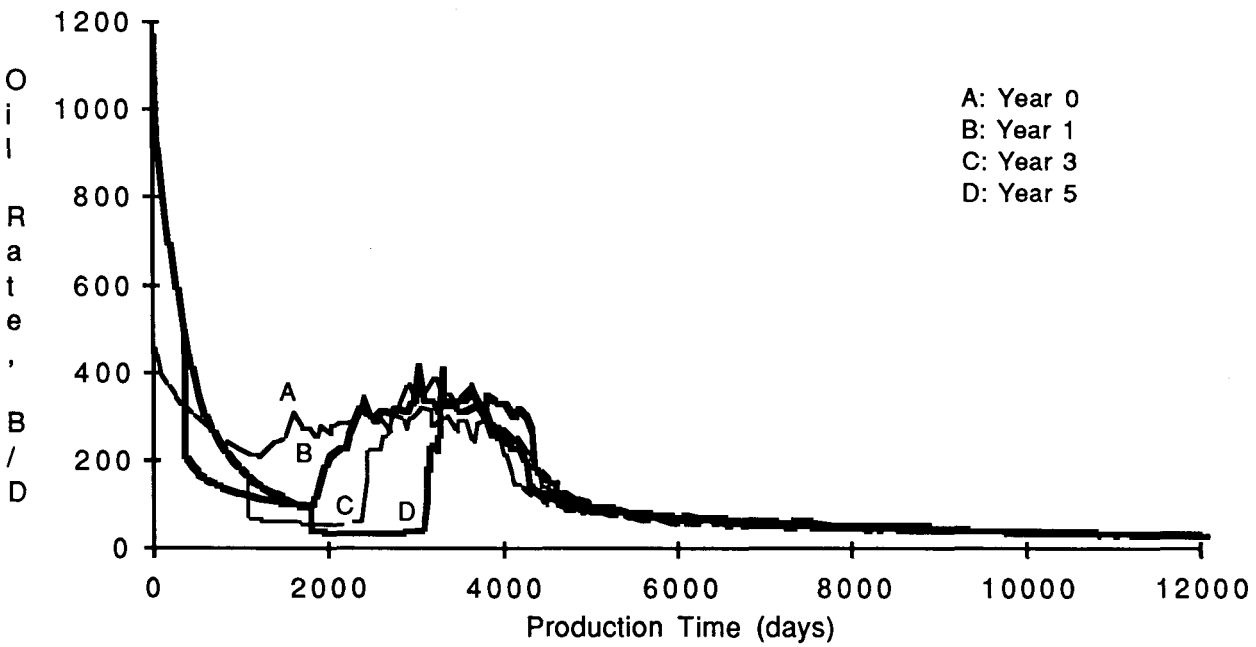


FIGURE 116. - Oil production rates at four waterflooding initiation times (150 md, 35° API, 40 acres, and 1,000 BPD well capacity).

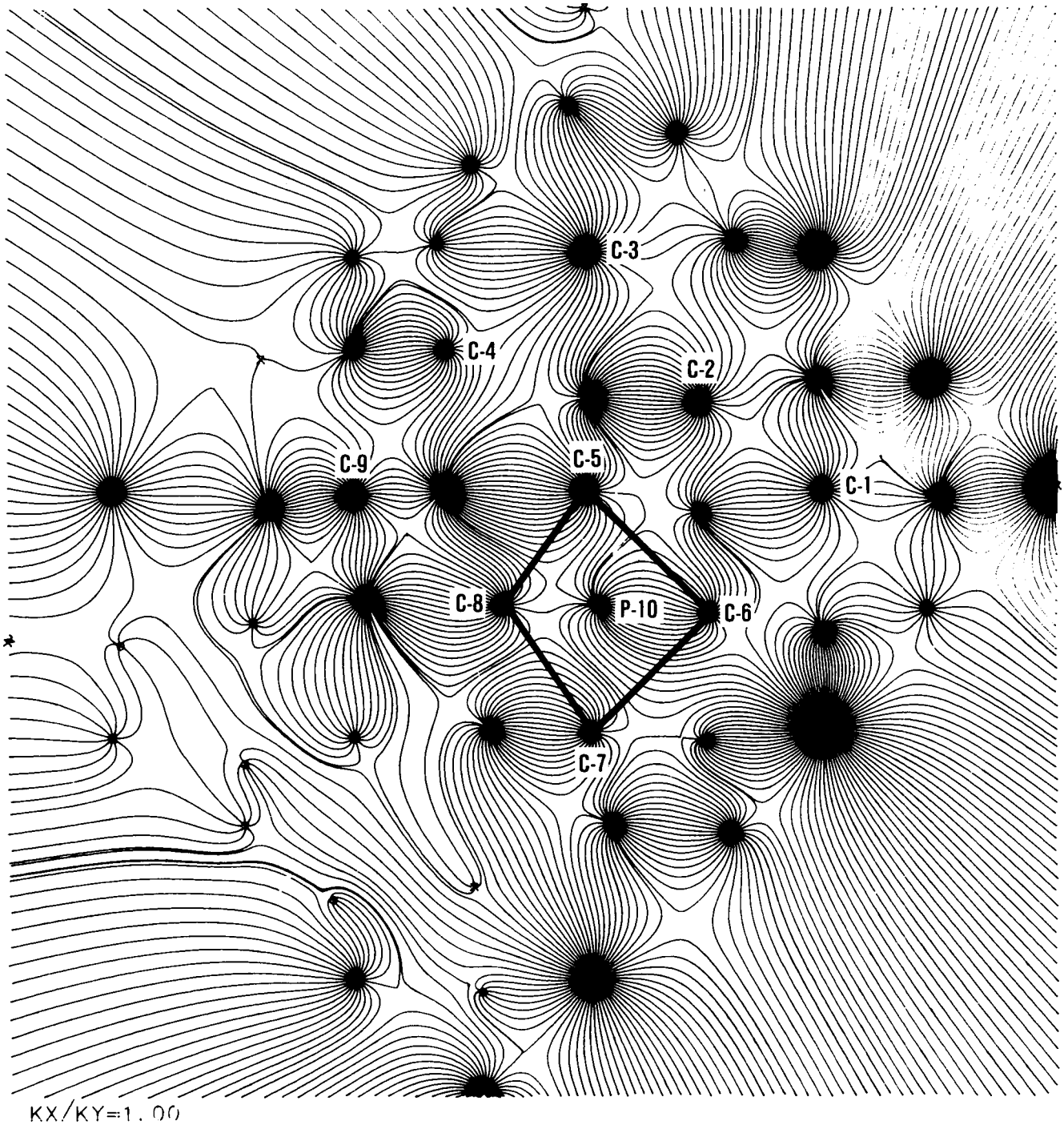


FIGURE 117. - Bell Creek TIP - streamlines for the preflush period.

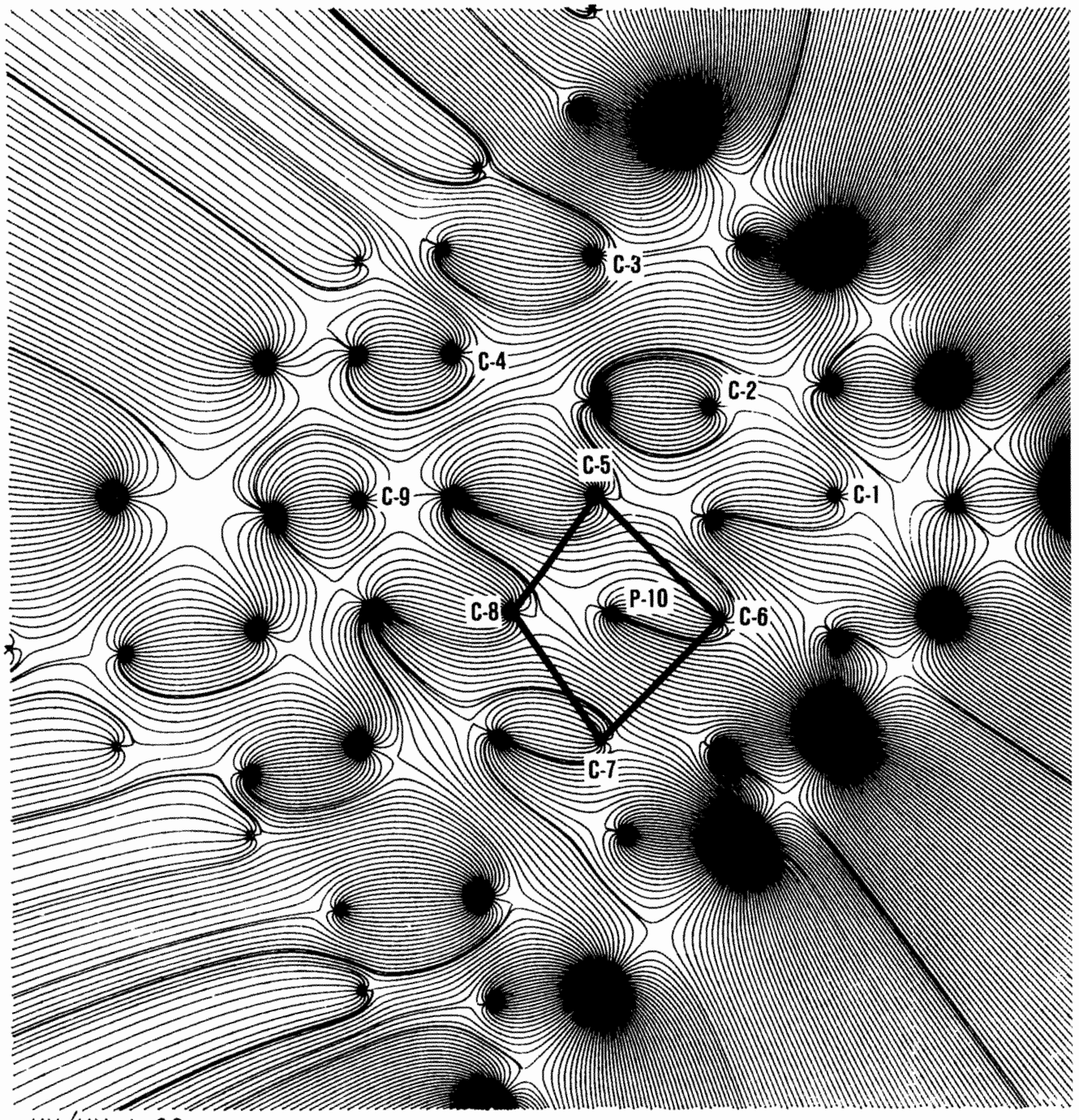


FIGURE 118. - Bell Creek TIP - streamlines for the chemical injection period.

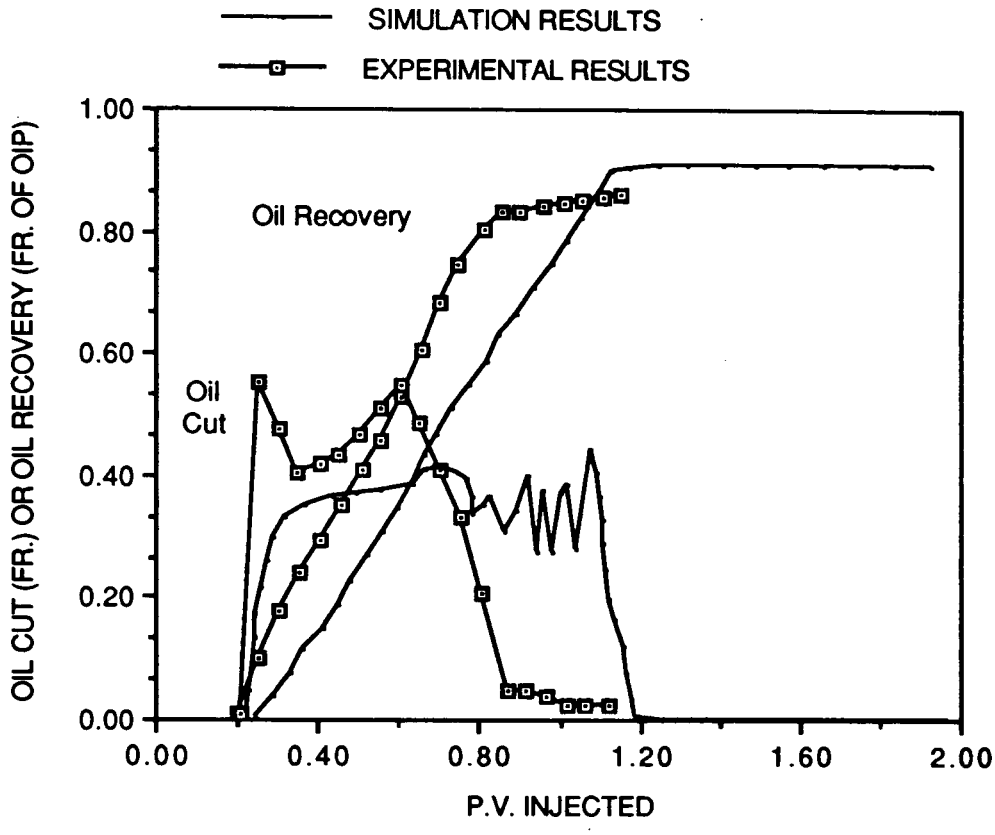


FIGURE 119. - Comparison of the experimental and simulated oil cut (fr.) and oil recovery (fr. of OIP) for the 0.03-PV surfactant slug coreflood.

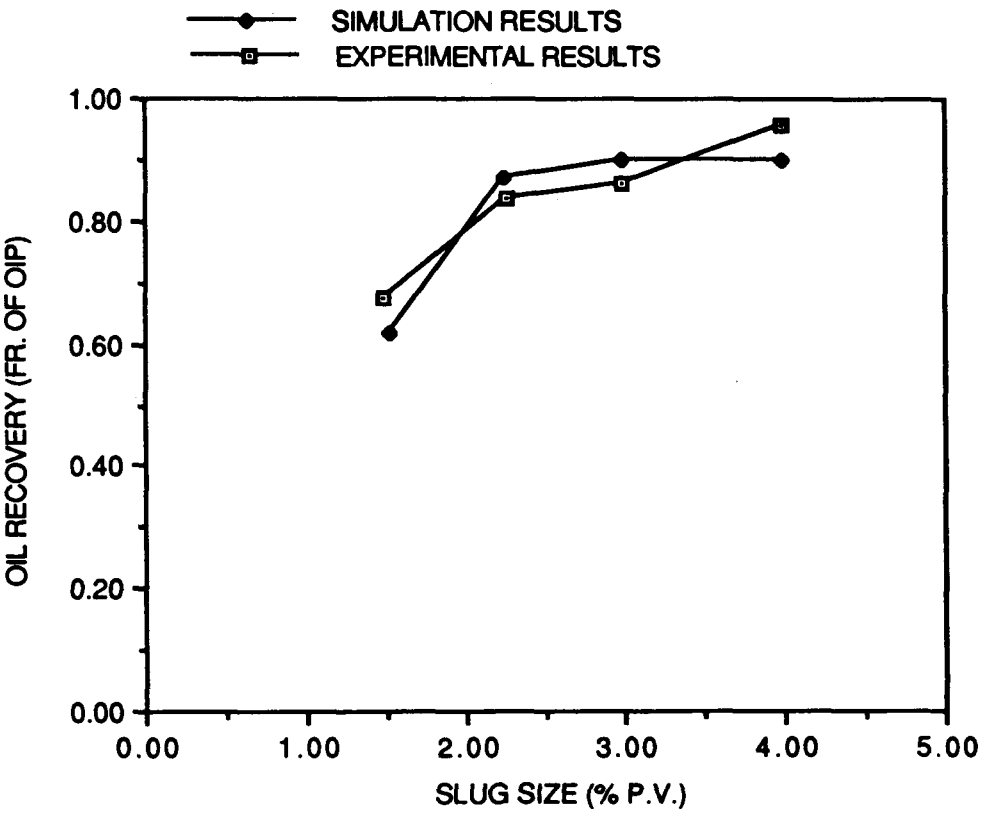


FIGURE 120. - Comparison of experimental and simulated oil recoveries (fr. of OIP) as a function of slug size (% PV).

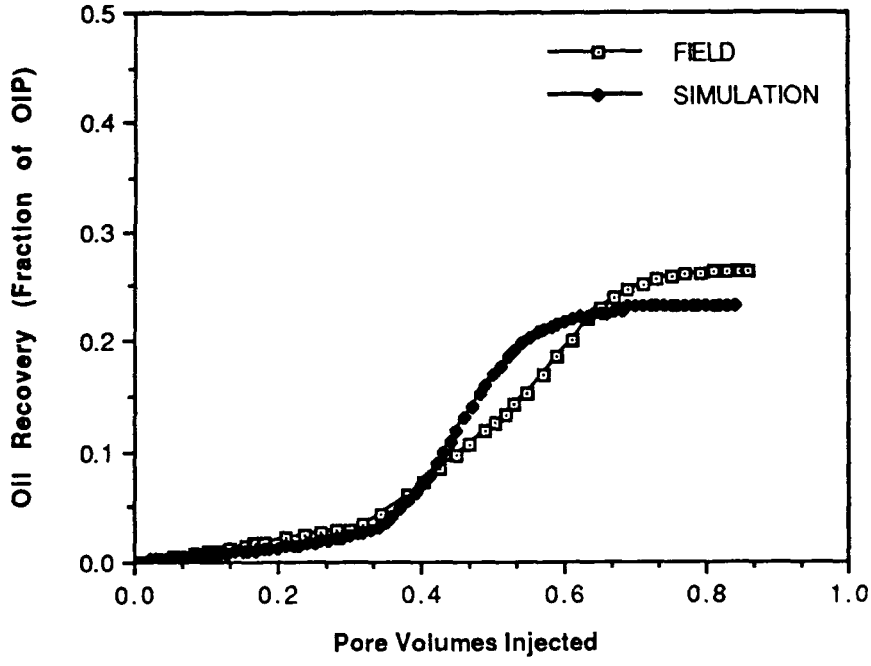


FIGURE 121. - Comparison of field and simulated oil recoveries.

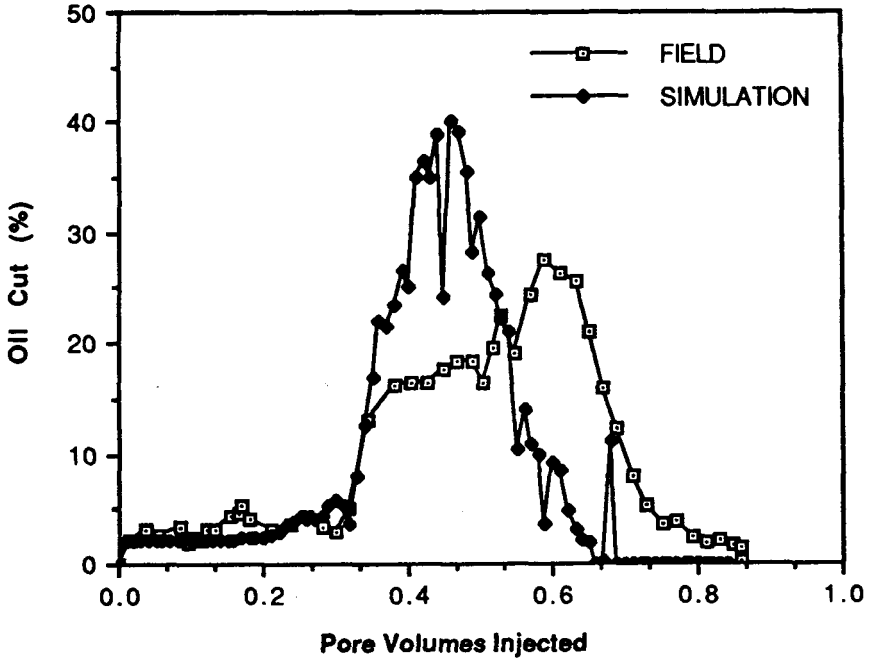


FIGURE 122. - Comparison of field and simulated oil cuts.

# CHAPTER 8. - METHODOLOGY FO RESERVOIR CHARACTERIZATION

## Methodology for Integrated Reservoir Characterization

Criteria for the identification of a barrier island system and the characteristics of its components are described in Chapter 4. Heterogeneities are classified, and their influence on production performance is summarized in tables 25 and 32 through 35. Wireline log interpretation procedures for the identification of reservoir architecture and framework delineation, distribution of petrophysical properties, and vertical distribution of water saturation in a sandstone deposit are also outlined in Chapter 4.

A log/core technique for the separation of facies by integrating log information with core descriptions was developed. Once the facies boundaries have been identified, the reservoir framework can be delineated. From the facies information and from petrophysical data, the stratigraphic cross sections were constructed for studying the architecture of barrier island sandstones. Methods for calculating the clay content index, 'sand cleanness' indices from analyses of available logs, and geological and petrographical data can then be described.

Sources of information and the sequence of information gathered from the literature, reservoir of interest, nearby reservoirs, analogous outcrops, and analogous modern deposits, leading to the construction of a quantitative geological model are organized as a flow chart in figure 123. This chart shows the integration of the geological model with the engineering model which is a geological-engineering model for future reservoir performance prediction. Geological and engineering data required for reservoir descriptions are outlined in tables 8 and 29. The chronology for determining necessary data at each stage of production is indicated in figure 77. The reliability of data is summarized in table 30.

Figure 124 summarizes geological and engineering elements that need to be assimilated for the construction of a quantitative, predictive hydrodynamic geological/engineering model.

Flow charts for constructing predictive geological, diagenetic, geochemical, structural, and engineering models were developed to facilitate the interdisciplinary integration. The procedure for supplementing the

subsurface data with quantitative data from analogous outcrops was also outlined. Based on the integrated geological/engineering model, flow charts were developed for mathematical simulations to predict performance at various stages of production.

## Reservoir Characterization Expert System

Reservoir characterization involves a synergistic approach to the integration of geological and engineering data. Reservoir characterization studies require both geological and engineering understanding which is not an easy task. The development of the expert system,[1] a technique of artificial intelligence (AI), provides a tool to use the knowledge base from reservoir characterization research by users who have little background in the integrative approach to reservoir characterization.

An expert system was developed in this study to advise users how to properly collect both geological and engineering data for building a hydrodynamic flow model. This established model was verified by comparing field production data with simulated results. Discrepancies found from simulation results indicate the need to refine the geological/engineering model. A verified reservoir model can then be used to predict the future performance of reservoirs. This system outlines the basic steps for characterizing a reservoir.

### Background

An expert system is a computer program that solves problems in much the same manner as human experts. It was not until the late 1970s that AI scientists began to realize that the problem-solving power of a program comes from the knowledge it possesses, not just from the formalism and inference schemes it employs. This realization led to the development of special-purpose computer programs that were expert in some narrow problem area. The process of building an expert system involves an "extraction" from human experts of their procedures, strategies, and rules of thumb for problem solving and building of this knowledge into a computer program. The heart of an expert system is the powerful knowledge that accumulates during system building. The knowledge is explicit and organized to simplify decision

making. Compared to human expertise, artificial expertise in an expert system is permanent, consistent, affordable, easy to transfer, and easy to document.

Many knowledge-based expert systems are now feasible for several domains of expertise. Some of the better-known expert systems have been used for diagnostic tools in the medical profession, chemical analyses, criminal investigations, and various applications in military strategy. Among other purposes are expert systems that help geologists and engineers in earth science applications. One known example is PROSPECTOR[2] which acts as a consultant to aid exploration geologists in their search for ore deposits. Given field data about a geological region, it estimates the likelihood of finding particular types of mineral deposits there. Other expert systems developed in earth science include DIPMETER ADVISER,[3] DRILLING ADVISER,[4] ELAS,[5] HYDRO,[6] LITHO,[7] MUD,[8] and XEOD.[9] Schlumberger's DIPMETER ADVISER infers subsurface geological structure by interpreting dipmeter logs and measurements of the conductivity of rock in and around a borehole as related to depth below the surface. Teknowledge's DRILLING ADVISER diagnoses the mostly likely causes of sticking and recommends a set of treatments to solve that problem. AMOCO's ELAS gives advice on how to control and interpret results from an interactive program for well log analysis and display. NL Baroid's MUD helps engineers maintain optimal drilling fluid properties. It does this by diagnosing the causes of problems with drilling fluids and suggesting treatments. The University of Alabama's XEOD determines clastic depositional environments based on the associations between 166 observable features and 58 environmental facies and subfacies. A set of features from a single bed or facies yields a set of possible environmental interpretations, ranked by likelihood based on certain values computed from the rules. In total, however, only a few expert systems that interpret formation heterogeneities are being applied in the earth sciences.

## Logical Flow of Reservoir Characterization Expert System

Figure 123 shows basic procedures for establishing and improving a reservoir model using an expert system. The system starts by establishing the stage of recovery and proposes a recovery mechanism to be modeled for the target reservoir. The reservoir data collection[10] falls into two major categories: geology and engineering.

## Geological Considerations

The reservoir characterization expert system considers geological data based on the following priorities: real reservoir data, previous information about the formation of interest from the literature, data of nearby reservoirs in the same formation, nearby analogous outcrop data, and information about depositionally analogous deposits in modern environments. When a geological model is not detailed enough for a given production stage and proposed recovery mechanism, the user is recommended to collect additional subsurface data until the environment of deposition can be positively identified. The determination of the deposition environment is important because predictable, characteristic properties of critical reservoir parameters exist in reservoirs deposited in similar depositional environments. After the depositional environment is identified, the geological model will be examined if core and other hard data adequate for the level of reservoir heterogeneities are currently viewed. Any inadequacy in the model requires a search for additional information. Information from literature gathered is followed by checking whether a nearby reservoir in the same formation is available. When available data indicate a favorable match with the reservoir being evaluated, depositional, diagenetic, and tectonic information is extracted, and quantitative engineering characteristics of all critical geological components are gathered for establishing or improving the geological model of the target reservoir. Similar procedures are recommended for nearby analogous outcrops of the same formation and depositionally analogous deposits in modern environments. The existing geological model will be supplemented with information available for all above data areas. This model will then be re-examined for its adequacy in describing reservoir heterogeneities required for the desired stage of production. An adequate geological model will be combined with the engineering model later to form a hydrodynamic flow model. Additional surface and/or subsurface data collected from the reservoir, related literature, and analogous outcrops and/or modern deposits are recommended if an adequate geological model cannot be constructed based on available data.

## Engineering Considerations

Engineering data are collected to identify reservoir heterogeneities and furnish required rock, rock-fluid, and fluid properties for use in mathematical simulations. Production/pressure and/or other general engineering data, depending on the reservoir's stage of production will also be examined for indications of reservoir heterogeneity. Other engineering tests such as wireline logs and well tests will supplement production and rock-fluid properties. The engineering information obtained will be combined with the geological model. The model will be further refined with a collection of further engineering data before a mathematical simulation of the model is conducted.

## Hydrodynamic Flow Model and Mathematical Simulation

The hydrodynamic flow model is an integration of geological and engineering models and shows the flow path in the reservoir rock. A mathematical simulator is used as a tool in this expert system to verify the hydrodynamic flow simulation.

An appropriate mathematical model for the target reservoir is selected. The simulation based on the hydrodynamic flow model is then performed to match the production history. Discrepancies identified by simulation require further improvement of the flow model. The model could be revised by collecting additional core data and engineering tests to better define the nature and magnitude of the responsible heterogeneities. The above model verification and refinement are continued, based on the field production performance, until a satisfactory model is obtained. This model can then be used to predict the fluid production and residual oil saturation distribution based on alternative production schemes.

## Features of Developed Expert System

To make this expert system versatile, the program was written in BASIC language under the environment of an IBM personal computer. The program is made from a series of simple "yes" or "no" questions. Based on answers received, the user might be asked different questions to construct, integrate, or verify the reservoir model. At the end of the program run, conclusions

will be made, and suggestions will be provided. Certain rules of thumb are provided for cases in which real data are difficult to obtain.

A "HELP" session is added in the program to explain certain key terms in the expert system that may not be familiar to users who can interrupt the program whenever they wish to use the "HELP" session.

Different from the standard rule-based expert system, the system developed in this study uses a conventional deterministic algorithm to reach the conclusion. This system simplifies a complicated logical flow chart into an easily used program.

## CONCLUSIONS

The following conclusions were made from this work:

1. The expert system developed in this research simplifies and converts complicated reservoir model-development work into an easily used program.

2. The program advises users how to collect data and verify the model and is the first phase of the reservoir characterization expert system.

## REFERENCES

1. Waterman, D. A. A Guide to Expert Systems. Addison-Wesley Publishing Co., Reading, Mass., 1985.

2. Gaschnig, J. PROSPECTOR: An Expert System for Mineral Exploration. Machine Intelligence, Infotech State-of-the-Art Report 9, No. 3, 1981.

3. Davis, R., H. Austin, I. Carlbom, B. Frawley, P. Purchnik, R. Sneiderman, and J. A. Gilreath. The Dipmeter Advisor: Interpretation of Geologic Signals. Proceedings IJCAI-81, 1981, pp. 846-849.

4. Hollander, C. R. and Y. Iwasaki. The Drilling Advisor: An Expert System Application. Fundamentals of Knowledge Engineering, Teknowledge Report, 1983.

5. Apte, Chidanand. Expert Knowledge Management of Multi-Level Modeling With an Application to Well-Log Analysis. Report LCSR-TR-41, Laboratory for Computer Science Research, Rutgers University, December 1982.

6. Gaschnig, J., R. Rebon, and J. Reiter. Development of a Knowledge-Based Expert System for Water Resource Problems. Report SRI 1619, AI Center, SRI International, Menlo Park, CA, August 1981.

7. Bonnet, A. and C. Dahan. Oil-well Data Interpretation Using Expert System and Pattern Recognition Technique. Proceedings IJCAI-83, 1983, pp. 185-189.

8. Kahn, G. and J. McDermott. MUD, a Drilling Fluids Consultant. Technical Report, Department of Computer Science, Carnegie-Mellon Univ., 1984.

9. Shultz, A. W. XEOD: An Expert System for Determining Clastic Depositional Environments. Geobyte, May 1988, pp. 22-32.

10. Szpakiewicz, M. J. Geological Problems Related to Characterization of Clastic Reservoirs for Enhanced Oil Recovery. Pres. at SPE/DOE Fifth Symposium on Enhanced Oil Recovery, Tulsa, OK, Apr. 20-23, 1984. SPE/DOE paper 14888. SPE Formation Evaluation, December 1987, pp. 449-460.

## CONSTRUCTION OF INTEGRATED ENGINEERING MODEL FOR PREDICTION OF FLUID FLOW PATTERN AND TRAPPING

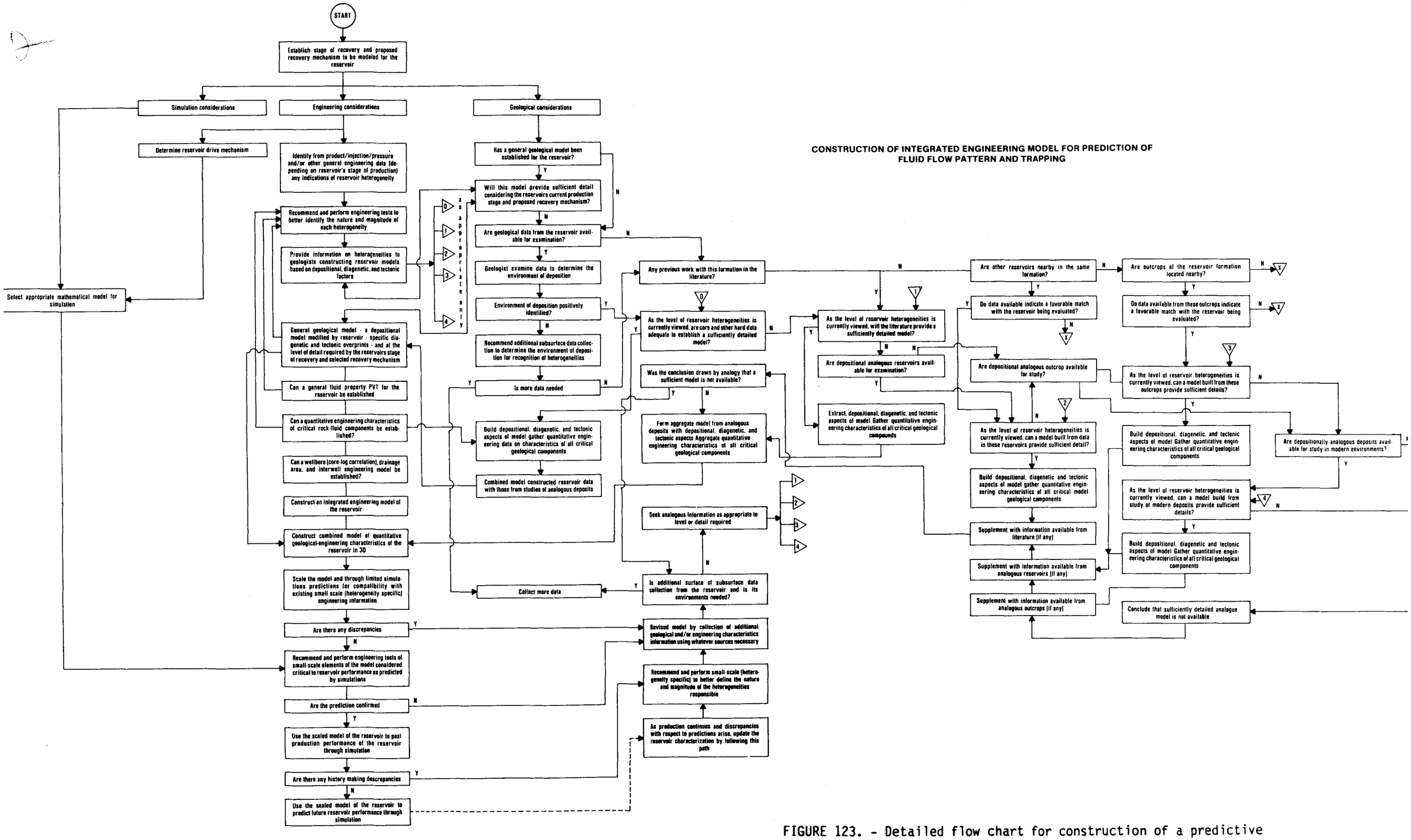


FIGURE 123. - Detailed flow chart for construction of a predictive hydrodynamic model.

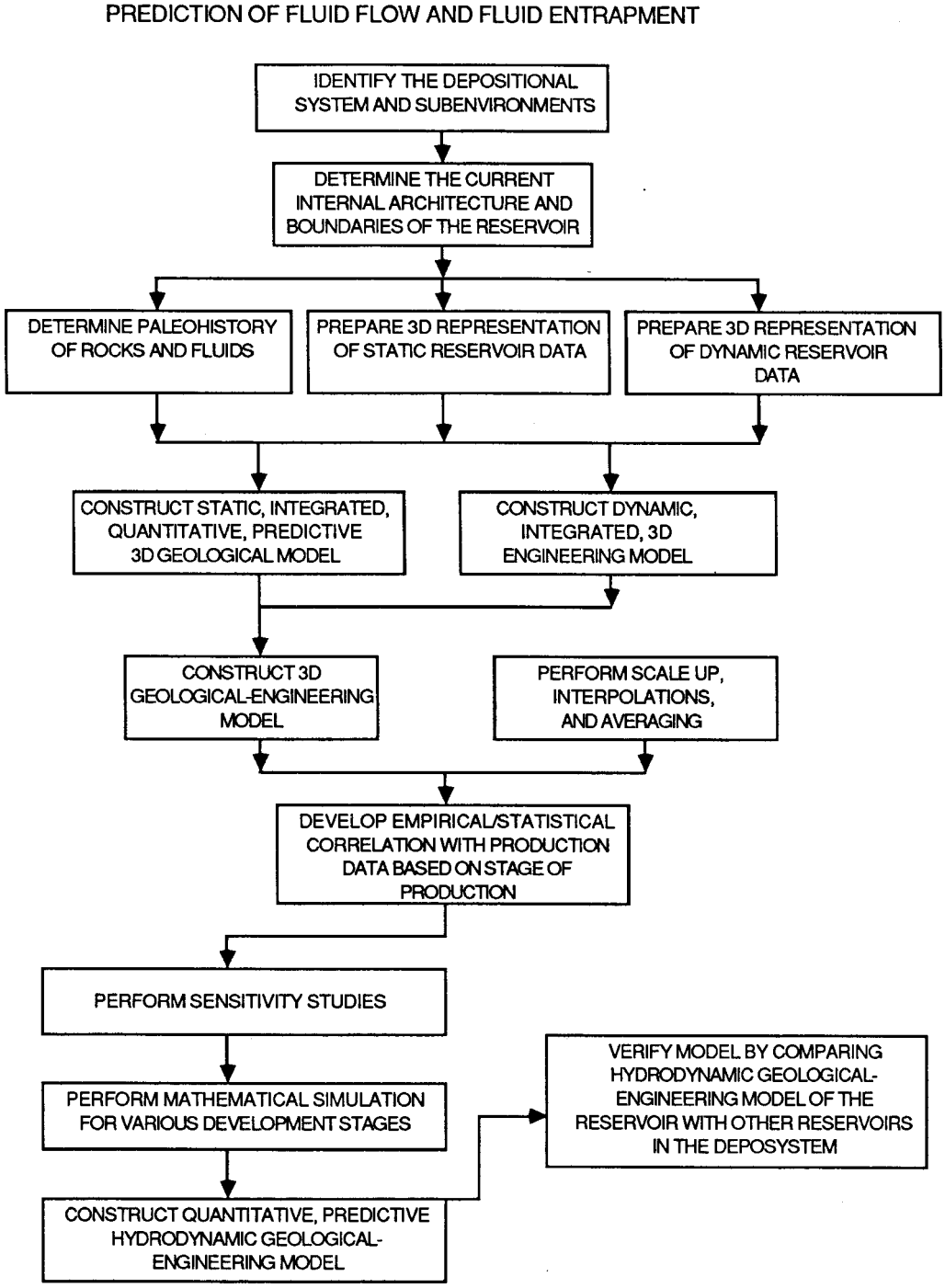


FIGURE 124. - Summary flow chart for development of an integrated, predictive hydrodynamic model showing interrelationship of discipines and timing of studies.

# CHAPTER 9. - SUMMARY OF GEOLOGICAL AND ENGINEERING MODELS OF BARRIER ISLAND SYSTEM BASED ON THE MUDDY FORMATION IN BELL CREEK OIL FIELD AND OUTCROPS IN NE WYOMING

## Geological Summary

### Depositional Aspects

#### Facies Divisions

Bell Creek (MT) field produces from Lower Cretaceous (Albian) barrier island sandstone and valley fill deposits of the Muddy formation.

Facies are distinguished on the basis of grain size, lithology, mineralogy, occurrence, and quantifiable proportions of sedimentary and biogenic structures. Permeability and porosity values correspond to the depositional energy which formed the facies. The foreshore, upper shoreface, upper part of middle shoreface, and washover facies were deposited by high-velocity currents, waves, and tides. They are commonly associated with the highest permeability and porosity values in Bell Creek field. Backshore and lower shoreface deposits are associated with intermediate to low values of permeability and porosity, whereas paralic and valley fill deposits exhibit the lowest permeability and porosity values.

Tidal channel fill and ebb and flood tidal delta facies are genetically associated with the barrier island depositional system. These facies are not emphasized in this model because of insufficient documentation in cores and outcrops.

#### Vertical Sequence of Facies

The vertical sequence of facies in barrier island deposits varies due to relative fluctuations in sea level which can shift the axis of the bar landward or seaward. A typical and complete sequence for regressive barrier island deposits can be described as (from bottom to top): marine shale, transition, lower shoreface, middle shoreface, upper shoreface, foreshore, backshore, washover, and lagoon facies. Within one cycle of barrier island facies, grain size and sorting generally increase toward the top, while shale content and amount of burrowing decrease toward the top. However, transgressive conditions also occur in the Muddy formation in Bell Creek Unit 'A' and are illustrated by the barrier island facies overlying and interfingering with lagoonal facies on the backbarrier side of the buildup.

The vertical sequence of facies is further complicated because stacked, incomplete sequences are often encountered. The stacking of barrier island cycles originated from the fluctuation of relative sea levels.

Generally, permeability and porosity increase upwards within a depositional cycle; however, the sequence is typically overlain by thin, lower permeability backshore and lagoonal deposits (fig. 88), and/or unconformably overlain by valley fill deposits.

## Associated Nonbarrier Deposits

Two postdeposition erosional events are indicated which resulted in ribbon-like valley cuts of different orientation and the low-relief valley cuts that and the low-relief valley cuts that reduced the thickness of barrier island deposits. Valley cuts are typically filled with mostly nonproductive fine-grained, clay-rich sediments. Valley fill deposits are commonly associated with other documented barrier island deposits. They are a dominant feature used to differentiate properties and productivity of the Muddy formation in Bell Creek field.

The common thickness of the valley fill sandstones in Bell Creek field is 4 to 11 ft. The average thickness of incised valley fill sediments is about 24 ft. Depths of incisions vary, and sometimes, they have completely removed the 30-ft-thick barrier island sand body and cut off hydraulic communication between major production units. More commonly, the valley incisions cut part-way through and their sediments communicate hydraulically with barrier island sandstones or are separated from barrier island sandstones by a few feet of lagoonal and estuarine deposits.

## Permeability Units

Three major permeability units can be distinguished in Bell Creek reservoir. The highest permeability unit consists of the foreshore, upper shoreface, middle shoreface, and washover facies. The intermediate unit contains the backshore and associated tidal sandstone facies, while the lower shoreface and lagoonal facies are the lowest permeability units. For this deposit, a three-layer model adequately describes petrophysical properties of the reservoir although in certain areas diagenesis significantly modified the normal, depositionally related permeability pattern.

## DIAGENETIC ASPECTS

Foreshore, shoreface, and washover facies have similar mineralogic and petrographic characteristics. These facies comprise sandstones which are moderately to well sorted, very fine to fine-grained quartzarenite and subarkose. Lower shoreface and some samples from the washover facies, however, tend to contain more clay cement and matrix. Individual barrier facies cannot be distinguished by framework mineralogy, grain size, or clay content alone.

Two distinct suites of clay exist: within barrier island sandstones kaolinite is twice as common as illite, whereas in valley fill sandstones and mudstones, smectite and kaolinite are the dominant clay minerals. Within the barrier island sandstone, kaolinite cement commonly forms coatings up to 30 microns thick on detrital grains formed as microporous monomineralic pore fillings. As little as 1% clay cement concentrated in pore throat regions has been shown to greatly reduce permeability. A concomitant increase in compaction further accents permeability reduction caused by clays blocking pore throats.

The distribution of clays had a significant influence on primary, secondary, and tertiary production patterns. Total clay and diagenetic clay distributions are similar to the distribution of average horizontal air permeability within the study area.

Aside from clays, which may account for up to 15% of rock, the only other volumetrically significant cement was calcite. Calcite is not common within cored samples at Bell Creek Unit 'A'; however, when it comprises more than 2 to 5% of the rock, permeability is generally less than a few 10's of millidarcies.

Early and late-stage leaching enhanced porosity in barrier island sandstones by creating oversized pores and corroding or completely removing unstable grains. Leaching created widespread secondary porosity within the upper facies of each barrier sequence.

Silicon cement occurs as syntaxial quartz overgrowths, and while not volumetrically significant, it provided sufficient consolidation to negate the effect of grain collapse after leaching.

## STRUCTURAL ASPECTS

Development and characteristics of the Muddy formation in the Bell Creek area; i.e., pattern of accumulation, submergence, erosion, and burial, are apparently tectonic related. The barrier island sands were deposited on structural paleo highs elevated by block movement of the basement. Observed reservoir architecture; i.e., stacking of barrier cycles and the relationship of major sandstone facies to the nonreservoir open marine and paralic facies, resulted from relative sea level changes caused by local and regional subsidence and uplift. The shifting of sand bodies seaward and landward followed the fluctuations of sea level. Erosional and depositional relationships between continental and marine environments resulted from the same mechanism. Large-scale tectonic movements caused major transgression spreading the sea over the Bell Creek area and covering the entire Muddy depositional complex with 200 ft of marine Mowry shales.

Postdepositional structural events included an uplift of the Black Hills and continued subsidence of the Powder River Basin which resulted in the present position of Bell Creek reservoir on the north-eastern flank of the basin.

Current tectonic features are site-specific but resemble the regional structural framework. Densely spaced NW-SE and NE-SW oriented small throw faults were documented in this study in Unit 'A' of Bell Creek field. Their role in conducting oil from a source rock to the reservoir is not clear. The Muddy formation is tightly encased in thick series of marine shales. Extensive late diagenesis documented in productive facies required large volumes of fluids to flush the reservoir. Oil and formation water entered and exited the sandstone body most probably through faults. The geothermal anomaly in Bell Creek field, with a temperature gradient nearly twice as high within the productive area as that around the edges, indicates a still active hydrodynamic system.

The ratio of fault throws to thickness of productive intervals varies from 0.5 to 2.0. In certain cases, the continuity of sandstone bodies is completely disrupted. The checking of formation and injected fluids in fault zones, even in case of small throws (5 to 10 ft), must be significant, considering the small average thickness of the oil-bearing sandstone (20 ft). Well test results corroborate the geologic conclusion that faults form

local barriers to flow. In addition, upthrown blocks produce more oil than water, whereas the results are opposite for downthrown tectonic blocks.

The relationship between conductivity along fault planes and associated fractures is not clear. However, there are strong indications of preferential flow of injected water along some NW-SE oriented faults.

Monitoring of changes in electrical resistivity provides a good indication of volumetric sweep and displacement efficiencies during the depletion of reservoirs. Separation of highly productive barrier island facies from nonbarrier and lower shoreface facies, based on application of Pickett's crossplot of formation resistivity obtained by plotting induction log values against the density log derived porosity proved successful.

Indices for clay content and log-derived heterogeneity index were successfully used for determining relative inhomogeneity in the reservoir sandstone.

## Engineering Summary

### Storage Capacity, Transmissivity, and Rock-Fluid Interaction

In the 4 square miles surrounding the TIP area of Unit 'A' of Bell Creek field, the storage capacity varied from 100 to 700% ft, the transmissivity varied from 10,000 to 100,000 md-ft, and the maximum net pay thickness was 26 ft. The preferential direction of flow during waterflood was along the strike of the barrier which coincided with NE regional and local fault direction. The NW trending faults provided local preferential flow channels. Initial oil saturation was about 74%, and mixed wettability behavior was indicated by imbibition tests performed on preserved cores.

The initial oil saturation distribution corresponded to the average distribution of air permeability in the study area. The average residual oil saturation after linedrive waterflooding was about 33% in the study area.

### Pressure, Drive Mechanism, and Prediction

The initial reservoir pressure was abnormally low. In addition, a good pressure communication existed throughout Unit 'A'.

The main reservoir drive mechanism was solution gas drive with a small gas cap and no appreciable water influx.

The linedrive waterflood provided a good areal sweep, whereas in the heterogeneous area of the field a poor vertical sweep efficiency resulted from permeability stratification.

The combined primary and secondary recovery efficiency of Unit 'A' was 55% of the original oil-in-place (OOIP), reducing the average oil saturation to about 33% in the study area. A micellar-polymer flood was responsible for recovering approximately 10% additional of the OOIP within the TIP area.

Primary reserve, initial production, and cumulative primary production followed the depositional trend of the barrier island system whose production quality was determined by superior depositional facies. Lower initial production regions corresponded with regions of high values of Dykstra-Parsons coefficients resulting from the stacking of facies, intercolation of barrier or nonbarrier facies, and diagenetic alteration.

Linedrive waterflood pushed the oil updip against the backbarrier and lagoonal facies where reservoir properties deteriorated. The cumulative secondary production was influenced by structural dip; therefore, downdip producers shared their reserves with all of the updip wells, shifting the area of highest cumulative production updip.

Based on results obtained from the evaluation of the geological model and waterflood simulation, infill drilling in heterogeneous regions of barrier island reservoirs is expected to produce substantial incremental oil production beyond linedrive waterfloods with 40-acre spacing. In the more homogeneous regions of the barrier island studied, the micellar-polymer flood was responsible for significant additional oil recovery.

# CHAPTER 10. - CONCLUSIONS FROM OVERALL STUDY

A hydrodynamic model derived from the integration of four partial geological models (depositional, diagenetic, structural, and interstitial fluids) provides an improved prediction of fluid movement and trapping in the reservoir. Information about the distribution and magnitude of geological heterogeneities can be supplemented by quantitative geological data from analogous reservoirs, outcrops, aquifers, and mines with similar evolutionary histories of the formation. Examples of quantitative geological information derived from integration of outcrop and subsurface data are as follows:

a. distribution of critical geological heterogeneities, their scale and predictability;
b. permeability, porosity, lithology and mineralogy distribution and their interrelationship; and
c. influence of lithology and mineralogy on permeability.

The barrier island depositional system was selected for NIPER reservoir characterization research because of its economic significance and a substantial amount of reserve remained as a target for EOR development. Bell Creek field was selected for detailed study from a list of candidate reservoirs because of the presence of an EOR project, the availability of subsurface data, and the presence of nearby analogous outcrops. The association of valley fill deposits which cut into the underlying barrier island facies was frequently observed in Bell Creek cores, associated outcrops, and several other barrier islands deposits. Valley incisions commonly cut into barrier island facies to varying degrees and typically comprise low quality to nonreservoir sediments. Valley incisions compartmentalize the production units in Bell Creek field and therefore are of critical importance to fluid flow. Valley incisions are associated with barrier island settings other than those at Bell Creek field; however, the pattern of valley cutting is site-specific.

Other common features which can be ascribed with a good deal of confidence to all barrier island systems include the sequence of facies for individual sedimentary cycles and original properties inherited from depositional processes, geometry and continuity of major flow units, and stacking pattern in progradational or regressive cycles. Features unique to the barrier island

depositional system include significant early diagenesis caused by the interaction of marine, brackish, meteoric, and continental-derived waters with unconsolidated sediment and the lateral association with paralic lagoonal or estuarine facies and marine-transitional facies, including ebb and flood tidal deltas. Diagenesis and faulting are the most important site-specific heterogeneities.

Superior reservoir properties were documented for foreshore, upper and middle shoreface, and washover, tidal channel and tidal delta splay facies. Lower permeability sediments prevail in most alluvial valley fills, lower shoreface, paralic facies, and those transitional to marine shales. Storage capacity and flow capacity tend to decrease toward the backbarrier side of the buildup but are highly variable within the barrier.

An integration of log and core data was used to distinguish highly productive from nonproductive intervals within the Muddy formation in non-cored areas. In addition, clay-rich zones and sand cleanness index were identified using wireline logs.

An integration of the subsurface core- and outcrop-derived geological model with production/injection data allowed the ranking of sedimentary, tectonic, and diagenetic heterogeneities relative to overall production performance. Conclusions from the intergration for individual production steps based on data from Unit 'A', Bell Creek field, are as follows:

1. Primary production was dominantly influenced by large-scale depositional heterogneities and moderately by medium-scale diagenetic heterogeneities, whereas the influence of structural heterogeneities (regional dipping and faulting) was low or negligible.

2. Secondary production was dominantly influenced by large-scale structural factors (structural dip but not faulting), moderately or dominantly influenced by medium-scale diagenetic heterogeneities, and moderately by large- to medium-scale depositional heterogeneities.

3. Tertiary production was dominantly influenced by large-, medium-, and small-scale depositional heterogeneities; locally by medium- to small-scale diagenetic heterogeneities; and by medium- to small-scale tectonics (faulting).

In the barrier island deposystem at Bell Creek field, a good correlation of the initial primary production rate with Dykstra-Parsons coefficients indicates that permeability stratification due to depositional and diagenetic factors adversely influenced primary production and residual oil saturation distribution. The high Dykstra-Parsons coefficient criterion may be used to identify regions where waterflooding has not sufficiently swept the formation. These areas can be the immediate target for a properly designed infill drilling program. Areas with low Dykstra-Parsons coefficients were effectively swept, and infill drilling would provide little advantage.

Sensitivity analysis indicates a significant effect of vertical to horizontal permeability ratio and permeability contrast between facies on the distribution of residual oil saturation. This type of contrast has been documented, for lower shoreface facies, valley fill facies, and near the unconformity between valley fill and barrier island sandstones in Bell Creek field.

In reservoirs with permeability layering such as that of Bell Creek field, where the higher permeability is at the top of the reservoir, the vertical distribution of permeability counteracts the action of gravity and favors oil flow. When the higher permeability is at the bottom of the reservoir, the vertical variations in permeability compound the effect of gravity and produce an earlier water breakthrough.

A single-layer model for barrier island facies of superior quality is capable of history matching the primary and secondary production performance of Bell Creek field. The engineering parameter that played the most critical role in the field simulation was relative permeability. Extensive research is still required to address the measurement, averaging, and scaleup of relative permeability data. Waterflood initiation time is an important consideration for the efficient development of barrier island reservoirs.

Micellar-polymer simulation of a five-spot pattern indicates that infill drilling associated with pattern waterflooding of the relatively homogeneous portion of a barrier island reservoir does not provide additional production beyond the linedrive waterflood phase. Therefore, the micellar-polymer flood was responsible for much of the production within the homogeneous portion of the reservoir. However, in highly heterogeneous areas the infill drilling and associated five-spot pattern waterflooding were most effective in the recovery

of trapped oil left behind after linedrive waterflooding. This was further confirmed by actual field results. Simulation studies indicated the incremental recovery was a result of improvement in areal and vertical sweep efficiencies. Streamline modeling of the TIP area indicates an unbalanced injection program during the tertiary phase of production due to reservoir heterogeneities in the TIP area.

Improved reservoir evaluation is obtainable through multidisciplinary integration of conventional reservoir data if updated knowledge of heterogeneities is provided and thorough analysis is performed.

A generic, comprehensive, stepwise methodology with abundant interconnection among disciplines is the key to successful scientific reservoir characterization. NIPER methodology is organized in a format that is easily adaptable to an expert system technique of artificial intelligence (AI) for effective and efficient reservoir characterization.

# APPENDIX A - SURVEY OF BARRIER ISLAND, STRAND PLAIN, AND SHELF SAND RIDGE RESERVOIRS

## TABLE A-1 - Reservoirs producing oil from barrier/strandplain deposits

| Field | State/County | Pay zone | OOIP | Cumulative production | Ultimate recovery | Ref. No. |
|---|---|---|---|---|---|---|
| | | | (millions of barrels) | | | |
| Elk Basin | WY/MT | Frontier FM (Second Wall Creek) | 998 | 467 | -- | 1 |
| Big Piney/ LaBarge | WY/Sublette | Almy | -- | 65 | 91 | 2 |
| Bell Creek | MT/ | Muddy SS | 244 | 77.5 | 150 | 2,4 |
| Patrick Draw | WY | Almond | 200-250 | -- | -- | 4 |
| Amelia Frio 6 | TX | | 47 | 27.5 | 34.2 | 7 |
| Lovell's Lake Frio | TX | Frio (Buna) | 20 | 10.3 | 10.6 | 7 |
| Lovell's Lake Frio | TX | Frio (Buna) | 42 | 30.2 | 30.2 | 7 |
| Aransas Pass | TX | Frio | 44 | 20.1 | 20.5 | 7 |
| Arnold David Chapman | TX | Frio | 21 | 10.3 | 10.7 | 7 |
| Bloomington 4600 | TX | Frio | 69 | 30.5 | 31.4 | 7 |
| Bonnie View | TX | Frio | 50 | 19.1 | 19.5 | 7 |
| Flour Bluff Phillips | TX | Frio | 37 | 18.7 | 18.8 | 7 |
| Francitas North | TX | Frio | 25 | 13.1 | 13.2 | 7 |
| Ganado West 4700 | TX | Frio | 44 | 13.5 | 23.4 | 7 |
| Greta 4400 | TX | Frio | 313 | 124.7 | 147.0 | 7 |
| Heyser 5400 | TX | Frio | 90 | 10.4 | 48.7 | 7 |
| Lake Pasture H-440S | TX | Frio | 132 | 37.7 | 74.0 | 7 |
| La Rosa 5400 | TX | Frio | 20 | 10.0 | 10.0 | 7 |
| La Rosa 5900 | TX | Frio | 23 | 12.0 | 14.2 | 7 |
| La Ward North | TX | Frio | 68 | 18.7 | 20.0 | 7 |
| Lolita Marginulia | TX | Frio | 32 | 16.2 | 17.2 | 7 |
| Lolita Ward Zone | TX | Frio | 29 | 17.4 | 18.0 | 7 |
| London Gin Doughty | TX | Frio | 24 | 14.2 | 15.0 | 7 |
| Magnet-Whithers | TX | Frio | 163 | 78.6 | 91.3 | 7 |
| Markham N-BCN Carlson | TX | Frio | 20 | 10.7 | 11.5 | 7 |
| Markham N-BCN Cornelius | TX | Frio | 36 | 9.7 | 22.0 | 7 |

TABLE A-1 - Reservoirs producing oil from barrier/strandplain deposits - Continued

| Field | Stat/County | Pay zone | OOIP | Cumulative production | Ultimate recovery | Ref. No. |
|---|---|---|---|---|---|---|
| | | | (millions of barrels) | | | |
| Maurbro Marginulina | TX | Frio | 51 | 24.7 | 26.0 | 7 |
| McFaddin 4400 | TX | Frio | 51 | 22.4 | 24.3 | 7 |
| Midway Main Midway | TX | Frio | 60 | 16.6 | 17.0 | 7 |
| M.E. O'Connor FQ-40 | TX | Frio | 45 | 17.3 | 18.0 | 7 |
| Old Ocean Armstrong | TX | Frio | 136 | 67.3 | 69.0 | 7 |
| Old Ocean Chenault | TX | Frio | 27 | 10.2 | 10.3 | 7 |
| Pickett Ridge | TX | Frio | 27 | 45.8 | 16.2 | 7 |
| Placedo 4700 Sand | TX | Frio | 77 | 41.4 | 45.0 | 7 |
| Plymouth Heep | TX | Frio | 113 | 53.4 | 55.4 | 7 |
| Portilla 7300 | TX | Frio | 25 | 11.7 | 12.6 | 7 |
| Portilla 7400 | TX | Frio | 75 | 42.3 | 46.7 | 7 |
| Sugar Valley N | TX | Frio | 21 | 6.3 | 6.5 | 7 |
| Laurence Taft 4000 | TX | Frio | | | | |
| Tom O'Connor | TX | Frio | 45 | 24.8 | 26.0 | 7 |
| 4400 | TX | Frio | 30 | 11.0 | 16.0 | 7 |
| Tom O'Connor 4500 Greta | TX | Frio | 59 | 15.9 | 33.0 | 7 |
| Tom O'Connor 5500 | TX | Frio | 261 | 77.7 | 140.0 | 7 |
| Tom O'Connor 5800 | TX | Frio | 422 | 244. | 252.0 | 7 |
| Tom O'Connor 5900 | TX | Frio | 549 | 246.3 | 337.0 | 7 |
| West Ranch Glasscock | TX | Frio | 127 | 50.3 | 53.0 | 7 |
| West Ranch Greta | TX | Frio | 223 | 73.9 | 111.0 | 7 |
| West Ranch Ward | TX | Frio | 69 | 36.2 | 37.0 | 7 |
| West Ranch 41-A | TX | Frio | 203 | 84.6 | 94.0 | 7 |
| West Ranch 98-A | TX | Frio | 82 | 45.3 | 47.0 | 7 |
| White Point E Brighton | TX | Frio | 119 | 64.5 | 66.0 | 7 |
| Withers North | TX | Frio | 100 | 49.0 | 50.0 | 7 |
| Aviators Mirando | TX | Jackson-Yegua | 37 | 10.1 | 10.3 | 7 |

TABLE A-1 - Reservoirs producing oil from barrier/strandplain deposits - Continu

| Field | State/County | Pay zone | OOIP | Cumulative production | Ultimate recovery | Ref. No. |
|---|---|---|---|---|---|---|
| | | | (millions of barrels) | | | |
| Colorado Cockfield | TX | Jackson-Yegua | 52 | 21.7 | 21.8 | 7 |
| Conoco Driscoll U 1G W | TX | Jackson-Yegua | 69 | 20.0 | 23.7 | 7 |
| Escobas Mirando | TX | Jackson-Yegua | 28 | 12.8 | 12.9 | 7 |
| Govt Wells, North G W | TX | Jackson-Yegua | 150 | 77.3 | 78.0 | 7 |
| Govt Wells, South G W | TX | Jackson-Yegua | 40 | 16.6 | 18.0 | 7 |
| Hoffman Dougherty | TX | Jackson-Yegua | 55 | 20.5 | 21.0 | 7 |
| Loma Novia Loma Novia | TX | Jackson-Yegua | 176 | 47.7 | 48.0 | |
| Lopez First Mirando | TX | Jackson-Yegua | 75 | 30.4 | 33.0 | 7 |
| Mirando City Mirando | TX | Jackson-Yegua | 46 | 12.1 | 12.1 | 7 |
| O'Hern Pettus | TX | Jackson-Yegua | 83 | 22.2 | 30.0 | 7 |
| Pettus Pettus | TX | Jackson-Yegua | 46 | 16.2 | 17.0 | 7 |
| Piedre Lumbre G W | TX | Jackson-Yegua | 95 | 20.7 | 22.0 | 7 |
| Prado Middle Loma Novia | TX | Jackson-Yegua | 38 | 10.4 | 23.7 | 7 |
| Seven Sisters G W | TX | Jackson-Yegua | 142 | 35.0 | 56.0 | 7 |

## TABLE A-2 - Reservoirs producing oil from shelf sand ridge deposits (Ultimate recovery >50 million barrels)

| Field | State | Pay zone | OOIP | Cumulative production | Ultimate recovery | Ref. No. |
|---|---|---|---|---|---|---|
| | | | | (millions of barrels) | | |
| House Creek | WY | Suxxex | -- | 8.7 | 20 | 2,3 |
| Heldt Draw | WY | Shannon | -- | | -- | 3 |
| Holler Draw | WY | Shannon | -- | | -- | 3 |
| Triangle U | WY | Shannon | -- | 10 | -- | 3 |
| Jepson Draw | WY | Shannon | -- | -- | -- | 3 |
| Flying E | WY | Shannon | -- | -- | -- | 3 |
| West House Creek | WY | Suxxex | -- | -- | -- | 3 |
| East Heldt Draw | WY | Shannon | -- | -- | -- | 3 |
| Teapot Dome NPR-3 | WY | Shannon | 181 | -- | -- | |
| Sussex | WY | Shannon/Sussex | -- | 59 | 66. | 2 |
| Sussex W | WY | | -- | 14.9 | 20.5 | 2 |
| Hartzog Draw | WY | Shannon | 350 STB | 32 STB | 100 | 5 |
| Meadow Creek | WY | Shannon/Sussex | -- | 96 | 108 | 2 |
| Meadow Creek | WY | Shannon/Sussex | -- | 10 | 10.1 | 2 |
| Culp Draw | WY | Shannon | -- | -- | -- | |
| Pine Tree | WY | Shannon | -- | -- | -- | |
| Pumpkin | WY | Shannon | -- | -- | -- | |
| Butte | WY | | -- | -- | -- | |
| Meadow Creek East | WY | Shannon/Sussex | -- | -- | -- | |
| Gas Draw | WY | Muddy FM (Gas Draw SS) | -- | 22 | 27 | 2 |
| Teapot East | WY | Shannon/Frontier | -- | 10.7 | 55 | 1 |
| | WY | Muddy | | | | |
| Olympic | OK | Olympic SS | -- | 12 | -- | 6 |

## REFERENCES

1. Moody, J. A., J. W. Mooney, and J. Spivak. 1968, Giant Oil Fields of North America, in Halbouty, M. T., ed., Geology of Giant Petroleum Fields, AAPG Memoir 14, 1970.

2. Galloway, W. E., T. E. Ewing, C. M. Garrett, N. Tyler and D. G. Bebout. Atlas of Major Texas Oil Reservoirs, Bureau of Economic Geology, Austin, TX., 1983.

3. Nehring, R. The Discovery of Significant Oil and Gas Fields in the United States. Report R-2654/2-USGS/DOE, 1981.

4. American Petroleum Institute. Reserves of Crude Oil, Natural Gas Liquids, and Natural Gas in the United States and Canada as of December 31, 1979. API Trans., v. 34, June 1980.

5. Crews, G. C., Barlow, Jr., J. A., and Haun, J. D. Upper Cretaceous Gammon, Shannon, and Sussex Sandstones, Central Powder River Basin, Wyoming. Proc. Wyoming Geol. Assoc. 28th Annual Field Conference 1976, pp. 9-19.

6. Conybeare, C. E. B. Geomorphology of Oil and Gas Fields in Sandstone Bodies Elsevier Publishing Co., New York, 1976.

7. McCubbin, D. G. Facies and Paleocurrents of Gallup Sandstone, Model for Alternating Deltaic and Strandplain Progradation (abs). AAPG, Bull. 56, 1972, p. 638.

## APPENDIX B - REPRESENTATIVE SEDIMENTOLOGIC ANALYSIS OF CORES: MUDDY FORMATION, BELL CREEK FIELD

(For location of cores refer to figure 10)

Other verified core descriptions are available in an Open File accessible at NIPER during office hours.

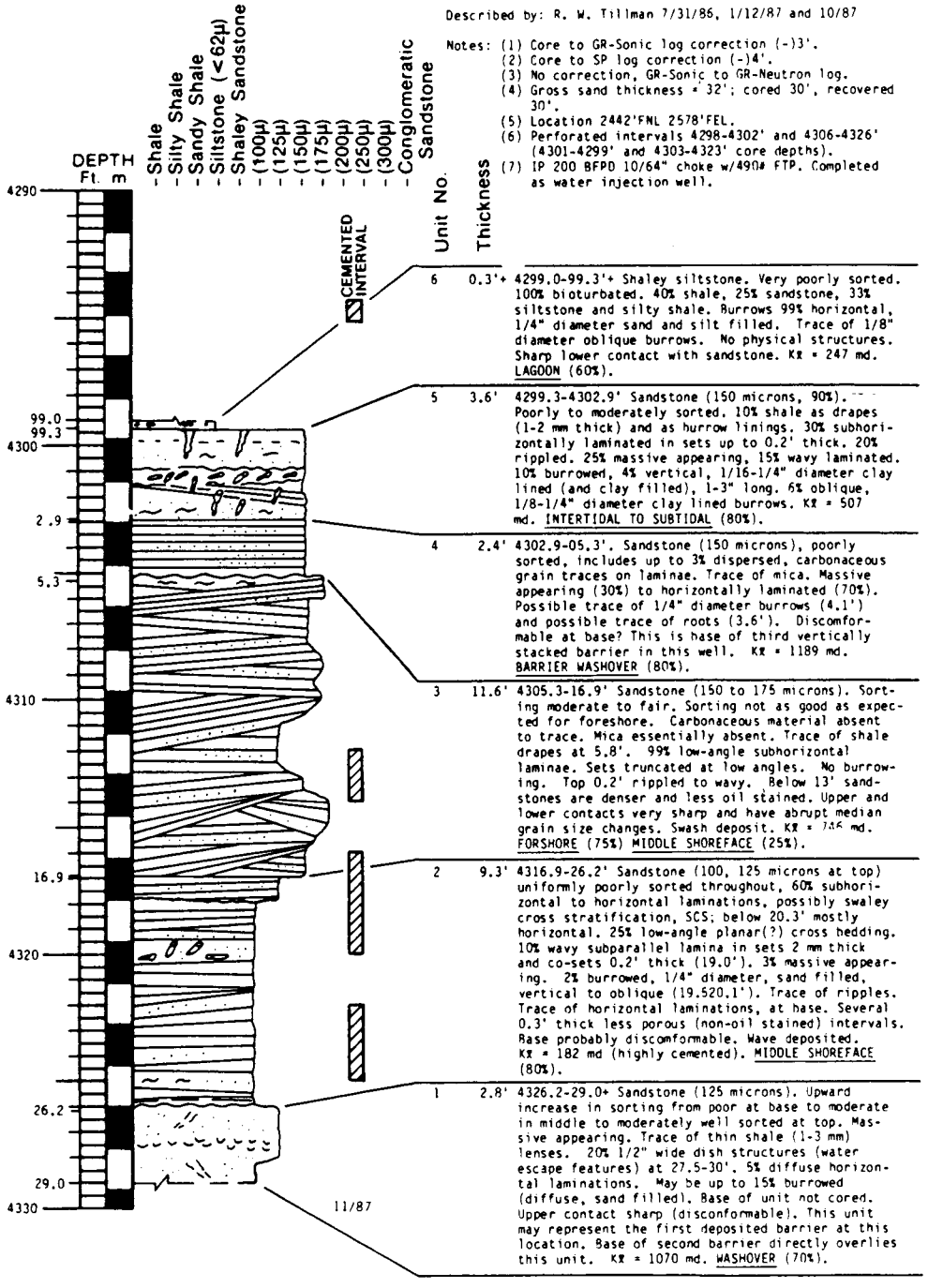


**FIGURE B-1. -Stratigraphic facies description; well W-16 in TIP area, completed as water injection well. Note highly clay-cemented layers within middle shoreface and foreshore facies.**

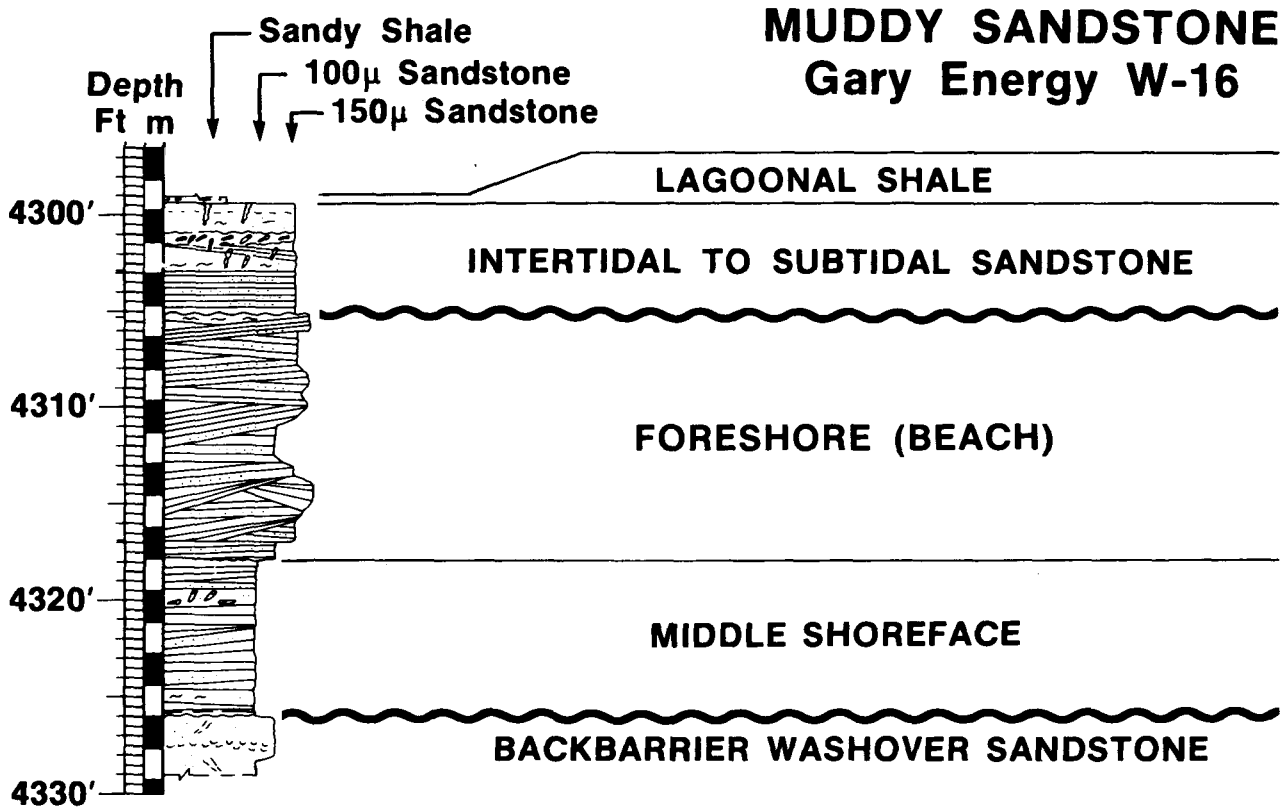


FIGURE B-2. -Summary of major genetic units in well W-16.

## APPENDIX C - REPRESENTATIVE SEDIMENTOLOGIC ANALYSIS OF OUTCROPS: MUDDY FORMATION, NEW HAVEN AREA, NE WYOMING
(For location of outcrops refer to figure 17)

Other verified outcrop profiles are available in an Open File accessible at NIPER during office hours.

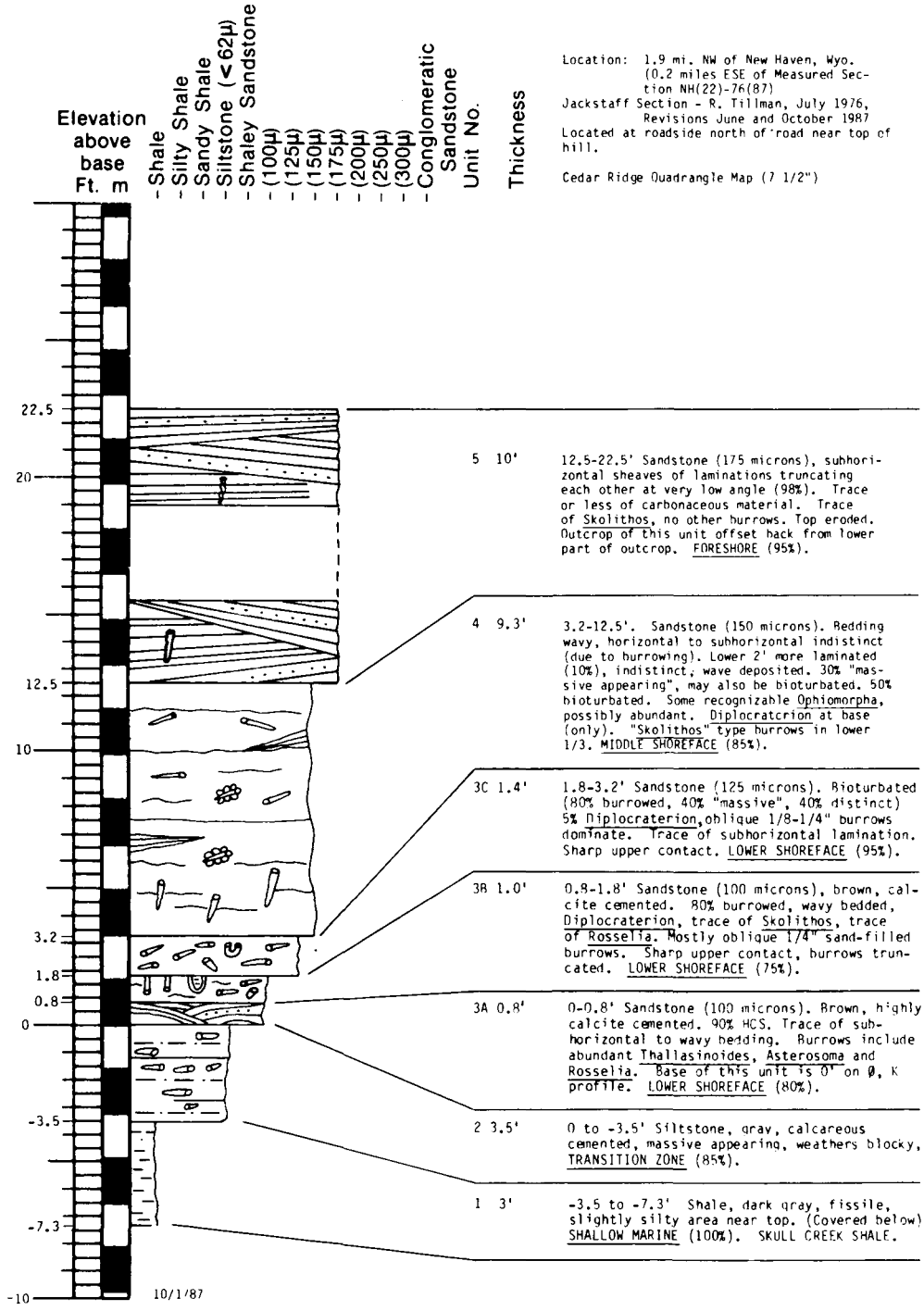


**FIGURE C-1. -Stratigraphic facies description; outcrop 22A, New Haven area, Wyoming. Measured section documents shallowing up (and coarsing up) sequence of barrier island sandstones representing one sedimentary cycle which is probably incomplete at top. The outcrop was sampled horizontally and vertically for distribution of petrophysical properties (study in progress).**

## APPENDIX D - INPUT PARAMETERS FOR CHEMICAL EOR SIMULATION

$a_4$ = Polymer adsorption parameter (dimensionless)
$a_{31}$ = Surfactant adsorption parameters (dimensionless)
$a_{32}$ = Surfactant adsorption parameters (ml/meq)
$A_{p1}, A_{p2}, A_{p3}$ = Polymer viscosity parameters (dimensionless)
$b_3$ = Surfactant adsorption parameter (dimensionless)
$b_4$ = Polymer adsorption parameter (1/wt%)
$b_{rk}$ = Parameter in permeability reduction factor equation (1/wt%)
$c_{pc}$ = Capillary pressure parameter (psi. $(\text{millidarcy})^{\frac{1}{2}}$)
$c_{rk}$ = Permeability reduction parameter $((\text{Darcy})^{\frac{1}{2}}/(\text{cP})^{1/3})$
$C$ = $\frac{qWt}{d\ Wx\ Wy\ Wz}$ Courant number (dimensionless)
$C^*_{2PLC}$ = Oil concentration at plait point in Type II(+) region (vol. fr.)
$C^*_{2PRC}$ = Oil concentration at plait point in Type II(-) region (vol. fr.)
$C_{3min}$ = Critical micelle concentration (vol. fr.)
$C_{SE1}$ = Effective salinity below which polymer viscosity is independent of salinity (meq/mL)
$C_{SEL}$ = Type II(-)/III effective salinity limit (meq/mL)
$C_{SEU}$ = Type III/II(+) effective salinity limit (meq/mL)
$D$ = Diffusion coefficient $ft^2/d$
$e_{1w}, e_{2w}, e_{3w}$ = Relative permeability exponent for aqueous, oleic, and microemulsion phases at low capillary number (dimensionless)
$e_{1c}, e_{2c}, e_{3c}$ = Relative permeability exponent for aqueous, oleic, and microemulsion phases at high capillary number (dimensionless)
$G_{11}, G_{12}, G_{13}$ = Interfacial tension parameters for water-microemulsion system (dynes/cm)
$G_{21}, G_{22}, G_{23}$ = Interfacial tension parameters for oil-microemulsion system (dynes/cm)
$k^\circ_{r1c}$ = Endpoint relative permeability for aqueous phase at high capillary number (dimensionless)
$k^\circ_{r2c}$ = Endpoint relative permeability for oleic phase at high capillary number (dimensionless)
$k^\circ_{r3c}$ = Endpoint relative permeability for microemulsion phase at high capillary number (dimensionless)
$k^\circ_{r1w}$ = Endpoint relative permeability for aqueous phase at low capillary number (dimensionless)
$k^\circ_{r2w}$ = Endpoint relative permeability for oleic phase at low capillary number (dimensionless)
$k^\circ_{r3w}$ = Endpoint relative permeability for microemulsion phase at low capillary number (dimensionless)
$m_{a0}, C_{a0}$ = Slope and intercept of maximum height of binodal curve (as a function of fraction of alcohol associated with surfactant) at zero salinity (vol. fr.)
$m_{a1}, C_{a1}$ = Slope and intercept of binodal curve at optimum salinity (vol. fr.)
$m_{a2}, C_{a2}$ = Slope and intercept of binodal curve at twice optimum salinity (vol. fr.)
$M_{C/OB}$ = Mobility ratio across the chemical front (dimensionless)
$M_{D/C}$ = Polymer drive/surfactant slug mobility ratio (dimensionless)
$M_{D/OB}$ = Overall mobility ratio (dimensionless)

$n_{pc}$ = Capillary pressure exponent (dimensionless)

$N_{Pe}$ = $\frac{L}{a_L}$, Peclet number (dimensionless)

$P_W$ = $\frac{WX}{a_L}$, Cell Peclet number (dimensionless)

$P_a$ = Exponent for calculating shear rate dependence of polymer viscosity (dimensionless)

$Q_V$ = Cation exchange capacity of reservoir clay (meq/mL of PV)

$S_{1rc}$ = Residual saturation of aqueous phase at high capillary number (fr. of PV)

$S_{2rc}$ = Residual saturation of oleic phase at high capillary number (fr. of PV)

$S_{3rc}$ = Residual saturation of microemulsion phase at high capillary number (fr. of PV)

$S_{1rw}$ = Residual saturation of aqueous phase at low capillary number (fr. of PV)

$S_{2rw}$ = Residual saturation of oleic phase at low capillary number (fr. of PV)

$S_{3rw}$ = Residual saturation of microemulsion phase at low capillary number (fr. of PV)

$S_p$ = Exponent for calculating salinity dependence of polymer viscosity (dimensionless)

$t_D$ = Dimensionless time (injected volume/pore volume)

$T_{11}$, $T_{12}$ = Capillary desaturation parameters for aqueous phase (dimensionless)

$T_{21}$, $T_{22}$ = Capillary desaturation parameters for oleic phase (dimensionless)

$T_{31}$,$T_{32}$ = Capillary desaturation parameters for microemulsion phase (dimensionless)

$W_s$ = Equivalent molecular weight of surfactant

**Greek Symbols**

$a_L$ = Longitudinal dispersivity (ft)

$a_1$,$a_2$,$a_3$,$a_4$, $a_5$ = Compositional microemulsion phase viscosity parameters (dimensionless)

$b_6$,$b_7$ = Effective salinity parameters (dimensionless)

$b_p$ = Effective salinity parameter for polymer viscosity (dimensionless)

$q_c$ = Coefficient in equivalent shear rate equation (day (Darcy)$^{\frac{1}{2}}$/ft sec)

$q_{\frac{1}{2}}$ = Shear rate at which polymer viscosity is one-half the polymer viscosity at zero shear rate ($sec^{-1}$)

$)_1$,$)_2$ = Water and oil viscosities (cP)

$s_{wo}$ = Interfacial tension between aqueous and oleic phases at low capillary number (dynes/cm)

**Subscripts**

| | | |
|---|---|---|
| 1 | = | Aqueous |
| 2 | = | Oleic |
| 3 | = | Microemulsion |
| c | = | High capillary number values or chemical front |
| l | = | Initial condition |
| OB | = | Oil bank |
| r | = | Residual |
| w | = | Waterflood or low capillary number values |